Détection de molécules biologiques par méthodes optiques

Qiqian Liu

Université Paris 13-UFR SMBH

N° attribué par la bibliothèque

THESIS

To obtain the rank of

DOCTOR OF PARIS SORBONNE NORD UNIVERSITY

Discipline: Chemistry

Presented and publicly supported by

Qiqian Liu

Development of nanovectors based on gold nanoparticles for Biomedical detection and treatment

Thesis director: Dr. Jolanda Spadavecchia and Pr. Marc Lamy de la Chapelle

JURY

Dr. Bich-thuy Doan	Université PSL	President
Pr. Claire Mangeney	Université Paris Descartes	Reporter
Pr. Nordin Felidi	Université Paris Diderot	Reporter
Dr. Jolanda Spadavecchia	Université Paris sorbonne Nord	Director
Pr. Marc Lamy de la Chapelle	Université du Mans	Co-director
Dr. Nadia Djaker	Université Paris sorbonne Nord	Supervisor

Acknowledgements

For this opportunity to present the results of my research:

I especially thank my thesis director Dr. Jolanda Spadavecchia for her guidance, but mostly her demand for excellence. I would like to express my gratitude to my co-director Pr. Marc Lamy de la chapelle for your guidance, the advice and support, and supervisors Nadia Djaker for the advice and support during these three years and for the good times spent together.

I would like to thank the members of the jury for this opportunity to present the results of my research:

Dr. Bich-thuy Doan (Chimie Paris Tech Université PSL), Pr. Claire Mangeney (Université Paris Descartes) Pr. Nordin Felidi (Université Paris Diderot).

Special thanks to Pr. Xiaowu Li for in vivo collaboration and Pr. Weiling Fu for SERS development. Dr. hui Liu for our precious in vivo collaboration。

I owe my gratitude to the whole laboratory's team, who built a welcoming, helpful, warm atmosphere work environment and for their help specially from Celia, Memona, Maroua, Hanane, Fatima.

I would like to thank my family specially my grandmother who has been always encouraged me during all these years and also my friends for their support and their unbreakable friendship during many years.

Accepted publication lists

1) **Qiqian Liu**, Pasquale Sacco, Eleonora Marsich, Franco Furlani, Celia Arib, Nadia Djaker, Marc Lamy de la Chapelle,Ivan Donati, and Jolanda Spadavecchia; Lactose-Modified Chitosan Gold (III)-PEGylated Complex-Bioconjugates: From Synthesis to Interaction with Targeted Galectin 1 Protein - Bioconjugate Chemistry 2018 29 (10), 3352-3361

2) **Qiqian Liu**, Fatima Aouidata, Pasquale Saccoc, Eleonora Marsichd, Nadia Djakera, Jolanda Spadavecchia; Galectin-1 protein modified gold (III)-PEGylated complex-nanoparticles: Proof of concept of alternative probe in colorimetric glucose detection - Colloids and Surfaces B: Biointerface , volume 185 1 January 2020, 110588

3) **Qiqian Liu**, Hui Liu, Pasquale Sacco, Nadia Djaker, Marc Lamy de la Chapelle, Eleonora Marsich, Xiaowu Li, Jolanda Spadavecchia ; CTL-Doxorubicin (DOX)-Gold complex Nanoparticles (DOX-AuGCs): Original Strategy to Enhance the Therapeutic Effect on Liver Cancer Model of Nude Mouse - nanoscale advances, 2020,2, 5231-5241

4) Celia Arib & **Qiqian Liu**, Nadia Djaker,Weiling Fu , Marc Lamy de la Chapelle, Jolanda Spadavecchia; Influence of the Aptamer Grafting on its Conformation and its Interaction with Targeted Protein – Plasmonics, 14, pages1029–1038(2019)

5) Hanane Moustaoui, a Justine Saber,a Ines Djeddi,a **Qiqian Liu**, ab Dania Movia, c Adriele Prina-Mello, c Jolanda Spadavecchia, Marc Lamy de la Chapellebd and Nadia Djaker; In situ protein corona study by scattering correlation spectroscopy: a comparative study between spherical and urchin-shaped gold nanoparticles nanoscale – 2019,11, 3665-3673

6) Jiaoqi Huang, Yang Zhang, Zhongquan Lin, Wei Liu, Xueping Chen, Yu Liu, Huiyan Tian, **Qiqian Liu**, Raymond Gillibert, Jolanda Spadavecchia, Nadia Djaker, Marc Lamy de la Chapelle, Yang Xiang and Weiling Fu; Femtomolar detection of nucleic acid based on functionalized gold nanoparticles nanophotonics - Volume 8, Issue 9, id.50, 9pp

7) Hanane Moustaoui, Justine Saber, Ines Djeddi, **Qiqian Liu**, Amadou Thierno Diallo, Jolanda Spadavecchia, Marc Lamy de la Chapelle, and Nadia Djaker; Shape and Size Effect on Photothermal Heat Elevation of Gold Nanoparticles: Absorption Coefficient Experimental Measurement of Spherical and Urchin-Shaped Gold Nanoparticles. J. Phys. Chem 2019, 123, 28, 17548–17554

8) Yu Liu, Yang Zhang, Morgan Tardivel, Médéric Lequeux, Xueping Chen, Wei Liu, Jiaoqi Huang, **Qiqian Liu**, Marc Lamy de la Chapelle & weiling Fu; Evaluation of the Reliability of Six Commercial SERS Substrates – Plasmonics, 15, pages743–752(2020)

In submission

9) Wafa Safar, Andra Tatar, Aymeric Leray, Monica Potara, **Liu Qiqian**, Mathieu Edely, Nadia Djaker, Jolanda Spadavecchia, Weiling Fu, Sarra Derouich, Nordin Felidj, Simion Astilean, Eric Finot, Marc Lamy de la Chapelle; New insight on the aptamer conformation and aptamer/protein interaction by surface enhanced Raman scattering and multivariate statistical analysis

List of abbreviations and acronyms

ATP:adenosine triphosphate

AuNP: Gold nanoparticle

Apt: aptamer

Apt w/T: aptamer with T

Apt wo/T aptamer without T

CNP : Chitosan nanoparticles

CTL : Chitlac

CS_2 carbon disulphide

CTAB : Cetyltrimethylammonium bromide

DNA : Deoxyribonucleic acid

DLS: Dynamic light scattering

DOX: Doxorubicin

EDC: 1-éthyl-3-(3-dimethylaminopropyl) carbodiimide

EGF: Epidermal Growth Factor

EFGR: epidermal growth factor receptor

EPR: Enhanced permeability and retention

FBS: Fetal bovin serum

FCS: Fluorescence correlation spectroscopy

GNF: Gold nanoflower

GNS: Gold nanosphere

GAGs: glycosaminoglycans

Galβ1-3GlcNAc: N-acetyl lactosamine

Gal-1: Protein Galectin-1

$HAuCl_4$: tetrachloroauric acid

(ICP-MS): inductively coupled plasma mass spectrometry

LSP: Localized surface plasmon

LSPR: Localized surface plasmon resonance

LC/MS: liquid chromatography coupled with mass spectrometry

TEM: Transmission Electroic Microscopy

mRNA: message Ribonucleic acid

MnSOD: Manganese superoxide dismutase

NHS: N-hydroxysuccinimide

OVA: ovalbumin

PBS: Phosphate buffered saline

PEG: Polyeethylene glycol

PSS: poly sodium styrene sulfonate

RNA: Ribonucleic acid

SCS: Scattering correlation spectroscopy

SERS: Surface enhanced Raman spectroscopy

TPL: two-photon imaging technology

UV-vis: Ultraviolet-visible

Table of contents

General introduction

During the recent years the use of nanoparticles in medical applications has been largely developed. For example, the nanoparticles are now commonly used in personal care products for skin, in food industries, in medical imaging, biomarkers detection or for drug delivery. Gold nanoparticles have especially attracted enormous scientific and technological interests for their unique optical properties, their ease to be synthesized or functionalized and their chemical stabilities.

The latest studies (drug delivery, diagnostics, biosensing, bio-imaging, theragnostic, and hazardous chemical sensing) [1] make gold nanoparticles one of the best candidates for biomedical applications such as targeted drug vector in the treatment of cancer, in biological detection or in biological imaging. However, knowledge on their possible toxicity and their impact on health is an essential element to be investigated before their application to humans. Thus, It is important to study their potential toxicity and biodistribution in animal model. Many studies show that when nanoparticles come into contact with a biological fluid, their surface is covered by macromolecules forming a 'corona'. Two consequences are resulting from such interaction: on one hand the nanoparticles may acquire new chemical and surface properties allowing them to interact more easily with biological objects as cells; on the other hand the conformation of adsorbed macromolecules may be altered leading to a loss of biological activity. In this context the study of the interaction between nanoparticles and biomolecules as well as the interaction between a bioreceptor grafted at the nanoparticle surface and a biomolecule is essential to understand the mechanism for the future biomedical applications in the drug delivery, the disease therapy or the analyte detection.

The aim of this thesis is to design and optimize a new hybrid nanoparticle which provides a good stability and could be used in several biomedical applications and providing highly sensitive detection of biomarkers and high therapeutic effects to target specifically the cancer cells. To do so, I have used a new method of synthesis exploiting the complexation of gold salts. This method allows not only the grafting of specific receptors at the nanoparticle surface but also the inclusion of therapeutic agents. This specific particle was tested first for the detection of Galectin-1 protein (a cancer biomarker) and of the glucose as well as for the treatment of the liver cancer in mice model. Moreover, since gold nanoparticles could interact with different biomolecules during their transport in the body, I also performed a study on the behavior of gold nanoparticles when they interact with a specific protein using spectroscopic methods.

A first bibliographical chapter describes the general information on nanoparticles: the different methods of synthesis and of surface functionalization as well as their physical chemical properties. Subsequently, I report on their main applications in the health fields, in particular for the biomarker's detection, for the nanovectorization and on their interaction with the biological environments.

A second chapter is devoted to the development of two gold nanoparticles for biomolecules detection. First part is gold polyethylene glycol and chitosan lactose modified nanoparticles for the Galectin-1 biomarker detection. Evidence suggests that galectin plays a considerable part in processes linked to tumorigenesis [2, 3], including transformation to a malignant form, and increased invasive properties of tumor cells. That is the reason why we selected it as detection target. Second part focuses on the Galectin-1 protein functionalized gold nanoparticles for the Glucose detection as galectins are a class of proteins that bind specifically to β-galactoside

sugars, such as N-acetyl lactosamine (Galβ1-3GlcNAc or Galβ1-4GlcNAc). That is the reason why we selected this protein to specifically detect glucose for cancer diagnosis.

A third chapter presents of a second nanovector with Doxorubicin which is used as an anti-cancer agent. The synthesis of this nanovector is done through the complexation of the gold salt with the doxorubicin molecules in the presence of chitlac (CTL) and polyethylene glycol (PEG). After having characterized the physico-chemical properties of the nanovectors, full in vivo experiments have been carried out for a series of biological analysis on nude mice. The efficiency of tumor reduction was evaluated and the biodistribution of nanovectors and its influence of the immune system were analyzed.

A fourth chapter presents the study of the interaction between a bioreceptor (an aptamer) grafted at the surface of a gold nanoparticle and its analyte (the MnSOD protein) depending on the analyte concentrations. For such study, we use scattering correlation spectroscopy to observe the nanoparticles in the presence of the analyte. This technique allows the determination of fundamental properties such as the binding constant of proteins with the aptamer, the thickness of the protein layer and the conformation of the protein during its adsorption on the nanoparticles. Additionally, we performed real time SERS measurements to observe the dynamic of the MnSOD/aptamer interaction.

To conclude this PhD thesis, the mains results will be summarized and some outlook will be introduced.

Chapter 1

Nanoparticles synthesis and applications in the health fields

Nanotechnology is a very wide and important interdisciplinary field which mainly focuses on the synthesis, the functionalization, the characterization, and the exploitation of nanostructured materials. The main characteristic of such materials is their size in the nanometer range, which constitutes a bridge between molecules and macroscopic systems.

Nanotechnology now includes nanobiology [4], nanoelectronics [5], nanomaterials [6-8], nanochemistry [9,10] and other disciplines. Since the microtechnology development, the human beings are getting deeper and deeper from the micro world down to the nanoscale and the level of understanding of the nano-objects has increased to an unprecedented level. The nanostructures are a key point for the next stage of scientific and technological developments. It will be a technological breakthrough, which could induce a new industrial revolution in the 21st century.

However, the nanomedicine, one of the nanotechnology fields, is still in its development stage and is a hot topic. This field consists in the application of nanotechnology concepts and techniques in the biomedical and pharmaceutical fields. Nowadays it is still growing constantly and it seeks to deliver a valuable set of research tools and clinical devices in the near future [11,12]. The nanoparticles can be selectively accumulated in specific cells or structures. But the strong permeability of nanoparticles not only provides effectiveness for the use of drugs, but also poses a potential threat to human health as nanoparticles with their small sizes can penetrate into cells and spread along the nerve cell synapses, blood vessels or lymphatic vessels.

This chapter is divided in two parts. The first part will be devoted to a bibliographic study on the different synthesis methods of gold nanoparticles, on their physical and chemical properties as well as on their surface functionalization. The second part will focus more specifically on their applications in the health fields.

1.1 Nanoparticles

Nanoparticles are defined as particles with a size in the range of 10-1000nm. They can have amorphous or crystalline atomic structure and their surfaces can act as carriers of biomolecules as proteins, DNA, Peptides, etc. To some degree, nanoparticles should be considered as a distinct state of the matter, in addition to the solid, liquid, gaseous, and plasma states, due to its distinct properties (large surface area and quantum size effects). For example, fullerene and carbon nanotubes are materials that form nanostructures in crystalline form, while graphite and diamond represent the carbon solid form. Many experiments choose the upper limit size of nanomaterials between 50 nm and 100 nm. The choice can be justified by the fact that some physical properties of nanoparticles converge on those of bulk when their size reaches these values. However, this size threshold varies with material type and cannot be the basis for such a classification. A legitimate definition extends this upper size limit to 1 micron, the sub-micron range being classified as nano. The recent advance in characterization tools and science (synthesis, understanding of physical phenomena) enabled the emergence of nanoscience and

nanotechnology. Nanoscience is the study of phenomena and material properties at the nanoscale, while nanotechnology is the application of the knowledge to create, produce and use materials exploiting nano-phenomenon. The differences between nanomaterials and “macro” materials can be explained by two parameters: surface effects and quantum effects. Surface effect is due to the very large surface area of nanomaterials. For instance, the chemical reactivity increases when the particle size decreases. Quantum effect is due to the delocalization of electrons on the surface and to their confinement in limited size. These factors give unique properties to nanomaterials, such as chemical property (surface reactivity, catalysis ...) and physical property (electric, electronic, thermal and optical).

In the following of this chapter, I will focus on gold nanoparticles.

1.1.1 Gold nanoparticles

Gold nanoparticles have in fact been used for a very long time. Indeed, gold nanoparticles would have been already produced in colloidal solutions around the 4th century BC in Egypt and China, for artistic purposes, notably in the famous cup of Lycurgus which dates from Roman Empire [13, 15]. The presence of gold nanoparticles in the glass of this cup gives special optical properties to it. When the cup is illuminated from the outside (reflected light), the glass appears green (Figure 1.1) while when it is illuminated from the inside (transmitted light), the glass appears red (Figure 1.1). This is due to the optical properties of the nanomaterials (mainly silver and gold nanoparticles) present within this cup, which by interacting with light will absorb and scatter the light.

Figure 1.1 Cup of Lycurgus

The, "soluble" gold was also used for healing purposes. This "soluble" gold intended for the treatment of certain diseases (melancholy, venereal disease or heart disease) was used until the Middle Ages [16, 17]. Currently we can still find gold colloidal solutions to treat rheumatoid arthritis [18], anxiety or the presence of gold nanoparticles in creams is used for anti-aging effects [18]. However, the beginning of gold colloid chemistry dates from the mid-19th century when Michael Faraday [17] synthesized gold nanoparticles by reducing tetrachloroaurate by white phosphorus in the presence of carbon disulphide (CS_2). At the beginning of the 20th century, Wilhelm Ostwald [17] will contribute to the development of the science of gold colloids. He was the first one to demonstrate that metallic nanoparticles have different properties from bulk materials and deduce that these properties are mainly determined by surface atoms as they have a low coordination number compared to core atoms and are therefore more mobile.

1.1.2 Synthesis of gold nanoparticles

There are several ways to synthesize gold nanoparticles. The most commonly used protocols are often categorized into two types of methods:

1) The top-down methods using physical–chemical processes that degrade a bulk material into smaller pieces, achieving the nanometric scale

2) The bottom-up methods that are the most used for nanomaterial synthesis. The synthesis of nanoparticles starts from smaller precursors, such as metallic salts or molecular seeds and forms nanostructures [19, 20]. Figure 1.2 shows the two common ways for the synthesis of nanoparticles.

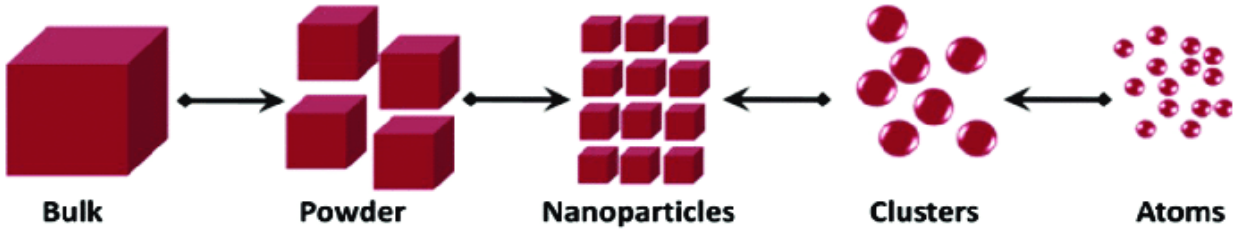

Figure 1.2 Top-down and bottom-up approaches for the synthesis of nanoparticles [20].

a) Synthesis of nanoparticles by "top-down" approach

Starting from a bulk material, it consists in transforming it into small particles of nanometric size. In this case, nanoparticles are mainly made by downsizing fragments of metals or metal oxides. As examples, one can cite:

1)Mechanosynthesis

Mechanosynthesis is a process of powder metallurgy. As the name suggests, it involves mechanical energy to reduce the grain size of the material. It is a process of grinding metal powders in order to reduce the size of the particles. This method cannot control the size and morphology of the particles because the structures are gradually fractionated until particles of nanometric sizes are obtained. The particles obtained by this method have a size of between 0.5 and 10 microns. This technique is very sophisticated and time consuming. Moreover, its efficiency and yield are not high [21].

2)Lithography

Lithography involves a nanometer mask made in a layer of polymer resin deposited on the surface of a substrate. The resin is subsequently exposed to radiation (UV, X, etc.) or to a beam of charged particles (electrons, ions). Unlike previous methods, lithography makes it easier to control the morphology and organization of nano-objects on a surface. Although this approach allows precise control of the size, shape and position of the structures, the quality of the nanoscale structures produced is not always optimal because of the (crystalline) defects generated during the development. In addition, the processing time is long and the major drawbacks are

its cost, low throughput and its resolution limit, due in particular to diffraction problems linked to the wavelength of the ray used (X or UV or e beam) [22,23].

b) Synthesis of nanoparticles by "Bottom-up" approach

Unlike the top-down approach, this approach makes it possible to obtain nanoparticles by nucleation and growth processes from a single atom or from atomic clusters. It involves the use of physico-chemical phenomena at the atomic and molecular scale to chemically transform a precursor into metallic particles. The assembly and positioning of atoms, molecules or particles allows the formation of simple or elaborate nanostructures. In general, in the "bottom-up" approach, there are two categories of reactions: reduction and decomposition reactions. These two reactions can take place in the gas, liquid or solid phase.
The chemical transformation routes grouped together under the name of “colloid chemistry” are particularly rich both in terms of the large number of compounds which have been able to be synthesized and in the flexibility of the processes making it possible to vary a large number of parameters. Since no general trend emerges from these methods, it is therefore important to determine the best synthesis method as well as the most suitable stabilizer for the intended application.

The physical synthesis for bottom-up method is based on homogeneous nucleation of supersaturated vapors followed by particle growth by condensation. Thus, depending on the chemical nature of the material, saturated vapors can be generated in various ways. The supersaturation can be carried out by cooling or by chemical reaction or by a combination of these two methods. Supersaturated vapors can grow homogeneously in the gas phase or heterogeneously on contact with the surface. Physical methods offer a greater variety of host matrices and the ability to more easily control the size, shape and local environment of the nanoparticles. However, they require heavier equipment and most of the time only allow the synthesis of materials in the form of thin films. The physical synthesis of nanoparticles can be initiated from solid, liquid or gaseous precursors [23].

1)Chemical (colloidal) nanoparticle production processes

Gold nanoparticles, maybe the most common class of nanoparticles, are generally synthesized by the reduction of gold salts, resulting in nucleation and growth of metallic particles in solution. Aqueous synthesis is nowadays commonly carried out by the citrate-reduction route that yields gold nanoparticles with a narrow and monomodal size distribution. The average particle diameter can be controlled on a size range between 2 and 200 nm through the stoichiometry of the reagents, i.e. precursor salt and reduction agent. The particles can be stabilized by citrate ions bound to the surface of the nanoparticles, resulting in negatively charged particles that repel each other by electrostatic repulsion. These are the oldest methods used for the preparation of nanoscale dispersions in matrices. The first use of the colloidal method dates back to Faraday, who prepared colloids of Au in 1857 [17]. Colloidal methods allow the preparation of large quantities of products and are suitable for the production of nanoparticles. These methods are based on fairly simple principles although it remains difficult to control certain reactions uniformly. They have the advantage of being relatively inexpensive and requiring less energy than other nanoparticle synthesis processes. They are also the easiest to use and are the basis of much of the production of nanomaterials. Among them, we distinguish in general two main routes for the gold nanoparticle synthesis:

Reductions by different ways: chemical reactions, electrochemistry, sonochemistry, photochemistry

Sol–gel chemistry and thermal decomposition of metal compounds in aqueous or organic media in the presence of surfactants (ligands or polymers).

Chemical reduction remains by far the most widely used method for the synthesis of nanoparticles. The metal nanoparticles are obtained here in a liquid medium. It can be carried out in aqueous or organic phase and the main reagents are as follows:

Metal salt + Reducing agent + Surfactant + Solvent

In this diagram, the salt is the precursor containing the metal. The solvent can be aqueous or organic (polyol, toluene for example) and must be polar, as it must have a dipole moment high enough to be able to break the bonds of the salt and dissolve it. The reducing agent is chosen to reduce the dissolved metal species that precipitate into metal particles. The surfactant acts as a protective agent of the metal particles by being adsorbed at the particle surface and thus preventing them from clumping together. The morphology as well as the size distribution of the nanoparticles are controlled by parameters such as the reduction kinetics and the nature of the surfactant.

2)Commun example of chemical reduction

Reduction by citrate

The best known method is the reduction of a gold salt by sodium citrate in aqueous solution. A century after the Faraday's synthesis, it was first developed in 1951 by Turkevich et al [24]. It allows the production of spherical nanoparticles through the reduction of tetrachloroauric acid ($HAuCl_4$) by citrate (figure 1.3). The beauty of this method lies in its simplicity and in the fact that it makes it possible to obtain stable and monodisperse colloids of gold by in situ reduction of gold salts in aqueous solution at a room temperature. In this synthesis, citrate acts as a reducing agent and as a surfactant because it prevents the particle aggregation by charging the particle surface. Further work on the synthesis of gold nanoparticles resulting from the reduction of gold salt by citrate has been carried out by Frens [25]. Thus in 1973, he showed that it was possible to control the average particle size by varying the ratio "concentration of gold salt" to "concentration of citrate" ($[HAuCl_4]$ / [citrate]). Thus, by reducing the amount of citrate used in the synthesis, we reduce the amount of citrate ions necessary for the stabilization of the particles causing the aggregation of small particles into large particles until the surface becomes large enough to be covered by existing citrate ions.

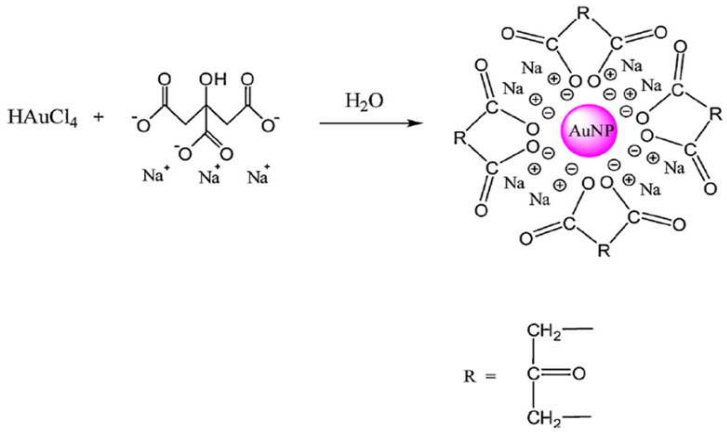

Figure1.3 Mechanism of Citrate reduction and growth of AuNPs

Reduction by borohydrides

Another synthesis which has revolutionized the world of colloidal gold nanoparticle chemistry is the synthesis of Brust and Schiffrin who, in 1994, allows the synthesis of gold nanoparticles of small size and controllable diameter [14] (Figure 1.4). This synthesis occurs in an organic solvent and consists of reducing tetrachloroauric acid with sodium tetrahydroborate, which is a strong reducing agent, in the presence of thiolated organic molecules. The latters will play the role of stabilizing agent by forming a protective layer around the nanoparticles, and avoid, or control, their aggregation. This synthesis has enabled the synthesis of gold nanoparticles surrounded by biocompatible polymers, such as thiolated polyethylene glycol (PEG), widely used in the biomedical fields.

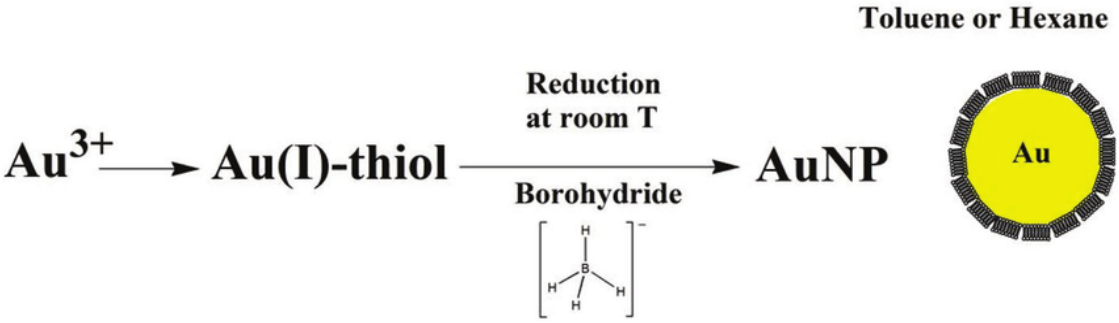

Figure 1.4 The Borohydrides Reduction

3) Synthesis of colloidal nanoparticles using biomolecules

These new ways of making gold nanoparticles are based on the use of the biological or chemical activities of biomolecules. In this case, the mechanism is similar to that of chemical synthesis. The only difference being that the reducing agents used are biomolecules such as enzymes [26], or natural metabolites present in plants [27], etc. This approach eliminates the use of harmful chemical as certain surfactants and stabilizers. This approach, which is known as green chemistry, is therefore a biocompatible and safer approach.

4)Stabilization against aggregation

The molecules bound at the nanoparticle surface not only control the growth of the particles during synthesis, but also prevent their aggregation. These surface molecules induce electrostatic repulsion or the formation of hydration layer on the surface and as a consequence repulsive forces between particles. Depending on the particle system, the core material and the solvent in which the particles are dispersed, the choice of the relevant stabilizer might produce very stable particles. First the molecules have to be bound to the particle by some attractive interactions (chemisorption, electrostatic attraction or hydrophobic interaction, most commonly provided by a head group of the molecule). Various chemical functional groups possess a certain affinity to inorganic surfaces. The most famous example is the thiol group that has a strong affinity for the gold. In many cases, this principle is already exploited during the synthesis. Polar or charged molecules provide solubility in polar or aqueous solvents while nanoparticles with apolar stabilizers such as hydrocarbon chains are only soluble in apolar organic solvents (hexane, toluene or chloroform).

1.1.3 Physico-chemical properties of gold nanoparticles

Nanoparticles synthesized by the reduction of gold in aqueous phase tend to have quasi-spherical morphologies as this shape presents the smallest surface area compared to other morphologies. Typically, the suspension of spherical gold nanoparticles presents a ruby red color due to the scattering of light by the nanomaterial, but the increase in size, as well as a change in the environment surrounding the nanoparticles, may modify the optical properties of the colloid [28,29].

a) Physical properties of Gold Nanoparticles

Gold nanoparticles with a diameter of a few to few tens of nanometers, whose basic units are small sized particles, have many physical characteristics that macroparticles do not have, such as optical effects, small size effects, surface effects, quantum effects or dielectric limits effect. These properties make gold nanoparticles widely used in materials, clinical medicine, food field, chemistry, ceramics, dyes and other fields

1)Optical properties

When an electromagnetic wave interacts with a metal, the free electrons in the conduction band can be excited. This interaction causes the collective oscillation of free electrons at a frequency imposed by the incident field. This oscillation is called plasmon and its oscillation resonance depends on the particle size and shape, the metal nature and the surrounding environment. Figure 1.5 shows the oscillation of plasmon and local enhancement. Gold nanoparticles can then selectively absorb and scatter the light. For nanoparticles smaller than 20 nm, the absorption is the main part, and the scattering only accounts for a small part. [30] The scattering increases for larger nanoparticles and provides the main contribution to the light interaction for nanoparticles larger than 50 nm. Because of plasmon, the optical properties of metallic nanoparticles have aroused considerable interest since the observation of an enhanced Raman scattering signal (SERS) from individual molecules adsorbed on the surface of nanoparticles [31-33]. From a fundamental point of view, the optical response of nano-objects provides access to their geometrical characteristics and therefore constitutes a powerful tool to analyze their properties. The specific optical properties of metal nanoparticles are a consequence of the appearance of surface plasmon resonance in their absorption spectrum. For gold, it is in the visible range of the

spectrum. Its characteristics, position and spectral widths, sensitivity to the polarization of light, depend both on the intrinsic properties of nanoparticles (composition, structure, size, shape) and on their local environment. Linear absorption or scattering spectroscopy thus provides information on nanoparticles under different environmental conditions. Furthermore, the optical response of a metal is directly related to the properties of electrons and the lattice via its dielectric constant. A modification of the electronic distribution therefore results in that of the optical properties.

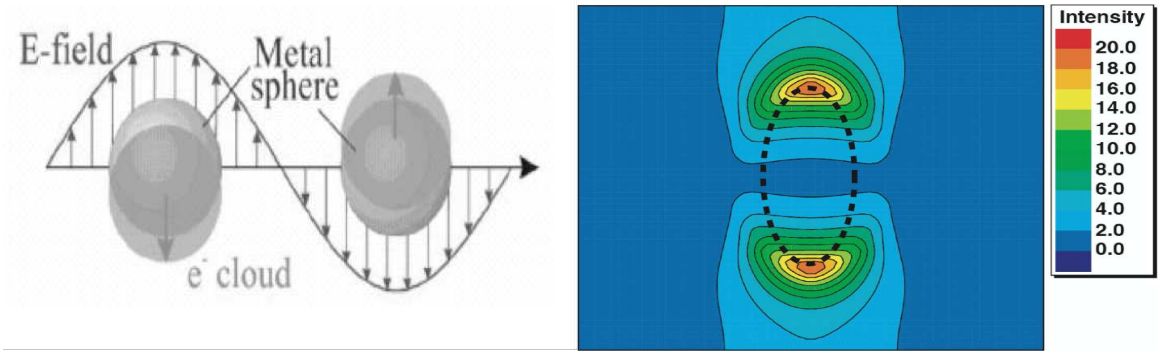

Figure 1.5 the oscillation of plasmon and local enhancement [31].

The size and the shape of gold nanoparticles have a strong influence on the surface plasmon resonance. [34] As the size of the particles increases, the plasmon resonance of the particle is shifted to longer wavelength. The resonance is located at a wavelength around 520nm for the smaller nanoparticles and can be shifted through the whole visible and even in the IR range for larger nanoparticles. By complementary color principle, gold colloidal solutions show colors ranging from red to blue (Figure 1.6), simply by changing the particle size. Similar behavior is also observable for elongated nanoparticle as nanorods. The colors changing could be used for colorimetry fast detection of different biomarkers.

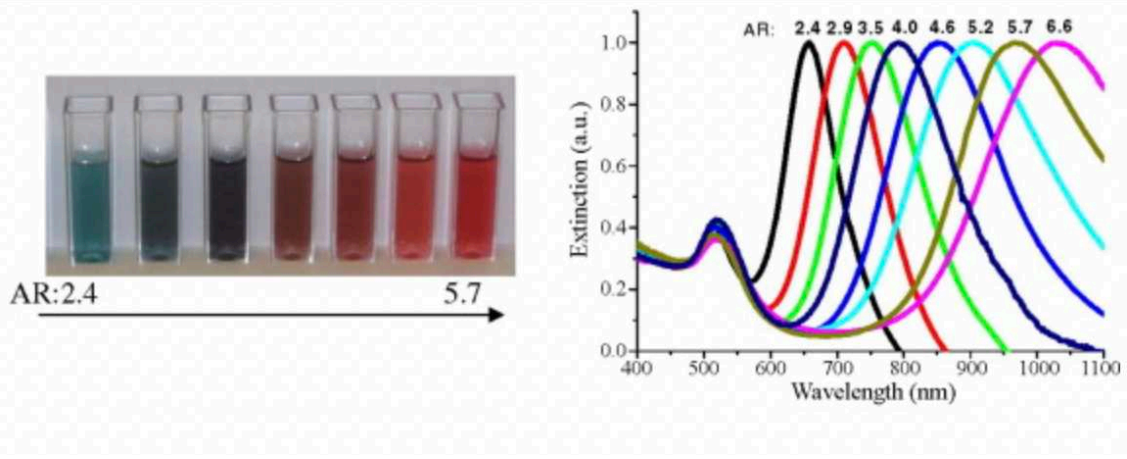

Figure1.6 The color change of nanoparticles induced by theirs size [34]

2)Surface effect

Due to the small size of the gold nanoparticles, the number of atoms at their surface is proportionally much higher than the number of atoms at the surface of bulk particles. The proportion

of surface atoms compared to the total number of atoms increases when the particle size decreases inducing a consequent modification of the surface energy and the surface binding energy. The various effects resulting from this are collectively referred to the surface effect. When the diameter of the gold nanoparticles reduced from 100 nm to 1 nm, the percentage of the atoms on the surface increase from 20% up to 99%. [32] In this latter case, the atoms are almost completely concentrated on the surface of the gold nanoparticles. Due to the vacancy effect of the surface, the surrounding is lacking adjacent atoms show insufficient atomic coordination, and the high surface energy makes the surface atoms have high reactivity and are extremely unstable.

b) Chemical properties of gold nanoparticles

Gold is a heavy metal and one of the most chemically stable elements. Gold nanoparticle has surface electronic states on some specific interfaces, and its Fermi energy level is located exactly in the forbidden band of the band structure along the crystal direction, forming a two-dimensional electron cloud. Thus, this one can only move parallel to the surface direction resulting with specific chemical properties. (surface properties, catalytic activity etc.) Gold nanoparticles have excellent biocompatibility and are harmless inside the human body, so the applications in the medical field are very large.

1)Fluorescence characteristics

When gold nanoparticles are coated with polyoctylphenylthiol group, pyrene group or other detection groups, all the groups can become fluorescent. The fluorescent gold nanoparticles have good application prospects in biophotonics and materials sciences.

2)Electrochemical characteristics

When cyclic voltammetry, differential pulse voltammetry and chronoamperometry were used to analyze the gold nanoparticles wrapped in the alkylthiol monolayer, it was found that there was an electric double layer capacitance on the surface of the gold nanoparticles, which is equivalent to a nanometer scale electrode, and the capacitance value increases with the decrease of the length of the alkyl chain of the coated particles. When the size of the gold nanoparticles decreases to a certain extent, the electrostatic attraction energy is bigger than the energy of thermal motion. [35] The stable ligand protecting the gold nanoparticles can produce a single electron transfer between the electrode and the probe, making it have a unique electrochemical redox activity, causing the electric double layer on the surface of the gold nanoparticles to be charged and discharged.

1.1.4 Bio-application of gold nanoparticles

As Gold nanoparticles have good stability, excellent conductivity, small size effect, specific optical properties (in particular plasmonic properties), surface effect and various catalytic characteristics, gold nanoparticles are now used in different applications, and more especially in the medical field. Since Au nanoparticles are biocompatible, they accept very easily on their surface a wide range of biological molecules such as amino acids, proteins, enzymes and DNA. Such biological molecules can be linked to nanoparticles in different ways: through functional groups (thiols, amines) to be directly bind to the surface or through bio-conjugate chemistry, forming new functional hybrid nanoparticles. The bound biomolecules can then be used in vitro or in

vivo for biomedical applications: such as biosensors for disease diagnosis, nanovectors for the disease treatment (drug delivery [36] or gene therapy [37]), targeted imaging contrast agents or photothermal therapy which is non-invasive and very effective method. However, although being biocompatible and used as therapeutic agents, there are still many uncertainties about their possible toxicity. Studies have shown that the toxicity of gold nanoparticles comes from their surface chemistry, shape and size, and need more investigations in the future.

a) Particle Functionalization

Chemical functional groups stabilizing the nanoparticles against aggregation can simply consist of an inert molecular chain (hydrocarbon chain or polyethylene glycol) or of functional groups which are in most cases linear molecules. In the case of water-soluble nanoparticles, these functional groups are often carboxylic acids stabilizing the nanoparticles by electrostatic repulsion. They can be exploited for the conjugation of other molecules to the particles. In the following of this chapter, I will focus on polyethylene glycol as a very important functional group

1)Poly (ethylene glycol)

Polyethylene glycol (PEG), is a linear polymer consisting of repeated units of CH_2-CH_2-O. Depending on the molecular weight the same molecular structure is also termed poly (ethylene oxide) or polyoxyethylene, PEO or POE, respectively. The polymer is well soluble in a number of organic polar and apolar solvents. In water the PEG is heavily hydrated, forming random coils with diameters much larger than proteins of comparable molecular weight. Due to its simple structure and chemical stability, it is a prototype of an inert and biocompatible polymer. The inertness and nontoxic properties of PEG give rise to a number of applications in medicine, chemistry or biotechnology: PEG is used for nonionic surfactants and as additive in cosmetics, pharmaceuticals and food. When bound to surfaces [38], PEG repels other molecules by steric effects. The incoming molecules are not attracted by electrostatic force and cannot penetrate the hydrated PEG layer. This results in inert hydrophilic surfaces with less “stickyness”. PEG-modified proteins [39] or drugs show increased water solubility and decreased immunogenicity in organisms as the antibodies bind much less to the drug or protein, resulting in an increased half-life in the blood stream. PEG-modified nanoparticles are more stable at high salt concentrations and in biological environments. They show less nonspecific binding to proteins and cells. [40-46] The modification of other molecules with PEG is often called “PEGylation”. For proteins, PEG is coupled to some amino acids, most commonly lysine and cysteine.

2)Biomolecules

Bioconjugation of colloidal nanoparticles is the “natural” extension of the described concepts of chemical functionalization with biomolecules. Nature offers a large variety of organic molecules of different composition, size and complexity that serve to provide structure and function to biological process and organisms. Examples include on the one hand small molecules like lipids, vitamins, peptides, sugars and larger ones such as natural polymers including proteins, enzymes, DNA and RNA. Conjugation of inorganic nanoparticles to biomolecules generates hybrid materials that can be used to let the nanoparticles interact specifically with biological systems. On the other hand, biomolecules can be seen as ordinary, though sometimes complex, molecules or polymers that can be exploited for the functionalization or spatial assembly of nanoparticles. Nanoparticle-biomolecule conjugates bring together the unique properties and functionality of both materials and more specifically the ability of biomolecules for highly specific binding by molecular recognition.

3) Polysaccharides

Among the wide number of polysaccharides available as potential candidates for biopolymer engineering, glycosaminoglycans (GAGs) belonging to the family of b (1–4)-linked linear polysaccharides, appear among the most promising ones. In particular, chitosan, composed of 2-amino-2-deoxy-d-glucose ($GlcNH_2$) residues with a variable number of randomly located N-acetyl-glucosamine groups (GlcNAc), revealed neither pathological inflammatory response in implantation models nor evidence of induced infection or presence of endotoxins and a low, if any, incidence on immunological reactions [47]. Recently chitosan and chitosan-based materials have been tested as biomaterials mimicking the cartilage matrix for a potential application in the repair of articular cartilage [48, 49]. The most interesting feature of chitosan as biomaterial is related to the presence of amino groups deriving from glucosamine units. The physico-chemical and biological properties of the polycation can be drastically modified exploiting the reactivity of glucosamine residues. Examples include acylation [50, 51], alkylation [52, 53] carboxymethylation [54] and quaternarization [55] of chitosan.

4)Proteins

Proteins are made up by a sequence of 20 different standard amino acids which are linked together by amide bonds and which possess different side chains residues. Naturally, each peptide or protein has one carboxylic and one primary amino group at its ends, while the amino acid side chains introduce additional functional groups or other properties depending on their molecular structure. The amino acid sequence determines the unique properties of each of a large number of possible structures, i.e. 20^n for a sequence of n amino acids, in terms of charge, polarity and hydrophobicity. These in turn determine the protein folding and thus its secondary and tertiary structures and that ultimately results in the functional biomolecule. In many cases, the specific function of a protein (enzyme, antibody...) is determined by its geometry and the physicochemical properties of the outer surface, given by the folded amino acid sequence. Often the inside of a protein is hydrophobic whereas hydrophilic amino acid side chains tend to point outwards into solution. Cysteine residues, even if far apart in the sequence, can come spatially close to each other in folded proteins and form stabilizing disulfide bonds. The thiol group of a terminal cystein residue can also be exploited as anchor group for the grafting of a peptide to the surface of nanoparticles.

5)Aptamer

Deoxyribonucleic acid (DNA) is a linear polymer containing the genetic information of organisms in form of the sequence of the four oligonucleotides being the monomeric building blocks. Besides its biological function, DNA can be employed as generic polymeric molecules of which the most prominent feature, duplex formation with a strand of complementary sequence, presents a very specific mechanism of molecular recognition. As this mechanism depends on the simple linear sequence of nucleotides, DNA can be used as “programmable” object with a very large number of possible sequences and conformations, and exploited as building block and structural element for the assembly of artificial structures, as it will be discussed later. Synthetic DNA oligomers of arbitrary sequences and with a large variety of functional end groups, which are commercially available, can be conveniently attached in aqueous solution to gold nanoparticles Aptamers are oligonucleotide or peptide molecules that bind to a specific target molecule by a S-Au bond, in the same way as for other ligand molecules [56-59]. Aptamers are usually created by selecting them from a large random sequence pool, but natural aptamers also exist in mRNA. Aptamers are usually added in quite large excess to the gold particles and they spontaneously bind to the nanocrystal surface

b) Biodetection by gold nanoparticles

1)Colorimetric fast detection

The functionalized nanoparticles surface could recognize specific targets inducing the nanoparticle aggregation and changing the solution color. J. Spadavecchia et al demonstrated that gold PEGylated nanoparticles conjugated with Galectin-1 protein can detect glucose through colorimetric modification [60]. Galectins (Gal) are a family of dimeric lectins, composed by two galactoside-binding sites implicated in the regulation of cancer progression and immune responses. In this study, the synthesis and the physical-chemical characterization of such nanoparticles (Gal-1-PEG-AuNPs) was performed and their ability to detect glucose in an aqueous solution was demonstrated in a wide concentration range varying from 100 pM up to 10 mM.

2)SERS detection

In Surface Enhanced Raman Scattering (SERS) [61], inelastic Raman scattering of light by molecules in close proximity to a metal nanoparticle surface can be greatly enhanced by several orders of magnitude through the excitation of surface plasmon. This effect can be used for the detection of biomolecules and the studies of interaction between nanoparticles and their environment.

c) Application of bioimaging and cancer photothermal therapy

Many cancer cells are covered with epidermal growth factor receptor (EFGR). So, the EFGR provides a new therapeutic target for cancer, meanwhile healthy cells will not clearly show this protein. [63] The combination of gold nanoparticles with anti-EFGR can be used to image cancer cells under dark field optical microscopy. For the commonly used spherical gold nanoparticles, the strong absorption of visible light makes the light energy can be converted into heat energy. Then the use of spherical gold nanoparticles assisted by laser thermal method can achieve selective destruction of cancer cells. Compared with normal cells, only half of the laser energy is needed to kill cancer cells and it does not damage benign cells. For the treatment or diagnosis of skin cancer, spherical gold nanoparticles are a good choice. However, because visible light does not easily penetrate biological tissues, spherical gold nanoparticles are powerless for the treatment or diagnosis of cancer in subcutaneous tissue

Gold nanorod particles with a suitable ratio are a good choice because of their strong ability to absorb and scatter light in the near infrared region (800-1200nm).

The application of gold nanorods have then attracted attention as a new marker material and a new contrast agent in cell imaging and photothermal therapy for the treatment of cancer. Indeed, their longitudinal plasmon resonance can be easily tuned in the near-infrared and thus in the optical range where the light can penetrate deeply in the tissues. In addition, gold nanoparticles can easily generate heat by near-infrared light absorption close to their plasmon resonance, so they have special advantages in the photothermal treatment of tumors.

When gold nanorods are injected [64] into mice, they flowed through blood vessels and two-photon imaging technology (TPL) can be used to obtain in-situ images of blood vessel

structures through the skin (See Figure.1.7). The recorded image is much brighter than for traditional fluorescent dyes (A single gold nanorod is 58 times brighter than a single rhodamine 6G molecule).

The nanoparticles can be modified with specific recognition elements as antibodies [64], and poly (sodium styrene sulfonate) (PSS) to prepare bioprobes. Subsequently, the gold nanorods modified with antibodies can specifically recognize the cancer cells overexpressing EGFR to label the cancer cells that can then be imaged by TPL. The results showed that using gold nanorods, the TPL imaging can penetrate down to 75μm into biological tissues. Under the same conditions, the image brightness is 3 times higher than two-photon auto fluorescence imaging (Figure 1.7).

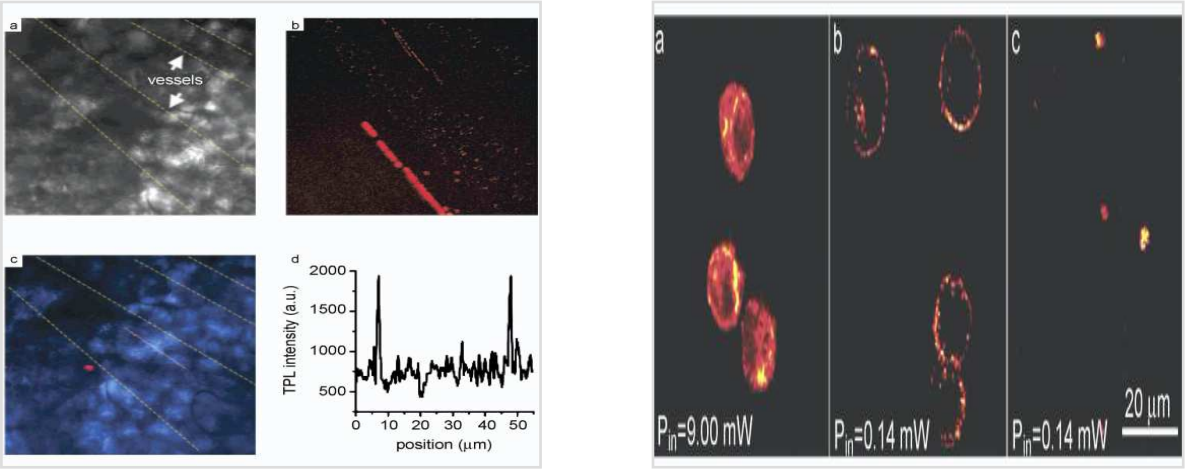

Figure 1.7 In vivo imaging of single gold nanorods in mouse ear blood vessels: (a) Transmission image with the two blood vessels indicated; (b) TPL image of gold nanorods flowing through the blood vessels; (c) Overlay of the transmission image and a single frame TPL image ;(d) TPL intensity profile from the linescan in c [62] Figure 1.7 Two photon images of cancer cells placed on a coverslip from a cell suspension: (a)Two photon autofluorescence image of unlabeled cells ;(b) TPL image of gold nanorods to label cells;(c)TPL image of no specifically labelled cells [62]

The dual role of diagnosis (imaging) and photothermal therapy. El Sayed et al. [65] reported that oligopeptide-labeled gold nanorods were used for nuclear labeling. Under a dark field optical microscope, cancer cells can be clearly distinguished from normal cells and 800nm laser irradiation can be selected. Cancer cells have been clearly killed (See Figure 1.8).

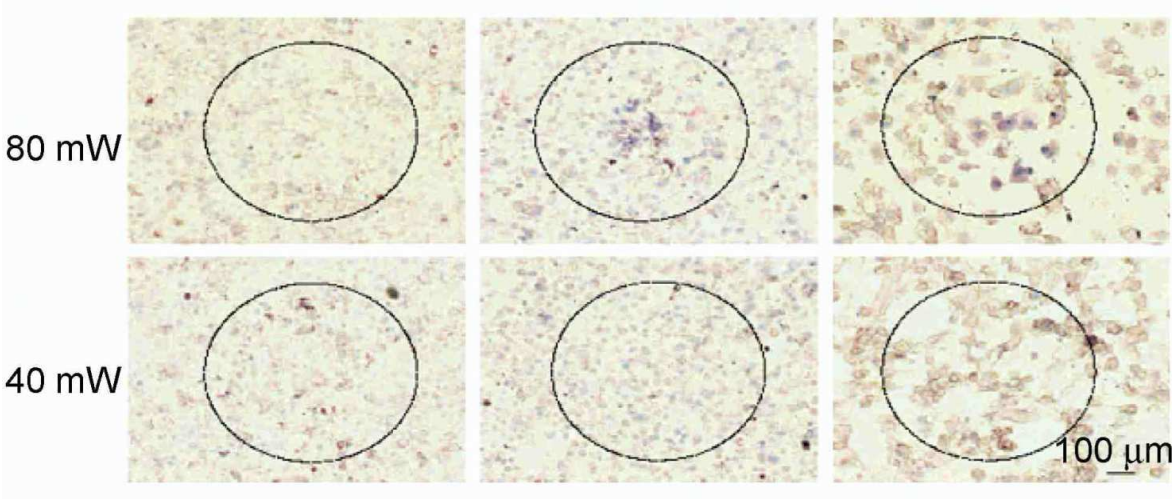

Figure 1.8 Selective photothermal therapy of cancer cells with anti-EGFR-Au nanorods incubate [67]

From all these results, gold particles are easy to prepare, and have special surface plasmon resonance characteristics that are continuously adjustable from the visible to near-infrared range. Gold particles are used as biomarkers and in biological detection, bioimaging, disease treatment, and information storage and other fields with broad application prospects. Although research in this area has just begun, it has achieved encouraging research results that have aroused widespread concern.

1.2 Nanovectors

In the fight against cancers, chemotherapy is along with radiotherapy and surgery, a weapon of actual choice. However, common anticancer molecules (such as alkylating agents, antimetabolites, plant alkaloids, topoisomerase inhibitors and antitumor antibiotics) have weak points due to their systemic administration:

The concentration of drugs through oral or injection administration within a short period of time in the body largely exceeds the actual need. Due to a lack of selectivity into the human body, fast metabolism and short half-life, the drug concentration quickly decreases in the body affecting their efficiency. Very large doses and excessive drug concentration are then required enhancing their side effects. Biomacromolecule drugs are easily degraded or inactivated by enzymes in the body. Their biological half-life is short, requiring repeated administration. Their diffusion in the body is also limited by the immune system or their penetration through biological barriers as cell membranes. The bioavailability of macromolecular drugs is low.

In recent years, the therapeutic arsenal has been enriched with more targeted therapies such as signal transduction modifiers (Gleevec®), enzyme inhibitors (Iressa® and Tarceva®), humanized antibodies (Avastin® and Cetuximab®), cell therapy or gene therapy. Even though the molecules in question are promising and exhibit more specificity for the tumor site, they still exhibit systemic toxicity, and the plasticity and genetic instability of tumors have been shown to be a limiting factor for this type of targeted therapy [66]. In addition, many tumors develop multi drug resistance, a phenomenon called MDR (or multidrug resistance) [67-69].

Faced with these problems, research has turned towards another strategy: the vectorization of well-known anti-cancer agents. Associating a molecule with a vector makes it possible to modify its pharmacokinetics and biodistribution. The desired aim is to promote the concentration of the active principle in the pathological tissue, to potentiate its local action, while reducing systemic toxicity. The vectorization strategy involves the association of a molecule with an object of nanometric dimensions (macromolecule or nano-object).

As the nanomaterials have a very small size and a very large surface area, the drug can be loaded onto their surface with high density, forming a high local concentration, and improving the utilization rate of the drug. In addition, the drug nanocarriers have the advantages of low toxicity, high efficiency, slow release, long-term effect and better drug stability. Moreover, they can recognize mutant cells, are non-toxic after drug release, will not accumulate in the body for a long time and have little side effects. They also have a stronger targeting release capability as bioreceptor can also be loaded at the nanocarrier surface. Therefore, nanocarrier is an emerging drug delivery technology with great development potential.

The formulation of nanovectors is therefore a key element in controlling the fate of the drugs in the body. The drugs enter in the human body through vectorization and is released on site, exerting a better drug treatment efficiency. The key to drug carrier technology is the choice of carrier material. At present, various polymer materials and inorganic materials have been used for carrier drug research, but the choice of materials must meet the requirements of tissue, blood, immunity and biocompatibility. In addition, the preparation of drug carriers is also very important because it will determine their biocompatibility and affects the efficiency of drugs delivery.

1.2.1 Delivery of anticancer drugs: targeting and delivery strategies

a) Passive and active targeting

The main objective of vectorization is to promote the accumulation of the anticancer drugs in the tumor. The injection or implantation directly into the tumor site allows to deliver the drug locally and thus avoiding the crossing of many biological barriers, but it is an invasive technique. Systematic administration also leads to passive accumulation of nanovectors in the tumor environment, through a phenomenon known as the "EPR effect", for "Enhanced Permeation and Retention" [70–72]. In fact, neoangiogenesis in tumors is imperfect, with new larger vessels than healthy ones, 200 nm on average and up to 700 nm, instead of 70 nm. The extravasation and accumulation of nanovectors (from 20 to 200 nm) in the interstitial spaces are therefore facilitated. In addition, lymphatic vessels are absent or non-functional within a tumor, which contributes to inefficient lymphatic drainage. Thus, nanovectors are not driven out of the tumor environment. It is this EPR effect that has been successfully exploited for the first generation of nanovectors, such as Doxil® [73]. However, passive targeting remains insufficient, a significant part of the anticancer drugs being distributed in the whole body and specifically at the tumor. This is why most of the recently developed nanovectors add to the formulation a biochemical and / or physical active targeting strategy. For biochemical targeting, it involves the decoration of the vectors with a bioreceptor allowing better recognition of the targeted tumor, in particular ligands specific to some receptors overexpressed at the surface of the tumor cells [66,69,72].These ligands can help to target the tumor cells, but also facilitate the entry of

nanovectors into these cells. The best-known example is the use of folic acid as its cellular receptor being overexpressed in many types of cancer [74].

b) Doxorubicin, an ideal candidate for vectorization in gold nanoparticles

Doxorubicin (DOX) is an anthracycline (a family of antibiotics). It is used to treat a wide variety of cancers, including leukemia, ovarian cancers, liver cancers and particularly advanced breast cancers [75]. My thesis is focused on this anticancer agent.

The DOX molecule (figure 1.8) is made of one aglycon nucleus and one sugar. The aglycon ring is a tetracyclic structure, with quinone and hydroquinone groups on rings B and C, a C4 methoxy substituent on ring D, and a short chain with a carbonyl on C9. Amino sugar or daunosamine (3-amino-2, 3, 6-trideoxy-L-fucosyl) is attached to ring A (C7) by a glycosidic bond [76]. The sugar part is hydrophilic whereas the anthraquinone nucleus is rather lipophilic, depending on the protonation state of the phenolic groups. Indeed, the molecule has ionizable functions (two phenolic groups on the B ring in position C11 and C6 with a pKa of 9.5 and 10.2 respectively, and an amine group on the sugar with a pKa of 8.3) [76]. The protonation of the amine group on the sugar improves its water solubility compared to the molecular form: doxorubicin hydrochloride is often used for this reason. The consequence of the charge bearing and the structure of the molecule is its ease to bind with proteins and cell membranes. Another consequence is that it can be used in both hydrophilic and lipophilic materials, and its affinity for such materials is highly dependent on pH conditions [77]. Doxorubicin is a popular research object: its anthracycline nucleus is responsible for its optical properties, and for the intrinsic fluorescence of the molecule. This molecule can therefore be easily assayed by UV-visible spectrophotometry. The distribution of DOX can also be visualized in tissues or cells, using fluorescence imaging [76]. Nevertheless, interpretations should be made with caution, as the intensity and fluorescence spectra of DOX strongly depend on its concentration and the nature of its microenvironment. In addition, the attachment of DOX to nanovectors via the anthracycline part quenches its fluorescence and may decrease its therapeutic properties. It is therefore often the sugar part that is used to graft it to the nanovectors.

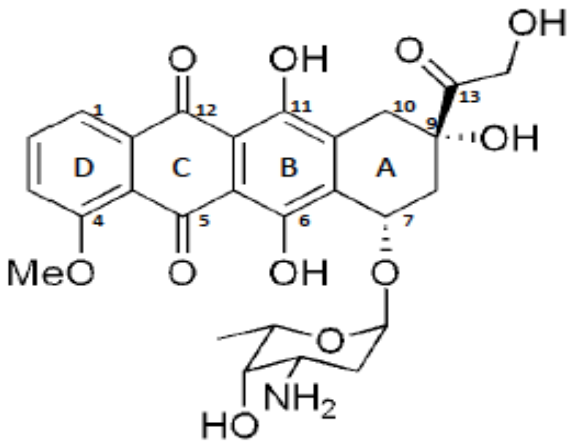

Figure1.8 Chemical structure of Doxorubicin

Although significant research efforts were made in this direction, few vectors have led to clinical trials, and only a handful has been approved for clinical use in humans. Doxorubicin is one of the few vector molecules available on the market, with Myocet, a formulation based on

liposomes (Enzon®®Pharmaceuticals, Piscataway, New Jersey), and Doxil/Caelyx, which are liposomes PEGylated (Centocor Ortho Biotech, Horsham, Pennsylvania, and Shering-Plow, North Ryde, New South Wales, Australia, respectively) [77]. These systems make it possible to passively target tumors by EPR effect [70]. Liposomal doxorubicin is efficient [78], but is generally used as a second-line treatment in case of relapse [79]. The side effects are certainly reduced, but not completely eliminated, in particular because of the persistence of a non-specific accumulation [76]. In addition to cardiotoxicity, there are persistent problems with palmar-plantar erythrodysesthesia (hand-foot syndrome). Faced with this observation, strategies consist in combining the liposomal formulations of DOX with other chemotherapies (combination with gemcitabine [80], carboplatin [81] or ifosfamide [82]), to reduce the quantities of injected drug, as proposed in several recent phase II clinical trials. Other approaches explore the modification of these liposomes with specific ligands, to increase the specificity of capture by tumor cells: for instance, ligand for the integrin receptor [83], ligand for the folate receptor [84], and all the different receptors specific to some specific cell lines [85, 86], and among them antibodies and peptides, such as the anti αv integrin antibody [87] and the peptide HVGGSSV [86]. Another strategy is the transfection of small interfering RNAs (siRNAs) to overcome resistance phenomena and to suppress the expression of efflux pumps [83]. In this context, the development of vectors other than liposomes for the delivery of DOX is needed. Hybrid gold nanoparticles provide an ideal platform for constructing such nano-objects.

c) Different generations of nanovectors

There are three generations of nanovectors schematically presented in Figure.1.9

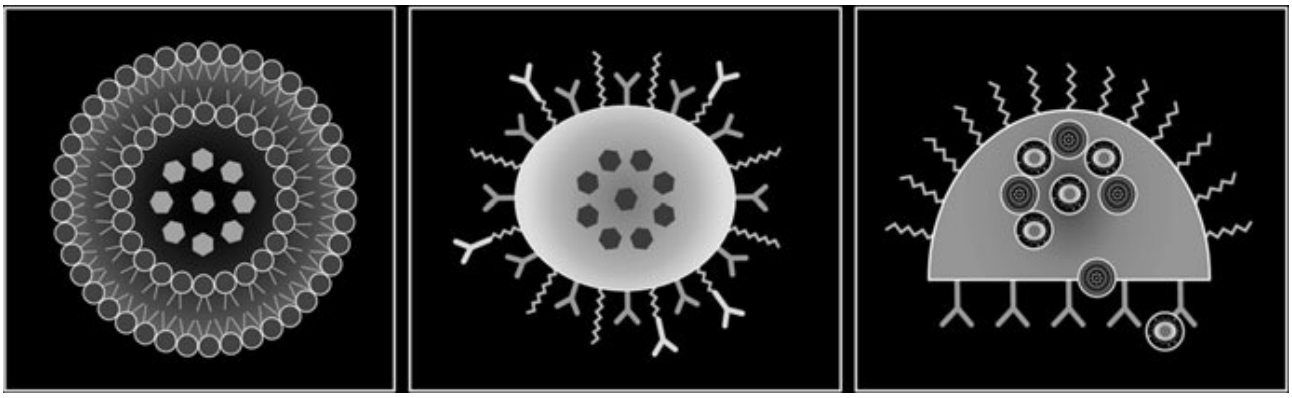

A **B** **C**

Figure. 1.9 Schematic presentation of three generations of nanovectors. A) First-generation of nanovectors: liposomes, including a container (double phospholipid bilayer membrane) and an active principle (dots) inserted inside the container. They target the tumor by EPR effect; B) Second-generation of nanovectors: they possess the ability to target their therapeutic action via antibodies and other biomolecules; they also propose remote activation, or responsiveness to environment; C)Third-generation nanovectors such as multistage agents are capable of more complex functions, such as time-controlled deployment of multiple active nanoparticles across various biological barriers and with different subcellular targets. [87]

1) The first generation of nanovectors target the tumor through passive mechanisms.

These products include liposomal drugs and polymer–drug conjugates [88], polymeric micelles [89], and dendrimers [90]. They are relatively simple but generally lack of an active targeting or controlled drug release components. Some surface modifications as the attachment of a PEG are frequently seen in this subclass. This modification produces nanovectors with substantially prolonged circulation time and, as a result, more likely passive tumor homing [91, 92]. Nanoparticles extravasate through the leaky vasculature and preferentially accumulate through the EPR effect. In this case of "passive targeting", the drugs may be released in the extracellular matrix and diffuse throughout the tissue for bioactivity. Some of these nanoparticles might also be taken up nonspecifically.

2) The second generation of nanovectors is hybrid systems with additional advanced functionalities

Such as the attachment of recognition elements on the nanovector surface specific to the targeted disease or a possibility for active/triggered release of the payload at the disease location through the use of physical remote energy [92, 93]. This category generally presents a progressive evolution of the first generation of nanovectors with emerging degrees of sophistication. Liposomes and other antibody targeted nanoparticles have been the most investigated example of the second generation [94,]. A variety of other targeting moieties besides antibodies are under extensive investigation worldwide, including ligands, aptamers, small peptides, and phage-display peptides binding to specific target cell surface markers or surface markers expressed in the disease microenvironment [101]. Examples of other nanocarriers in the first and second generations include metal nanoparticles for use in diagnostics and therapy [95, 96], albumin-bound paclitaxel nanoparticles approved for use in metastatic breast cancer [97], drug–polymer construct dendrimers, and polymeric micelles [98].

3)The third generation of nanovectors includes therapeutic and diagnostic multicomponents and multifunctional constructs with logic-embedded functions.

These systems aim at overcoming a variety of obstacles in order to efficiently reach their target, representing a paradigm shift when compared to the previous two generations of nanovectors [99]. The third-generation multicomponent carriers comprise a number of nanoengineered components with the advantage of decoupling functions such as biorecognition, cytotoxicity, and bio-barrier avoidance to separate nanocomponents acting in a synergistic pre-programmable and sequential manner, encoded in the properties of the material.

d) Interaction of nanoparticles with biological media

It is important to understand the interaction mechanisms involved when nanoparticles are placed in biological media. This is an even more important point for nanomedicine research. Understanding these interactions can help us to understand not only their cellular internalization, but also their biodistribution within the body and therefore to estimate their possible therapy efficiency or toxicity. In general, nanoparticles enter in the cells through different internalization mechanisms. Figure 6.1 shows the different internalization pathway to enter in the organisms and in the cells [100]. The small size of nanoparticles allows them to enter in the human body by inhalation, ingestion, or through the skin contact. Once they are in the extracellular fluid, they will be conjugated with biomolecules presented in the media, which allows them to internalize in the cells.

1.2.2 Cellular Internalization

Nanomedicines are totally based on nanoparticles which must cross the cell membranes by different mechanisms. The plasma membrane is a dynamic structure allowing the separation between the intracellular medium (the cytoplasm) and the extracellular environment, while regulating the entry and exit of molecules. The small molecules essential for cell survival (amino acids, sugars and ions) can enter the cell simply by crossing the plasma membrane via pumps or protein channels anchored in the membrane.

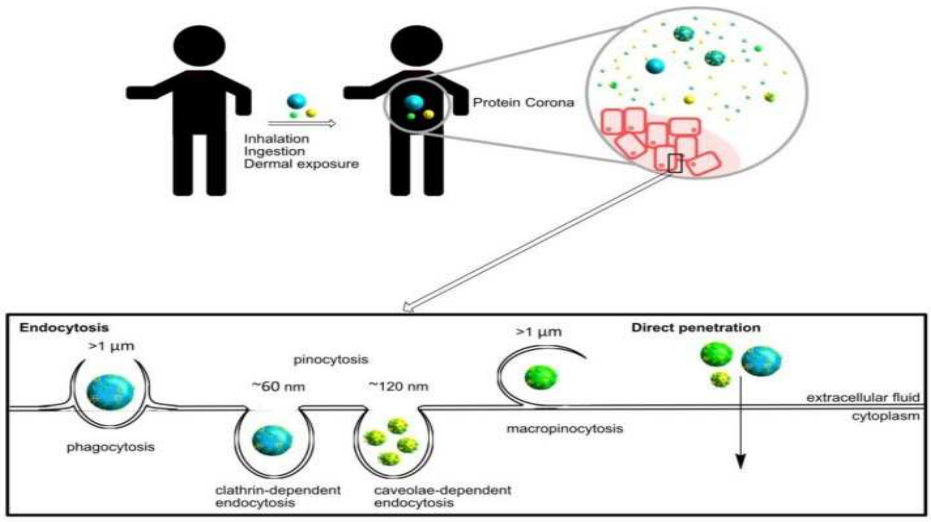

Figure 2.0 Schematic representation of internalization pathways for nanoparticles (NPs) in the human body and in the cells.[101]

In general, the different mechanisms include 6 ways for internalization:

a) the phagocytosis is an endocytosis mechanism mainly used by immune cells (macrophages, neutrophils and dendritic cells). It constitutes a defense system against foreign organisms and eliminates cell dead by apoptosis
b) the micropinocytosis is characterized by the formation of very small vesicles (60-120 nm) which are called micropinosomes [101]. Internalization by this route is only possible through the presence of growth factors or mitogenic agents.

c) The macropinocytosis is characterized by the formation of very large vesicles (up to 5 µm) which are called macropinosomes [101]. Internalization by this route is only possible through the presence of growth factors or mitogenic agents.

d) The clathrin-dependent endocytosis is characterized by the formation of vesicles from 60 to 120 nm [102], covered with a protein membrane composed mainly of clathrines. This internalization path is only possible by activation of membrane receptors through specific ligands such as immunoglobulins, transferrin, insulin, LDL or even EGF.

e) The caveolae-dependent endocytosis causes the formation of small vesicles in the cell. It is a process used by the cell to transport molecules, but the mechanisms that control this path are still poorly understood.

f) The direct penetration occurs for very small nanoparticles. The penetration doesn't need any force process.
The nanoparticles (NPs) size directly affects the internalization process. In fact, nanoparticles in the range of 10–100 nm achieve higher cellular uptake but the smaller ones imply a higher energy cost to the cells [103]. Usually, NPs larger than 100 nm are internalized by specialized phagocytic cells (such as macrophages or dendritic cells) which allows targeted design. Furthermore, the optimal size for internalization inside the cells is strongly linked to the NPs surface chemistry. In general, Van der Waals or electrostatic forces are critical in the NP interactions with biomolecules and cells. In fact, several studies show correlation between zeta potential and endocytosis/exocytosis mechanisms [104]. Then, specific cellular internalization mechanisms could be targeted to favor specific interactions (i.e., employing affinity ligands) as opposed to nonspecific interactions (i.e., hydrophobic). In this sense, antibody-coated NPs present an internalization potential in targeted cells four to eight times higher than positively or negatively charged NPs without the affinity component [104]. Besides the use of antibodies for targeting delivery, non-specific interactions through chemical elements are always present and influence target affinities, which must be always taken into consideration.
Protein adsorption also depends on the NP shape and, consequently, affects the cellular uptake. It seems that spherical and highly homogeneous NP conjugates have better cellular uptake than amorphous and non-geometrically symmetric nanoconjugates. Moreover, several authors claim that shape could be employed to prevent non-specific cellular internalization in the targeted cells.
In view of the bibliographic data, it is important to not only study the physicochemical properties of nanoparticles and their interaction with the proteins, but also study the efficiency of nanovectors in vivo for the cancer therapy efficiency. Thus, it's crucial to have a deep investigation in vivo experiments and to understand the interaction between protein and nanoparticles as it will be presented in the two following chapters devoted to the specific biomarker's detection and to the study of in vivo efficiency of a nanovector.

1.3 Bibliographic references

1 Mahato, K., Nagpal, S., Shah, M.A. *et al.* Gold nanoparticle surface engineering strategies and their applications in biomedicine and diagnostics. *3 Biotech* **9,** 57 (2019).

2 Radosavljevic G, Volarevic V, Jovanovic I, Milovanovic M, Pejnovic N, Arsenijevic N, Hsu DK, Lukic ML (April 2012). "The roles of Galectin-3 in autoimmunity and tumor progression". Immunologic Research. **52** (1–2): 100–10.

3 Reticker-Flynn NE, Malta DF, Winslow MM, Lamar JM, Xu MJ, Underhill GH, Hynes RO, Jacks TE, Bhatia SN (2012). Nature Communications.

4 Zadegan, Reza M.; Norton, Michael L. (June 2012). Int. J. Mol. Sci. 13 (6): 7149–7162.

5 Beaumont, Steven P. (September 1996). "III–V Nanoelectronics". Microelectronic Engineering. 32 (1): 283–295.

6 Buzea, Cristina; Pacheco, Ivan; Robbie, Kevin (2007). "Nanomaterials and Nanoparticles: Sources and Toxicity". Biointerphases. 2 (4): MR17–MR71.

7 Hubler, A.; Osuagwu, O. (2010). "Digital quantum batteries: Energy and information storage in nanovacuum tube arrays". Complexity: NA.

8 Portela, Carlos M.; Vidyasagar, A.; Krödel, Sebastian; Weissenbach, Tamara; Yee, Daryl W.; Greer, Julia R.; Kochmann, Dennis M. Proceedings of the National Academy of Sciences. 117 (11): 5686–5693.

9 Eldridge, T. (8 January 2014). "Achieving industry integration with nanomaterials through financial markets". Nanotechnology_Now.

10 Langer, Robert (2010). "Nanotechnology in Drug Delivery and Tissue Engineering: From Discovery to Applications". Nano Lett. 10 (9): 3223–30.

11 Kingshott, Peter. "Electrospun nanofibers as dressings for chronic wound care" (PDF). Materials Views. Macromolecular Bioscience.

12 Xiang, Dong-xi; Qian Chen; Lin Pang; Cong-long Zheng (17 September 2011). "Inhibitory effects of silver nanoparticles on H1N1 influenza A virus in vitro". Journal of Virological Methods. 178 (1–2): 137–142.

13 Wagner V, Dullaart A, Bock AK, Zweck A (October 2006). "The emerging nanomedicine landscape". Nature Biotechnology. 24 (10): 1211–7.

14 Freitas RA (March 2005). "What is nanomedicine?"(PDF). Nanomedicine. 1 (1): 2–9.

15 Daniel, M.-C. and D. Astruc, Gold Nanoparticles: Assembly, Supramolecular Che- mistry, Quantum-Size-Related Properties, and Applications toward Biology, Cata- lysis, and Nanotechnology. Chemical Reviews, 2004. 104(1): p. 293-346.

16 Thakor, A.S., et al., Gold nanoparticles: a revival in precious metal administration to patients. Nano Lett, 2011. 11(10): p. 4029-36.

17 Kim, J.H., et al., Anti-glycation effect of gold nanoparticles on collagen. Biol Pharm Bull, 2012. 35(2)

18 Khan S., Alam F., Azam A., Khan A.U. Gold nanoparticles enhance methylene blue-induced photodynamic therapy: A novel therapeutic approach to inhibit Candida albicans biofilm. Internat. J. Nanomed. 2012; 7:3245.

19 Khan M.S., Vishakante G.D., Siddaramaiah H. Gold nanoparticles: A paradigm shift in biomedical applications. Adv. Colloid Interface Sci. 2013 ; 1:44–58.

20 Beltrame, P; Comotti, M; Della Pina, C; Rossi, M: Appl. Catal. A-Gen. 297 (2006) 1-

21 WangCG, ChenY, WangTT, etal. Chem. Mater.,2007,19: 5809 —5811

22 WangCG, ChenY, WangTT, etal. Adv. Funct.Mater.,2008, 18: 355 —361

23 KreibigU,VollmerM.OpticalPropertiesofMetalClusters.Berlin: Springer2Verlag , 1995

24 Fraday., M. Philos. Trans.,1857, 147, 145.25. Frens.G., Nature Phys. Sci.. Zhao P., Li N., Astruc D. State of the art in gold nanoparticle synthesis. Coord. Chem. Rev. 2013; 257: 638–665.

25 Khan S., Alam F., Azam A., Khan A.U. Gold nanoparticles enhance methylene blue-induced photodynamic therapy: A novel therapeutic approach to inhibit Candida albicans biofilm. Internat. J. Nanomed. 2012 ;7:3245.

26 Pelaz B, Charron G, Pfeiffer C, Zhao YL, de la Fuente JM, Liang XJ, Parak WJ, del Pino P. 2013. Interfacing engineered nanoparticles with biological systems: anticipating adverse nano-bio interactions. Small 9, 1573–1584.

27 Peng ZG, Hidajat K, Uddin MS. 2004. Adsorption of bovine serum albumin on nanosized magnetic particles. J. Colloid Interface Sci. 271, 277–283.

28 Sperling. R.A, Rivera Gil. P, Zhang. F, Zanella. M and Parack. W. J., Chem. Soc. Rev.,2008, 37, 1896-1908.

29 Haruta. M, Tsubota. S, Kobashi.T, Kageyama. H, Genet M. J and Delmon. B.; J. Ctal., 1993, 144, 175.

30 Lim. S. H, Phonthammachai. N, Zhong. Z, Teo. J. and White. T. J., Langmuir, 2009, 25, 9480-9486.

31 Ueda. A, Oshima. T and Haruta. M., Applied Catlysis B: Environmental,1997, 12, 81-93. Nguyen. L. Q, Salim. C. and Hinode. H., Applied Catalysis A: General, 2008, 347, 94- 99.

32 Bernadette M. Quinn, Peter Liljeroth, Virginia Ruiz, Timo Laaksonen, and JAmChem-Soc,2003,125(22):6644

33 Baptista. P, Pereira. E, Eaton. P, Doria. G, Miranda. A, Gomes. I, Quaresma. P and Franco. R., Anal. Bioanal. Chem.,2008, 391, 943-950.

34 Cail. W, Gao. T, Hong. H and Sun. J., Nanotechnol. Sci. Appl., 2008, 1, 17-32.

35 Molinaro G, Leroux J, Damas J, Adam A. Biocompatibility of thermosensitive chitosan-based hydrogels: an in vivo experimental approach to injectable biomaterials. Biomaterials 2002;23: 2717–22.

36 Madihally SV, Matthew HWT. Porous chitosan scaffolds for tissue engineering. Biomaterials 1999;20:1133–42.

37 H. M. Zareie, C. Boyer, V. Bulmus, E. Nateghi, T. P. Davis: "Temperature-Responsive Self-Assembled Monolayers of Oligo(ethylene glycol): Control of Biomolecular Recognition", ACS Nano 2008, 2(4), 757-765.

38 F. M. Veronese: "Peptide and protein PEGylation: a review of problems and solutions", Biomaterials 2001, 22, 405 - 417. 41.W. Liu, M. Howarth, A. B. Greytak, Y. Zheng, D. G. Nocera, A. Y. Ting, M. G. Bawendi: "Compact Biocompatible Quantum Dots Functionalized for Cellular Imaging", J. Am. Chem. Soc. 2008, 130(4), 1274-1284.

39 R. Gref, M. Lück, P. Quellec, M. Marchand, E. Dellacherie, S. Harnisch, T. Blunk, R. H. Müller: "`Stealth' corona-core nanoparticles surface modified by polyethylene glycol (PEG): influences of the corona (PEG chain length and surface density) and of the core composition on phagocytic uptake and plasma protein adsorption", Colloids and Surfaces B 2000, 18(3-4), 301-313.

40 B. Ballou, B. C. Lagerholm, L. A. Ernst, M. P. Bruchez, A. S. Waggoner: "Noninvasive Imaging of Quantum Dots in Mice", Bioconjugate Chemistry 2004, 15(1), 79-86.

41 Y. L. Liu, M. K. Shipton, J. Ryan, E. D. Kaufman, S. Franzen, D. L. Feldheim: "Synthesis, stability, and cellular internalization of gold nanoparticles containing mixed peptide-poly(ethylene glycol) monolayers", Analytical Chemistry 2007, 79(6), 2221-2229.

42 L. van Vlerken, T. Vyas, M. Amiji: "Poly (ethylene glycol)-modified Nanocarriers for Tumor-targeted and Intracellular Delivery", Pharmaceutical Research 2007, 24(8), 1405.

43 H. Skaff, T. Emrick: "The use of 4-substituted pyridines to afford amphiphilic, pegylated cadmium selenide nanoparticles", Chemical Communications 2003, 2003(1), 52-53.

44 C. J. Fee, J. M. V. Alstine: "Prediction of the Viscosity Radius and the Size Exclusion Chromatography Behavior of PEGylated Proteins", Bioconjugate Chemistry 2004, 15(6), 1304-1313.

45 Buckmaster.R, Hanada. T, Kawazoe. Y, Cho. M-W, Yao. T, Urushihara. N and Yamamoto. A., Nano Lett.,2005, 5, 771-776.

46 Shen.H, Chen. B, Lu. G, Ning. T, Guan. D, Zhou. Y and Chen. Z., Nanotechnology, 2006, 17, 4274-4277.

47 Asoh.H, Arai.F and Ono.S., Electrochem. Commun.,2007, 9, 535-539.

48 Jolanda and al.Colloids and Surfaces B: Biointerfaces 185 (2020) 110588

49 WangH ,HuffTB, ZweifelDA,etal. Proc. Natl. Acad. Sci. USA, 2005, 102 : 15752 —15756

50 DurrNJ,LarsonT ,SmithDK,etal. NanoLett. ,2007,7:941— 945

51 JainPK, El2 SayedIH, El2Sayed MA. Nanotoday, 2007,1:18— 29

52 Godin B et al (2010) An integrated approach for the rational design of nanovectors for biomedical imaging and therapy. Adv Genet 69:31–64

53 Duncan R (2003) The dawning era of polymer therapeutics. Nat Rev Drug Discov 2(5):347–360

54 C. A. Mirkin, R. L. Letsinger, R. C. Mucic, J. J. Storhoff: "A DNA-Based Method For Rationally Assembling Nanoparticles Into Macroscopic Materials", Nature 1996, 382, 607-609.

55 L. M. Demers, C. A. Mirkin, R. C. Mucic, I. Robert A. Reynolds, R. L. Letsinger, R. Elghanian, G. Viswanadham: "A Fluorescence-Based Method for Determining the Surface Coverage and Hybridization Efficiency of Thiol-Capped Oligonucleotides Bound to Gold Thin Films and Nanoparticles", Analytical Chemistry 2000, 72(22), 5535-5541.

56 L. He, M. D. Musick, S. R. Nicewarner, F. G. Salinas, S. J. Benkovic, M. J. Natan, C. D. Keating: "Colloidal Au- Enhanced Surface Plasmon Resonance for Ultrasensitive Detection of DNA Hybridization", Journal of the American Chemical Society 2000, 122(38), 9071-9077.

57 R. Jin, G. Wu, Z. Li, C. A. Mirkin, G. C. Schatz: "What Controls the Melting Properties of DNA-Linked Gold Nanoparticle Assemblies?" Journal of the American Chemical Society 2003, 125(6), 1643-1654.

58 R. L. Letsinger, R. Elghanian, G. Viswanadham, C. A. Mirkin: "Use of a Steroid Cyclic Disulfide Anchor in Constructing Gold Nanoparticle-Oligonucleotide Conjugates", Bioconj. Chem. 2000, 11, 289-291.

59 Z. Li, R. Jin, C. A. Mirkin, R. L. Letsinger: "Multiple thiol-anchor capped DNA–gold nanoparticle conjugates", Nucleic Acids Research 2002, 30(7), 1558-1562.

60 Kubota N, Tatsumoto N, Sano T, Toya K. A simple preparation of half N-acetylated chitosan highly soluble in water and aqueous organic solvents. Carbohydr Res 2000; 324:268–74.

61 J. Kneipp, H. Kneipp, K. Kneipp: "SERS-a single-molecule and nanoscale tool for bioanalytics", Chemical Society Reviews 2008, 37(5), 1052-1060.

62 Sorlier P, Denuzie"re A, Viton C, Domard A. Relation between the degree of acetylation and the electrostatic properties of chitin and chitosan. Biomacromolecules 2001; 2:765–72.

63 Sashiwa H, Shigemasa Y. Chemical modification of chitin and chitosan 2: preparation and water soluble property of N-acylated or N-alkylated partially deacetylated chitins. Carbohydr Polym 1999; 39:127–38

64 Yang T-C, Chou C-C, Li C-F. Preparation, water solubility and rheological property of the N-alkylated mono or disaccharide chitosan derivatives. Food Res Int 2002; 35:707–13.

65 J. Klostergaard, C.E. Seeney, Magnetic nanovectors for drug delivery, Maturitas. 73 (2012) 33–44.

66 Z. Gao, L. Zhang, Y. Sun, Nanotechnology applied to overcome tumor drug resistance, Journal of Controlled Release. 162 (2012) 45–55.

67 C.-M.J. Hu, L. Zhang, Nanoparticle-based combination therapy toward overcoming drug resistance in cancer, Biochemical Pharmacology. 83 (2012) 1104–1111.

68 A. Shapira, Y.D. Livney, H.J. Broxterman, Y.G. Assaraf, Nanomedicine for targeted cancer therapy: Towards the overcoming of drug resistance, Drug Resist Update. 14 (2011) 150–163

69 F. Danhier, O. Feron, V. Préat, to exploit the tumor microenvironment: Passive and active tumor targeting of nanocarriers for anti-cancer drug delivery, Journal of Controlled Release. 148 (2010) 135–146.

70 S. Dufort, L. Sancey, J.-L. Coll, Physico-chemical parameters that govern nanoparticles fate also dictate rules for their molecular evolution, Adv. Drug Deliv. Rev. 64 (2012) 179–189.

71 H. Maeda, J. Wu, T. Sawa, Y. Matsumura, K. Hori, Tumor vascular permeability and the EPR effect in macromolecular therapeutics: a review, J Control Release. 65 (2000) 271–284.

72 Y. (Chezy) Barenholz, Doxil® — The first FDA-approved nano-drug: Lessons learned, J Control Release. 160 (2012) 117–134.

73 P. Mohan, N. Rapoport, Doxorubicin as a molecular nanotheranostic agent: effect of doxorubicin encapsulation in micelles or nanoemulsions on the ultrasound-mediated intracellular delivery and nuclear trafficking, Mol. Pharm. 7 (2010) 1959–1973.

74 T. Islam, L. Josephson, Current state and future applications of active targeting in malignancies using superparamagnetic iron oxide nanoparticles, Cancer Biomark. 5 (2009) 99–107.

75 L.M. Kaminskas, V.M. McLeod, B.D. Kelly, G. Sberna, B.J. Boyd, M. Williamson, et al., A comparison of changes to doxorubicin pharmacokinetics, antitumor activity, and toxicity mediated by PEGylated dendrimer and PEGylated liposome drug delivery systems, Nanomedicine: Nanotechnology, Biology and Medicine. 8 (2012) 103–111.

76 DOXIL_PI_Booklet.pdf, (n.d.).

77 M.R. Mirza, B. Lund, J.C. Lindegaard, N. Keldsen, A. Mellemgaard, R. dePont Christensen, et al., A phase II study of combination chemotherapy in early relapsed epithelial ovarian cancer using gemcitabine and pegylated liposomal doxorubicin, Gynecologic Oncology. 119 (2010) 26–31.

78 P. Power, G. Stuart, A. Oza, D. Provencher, J.R. Bentley, W.H. Miller Jr, et al., Efficacy of pegylated liposomal doxorubicin (PLD) plus carboplatin in ovarian cancer patients who recur within six to twelve months: A phase II study, Gynecologic Oncology. 114 (2009) 410–414.

79 F. Joly, E. Sevin, A. Lortholary, F. Priou, J.F. Paitel, M. Fabbro, et al., Association of pegylated liposomal doxorubicin and ifosfamide in early recurrent ovarian cancer patients: A Multicenter Phase II Trial, Gynecologic Oncology. 116 (2010) 312–316.

80 J. Jiang, S. Yang, J. Wang, L. Yang, Z. Xu, T. Yang, et al., Sequential treatment of drug-resistant tumors with RGD-modified liposomes containing siRNA or doxorubicin, European Journal of Pharmaceutics and Biopharmaceutics. 76 (2010) 170–178.

81 G.D. Bothun, A. Lelis, Y. Chen, K. Scully, L.E. Anderson, M.A. Stoner, Multicomponent folate-targeted magnetoliposomes: design, characterization, and cellular uptake, Nanomedicine: NBM. 7 (2011) 797–805. 85 R.E. Eliaz, S. Nir, C. Marty, F.C. Szoka Jr, Determination and modeling of kinetics of cancer cell killing by doxorubicin and doxorubicin encapsulated in targeted liposomes, Cancer Res. 64 (2004) 711–718.

82 A. Lowery, H. Onishko, D.E. Hallahan, Z. Han, Tumor-targeted delivery of liposome- encapsulated doxorubicin by use of a peptide that selectively binds to irradiated tumors, Journal of Controlled Release. 150 (2011) 117–124.

83 Muzzarelli RAA, Tanfani F, Emanuelli M, Mariotti S. N- (carboxymethylidene)chitosans and N-(carboxymethyl)chitosans: novel chelating polyampholytes obtained from chitosan glyoxy- late. Carbohydr Res 1982; 107:199–214.

84 Murata J, Ohya Y, Ouchi T. Possibility of application of quaternary chitosan having pendant galactose residues as gene delivery tool. Carbohydr Polym ,1996; 29:69–74.

85.Lee CC et al (2005) Designing dendrimers for biological applications. Nat Biotechnol 23(12):1517–1526

86 Torchilin VP (2005) Recent advances with liposomes as pharmaceutical carriers. Nat Rev Drug Discov 4(2):145–160

87 Harris JM, Chess RB (2003) Effect of pegylation on pharmaceuticals. Nat Rev Drug Discov 2(3):214–221

88 Park S, Jeong EJ, Lee J, et al. Preparation and characterization of nonaarginine-modified chitosan nanoparticles for siRNA delivery. Carbohydrate Polymers. 2013;92:57–62.

89 Duncan R (2006) Polymer conjugates as anticancer nanomedicines. Nat Rev Cancer 6(9):688–701

90 Brannon-Peppas L, Blanchette JO (2004) Nanoparticle and targeted systems for cancer therapy. Adv Drug Deliv Rev 56(11):1649–1659

91 Farokhzad OC, Langer R (2009) Impact of nanotechnology on drug delivery. ACS Nano16–2096. Brannon-Peppas L, Blanchette JO (2004) Nanoparticle and targeted systems for cancer therapy. Adv Drug Deliv Rev 56(11):1649–1659

92.Kale AA, Torchilin VP (2007) "Smart" drug carriers: PEGylated TATp-modified pH-sensitive liposomes. J Liposome Res 17(3–4):197–203

93.Hajitou A, Pasqualini R, Arap W (2006) Vascular targeting: recent advances and therapeutic perspectives. Trends Cardiovasc Med 16(3):80–88

94 Gindy ME, Prud'homme RK (2009) Multifunctional nanoparticles for imaging, delivery and targeting in cancer therapy. Expert Opin Drug Deliv 6(8):865–878

95 Latorre M, Rinaldi C (2009) Applications of magnetic nanoparticles in medicine: magnetic fluid hyperthermia. P R Health Sci J 28(3):227–238

96 Chuang VT, Kragh-Hansen U, Otagiri M (2002) Pharmaceutical strategies utilizing recombinant human serum albumin. Pharm Res 19(5):569–577

97 Ferrari M (2010) Frontiers in cancer nanomedicine: directing mass transport through biological barriers. Trends Biotechnol 28(4):181–188

98 Sakhrani, N.M. and H. Padh, Organelle targeting: third level of drug targeting. Drug Design, Development and Therapy, 2013. 7

99 Parkar, N.S., et al., Vesicle Formation and Endocytosis: Function, Machinery, Mechanisms, and Modeling. Antioxidants & Redox Signaling, 2009. 11(6)

100 Yameen B., Choi W.I., Vilos C., Swami A., Shi J., Farokhzad O.C. Insight into Nanoparticle Cellular Uptake and Intracellular Targeting. J. Control. Release. 2014; 190:485–499.

101 Hu G., Jiao B., Shi X., Valle R.P., Fan Q. Zuo Y.Y. Physicochemical Properties of Nanoparticles Regulate Translocation across Pulmonary Surfactant Monolayer and Formation of Lipoprotein Corona. ACS Nano. 2013;7: 10525–10533.

102 Shang L., Nienhaus K., Nienhaus G. Engineered Nanoparticles Interacting with Cells: Size Matters. J. Nanobiotechnol. 2014; 12:5

103 Zhao J., Stenzel M.H. Entry of Nanoparticles into Cells: The Importance of Nanoparticle Properties. Polym. Chem. 2018;9: 259–272

104 Wilhelm C., Billotey C., Roger J., Pons J.N., Bacri J., Gazeau F. Intracellular Uptake of Anionic Superparamagnetic Nanoparticles as a Function of Their Surface Coating. Biomaterials. 2003;24: 1001–1011.

Chapter 2

Development of a new hybrid nanoparticle synthesized by gold complexing for the detection of biomarkers

This chapter will be dedicated to the development of hybrid nanoparticles for the biomarker detections. The nanoparticle surface was first functionalized with Lactose-Modified Chitosan (CTL) to specifically interact with the biomarkers. The nanoparticles were first used in the detection of Galectin-1 protein and then in the colorimetric detection of glucose via its interaction with Galectin-1 protein.

2.1 Lactose-modified chitosan gold (III)-PEGylated complex –bioconjugates: from synthesis to interaction with targeted Galectin-1 protein

2.1.1 Chitosan

Chitosan (figure2.1) is a linear polysaccharide composed of randomly distributed β-(1→4)-linked glucosamine (deacetylated unit) N-acetyl-D-glucosamine (acetylated unit). It is produced by treating the chitin shells of shrimp and other crustaceans with an alkaline substance, such as the sodium hydroxide. The chitosan has a large number of commercial and biomedical uses. It can be used in agriculture as a seed treatment and biopesticide, helping plants to fight fungal infections. In winemaking, it can be used as a fining agent, also helping to prevent spoilage. In industry, it can be used in a self-healing polyurethane paint coating . In medicine, it is useful in bandages to reduce bleeding and as an antibacterial agent. It can also be used to help the drug delivery through the skin. Chitosan and derivatives have been explored in the development of nanomaterials, bio-adhesives, wound dressing materials[1,2], improved drug delivery systems[3], enteric coatings[4] and in medical devices[5,6]. Chitosan nanofiber membranes have a high degree of biocompatibility and may support new bone formation.

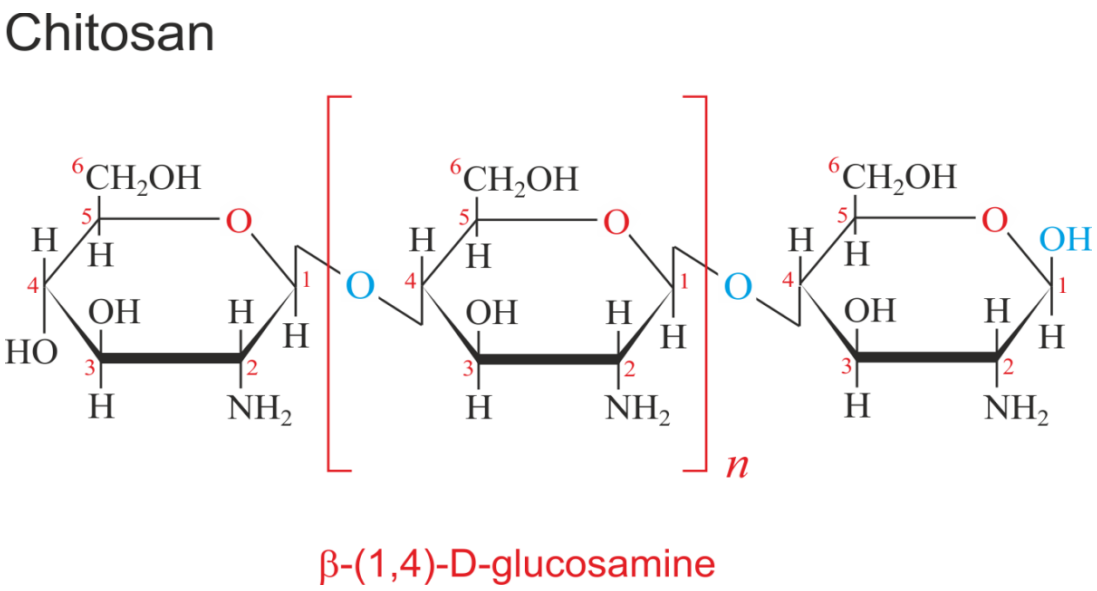

Figure 2.1 Chemical structure of chitosan

2.1.2 Lactose-Modified Chitosan

The Lactose-Modified Chitosan (CTL, Figure2.2) is a derivative of Chitosan with branched polysaccharide synthesized via reductive N-alkylation of primary amines by lactose moieties. CTL is a ternary heteropolysaccharide composed of β-1 → 4 linked glucosamine (D unit), N-acetyl-glucosamine (A unit), and N-Lactit-1-yl glucosamine (L unit) sugars. Firstly, proposed in 1982 by Yalpani [7,8], CTL has been reconsidered as a chemically modified chitosan able to show interesting biological and physico-chemical properties. Thus, the lactose residues grafted on the chitosan backbone give specific advantages with respect to the original polymer and most of the commercial chitosans. They have a higher solubility at neutral pH, a miscibility with polyanions to form soluble complexes without associative phase separation, and the possibility to form gels when it is mixed with boric acid that plays the role of cross linker under physiological conditions of pH and osmolarity. They represent interesting natural polymers for the development of biomaterials for tissue regeneration. In particular, CTL has shown to induce aggregation of articular chondrocytes [9] or to stimulate the production of collagen and glycosaminoglycans within an otherwise inert 3D architecture [10]. Similar biological activity has been noticed on an osteoblast-like cell line.[11] The biological significance of CTL has been traced back by some authors through the interaction between the dangling lactitol moieties and a s-type lectin (the galectin-1) bridging the polysaccharide and the integrin on the cell surface. This recognition allows then the downstream signaling cascade to be activated.[12] The almost ubiquitous presence of galectins in biological tissues is considered to be the cause of the cell-unspecific role of CTL.

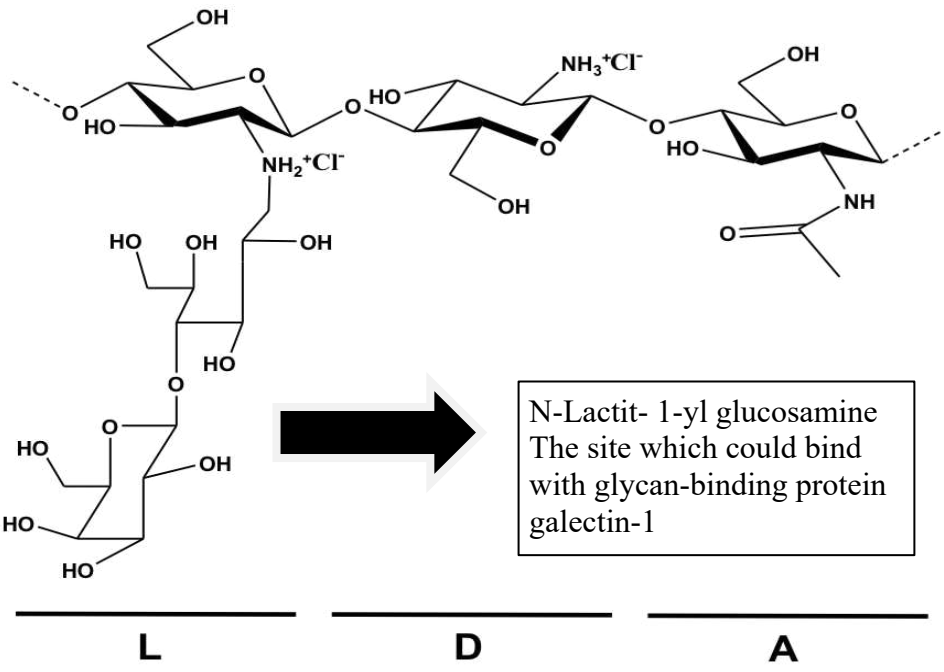

Figure 2.2 Structure of CTL with 3 units

2.1.3 The Galectin -1

Galection-1 shown in Figure 2.3 is a protein differentially expressed in various normal and pathologic tissues and it displays a wide range of activities in biological processes. The galectin-1 protein is 135 amino acids in length and highly conserved across species. It can be found in the nucleus, the cytoplasm, at the cell surface and in the extracellular space. Galectins in general lack a traditional signal sequence, but are still secreted across the plasma membrane.

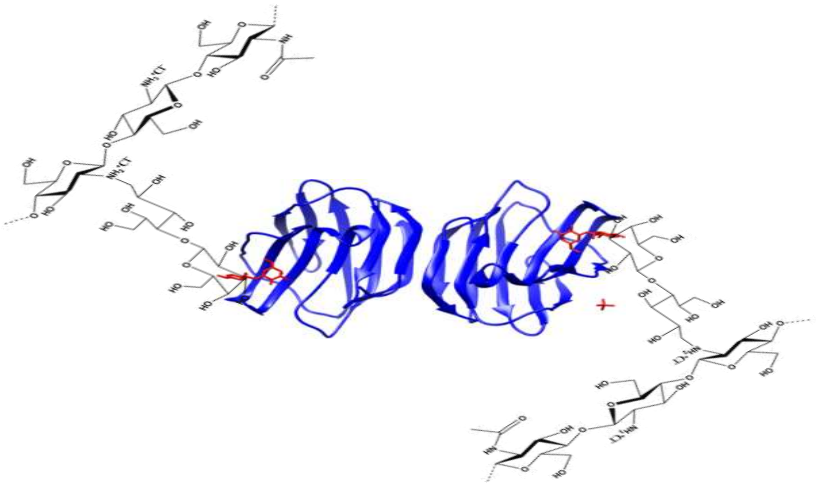

Figure 2.3 The interaction of Gal-1 with CTL

Galectin-1 contains a single carbohydrate recognition domain (in red color in the figure 2.3) through which it can bind with glycans (CTL) both as a monomer and as a homodimer.

Studies show an over expression of Gal-1 in different cancers such as colon, liver, breast, lung, head and neck, ovarian, prostate carcinomas, and Hodgkin's lymphoma [13]. This expression appears to have strong influence on the tumor progression at different steps such as angiogenesis, apoptosis, cell migration, and metastatic spread. It has been recently demonstrated that the Gal-1 over expression is correlated with the tumor aggressiveness, the patient survival, and the prognosis [14]. Several studies identify this lectin as a promising therapeutic and prognostic marker. Detecting and identifying this protein in biological media can then be of primary importance. However, its specific recognition needs the interaction with a bioreceptor providing a high affinity with Gal-1. The bioreceptor must be grafted at the surface of sensing transducer that could induce the capture of the analyte to be detected. Topologically, Gal-1 represents a particularly interesting challenge for targeting synthetic and multivalent ligands [15], since it is a rigid dimer [16] with two binding sites in opposite directions. The positions of the binding sites compete with each other at linear distance up to 6 nm. Since the main biological targets of Gal-1 reside on the cell surface, one strategy for targeting Gal-1 is to use structures that mimic dGal-1 often considered as a cancer biomarker, thus its important make a fast-specific early diagnosis and point of care for the patients. The following publication is the first time a proof of concept which open a way by using CTL as a bioreceptor on the surface of gold nanoparticles to detect Gal-1 in different concentrations and characterizethe interaction between the Gal-1 and Lactose-modified chitosan gold (III)-PEGylated nanoparticles with different equipment

2.2 Publication 1

Lactose-Modified Chitosan Gold (III)-PEGylated Complex- Bioconjugates: From Synthesis to Interaction with Targeted Galectin-1 Protein

Bioconjugate Chemistry

Article

Cite This: *Bioconjugate Chem.* XXXX, XXX, XXX−XXX

pubs.acs.org/bc

Lactose-Modified Chitosan Gold(III)-PEGylated Complex-Bioconjugates: From Synthesis to Interaction with Targeted Galectin-1 Protein

Qiqian Liu,[†,#] Pasquale Sacco,[‖,#] Eleonora Marsich,[⊥] Franco Furlani,[‖] Celia Arib,[†] Nadia Djaker,[†] Marc Lamy de la Chapelle,[‡,§] Ivan Donati,[‖] and Jolanda Spadavecchia*[,†]

[†]CNRS, UMR 7244, CSPBAT, Laboratoire de Chimie, Structures et Propriétés de Biomateriaux et d'Agents Therapeutiques, Université Paris 13, Sorbonne Paris Cité, 93000 Bobigny, France

[‡]Institut des Molécules et Matériaux du Mans (IMMM - UMR CNRS 6283), Le Mans Université, Avenue Olivier Messiaen, 72085 Le Mans cedex 9, France

[§]Department of Clinical Laboratory Medicine, Southwest Hospital, Third Military Medical University, 400038 Chongqing, China

[‖]Department of Life Sciences, University of Trieste, Via L. Giorgieri 5, I-34127 Trieste, Italy

[⊥]Department of Medicine, Surgery and Health Sciences, University of Trieste, Piazza dell'Ospitale 1, I-34129 Trieste, Italy

Supporting Information

ABSTRACT: Galectins (Gal) are a family of glycan-binding proteins characterized by their affinity for β-galactosides. Galectin-1 (Gal-1), a dimeric lectin with two galactoside-binding sites, regulates cancer progression and immune responses. Coordination chemistry has been engaged to develop versatile multivalent neo-glycoconjugates for binding Gal-1. In this study we report a fast and original method to synthesize hybrid gold nanoparticles in which a hydrochloride lactose-modified chitosan, named CTL, is mixed with dicarboxylic acid-terminated polyethylene glycol (PEG), leading to shell-like hybrid polymer-sugar-metal nanoparticles (CTL-PEG-AuNPs). The aim of this paper is to preliminarily study the interaction of the CTL-PEG-AuNPs with a target protein, namely, Gal-1, under specific conditions. The molecular interaction has been measured by Transmission Electron Microscopy (TEM), UV−vis, and Raman Spectroscopy on a large range of Gal-1 concentrations (from 0 to 10^{-12} M). We observed that the interaction was strongly dependent on the Gal-1 concentration at the surface of the gold nanoparticles.

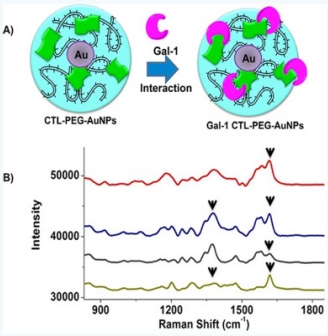

INTRODUCTION

Gold nanoparticles (AuNPs) are used in various fields as medical nanovectors, transducers, or nanosensors.[1] The research on new synthesis methods is still an active field in order to optimize the AuNPs properties for such applications.[2−4] In a previous study we have investigated a fast synthesis method to realize polymer-modified AuNPs using dycarboxylic PEG, collagen, or bisphosphonate (BPO) as stabilizers in order to demonstrate high stability and efficacy under realistic biomedical conditions.[5−8] Other authors have synthesized hybrid metal nanoparticles based on chitosan and chitosan-derivatives as sugar stabilizers for various applications in the field of the nanomedicine.[9−13]

Lactose-modified chitosan, CTL (in other papers termed Chitlac), is a branched polysaccharide synthesized via reductive *N*-alkylation of primary amines by lactose moieties (Figure S1 in Supporting Information).[14] CTL is a ternary heteropolysaccharide composed of β-1 → 4 linked glucosamine (D unit), *N*-acetyl-glucosamine (A unit), and *N*-Lactit-1-yl glucosamine (L unit) sugars. The presence of lactose residues grafted on the chitosan backbone ensures some advantages with respect to the original polymer, such as a higher solubility at neutral pH than most of commercial chitosans, miscibility with polyanions to form soluble complexes without associative phase separation, and the possibility to form gels upon mixing with boric acid as cross-linker under physiological conditions of pH and osmolarity.[15] From the biological point of view, it has been proven that CTL fosters the aggregation of an osteoblast-like cell line *in vitro*, stimulates the cell proliferation, and enhances the alkaline phosphatase activity.[16] Contextually, the aggregation of chondrocytes and the stimulation of collagen and glycosaminoglycans production was also demonstrated.[17,18] It was found that the bioactivity of CTL is ascribed to the specific interaction between the lactitol groups of the polymer and the β-galactoside-binding protein Galectin-1.[19,20]

Galectin-1 (Gal-1) is a protein differentially expressed in various normal and pathologic tissues and displays a wide

Received: July 23, 2018
Revised: September 12, 2018
Published: September 14, 2018

DOI: 10.1021/acs.bioconjchem.8b00520
Bioconjugate Chem. XXXX, XXX, XXX−XXX

Scheme 1. Representation of the Synthesis of CTL-PEG-AuNPs[a]

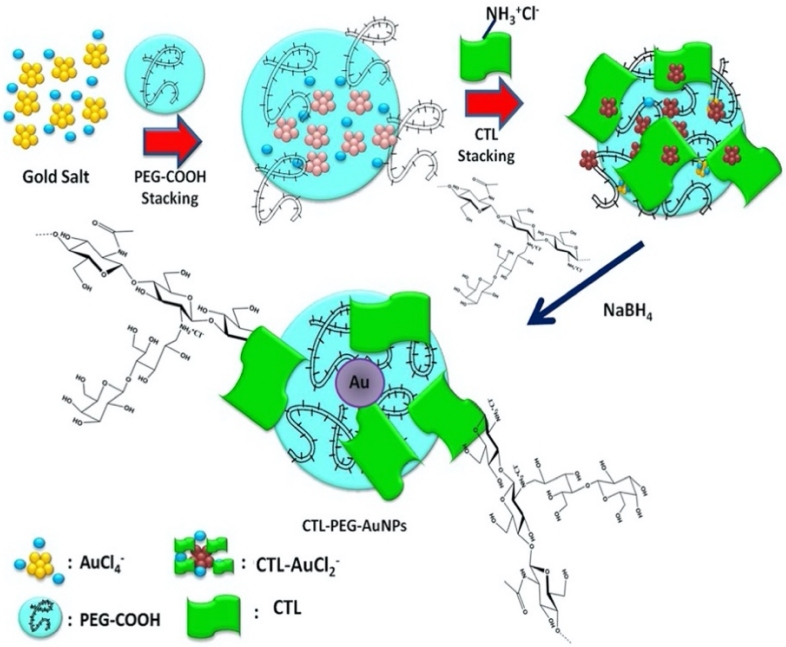

[a]Please note that drawings are not in scale and are not intended to be representative of the full sample composition.

range of activities in biological processes. Increased Gal-1 expression has been reported in different tumors such as colon, breast, lung, head and neck, ovarian, prostate carcinomas, and Hodgkin's lymphoma.[21−27] The expression of this protein in various cancer cells appears to affect tumor progression steps, mainly angiogenesis, apoptosis, cell migration, and metastatic spread. It has been recently demonstrated that Gal-1 overexpression positively correlates to tumor aggressiveness, poor patient survival, and prognosis.[28] Several studies identify this lectin as a promising therapeutic and prognostic marker in cancer.[29] Topologically, Gal-1 represents a particularly interesting challenge for targeting with synthetic, multivalent ligands[30] since it is a rigid dimer[31] with two binding sites oriented in opposite directions. The positions of the binding sites compete with each other at linear distance up to 6 nm. Since the main biological targets of Gal-1 reside on the cell surface, one strategy for targeting Gal-1 is to use structures that mimic the fluidity and adaptability of cellular membranes. Detecting and identifying this protein in biological media can then be of primary importance. However, its specific recognition needs the interaction with a bioreceptor providing a high affinity with Gal-1. The bioreceptor must be grafted at the surface of sensing transducer that could induce a modification of its affinity with the analyte to be detected. Most of the methods used to detect biomolecules require strict molecular recognition events.[32] In these latter cases, grafted biomolecules at the AuNP surface can act as bioreceptors having a high affinity for the targeted analytes.[33] The analyte target detection depends on the affinity constant of the bioreceptor to the targeted analyte.[34] The goal of the present paper is to preliminarily investigate the possibility of exploiting the interaction between CTL and Gal-1 for the development of a nanocarrier system based on CTL-decorated AuNPs for the detection and the tracking of the lectin protein.

We would like to understand whether the grafting will modify the interaction and thus if some parameters can be optimized in order to improve this interaction in terms of sensing purposes. The specific binding affinity between CTL and Gal-1 was ascertained and quantified by means of Surface Plasmon Resonance. Shell-like hybrid CTL-PEG-gold nanoparticles (CTL-PEG-AuNPs) were synthesized and characterized. The interaction between Gal-1 and CTL-PEG-AuNPs was then investigated using Localized Surface Plasmon (LSP), Transmission Electron Microscopy (TEM), and Raman spectroscopy as analytical tools.

■ RESULTS AND DISCUSSION

CTL-Galectin 1 Binding Affinity. In a previous paper,[1] we looked experimentally for the existence of the interaction between the polymer CTL and the lectin Gal-1 able to induce specific biological responses.

Herein, the Surface Plasmon Resonance (SPR) technique was exploited to demonstrate *in vitro* the presence of a molecular interaction between Gal-1 and CTL, and the equilibrium binding constants were calculated. To this aim CTL was immobilized on the chip via amidation chemistry. SPR signals were recorded using different concentrations of Gal-1 and corrected for the contribution of the solvent as shown in Figure S3 in Supporting Information. SPR analysis performed on nonderived polysaccharide (chitosan) allows a clear deduction that the specific interaction exists only in the case of CTL (data not shown). Interestingly, for CTL the SPR signal for concentrations of Gal-1 equal to or greater than 1 μM does not seem to reach a constant value, indicative of the achievement of a steady state. On the contrary, in the time interval in which the plateau would be expected, the signal increases linearly with slopes increasing with Gal-1 concentrations.

DOI: 10.1021/acs.bioconjchem.8b00520
Bioconjugate Chem. XXXX, XXX, XXX−XXX

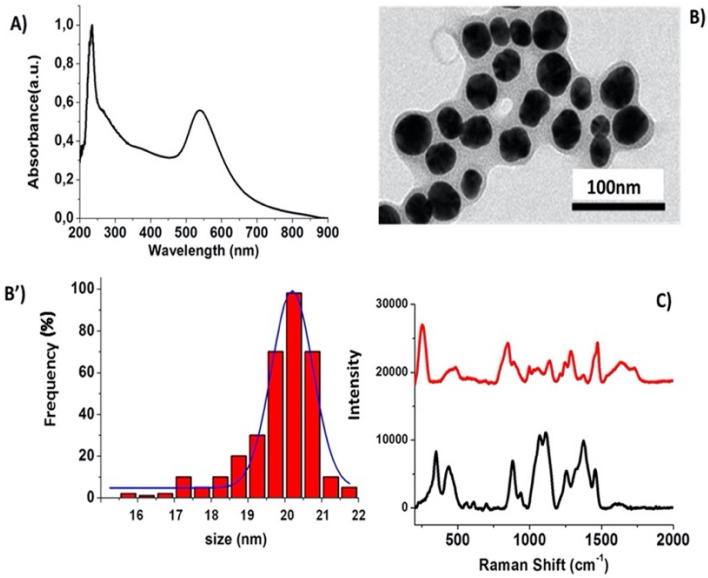

Figure 1. (A) Normalized UV−vis absorption spectrum of CTL-PEG-AuNPs, (B) TEM images of CTL-PEG-AuNPs, and size distribution histogram (B′). (C) Raman spectrum of CTL-PEG-AuNPs (red line) compared to free CTL spectrum as control (black line). (B) Scale bar: 100 nm. (C) Raman spectra. Experimental conditions: λ_{exc} = 785 nm; laser power 20 mW; accumulation time 180 s.

The analysis of the kinetic data (see Supporting Information) was carried out by adopting a model unimolecular (1:1) for the protein−substrate system providing the values of the kinetic association constant ($k_a = 6 \times 10^3$ M^{-1} s^{-1}) and kinetic dissociation constant ($k_d = 6 \times 10^{-2}$ s^{-1}) of the complex. The calculated affinity constant, defined as $K_A = k_a/k_d$, was 1×10^5 M^{-1}. The affinity constant was also calculated independently using the steady state values of the temporal trace at the different protein concentrations. The value of K_A obtained from the kinetic data was comparable with those obtained from the responses to equilibrium: 1×10^5 M^{-1} in the first case and 4×10^5 M^{-1} in the second one.

Gal-1 binds relatively strongly to CTL, in fact the calculated affinity constant (1×10^5 M^{-1}) is stronger than that reported in literature by Miller et al. for the binding of Gal-1 with the disaccharide lactose (Gal-β(1 → 4)-Glc).[36] The multivalent structure of CTL may contribute to this high analogy for Gal-1, something that is viewed with many cell-surface glycoconjugates that bear multiple galectin-binding sites.[37,38] Moreover this value is in the same range of values reported for the affinity constants for binding to both linear and complex branched glycans bearing terminal β(1 → 4)-linked galactose side chains.[39]

Formation Mechanism of CTL-PEG-AuNPs. In the past years Spadavecchia et al. have extensively investigated the synthesis of hybrid nanoparticles and the effect of various surfactant agents on the growth process.[5,6] Recently, Furlani-Sacco et al. have developed colloidal coacervates using the bioactive chitosan-derivative CTL by ionotropic gelation.[11] Contextually, other authors have designed a nanocomposite hydrogel based on natural polysaccharides, CTL, and gold nanoparticles with considerable antimicrobial activity.[20]

After demonstrating the existence of a high binding affinity between CTL and Gal-1, the objective of this paper was to evaluate the interaction between Gal-1 and CTL under formation of stable complexes of PEGylated Au (III)-CTL as active excipients of gold nanoparticles. The major discrepancy with other chemical procedures is that PEG and CTL participate in the stabilization of AuNPs via complexation between their ketone and amino groups with chloride auric ions. In our case, the formation of gold NPs from $AuCl_4^-$ comprises the following steps (Scheme 1):

1. Complexation of PEG with $AuCl_4^-$ and initial reduction of the polymer−metal complex to generate gold clusters.[7]
2. Stacking process of CTL by electrostatic adsorption onto the PEGylayed gold clusters.
3. Final reduction of metal ions at the vicinity of the clusters, growth of AuNPs and colloidal stabilization through the dicarboxylic PEG and CTL polymers.

In the first step, PEG dicarboxylic acid (PEG) is added into $HAuCl_4$ aqueous solution, to complex with it as previously described.[6,7] In the second step, the positively amino charged ($-NH_3^+$ and $-NRH_2^+$) groups of CTL in water solution favor strong electrostatic interactions with the negatively charged complex PEG-$AuCl_4^-$, the latter playing a strategic role in the growth process of AuNPs.[6] The addition of CTL in the PEG-$AuCl_4^-$ solution increases the kinetics of reduction by a further complexation with the Au ions.[6] Such an effect controls the simultaneous chemical and steric arrangement of CTL and PEG between $AuCl_4^-$ on the surface of gold seeds during the growth process of nanoparticles. In the third step, the reduction by $NaBH_4$ induces the growth process of hybrid nanoparticles.

All products were entirely characterized by UV−vis absorption spectroscopy, TEM, and Raman spectroscopy. The UV−visible spectrum of CTL-PEG-AuNPs was characterized by a surface plasmon band at 530 nm and a peak at 234 nm assigned to the CTL-PEG absorption (Figure 1A; Figure S4 in Supporting Information), which confirms the formation of AuNPs. In addition, the bright violet-blue color of the resulting nanoparticles and the UV−vis spectra remained unaltered after six months at room temperature validating the realization of stable colloidal solution.

DOI: 10.1021/acs.bioconjchem.8b00520
Bioconjugate Chem. XXXX, XXX, XXX−XXX

Scheme 2. Schematic Representation of Interaction Mechanism of Galectin-1 onto CTL-PEG-AuNPs (A) and Subsequent Conformational Change of Galectin Molecules under Specific Concentrations of Protein (B)[a]

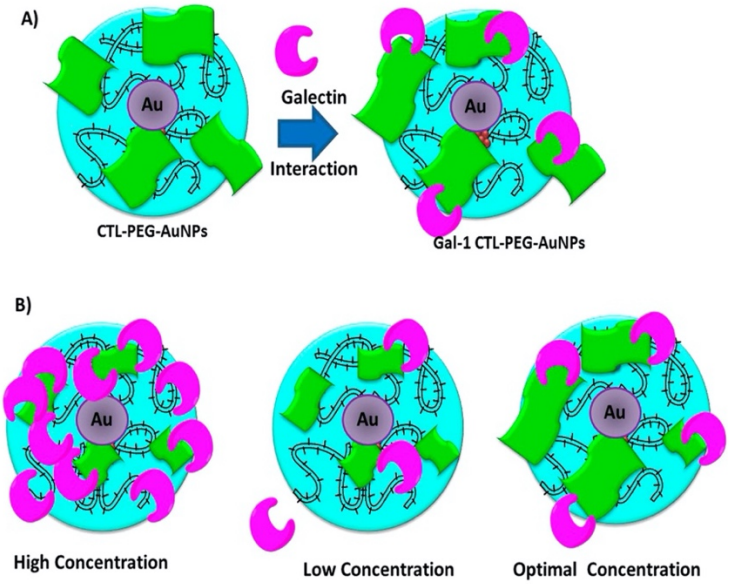

[a]Please note that drawings are not to scale and are not intended to be representative of the full samples composition.

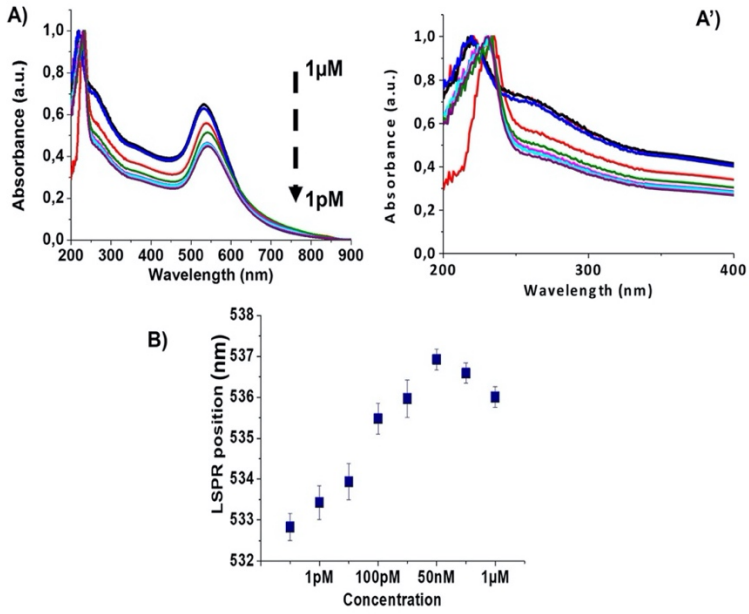

Figure 2. (A) UV–vis absorption spectra in the range 200–900 nm of CTL-PEG-AuNPs before (black line) and after (red line) interaction of Galectin-1 (from 1 μM to 1 pM) under straight condition (NaCl 0.9%). (A′) Enlargement of UV–vis absorption spectra in the range 200–400 nm of CTL-PEG-AuNPs before and after interaction of Galectin-1. (B) Evolution of the CTL-PEG-AuNPs plasmonic bands versus the Gal-1 concentration.

Representative TEM images of the colloidal solutions are shown in Figure 1 panel B. CTL-PEG-AuNPs exhibit a thin distribution in size and shape, with an average size of 20 ± 0.5 nm as estimated from 450 particles on a given TEM image. Anyway, some of the particles showed a somewhat faceted shape as a result of their nanocrystalline nature. Spadavecchia et al. have studied the synthesis of analogous nanomaterials using dicarboxylic PEG[5,6,8,35,40] obtaining PEG-AuNPs with a smaller size, i.e., about 6.7 ± 0.5 nm.[8] On the basis of previous studies[8,35,40] we assumed that, when CTL was added to the complex with the PEG-$AuCl_4^-$, the chemical and steric arrangement between PEG and CTL influences the final size of the nanoparticles.

The Raman spectra of free CTL and CTL-PEG-AuNPs in water exhibit many bands in the region 500–2000 cm^{-1} (Figure 1C). The wide band observed around 1600 cm^{-1} on

DOI: 10.1021/acs.bioconjchem.8b00520
Bioconjugate Chem. XXXX, XXX, XXX–XXX

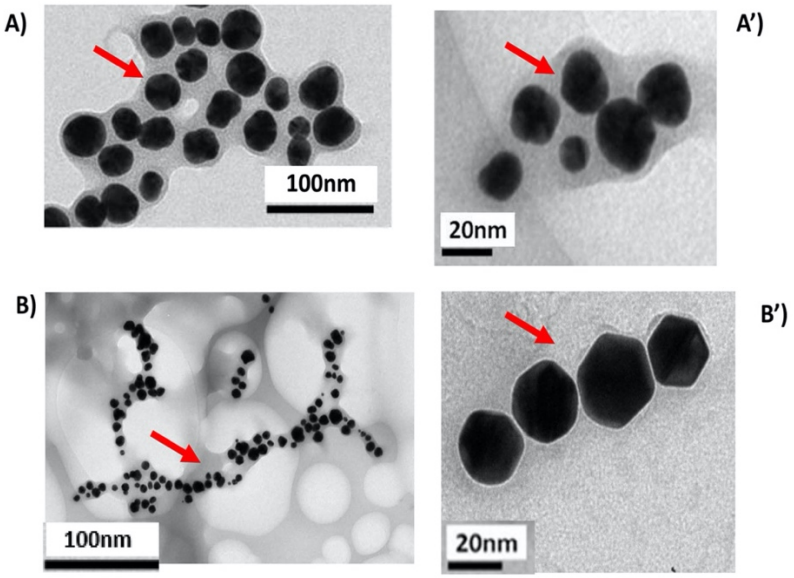

Figure 3. TEM images of CTL-PEG-AuNPs before (A,A′) and after interaction with Galectin-1 (B,B′). Scale bars: 100 nm; 20 nm (low A,B and high B,B′ magnification). Directional arrows showing a metal core of around 20 nm and suggesting the presence of an organic CTL-PEG layer of few nanometers.

the CTL-PEG-AuNPs of Raman spectra is assigned to the water. One of the Raman fingerprints of the CTL-PEG-AuNPs is the presence of a band around 263 cm^{-1} and disappearance of a double peak at 446−485 cm^{-1}. These bands can be assigned to the gold chloride stretches, ν (Au−Cl) and δ (OAuO) in aliphatic chains, and is clear evidence of the formation of a complex between $AuCl_2^-$, PEG and CTL in solution. The common peak at 430 cm^{-1} is due to the vibrations δ (OH···O), ν (OH···O) of the PEG. Based on the spectrochemical and previously theoretical results, we assumed that Au^{3+} ions promoted the deprotonation of the PEG.[35] The spectra of PEG molecules free as control were previously described in the literature[35,8] (Figure S1-A in Supporting Information). Only a few bands remain as the two bands around 1000 cm^{-1} and the one around 1620 cm^{-1}. The other ones are less intense or have completely disappeared. For instance, the strong band at 1375 cm^{-1} assigned to C═O carbonyl stretching of CTL disappears after formation of gold nanoparticles. A double peak at 1065−111 cm^{-1} due to C−O−C stretching in backbone of CTL disappears after PEG stacking onto gold nanoparticles. Furthermore, new bands also appear as an intense triplet at 1211−1243−1289 cm^{-1} due to C−O plane deformation of carboxylic acid and a strong peak at 1471 cm^{-1} assigned to ν C−C stretching. These bands are due to the variation of the steric conformation of the polymers and become more prominent upon complexation, as described previously.[35,40]

Galectin Active Interaction. Galectins are a family of glycan-binding proteins qualified by their affinity for β-galactosides and the presence of typical carbohydrate recognition domains (CRDs).[41] Several studies have shown that the linker's role, responsible for the intramolecular interactions of CRDs, is associated with the ability to induce a specific biological response.[42] For these reasons, galectins are hopeful candidates as diagnostic markers and novel drug targets for human diseases.[43−45]

CTL-PEG-AuNPs were used as building blocks to observe the biomolecular interaction with Galectin-1 (Gal-1) as protein that plays a key role in some biological processes. In order to achieve the mechanism of interaction between Gal-1 and CTL-PEG-AuNPs, Gal-1 proteins were incubated at different concentrations in the AuNPs solutions (Scheme 2). Gal-1 interacts through high binding affinity with CTL as showed by SPR measurements. The protein interaction with CTL-PEG-AuNPs was evaluated by UV−visible absorption (Figure 2). As a matter of fact, the extinction spectrum of the AuNPs is characterized by the plasmon resonance that is strongly dependent on the AuNPs environment, especially to any modification of the local dielectric constant. As a consequence, when Gal-1 interacts with CTL-PEG-AuNPs, it will modify the local environment, thus inducing a shift of the plasmon band. When Gal-1 was added to CTL-PEG-AuNPs in the range from 1 μM to 1 pM, we observed a dynamic variation of the plasmon position and width depending on the Gal-1 amount. Lowering the concentration of protein from 1 μM to 1 pM, we observed that the plasmon band red-shifted with a decrease of its width. Therefore, we assumed that the grafting of Gal-1 onto CTL-PEG-AuNPs surface induced some agglomeration of the nanoparticles due to the interaction with Gal-1 at the gold surface. The weak red shift and the decrease of the plasmon band can then be explained by a lower nanoparticle aggregation and a dissociation of agglomerates after the addition of Gal-1 at a concentration of 1 nM (Scheme 2). It means that from 1 μM up to 1 pM, Gal-1 interacts with the CTL-PEG-AuNPs inducing very small changes on the plasmon band (modification of the dielectric constant around the AuNPs with the addition of Gal-1 proteins and maybe few dissociations). At concentrations higher than 1 nM, a large number of Gal-1 proteins are expected to interact with the CTL-PEG-AuNPs forming a Gal-1 monolayer at the AuNPs surface. From 1 nM, the number of the Gal-1 is then large enough to prevent any interactions between the proteins on CTL-PEG-AuNPs, thus inducing the dissociation of the

DOI: 10.1021/acs.bioconjchem.8b00520
Bioconjugate Chem. XXXX, XXX, XXX−XXX

nanoparticle agglomerates. Hence, at these concentrations we observed a blue shift of the peak due to the CTL-PEG layer from 234 to 217 nm (Figure 2A′) with the consequent decrease of the plasmon band. This effect can be due to the formation of a shell of proteins adsorbed onto the CTL-PEG-AuNPs that incessantly exchange with CTL at high concentration of Gal-1 in the environment. With the saturation of the surface of the AuNPs, we can suppose that it could induce a better orientation of the Gal-1 or a change of its conformation due to chemical hindrance and also due to protein conformation changes. The evolution of the CTL-PEG-AuNPs plasmonic bands versus the Gal-1 concentration is displayed in Figure 2B.

The protein interaction with CTL-PEG-AuNPs was also characterized by TEM. Such bioconjugates have a spherical shape (Figure 3A,B) with a diameter close to 20 nm. Following Gal-1 interaction onto CTL-PEG-AuNPs, we observed characteristic linear chain likely (Figure 3B,B′) objects, due to the preferential location of CTL-PEG and Gal-1 onto the particle surface.

The Gal-1 interaction was confirmed by DLS and Zeta potential measurements (Table S1 in Supporting Information). The hydrodynamic diameter of CTL-PEG-AuNPs was slightly higher (about 5 nm) than the radius determined by TEM analyses. This discrepancy should take into account the overestimation of the hydrodynamic diameter due to the surrounding water molecules. Besides, the ζ-potential measurements show that CTL-PEG-AuNPs and Gal-1 CTL-PEG-AuNPs were colloidally stable at physiological pH (ζ-potential = -29 ± 2 mV, for CTL-PEG-AuNPs and -25 ± 1 mV for Gal-1 CTL-PEG-AuNPs with a PDI equal to 0.3 ± 2).

The stability of CTL-PEG-AuNPs and Gal-1 CTL-PEG-AuNPs was verified in solution by visualizing the Localized Surface Plasmon (LSP) band at 530 nm. The analysis was carried out at pH 4 and electrolytic conditions up to 3 months. The synthesized CTL-PEG-AuNPs and Gal-1 CTL-PEG-AuNPs showed an almost negligible change in the LSP band position in the time frame investigated (Figure S2A,B in Supporting Information). The LPS band intensity was almost constant in the first 15 days of incubation, thus indicating the perfect stability of the systems. A slight (tolerable) reduction of LPS band intensity was noticed at 1 month. If the incubation is prolonged up to 3 months, a marked reduction of the absorbance was detected for both CTL-PEG AuNPs and Gal-1 CTL-PEG-AuNPs, thus suggesting that the systems were almost unstable for long storage purposes.

The successful interaction of Gal-1 onto CTL-PEG-AuNPs surface was established by Raman spectroscopy at different Gal-1 concentrations (Figure 4). The detection of the fingerprint of CTL and PEG-COOH at the AuNPs surface was demonstrated through the observation of the Raman bands at 1137 cm^{-1}, 1270 cm^{-1}, and 1455 cm^{-1} due to the vibration of C−O−H, C−O−C, and C−O chemical groups, respectively (Figure 4A,A′). After the Gal-1 binding, the amide II (1587−1620 cm^{-1}) and amide III (1200−1300 cm^{-1} regions), as well as modifications in protein local environments, confirmed the protein interaction (Figure 4A,A′). When the protein concentration decreased from 500 nM to 1 pM, the fingerprint of amide band was masked by water peak at 1600 cm^{-1} due to the ionic environment.

By evaluating the Raman results it was possible to confirm that the chemical and steric conformation of Gal-1 depend on molecule concentration that influences in turn the bioconjugation with CTL-PEG-AuNPs. In fact, the self-assembly of the Gal-1 on the CTL-PEG-AuNPs will take place due to their great packing density as well as the force repulsion between the negatively charged Gal-1.[30,46] However, the self-assembly of the Gal-1 on the CTL-PEG-AuNPs from 1 μM to 1 nM shows amide bands; in the presence of lower Gal-1 concentrations (from 1 μM to 1 pM) amide bands progressively disappear. This phenomenon is probably due to the swelling of polymers in water that interferes with protein steric conformation at low concentration. Similar analyses of Gal-1 interaction (UV−vis and Raman) (Figure S5 in Supporting Information) were carried out in the presence of PEG-AuNPs as control, under the same experimental conditions, confirming the selectivity of interaction between CTL-PEG-AuNPs and Gal-1. In fact, after incubating PEG-AuNPs and Gal-1 at maximal concentration (1 μM), we did not observe any signal variation.

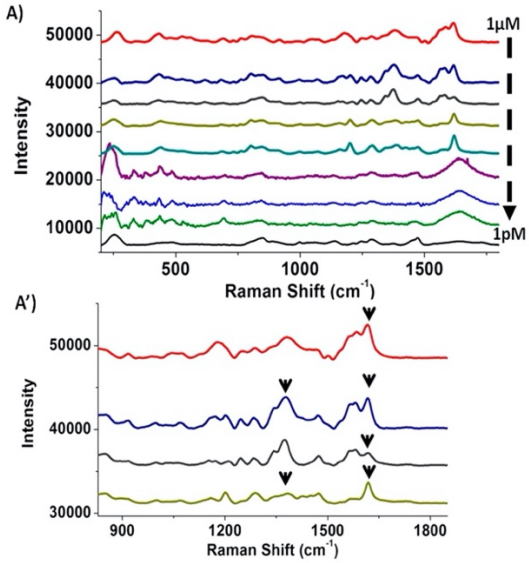

Figure 4. (A) Raman spectra of the CTL-PEG-AuNPs (red line) and Gal-1 CTL-PEG-AuNPs (Galectin-1 concentration range 1 μM − 1 pM) compared to free CTL (black line). (A′) Zoom Raman spectra of Gal-1 CTL-PEG-AuNPs from 1 μM to 500 nM; directional arrows show the characteristic peaks during protein interaction. Experimental conditions: λ_{exc} = 785 nm; laser power 20 mW; accumulation time 180 s.

Selectivity of Galectin versus CTL-PEG-AuNPs. To confirm the selectivity of Gal-1 versus CTL, a preliminary test in the presence of collagen type I was carried out. Collagen (Col) is one of several structural proteins in the extracellular matrix (ECM) overexpressed in many type of cancer. For this purpose it has been entirely used in biomedical and biomaterial applications.[47] Col solution and Col/Gal-1 mixture solution were incubated at room temperature with CTL-PEG-AuNPs at 1 μM for 18 h, and the interaction was monitored by UV−vis and Raman spectroscopy.

Figure 5A shows a shift of the plasmon position from 530 nm before interaction (black line) to 539 nm after the binding (red line) with the Col/Gal-1 mixture. A weakly widened peak at 640 nm is probably due to agglomeration between gold particles after the capture of the protein at the particle surface due to modification of the surface charges.

The protein interaction was confirmed by Raman spectroscopy. After the Col-Gal-1 interaction onto CTL-PEG-AuNPs,

DOI: 10.1021/acs.bioconjchem.8b00520
Bioconjugate Chem. XXXX, XXX, XXX−XXX

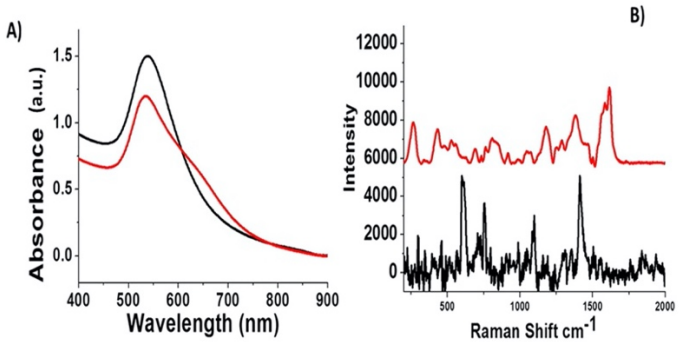

Figure 5. (A) Normalized UV−vis absorption spectrum of CTL-PEG-AuNPs before (black line) and after (red line) incubation with a mixture of Collagen (I) and Gal-1 at 1 μM. (B) Raman spectrum of CTL-PEG-AuNPs (red line) after interaction with a mixture of Collagen (I) and Gal-1 at 1 μM, compared to free CTL-PEG-AuNPs spectrum as control (black line). Raman spectra experimental conditions: λ_{exc} = 785 nm; laser power 20 mW; accumulation time 180 s.

the Raman spectrum is perfectly equivalent to Raman spectra related to single Gal-1 interaction onto CTL-PEG-AuNPs. Indeed the amide II (1587−1620 cm^{-1}) and amide III (1200−1300 cm^{-1} regions), confirmed that the Gal-1 protein is effectively captured at the AuNPs surface (Figure 5B). Moreover, the spectroscopical fingerprint of collagen is not observable. In order to assume the success of this analysis, we checked the interaction of Col *free* onto CTL-PEG-AuNPs as control (Figure S6A,B in Supporting Information), under the same experimental conditions. Figure S6 shows that, when Col was added to CTL-PEG-AuNPs, a negligible blue shift was observed in UV−vis spectra at 1 pM probably due to the chemical exchange between Col and PEG onto AuNPs surface (Figure S6A red line). However, at 1 μM, we noticed a decreased and widened peak, with a strong red shift at 680 nm due to the aggregation of AuNPs. The comparative Raman spectra at 1 pM (red line) and 1 μM (blue line) (Figure S6B Supporting Information) did not show any remarkable spectroscopical modification. This means that there was no capture of the Col at the AuNPs surface even at high concentration of Col. We thus can conclude that the CTL-PEG-AuNPs surface selectively interacts with the Gal-1.

■ CONCLUSIONS

In this paper, we studied for the first time the biointeraction between Galectin-1 and CTL-PEGylated gold nanoparticles. The analysis of the UV−visible and Raman spectra allowed us to highlight the formation of agglomerates due to high binding affinity between Gal-1 and CTL onto gold nanoparticles. We observed some dissociation for specific Gal-1 concentrations giving evidence of the interaction of the protein with the CTL by SPR experiments. This paper allows a better understanding of the interaction mechanism (chemical structure modifications, kinetic interaction) and the sensing optimization since the detection sensitivity is directly related to the affinity of the bioreceptor to the analyte. Further investigations are further needed to assess the *in vitro* and *in vivo* selectivity of the present system toward different cancer models.

■ MATERIALS AND METHODS

Materials. Tetrachloroauric acid ($HAuCl_4$), sodium borohydride ($NaBH_4$), dicarboxylic polyethylene glycol (PEG)-600 (PEG), sodium chloride (NaCl 0.9%), phosphate-buffered solution (PBS), and collagen type I were all provided by Sigma-Aldrich at maximum purity grade. Recombinant Human Galectin-1 (Lot# 0707271-1) was purchased from PeproTech (Rocky Hill, NJ, USA). Hydrochloride CTL was kindly provided by BiopoLife S.r.l. (Trieste, Italy). The chemical composition of CTL was determined by ^{1}H NMR spectroscopy and resulted in a fraction of deacetylated units (F_D) 0.36, fraction of lactose-modified units (F_L) 0.56, and fraction of acetylated units (F_A) 0.08. The physical properties were determined by viscometry: the intrinsic viscosity, $[\eta]$, of CTL was checked at 25 °C by means of a CT 1150 Schott Geräte automatic measuring apparatus and a Schott capillary viscometer. A buffer solution composed by 20 mM AcOH/AcNa, pH 4.5, and 100 mM NaCl was used as solvent.[11] The resulting $[\eta]$ was 511 mL/g. The estimated viscosity average molecular weight, M_v of CTL was around 870 000.

Surface Plasmon Resonance Analysis. The interaction between CTL and Gal-1 was assessed by means of a Biacore TM 2000 Instrument (BIAcore, Uppsala, Sweden) using a Chip sensor CM5 (GE Healthcare). CTL was immobilized on the chip following manufacturer's instructions. Briefly, CTL was dissolved in AcOH/AcNa buffer, pH 4.5, at a concentration of 0.05 g/L. Subsequently, CTL was injected (30 μL/min) on the chip surface until a SPR signal of approximately 800 RU was observed.

Gal-1 solubilization and binding measurements were performed in PBS buffer, pH 7, supplemented with dithiothreitol (DTT-2 mM) and P20 detergent (0.005%). Gal-1 solutions in a range of concentrations 0.12−8 μM were injected over the sensor chip surface at 30 μL/min. Flow channel Fc1 has been used as negative control. The chip was regenerated by injection of lactose 10 mM. Data analysis has been performed by the BIA evaluation 3.2 Software (Biacore). A Langmuir 1:1 model was used for the calculation of rate constants (for details see Supporting Information).

Preparation of CTL and Galectin Protein Solutions. CTL was solubilized at a concentration equal to 1 mg/mL in Milli-Q water (final pH around 3). Galectin powder was solubilized in water and then diluted in order to obtain solutions with concentrations comprised within the range 1 μM − 1 pM. Molar concentrations of Galectin-1 were determined taking into account that the molecular weight of Galectin-1 is equal to 14.5 kDa.

Preparation of Collagen and Galectin Protein Solutions (Selectivity Test). Galectin and Collagen were solubilized in water and mixed together to obtain a solution at concentration of 1 μM.

DOI: 10.1021/acs.bioconjchem.8b00520
Bioconjugate Chem. XXXX, XXX, XXX−XXX

Synthesis of CTL-PEG-AuNPs. Colloids of CTL-PEG-coated AuNPs (CTL-PEG-AuNPs) were synthesized by a well-established chemical reduction process described in Scheme 1. Briefly, 250 μL of PEG solution (0.5 mM) was added to 20 mL of tetrachloroauric acid solution (2.4×10^{-4} M) under stirring at room temperature. Then, 5 mL of CTL solution (1 mg/mL) and 2 mL of aqueous 0.01 M $NaBH_4$ were added drop by drop with precaution until solution turned into a violet color. The concentration was estimated by standard mathematical calculations in colloidal solution.

Determination of CTL-PEG-AuNPs Concentration. AuNPs concentration was determined by exploiting standard mathematical calculations in colloidal solution. Lambert–Beer law ($A = \varepsilon\ C\ l$) was used to determine colloids concentration. In this equation, A is the maximum absorbance (corresponding to the Surface Plasmon Resonance Band at around 530–540 nm) of the UV–visible spectrum, ε is the molar extinction coefficient (equal to 3.07×10^{10} M^{-1} cm^{-1}), C is the molar concentration of colloids, and l is the optical length of cuvette (1 cm). The resulting C was multiplied for the dilution factor to obtain the concentration of colloids.

Bioconjugation of CTL-PEG-AuNPs with Gal-1. The interaction of Gal-1 protein with CTL-PEG-AuNPs surface was obtained exploiting the procedures depicted in Scheme 2. Briefly, 5 mL of CTL-PEG-AuNPs (42 nM) were added into separate tubes containing 50 μL of Gal-1 (from 1 μM to 1 pM; PBS pH 7; NaCl 0.15 M). After 18 h of incubation, the CTL-PEG-AuNPs/Gal-1 suspension was centrifuged twice at 5000 rpm for 10 min to eliminate the excess of Gal-1 and then the pellets were redispersed in 1 mL of Milli-Q water as described previously.[8]

Physical-Chemical Characterization. All the measurements were accomplished in triplicate to confirm the reproducibility of the synthetic and analytical procedures.

UV/vis Measurements. Absorption spectra were recorded using a double-beam Varian Cary 500 UV–vis spectrophotometer (Agilent, France). UV–vis spectra of the AuNPs were achieved in water at concentration of 42 nM in the 200–900 nm spectral range.

Transmission Electron Microscopy (TEM). Transmission Electron Microscopy (TEM) images were recorded with a JEOL JEM 1011 microscope operating (JEOL, USA) at an accelerating voltage of 100 kV. TEM specimens were prepared after separating the surfactant from the metal particles by centrifugation under a protocol described previously.[8]

Raman Spectroscopy. The Raman experiments have been performed on an Xplora spectrometer (Horiba Scientifics-France) under a protocol described previously.[8]

Dynamic Light Scattering (DLS) and Zeta Potential Measurements. The size and zeta potential measurements were performed using a Zetasizer Nano ZS (Malvern Instruments, Malvern, UK) equipped with a He–Ne laser (633 nm, fixed scattering angle of 173°) at room temperature as described previously.[35]

Stability of CTL-PEG-AuNPs and Gal-1 CTL-PEGAuNPs as a Function of pH. The stability of nanoparticles was detected by UV–vis. All nanoparticles were dissolved in PBS buffer, NaCl 0.15 M, pH 4 and stored for 3 months (Figure S2 in Supporting Information).

■ ASSOCIATED CONTENT

Supporting Information

The Supporting Information is available free of charge on the ACS Publications website at DOI: 10.1021/acs.bioconjchem.8b00520.

Supplementary figures, schemes and tables are provided (PDF)

■ AUTHOR INFORMATION

Corresponding Author

*E-mail: jolanda.spadavecchia@univ-paris13.fr.

ORCID

Pasquale Sacco: 0000-0002-4483-5099
Franco Furlani: 0000-0001-5986-1727
Nadia Djaker: 0000-0001-7912-5436
Ivan Donati: 0000-0003-3752-8346
Jolanda Spadavecchia: 0000-0001-6697-1174

Author Contributions

The manuscript was written through contributions of all authors. All authors have given approval to the final version of the manuscript.

Author Contributions

#These authors (Qiqian Lisu, Pasquale Sacco) contributed equally.

Notes

The authors declare no competing financial interest.

■ ACKNOWLEDGMENTS

This work has been partly performed on the CNanoMat platform of the University Paris 13. This study was supported by the University of Trieste (FRADONATI2016-17) and by the INTERREG V-A ITALIA-SLOVENIA 2014-2020 BANDO 1/2016 ASSE 1 - project BioApp 1472551605.

■ REFERENCES

(1) Marcon, P., Marsich, E., Vetere, A., Mozetic, P., Campa, C., Donati, I., Vittur, F., Gamini, A., and Paoletti, S. (2005) The role of Galectin-1 in the interaction between chondrocytes and a lactose-modified chitosan. *Biomaterials 26* (24), 4975–84.

(2) Sapsford, K. E., Algar, W. R., Berti, L., Gemmill, K. B., Casey, B. J., Oh, E., Stewart, M. H., and Medintz, I. L. (2013) Functionalizing Nanoparticles with Biological Molecules: Developing Chemistries that Facilitate Nanotechnology. *Chem. Rev. 113* (3), 1904–2074.

(3) Moore, T. L., Rodriguez-Lorenzo, L., Hirsch, V., Balog, S., Urban, D., Jud, C., Rothen-Rutishauser, B., Lattuada, M., and Petri-Fink, A. (2015) Nanoparticle colloidal stability in cell culture media and impact on cellular interactions. *Chem. Soc. Rev. 44* (17), 6287–6305.

(4) Jans, H., Liu, X., Austin, L., Maes, G., and Huo, Q. (2009) Dynamic Light Scattering as a Powerful Tool for Gold Nanoparticle Bioconjugation and Biomolecular Binding Studies. *Anal. Chem. 81* (22), 9425–9432.

(5) Politi, J., De Stefano, L., Longobardi, S., Giardina, P., Rea, I., Methivier, C., Pradier, C. M., Casale, S., and Spadavecchia, J. (2015) The amphiphilic hydrophobin Vmh2 plays a key role in one step synthesis of hybrid protein-gold nanoparticles. *Colloids Surf., B 136*, 214–21.

(6) Spadavecchia, J., Apchain, E., Alberic, M., Fontan, E., and Reiche, I. (2014) One-step synthesis of collagen hybrid gold nanoparticles and formation on Egyptian-like gold-plated archaeological ivory. *Angew. Chem., Int. Ed. 53* (32), 8363–6.

(7) Spadavecchia, J., Perumal, R., Barras, A., Lyskawa, J., Woisel, P., Laure, W., Pradier, C. M., Boukherroub, R., and Szunerits, S. (2014)

DOI: 10.1021/acs.bioconjchem.8b00520
Bioconjugate Chem. XXXX, XXX, XXX–XXX

Amplified plasmonic detection of DNA hybridization using doxorubicin-capped gold particles. *Analyst 139* (1), 157−64.
(8) Spadavecchia, J., Movia, D., Moore, C., Maguire, C. M., Moustaoui, H., Casale, S., Volkov, Y., and Prina-Mello, A. (2016) Targeted polyethylene glycol gold nanoparticles for the treatment of pancreatic cancer: from synthesis to proof-of-concept in vitro studies. *Int. J. Nanomed. 11*, 791−822.
(9) Tammam, S. N., Khalil, M. A. F., Abdul Gawad, E., Althani, A., Zaghloul, H., and Azzazy, H. M. E. (2017) Chitosan gold nanoparticles for detection of amplified nucleic acids isolated from sputum. *Carbohydr. Polym. 164*, 57−63.
(10) Donati, I., Travan, A., Pelillo, C., Scarpa, T., Coslovi, A., Bonifacio, A., Sergo, V., and Paoletti, S. (2009) Polyol Synthesis of Silver Nanoparticles: Mechanism of Reduction by Alditol Bearing Polysaccharides. *Biomacromolecules 10* (2), 210−213.
(11) Furlani, F., Sacco, P., Marsich, E., Donati, I., and Paoletti, S. (2017) Highly monodisperse colloidal coacervates based on a bioactive lactose-modified chitosan: From synthesis to characterization. *Carbohydr. Polym. 174*, 360−368.
(12) Manivasagan, P., Bharathiraja, S., Bui, N. Q., Lim, I. G., and Oh, J. (2016) Paclitaxel-loaded chitosan oligosaccharide-stabilized gold nanoparticles as novel agents for drug delivery and photoacoustic imaging of cancer cells. *Int. J. Pharm. 511* (1), 367−379.
(13) Collado-Gonzalez, M., Montalban, M. G., Pena-Garcia, J., Perez-Sanchez, H., Villora, G., and Diaz Banos, F. G. (2017) Chitosan as stabilizing agent for negatively charged nanoparticles. *Carbohydr. Polym. 161*, 63−70.
(14) Donati, I., Stredanska, S., Silvestrini, G., Vetere, A., Marcon, P., Marsich, E., Mozetic, P., Gamini, A., Paoletti, S., and Vittur, F. (2005) The aggregation of pig articular chondrocyte and synthesis of extracellular matrix by a lactose-modified chitosan. *Biomaterials 26* (9), 987−98.
(15) (a) Marsich, E., Travan, A., Feresini, M., Lapasin, R., Paoletti, S., and Donati, I. (2013) Polysaccharide-Based Polyanion−Polycation−Polyanion Ternary Systems in the Concentrated Regime and Hydrogel Form. *Macromol. Chem. Phys. 214* (12), 1309−1320. (b) Sacco, P., Furlani, F., Cok, M., Travan, A., Borgogna, M., Marsich, E., Paoletti, S., and Donati, I. (2017) Boric Acid Induced Transient Cross-Links in Lactose-Modified Chitosan (Chitlac). *Biomacromolecules 18* (12), 4206−4213. (c) Cok, M., Sacco, P., Porrelli, D., Travan, A., Borgogna, M., Marsich, E., Paoletti, S., and Donati, I. (2018) Mimicking mechanical response of natural tissues. Strain hardening induced by transient reticulation in lactose-modified chitosan (chitlac). *Int. J. Biol. Macromol. 106*, 656−660.
(16) Travan, A., Marsich, E., Donati, I., Foulc, M.-P., Moritz, N., Aro, H. T., and Paoletti, S. (2012) Polysaccharide-Coated Thermosets for Orthopedic Applications: From Material Characterization to In Vivo Tests. *Biomacromolecules 13* (5), 1564−1572.
(17) Lei, M., Liu, S.-q., and Liu, Y.-l. (2008) Resveratrol protects bone marrow mesenchymal stem cell derived chondrocytes cultured on chitosan-gelatin scaffolds from the inhibitory effect of interleukin-1β. *Acta Pharmacol. Sin. 29*, 1350.
(18) Marsich, E., Borgogna, M., Donati, I., Mozetic, P., Strand, B. L., Salvador, S. G., Vittur, F., and Paoletti, S. (2008) Alginate/lactose-modified chitosan hydrogels: a bioactive biomaterial for chondrocyte encapsulation. *J. Biomed. Mater. Res., Part A 84* (2), 364−76.
(19) Mendoza, G., Regiel-Futyra, A., Andreu, V., Sebastián, V., Kyzioł, A., Stochel, G., and Arruebo, M. (2017) Bactericidal Effect of Gold−Chitosan Nanocomposites in Coculture Models of Pathogenic Bacteria and Human Macrophages. *ACS Appl. Mater. Interfaces 9* (21), 17693−17701.
(20) Marsich, E., Travan, A., Donati, I., Di Luca, A., Benincasa, M., Crosera, M., and Paoletti, S. (2011) Biological response of hydrogels embedding gold nanoparticles. *Colloids Surf., B 83* (2), 331−9.
(21) Barrow, H., Rhodes, J. M., and Yu, L. G. (2011) The role of galectins in colorectal cancer progression. *Int. J. Cancer 129* (1), 1−8.
(22) Dalotto-Moreno, T., Croci, D. O., Cerliani, J. P., Martinez-Allo, V. C., Dergan-Dylon, S., Méndez-Huergo, S. P., Stupirski, J. C., Mazal, D., Osinaga, E., Toscano, M. A., Sundblad, V., Rabinovich, G. A., and Salatino, M. (2013) Targeting Galectin-1 Overcomes Breast Cancer-Associated Immunosuppression and Prevents Metastatic Disease. *Cancer Res. 73* (3), 1107−1117.
(23) Szöke, T., Kayser, K., Baumhäkel, J. D., Trojan, I., Furak, J., Tiszlavicz, L., Horvath, A., Szluha, K., Gabius, H. J., and Andre, S. (2005) Prognostic Significance of Endogenous Adhesion/Growth-Regulatory Lectins in Lung Cancer. *Oncology 69* (2), 167−174.
(24) Saussez, S., Camby, I., Toubeau, G., and Kiss, R. (2007) Galectins as modulators of tumor progression in head and neck squamous cell carcinomas. *Head & Neck 29* (9), 874−884.
(25) Chow, S. N., Chen, R. J., Chen, C. H., Chang, T. C., Chen, L. C., Lee, W. J., Shen, J., and Chow, L. P. (2010) Analysis of protein profiles in human epithelial ovarian cancer tissues by proteomic technology. *Eur. J. Gynaecol Oncol 31* (1), 55−62.
(26) Laderach, D. J., Gentilini, L. D., Giribaldi, L., Delgado, V. C., Nugnes, L., Croci, D. O., Al Nakouzi, N., Sacca, P., Casas, G., Mazza, O., Shipp, M. A., Vazquez, E., Chauchereau, A., Kutok, J. L., Rodig, S. J., Elola, M. T., Compagno, D., and Rabinovich, G. A. (2013) A unique galectin signature in human prostate cancer progression suggests galectin-1 as a key target for treatment of advanced disease. *Cancer Res. 73* (1), 86−96.
(27) Gandhi, M. K., Moll, G., Smith, C., Dua, U., Lambley, E., Ramuz, O., Gill, D., Marlton, P., Seymour, J. F., and Khanna, R. (2007) Galectin-1 mediated suppression of Epstein-Barr virus−specific T-cell immunity in classic Hodgkin lymphoma. *Blood 110* (4), 1326−1329.
(28) Thijssen, V. L., Heusschen, R., Caers, J., and Griffioen, A. W. (2015) Galectin expression in cancer diagnosis and prognosis: A systematic review. *Biochim. Biophys. Acta, Rev. Cancer 2*, 235−47.
(29) Astorgues-Xerri, L., Riveiro, M. E., Tijeras-Raballand, A., Serova, M., Neuzillet, C., Albert, S., Raymond, E., and Faivre, S. (2014) Unraveling galectin-1 as a novel therapeutic target for cancer. *Cancer Treat. Rev. 40* (2), 307−19.
(30) Pieters, R. J. (2006) Inhibition and Detection of Galectins. *ChemBioChem 7* (5), 721−728.
(31) Bourne, Y., Bolgiano, B., Liao, D.-I., Strecker, G., Cantau, P., Herzberg, O., Feizi, T., and Cambillau, C. (1994) Crosslinking of mammalian lectin (galectin-1) by complex biantennary saccharides. *Nat. Struct. Mol. Biol. 1*, 863.
(32) Rajeeva, B. B., Hernandez, D. S., Wang, M., Perillo, E., Lin, L., Scarabelli, L., Pingali, B., Liz-Marzán, L. M., Dunn, A. K., Shear, J. B., and Zheng, Y. (2015) Regioselective Localization and Tracking of Biomolecules on Single Gold Nanoparticles. *Advanced Science 2* (11), 1500232.
(33) Richman, S. A., Kranz, D. M., and Stone, J. D. (2009) Biosensor detection systems: engineering stable, high-affinity bioreceptors by yeast surface display. *Methods in molecular biology (Clifton, N.J.) 504*, 323−50.
(34) Vo-Dinh, T. (2008) Nanosensing at the single cell level(). *Spectrochim. Acta, Part B 63* (2), 95−103.
(35) Moustaoui, H., Movia, D., Dupont, N., Bouchemal, N., Casale, S., Djaker, N., Savarin, P., Prina-Mello, A., de la Chapelle, M. L., and Spadavecchia, J. (2016) Tunable Design of Gold(III)-Doxorubicin Complex-PEGylated Nanocarrier. The Golden Doxorubicin for Oncological Applications. *ACS Appl. Mater. Interfaces 8* (31), 19946−57.
(36) Miller, M. C., Nesmelova, I. V., Platt, D., Klyosov, A., and Mayo, K. H. (2009) The carbohydrate-binding domain on galectin-1 is more extensive for a complex glycan than for simple saccharides: implications for galectin-glycan interactions at the cell surface. *Biochem. J. 421* (2), 211−21.
(37) Collins, B. E., and Paulson, J. C. (2004) Cell surface biology mediated by low affinity multivalent protein-glycan interactions. *Curr. Opin. Chem. Biol. 8* (6), 617−25.
(38) Bumba, L., Laaf, D., Spiwok, V., Elling, L., Kren, V., and Bojarova, P. (2018) Poly-N-Acetyllactosamine Neo-Glycoproteins as Nanomolar Ligands of Human Galectin-3: Binding Kinetics and Modeling. *Int. J. Mol. Sci. 19* (2), 372.

DOI: 10.1021/acs.bioconjchem.8b00520
Bioconjugate Chem. XXXX, XXX, XXX−XXX

(39) Stowell, S. R., Arthur, C. M., Mehta, P., Slanina, K. A., Blixt, O., Leffler, H., Smith, D. F., and Cummings, R. D. (2008) Galectin-1, −2, and −3 exhibit differential recognition of sialylated glycans and blood group antigens. *J. Biol. Chem. 283* (15), 10109−23.
(40) Marguerit, G., Moustaoui, H., Haddada, M. B., Djaker, N., Chapelle, M. L., and Spadavecchia, J. (2018) Taxanes Hybrid Nanovectors: From Design to Physico-Chemical Evaluation of Docetaxel and Paclitaxel Gold (III)-PEGylated Complex Nanocarriers. *Particle & Particle Systems Characterization 35* (2), 1700299.
(41) Johannes, L., Wunder, C., and Shafaq-Zadah, M. (2016) Glycolipids and Lectins in Endocytic Uptake Processes. *J. Mol. Biol. 428*, 4792.
(42) Cousin, J. M., and Cloninger, M. J. (2016) The Role of Galectin-1 in Cancer Progression, and Synthetic Multivalent Systems for the Study of Galectin-1. *Int. J. Mol. Sci. 17* (9), 1566.
(43) Chuang, C.-H., Du, Y.-C., Wu, T.-F., Chen, C.-H., Lee, D.-H., Chen, S.-M., Huang, T.-C., Wu, H.-P., and Shaikh, M. O. (2016) Immunosensor for the ultrasensitive and quantitative detection of bladder cancer in point of care testing. *Biosens. Bioelectron. 84*, 126−132.
(44) Ebrahim, A. H., Alalawi, Z., Mirandola, L., Rakhshanda, R., Dahlbeck, S., Nguyen, D., Jenkins, M., Grizzi, F., Cobos, E., Figueroa, J. A., and Chiriva-Internati, M. (2014) Galectins in cancer: carcinogenesis, diagnosis and therapy. *Annals of Translational Medicine 2* (9), 88.
(45) Besford, Q. A., Wojnilowicz, M., Suma, T., Bertleff-Zieschang, N., Caruso, F., and Cavalieri, F. (2017) Lactosylated Glycogen Nanoparticles for Targeting Prostate Cancer Cells. *ACS Appl. Mater. Interfaces 9* (20), 16869−16879.
(46) Belitsky, J. M., Nelson, A., Hernandez, J. D., Baum, L. G., and Stoddart, J. F. (2007) Multivalent interactions between lectins and supramolecular complexes: Galectin-1 and self-assembled pseudopolyrotaxanes. *Chem. Biol. 14* (10), 1140−51.
(47) Xu, B., Chow, M.-J., and Zhang, Y. (2011) Experimental and Modeling Study of Collagen Scaffolds with the Effects of Crosslinking and Fiber Alignment. *Int. J. Biomater. 2011*, 172389.

DOI: 10.1021/acs.bioconjchem.8b00520
Bioconjugate Chem. XXXX, XXX, XXX−XXX

Supporting information

Lactose-modified chitosan gold (III)-PEGylated complex-bioconjugates: from synthesis to interaction with targeted Galectin-1 protein

Qiqian Liu[1‡], Pasquale Sacco[4‡], Eleonora Marsich[5], Franco Furlani[4], Celia Arib[1], Nadia Djaker[1], Marc Lamy de la Chapelle, [2,3] Ivan Donati[4], Jolanda Spadavecchia[1*]

[1] *CNRS, UMR 7244, CSPBAT, Laboratoire de Chimie, Structures et Propriétés de Biomateriaux et d'Agents Therapeutiques Université Paris 13, Sorbonne Paris Cité, Bobigny, France*

[2]*Institut des Molécules et Matériaux du Mans (IMMM - UMR CNRS 6283),Le Mans Université, Avenue Olivier Messiaen, 72085 Le Mans cedex 9, France.*

[3]*Department of Clinical Laboratory Medicine, Southwest Hospital, Third Military Medical University, Chongqing, China*

[4]*Department of Life Sciences, University of Trieste, Via L. Giorgieri 5, I-34127 Trieste, Italy*

[5] *Department of Medicine, Surgery and Health Sciences, University of Trieste, Piazza dell'Ospitale 1, I-34129 Trieste, Italy*

Corresponding Author*: jolanda.spadavecchia@univ-paris13.fr

ADDITIONAL FIGURES

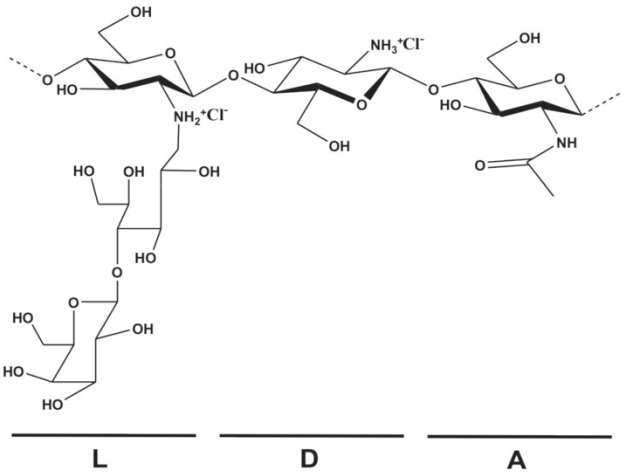

Figure S1. Schematic representation of CTL structure.

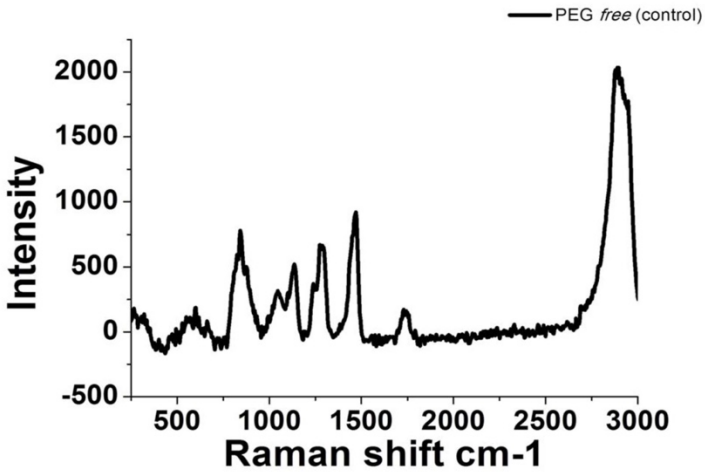

Figure S1-A: Raman spectra of the PEG *free* as control. Experimental conditions: λ_{exc} = 785 nm; laser power 20 mW; accumulation time 180 s.

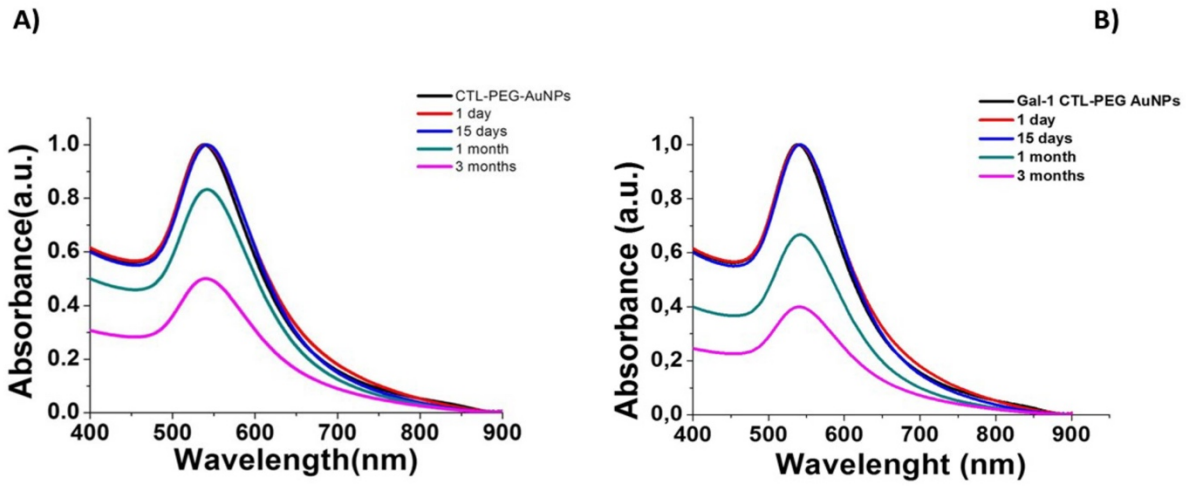

Figure S2. Changes in the UV-Vis absorption spectra of CTL-PEG-AuNPs (A) and Gal-1 CTL-PEG-AuNPs (B) when incubated in buffer solution at pH 4.0 and up to three months.

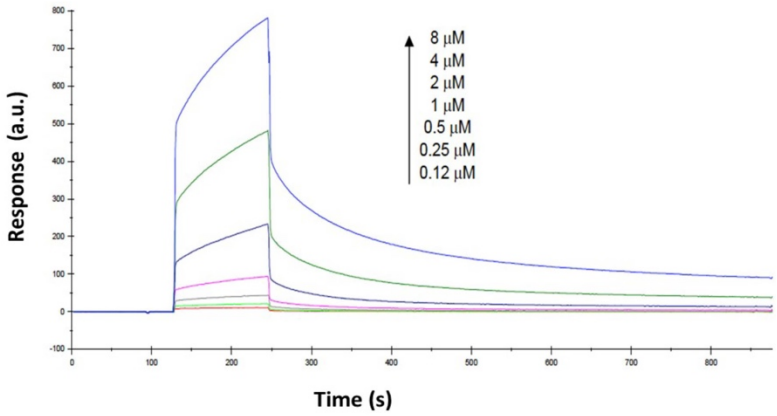

Figure S3. Sensorgram curves of the binding of Gal-1 to CTL after baseline adjustment. Increasing concentrations of Gal-1 were used, as shown in the graph. All the curves were subtracted from solvent signals. Data loaded from the instrument result files were analyzed as sensorgrams using the BIAevaluation 3.2 Software (Biacore), following the steps indicated in the user manual. For kinetic data evaluation, sensorgram data fitting for simultaneous ka/kd was performed using a simple model for 1:1 (Langmuir) binding. Software default settings parameters were chosen. Fitting of the curves to the 1:1 interaction model was performed using global settings for ka and kd and analyte concentration

was used as input values for the fitting procedure. The suitability of the fitting model was confirmed by analysis of the systematic deviations (scatter) between the experimental and the fitted data in the residual plots and by a chi^2 equal to 5.8. For evaluation of steady state affinity data, a plot of Req against protein concentration was created, using software tools and this plot was fitted to the general fitting model "Steady state affinity".

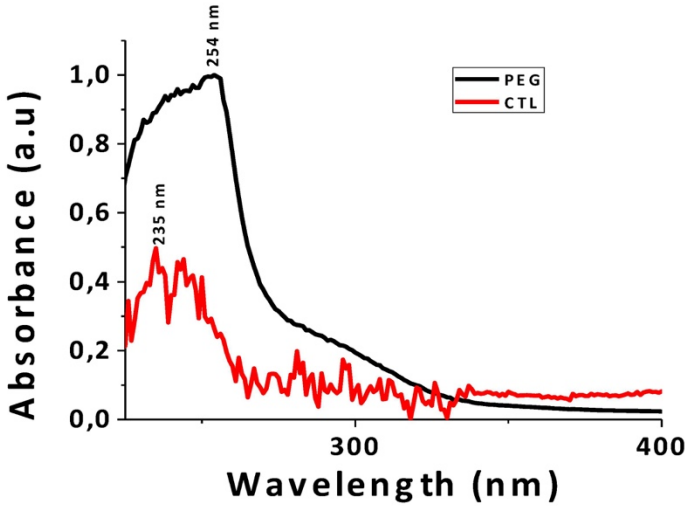

Figure S4. UV-Vis absorption spectra of CTL and PEG as control in the range 200-900 nm.

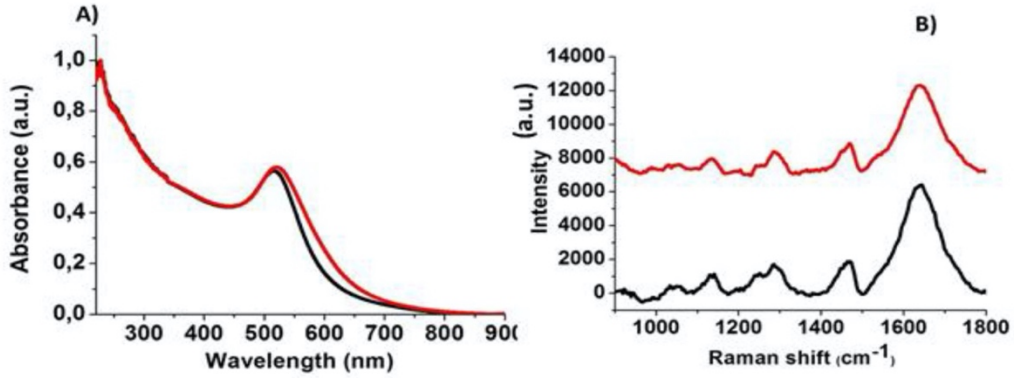

Figure S5. A) UV-Vis absorption spectra of PEG-AuNPs before (black line) and after interaction with Gal-1 at 1 μM (red line) in the spectroscopical range 200-900 nm. B) Raman spectra of the PEG-AuNPs (black line) and Gal-1 PEG-AuNPs (Gal-1 1 μM) (red line). Experimental conditions: λ_{exc} = 785 nm; laser power 20 mW; accumulation time 180 s.

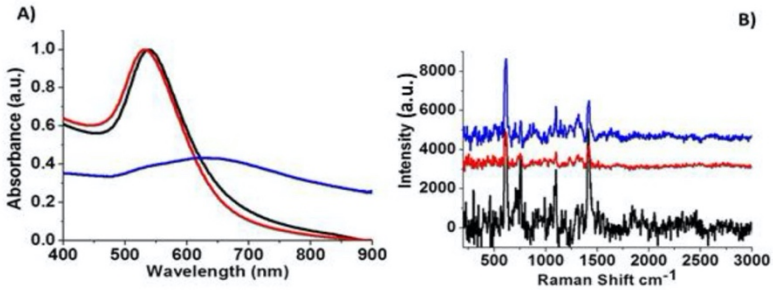

Figure S6. A) UV-Vis absorption spectra of CTL-PEG-AuNPs before (black line) and after interaction with Col at 1 pM (red line) and at 1 μM (blue line) in the spectroscopical range 400-900 nm. B) Raman spectra of the CTL-PEG-AuNPs (black line) and Col-CTL-PEG-AuNPs (Col concentration 1 pM (red line) and 1 μM (blue line)). Experimental conditions: λ_{exc} = 785 nm; laser power 20 mW; accumulation time 180 s.

ADDITIONAL TABLES

Table S1. ζ-potential and hydrodynamic diameter of CTL-PEG-AuNPs (control) and Gal-1-CTL-PEG-AuNPs.

Synthetic product	ζ-potential (mV)	Hydrodynamic diameter (nm)	PDI
CTL-PEG-Au NPs	-29 ± 2	18 ± 2	0.3 ± 2
Gal-1-CTL-PEG-AuNPs	-25 ± 1	30 ± 2	0.7 ± 2

2.3 Conclusion

In this publication, we studied for the first time the bio-interaction between Gal-1 and CTL-PEGylated gold nanoparticles. The analysis of the UV-visible and Raman spectra allowed us to highlight the formation of agglomerates of gold nanoparticles due to high binding affinity between Gal-1 and CTL onto gold nanoparticles. We observed some dissociation of gold nanopartciles for specific Gal-1 concentrations giving evidence of the interaction of the protein with the CTL by SPR analyze. This publication provides us a better understanding of the interaction mechanism (chemical structure modifications, kinetic interaction) and allows an optimisation of the sensing abilities since the detection sensitivity is directly related with the affinity of the bioreceptor to the analyte.

Nowadays there are many methods for specific detection of proteins, we could specially divide in two categories: the separation methods and the antibody dependent methods

The former methods include: high-performance liquid chromatography (HPLC) to detect proteins or peptides and liquid chromatography coupled with mass spectrometry (LC/MS) to detect proteins at low concentrations (ng/mL to pg/mL) in blood and body fluids.

The latter methods includes: immune sorbent assay (ELISA, detection of proteins down to pg/mL, the immunoprecipitation (technique of precipitating a protein antigen out of solution using an antibody), the immunoeletrophoresis (separation and characterization of proteins based on electrophoresis and reaction with antibodies), the Western blot(coupling of the gel electrophoresis and the incubation with antibodies to detect specific proteins in a sample of tissue) and the protein immunostaining (immunostaining is any use of an antibody -based method to detect a specific protein in a sample)

All these methods are time consuming and need complex sample preparations. They only provide a detection method but have no therapeutic purpose. Conversely, the nanoparticles could provide theranostic effect that is a clear advantage for such kind of objects. In this work, we first demonstrated the easy and fast cancers biomarker detection using AuNP bearing CTL whereas we will demonstrate in the following chapter (chapter 3) their ability to target specific cancer cells and be used as nanovector for cancer therapy.

This work was carried out in collaboration with the Department of Life Sciences of the University of Trieste and the CTL was provided by Doctor Pasquale Sacco.

2.4 Galectin-1 protein modified gold (III)-PEGylated complex-nanoparticles: Proof of concept of alternative probe in colorimetric glucose detection

2.4.1 Glucose

Glucose is a vital substance for human being and plays an important role in cell metabolism. It is needed in many cells for energy processes, its metabolism providing energy in the form of adenosine triphosphate (ATP). It is also essential for the synthesis of important cellular

constituents: macromolecules containing sugars such as glycoproteins and nucleic acids. But cancer is a disease at the cellular level involving heritable disorders in cellular control mechanism. Cancer cells also need to adapt their metabolism to survive and multiply under the metabolically compromised conditions provided by the tumor-microenviroment .Tumor cells alter their metabolism to maintain unregulated cellular proliferation and survival, but this transformation leaves them reliant on constant supply of nutrients and energy. They alter their metabolism to support their rapid proliferation and expansion across the body. After the discovery of the altered cancer cell metabolism in 1930, lot of studies have shed light on several aspects of cancer metabolism with a common goal to find new ways for effectively eliminating tumor cells by targeting their energy metabolism. Research has directed most of its resources to elucidate the causes, to prevent its apparition and possibly to cure for cancer. Yet the process has been elusive claiming human lives more than ever. This disease is a manifestation of etiological and pathological disturbances of mechanisms that control cell division, differentiation and metabolism. 50% of all human tumors carry genetic alterations that lead to the inactivation of some tumor suppressor proteins. Cancer cells are shown to experience characteristic changes in their metabolic programs, including increased uptake of glucose, enhanced rates of glutaminolysis and fatty acids synthesis, suggesting that metabolic shifts supports tumor cells growth and survival. Otto Warburg observed that, even in the presence of oxygen, human and animal tumors prefer to convert glucose into lactate instead of utilizing the mitochondrial metabolism and the oxidative phosphorylation chain for energy production .His observation is supported by the elevated levels of lactate dehydrogenase that have been found in various cancers .This preferred conversion of glucose to lactate in the presence of oxygen is known as aerobic glycolysis or the “Warburg effect”. Readers are referred to these recent excellent reviews on the regulation of glucose metabolism in cancer cells [19], [20], [21], [22]. Thus, it’s very important to make a fast detection with glucose.

There are many different methods to detect Glucose: like Copper-iodometric methods, enzymatic methods, Glucose meters, Non-enzymatic glucose sensors, high performance liquid chromatography (HPLC), etc. But the colorimetric glucose detection using nanoparticles is a novel method that gives new perspectives of analysis. In this publication we provided an evidence that the Gal-1 interacts with glucose under gold complex and we have experimented two synthesis methods: the first one is the bioconjugation of Gal-1 onto PEG-AuNPs (Gal-1 ON PEG

AuNPs) whereas the other one is the bioconjugation of Gal-1 into PEG-AuNPs (Gal-1 IN PEG-AuNPs), interestingly these two methods give different results (figure2.4)

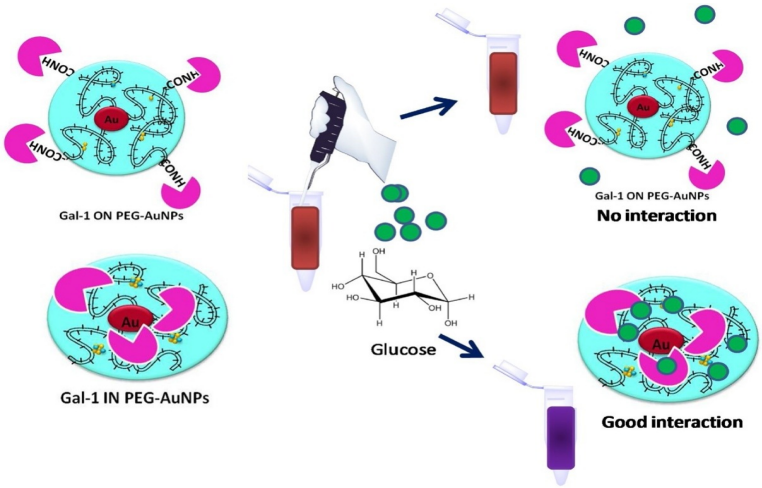

Figure 2.4 Method in and method on in different results

2.5 Publication 2

Galectin-1 protein modified gold (III)-PEGylated complex-nanoparticles: Proof of concept of alternative probe in colorimetric glucose detection

Colloids and Surfaces B: Biointerfaces 185 (2020) 110588

Contents lists available at ScienceDirect

Colloids and Surfaces B: Biointerfaces

journal homepage: www.elsevier.com/locate/colsurfb

Galectin-1 protein modified gold (III)-PEGylated complex-nanoparticles: Proof of concept of alternative probe in colorimetric glucose detection

Qiqian Liu[a,b], Fatima Aouidat[a], Pasquale Sacco[c], Eleonora Marsich[d], Nadia Djaker[a], Jolanda Spadavecchia[a,b,*]

[a] CNRS, UMR 7244, NBD-CSPBAT, Laboratoire de Chimie, Structures et Propriétés de Biomatériaux et d'Agents Thérapeutiques Université Paris 13, Sorbonne Paris Cité, Bobigny, France
[b] Department of Clinical Laboratory Medicine, Southwest Hospital, Third Military Medical University, Chongqing, China
[c] Department of Life Sciences, University of Trieste, Via L. Giorgieri 5, I-34127 Trieste, Italy
[d] Department of Medicine, Surgery and Health Sciences, University of Trieste, Piazzale Europa 1, I-34127 Trieste, Italy

ARTICLE INFO

Keywords:
Galectin-1
AuNPs
Biomolecules colloid functionalization
LSPR
SERS

ABSTRACT

Galectins (Gal) are a family of dimeric lectins, composed by two galactoside-binding sites implicated in the regulation of cancer progression and immune responses. In this study, we report for the first time the synthesis and the physical-chemical characterization of galectin-1-complex-gold COOH-terminated **polyethlenglicole** (PEG)-coated NPs **(Gal-1 IN PEG-AuNPs)** and their ability to recognize glucose in an aqueous solution with a concentration varying from 10 mM to 100 pM. The chemical protocol consistsof three steps: (*i*) complexation between galectin-1Gal-1 and tetrachloroauric acid ($HAuCl_4$) to form gold-protein grains; (*ii*) staking process of COOH-terminated **polyethlenglicole** molecules (PEG) onto Gal-1-Au complex and (*iii*) reduction of hybrid metal ions to obtain a colloidal stable solution. During the complexation, the spectral signatures related to the Gal-1 orientation on the gold surface have been found to change due to its protonation state. The effective glucose monitoring was detected by UV–vis, Raman spectroscopy and Transmission Electron Microscopy (TEM). Overall, we observed that the interaction is strongly dependent on the Gal-1 conformation at the surface of gold nanoparticles.

1. Introduction

Gold-based nanomaterials have been catching much attention in many areas, such as chemistry, physics, materials science, and biosciences, because of their size- and shape-dependent optic, electric, and catalytic properties [1–3]. Synthesis of spherical gold nanoparticles (AuNPs) involves the chemical reduction of chloroauric acid ($HAuCl_4$) by using sodium borohydride ($NaBH_4$) and sodium citrate as the reducing agents, thus lowering particle size up to 2–10 and 10–40 nm, respectively [4,5]. The "green" approach for synthesizing gold nanoparticles (AuNPs) by using natural macromolecules has been attracted growing interest over the last few decades [6,7]. The green natural compounds were reported to favour the synthesis of well-dispersed AuNPs [8]. Among screened bio-macromolecules, proteins have been widely used in nanocluster (< 1 nm) synthesis, hence representing ideal candidates for AuNPs formation [9].

In the latest years, Spadavecchia et al. have in-depth investigated the synthesis of hybrid nanoparticles based on drugs and/or biomolecules-gold-complex by an experimental approach named "Method IN", in which the drugs or biomolecules interact actively with gold salt ($HAuCl_4$) by chelation bonding. A biocompatible polymer molecule (PEG diacid) acts as surfactant, in order to form hybrid gold nanoparticles upon reduction by $NaBH_4$ [10–12].

The same authors have synthetized hybrid metal nanoparticles based on chitosan and on chitosan-derivatives as sugar stabilizers, for the detection and the tracking of the galectin-1 protein as biomarker [13]. Galectin-1 (Gal-1) is a lectin differentially expressed in different tissues, and plays a key role in biological systems [14]. It has been recently unveiled that Gal-1 over expression is correlated with tumour aggressiveness [15]. Some studies claim the thesis that this protein might represent a promising therapeutic marker in cancer [14,16].

Some structural studies with Gal-1 have explored its binding to simple carbohydrates, especially lactose and *N*-acetyl-lactosamine [17]. However, it was established that Gal-1 interacts at the cell surface with

* Corresponding author at: CNRS, UMR 7244, NBD-CSPBAT, Laboratoire de Chimie, Structures et Propriétés de Biomatériaux et d'Agents Thérapeutiques Université Paris 13, Sorbonne Paris Cité, Bobigny, France.
E-mail address: jolanda.spadavecchia@univ-paris13.fr (J. Spadavecchia).

https://doi.org/10.1016/j.colsurfb.2019.110588
Received 18 July 2019; Received in revised form 20 September 2019; Accepted 14 October 2019
Available online 15 October 2019

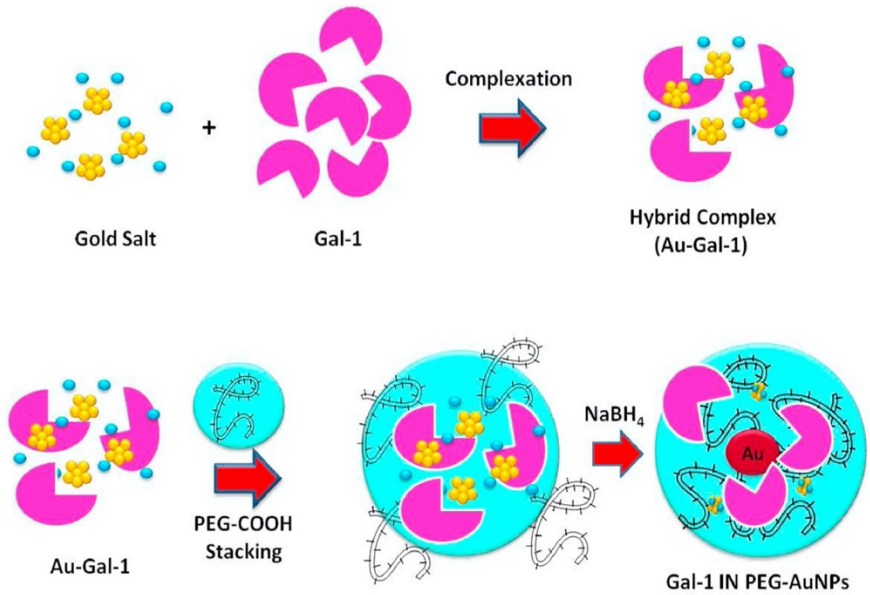

Scheme 2. Representation of the synthesis of Gal-1 IN PEG-AuNPs (Please note that drawings are not in scale and are not intended to be representative of the full samples composition).

2.8. Incubation of Gal-1 ON PEG-AuNPs and Gal-1 IN PEG-AuNPs with Glucose

The interaction of Glucose with Gal-1 ON PEG-AuNPs and Gal-1 IN PEG-AuNPs surface was achieved through the protocols **of incubation** described below: 900 µL of Gal-1 ON PEG-AuNPs and Gal-1 IN PEG-AuNPs (1 mM) were added into separate tubes containing 100 µL of Glucose (from 10 mM to 100 pM; PBS pH 7; NaCl 0.15 M). After 18 h of incubation, the NPs/Glucose suspension was centrifuged twice at 5000 rpm for 10 min to eliminate the excess of Glucose and then the pellets were redispersed in 1 mL of Milli-Q water.

2.9. Physical-Chemical characterization

All characterizations were carried out in triplicate determinations as described previously [13,28,29].

2.10. UV/Vis measurements

Absorption spectra were recorded by using a double-beam Varian Cary 500 UV–vis spectrophotometer (Agilent, France). UV–vis spectra of the NPs were recorded in water at a concentration of 1 mM in the 200–900 nm spectral range.

2.11. Transmission Electron Microscopy (TEM)

Transmission Electron Microscopy (TEM) images were recorded with a JEOL JEM 1011 microscope operating (JEOL, USA) at an accelerating voltage of 100 kV. TEM specimens were prepared after separating the surfactant from the metal particles by centrifugation under a protocol described elsewhere [28,21].

2.12. Raman Spectroscopy

The Raman experiments have been performed on an Xplora spectrometer (Horiba Scientifics-France)witha protocol described previously [28].

2.13. Dynamic light scattering (DLS) and Zeta potential measurements

The size and zeta potential measurements were performed by using a Zetasizer Nano ZS (Malvern Instruments, Malvern, UK) equipped with a He-Ne laser (633 nm, fixed scattering angle of 173°) at room temperature as described previously [28].

2.14. Stability of Gal-1 IN-PEG-AuNPs versus pH

The stability of Gal-1 ON-PEG AuNPs was described previously [13], the stability of Gal-1 IN-PEGAuNPs was detected by UV–vis. All nanoparticles were dissolved in PBS solution 10 mM at pH 5.5 and stored for 3 months (Figure S1 in Supporting Information).

3. Results and discussion

Functional protein–nanoparticle bioconjugates are gaining increasing attention in biomedical sectors such as drug delivery and biosensing [32].

Parak et al., have implemented a methodology to obtain protein–gold nanoparticle bioconjugates with a focus on site-specific attachment of protein on AuNPs [9]. The same authors have demonstrated that lysine groups are involved during the growth of nanoparticles formation.

This study aims at explaining the formation of stable complexes of PEGylated Au (III)–Gal-1 as building blocks of gold nanoparticles

The final goal is to evaluate the grafting of the Galectin-1 protein (Gal-1) at the surface of the PEG-AuNPs by carbodiimide chemistry (**method ON**) and chelation bond (**method IN**) in order to study the interactions with glucose under two different chemical conformations.

3.1. Conjugation of Gal-1 onto (Gal-1 ON PEG-AuNPs) and into (Gal-1 IN PEG-AuNPs) PEG-AuNPs

Previously, Spadavecchia et al. have grafted pegylated gold nanoparticles (PEG-AuNPs) with biomolecules by several chemical methodologies in order to evaluate therapeutic efficiencies [13,27,10,30]. Huang et al. adsorbed galectin-1 molecules onto citrate gold nanoparticles by an electrostatic approach in order to increase protein binding affinity to receptors by cross-linking CD45 on T cells [31].

Herein we designed and characterized the grafting of Gal-1 at the surface of the pegylated gold nanoparticles through the formation of amide links between the −COOH groups embedding the surface of the PEG-AuNPs and the -NH_2 groups of the protein by activation with EDC/NHS (method ON) (scheme 1).

The protocol used for the production of Gal-1 IN PEG-AuNPs involves the formation of Au (III)-Gal-1 complexes (Gal-1-$AuCl_4^-$), followed by PEG interactions with Gal-1-$AuCl_4^-$ clusters and formation of AuNPs. To the best of our knowledge, examples of AuNPs formation from stable Au^{3+} ions-Gal-1 complexes cannot be found in the scientific literature (method IN) (Scheme 2).

The aim of this paper is to assess the interactions between Gal-1 and glucose under formation of stable complexes of PEGylated Au(III) as active excipients of gold nanoparticles. The major discrepancy with other chemical procedures is that in our study Gal-1 participates to the nucleation and growth of AuNPs *via* complexation between the ketone of Asn 50 and the amino groups of phenylalanine side chains (Phe39, Phe49, Phe126) with chloride auric ions. In our case, the formation of gold NPs from $AuCl_4^-$comprehendsthe following steps (Scheme 2):

(1) Chelation of Gal-1 with $AuCl_4^-$ and inceptive reduction of the protein-metal complex to produce gold clusters;
(2) Embedding process of PEG by electrostatic adsorption onto the Gal-1gold clusters;
(3) Final reduction of metal ions and growth of a stable colloidal solution (AuNPs) through dicarboxylic PEG polymers.

In the first step, Gal-1 is added into $HAuCl_4$ aqueous solution to complex with him. In the second step, the PEG polymer chains diacide in water solution embedding a complex Gal-1-$AuCl_4^-$,plays a key role in the growth process of AuNPs. The addition of PEG in the Gal-1-$AuCl_4^-$solution improves the reduction kinetics through complexation with the Au ions [34]. This effect regulates the simultaneous chemical and steric arrangement of Gal-1 and PEG between $AuCl_4$- on the surface of gold seeds during the growth of nanoparticles. In the third step, the final reduction of metal ions in the presence of $NaBH_4$, generates the hybrid nanoparticles.

3.2. Physicochemical evaluation of Gal-1 ON PEG-AuNPs and Gal-1 IN PEG-AuNPs

The interaction between Gal-1 and PEG-AuNPs was monitored by UV–vis absorption spectra.

Fig. 1A shows the localized surface plasmon (LSP) band of PEG-AuNPs before (Fig. 1A, blue line) and after immobilization of Gal-1 by carbodiimide chemistry (Gal-1 ON PEG-AuNPs) (Fig. 1A, black line). After immobilization of Gal-1 onto PEG-AuNPs (Gal-1 ON PEG-AuNPs) the colour of the solution changes and the colloidal solution was characterized by UV–vis spectroscopy. The Gal-1 ON PEG-AuNPs showed a broad LSP peak at 548 nm, due to the change of localized refractive index of PEG-AuNPs [28]. The notable red-shift of the LSP band with a peak broadening in the Gal-1 ON PEG-AuNPs spectra, indicate a linear increase in particle size and modification of the nanoparticles surface [35]. Based on the UV–vis spectrum of Gal-1 ON PEG-AuNPs, we assume that such increase could be associated to the successful conjugation of the AuNPs surface with Gal-1, and the ulterior AuNPs agglomeration associated to the formation of classical van der Waals inter-protein interactions [28].

Concerning the chelation method (method IN), we observed a blue-shift from 548 nm to 538 nm (Fig. 1A, red line), due to π-π* electronic transitions between the Gal-1 and $AuCl_4^-$ ions, giving a common demonstration of the complex formation. The different shift of the plasmon band, indicate that each chemical protocol applied (ON and IN) is answerable of different chemical behavior of the Gal-1 from PEG-AuNPs. This will have remarkable impacts on the steric conformation of the Gal-1 at the PEG-AuNPs surface and distinct grafting kinetic. Infact, the chemical grafting will impact the steric place of the Gal-1. In the case of the carbodiimide grafting (EDC/NHS), the Gal-1 is situated directly at the gold surface embedded by a PEG layer while for the chelation method, the Gal-1 will be placed into the core of gold, surface

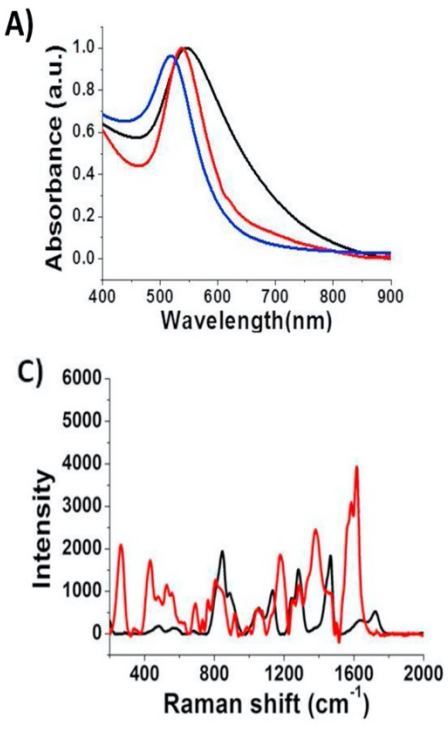

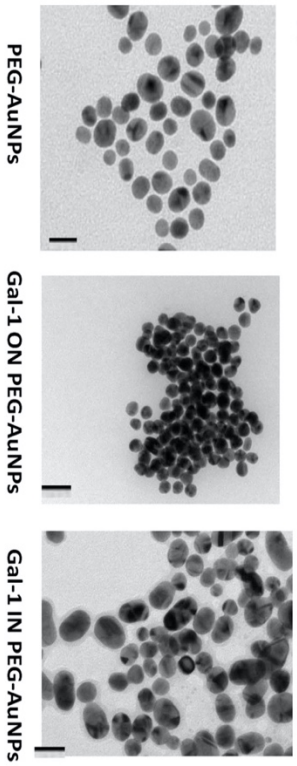

Fig. 1. (A) Normalized UV–vis absorption spectrum of **PEG-AuNPs** (blue line), **Gal-1 ON PEG-AuNPs** (black line), **Gal-1 IN PEG-AuNPs** (red line) in the spectral range (400–900 nm). **(B)** TEM images of PEG-AuNPs before and after conjugation of Gal-1 protein by carbodiimide chemistry (Gal-1 ON PEG-AuNPs) and chelation reaction **(**Gal-1 IN PEG-AuNPs) Scale bars: 50 nm; 10 nm. **(C)** Raman spectra of the Gal-1 IN PEG-AuNPs (red line) and Gal-1 ON PEG-AuNPs Experimental conditions: λ_{exc} = 785 nm; laser power 20 mW; accumulation time 180 s (For interpretation of the references to colour in this figure legend, the reader is referred to the web version of this article).

Table 1
z-potential and hydrodynamic diameter of PEG-AuNPs, Gal-1 ON PEG-AuNPs and Gal-1 IN PEG-AuNPs by carbodiimide and chelation chemistry.

Synthetic product	Zeta potential (mV)	Hydrodynamic diameter (nm)	PDI
PEG-AuNPs	−22 ± 1	10 ± 2	0.3 ± 2
Gal-1 ON PEG-AuNPs	−28 ± 1	15 ± 3	0.3 ± 2
Gal-1 IN PEG-AuNPs	−33 ± 1	30 ± 2	0.3 ± 2

folded of the PEG layer. This chemical attitude is due to a specific adsorption onto cristallographic gold facets [1.1.0] of Gal-1, that allows a different steric conformation of chemical groups during nucleation and growth process of PEG-AuNPs. This behavior was confirmed by TEM Images.

Fig. 1B displays a spherical pegylated gold nanoparticles showing a diameter of about 10 ± 2, in nice agreement with what observed previously [28]. After carbodiimide grafting, the Gal-1 ON PEG-AuNPs appears as circular agglomerate of nanoparticles decorated of a dense layer of polymer. Though the size of single protein was about 5 nm [36], we believe that Gal-1 takes a better place of PEG molecules onto the particles, with a specific steric arrangement. On the contrary, the shape of Gal-1 ON PEG-AuNPs, Gal-1 IN PEG-AuNPs displays spherical gold nanoparticles, piled in a shell of PEG, with an almost analogous diameter of around 30 ± 2 nm (Fig. 1B**).** The Gal-1grafting is confirmed by DLS and Zeta potential measurements (Table 1). The hydrodynamic diameter is increased by around 10 nm, which means an increase of 5 nm of the hydrodynamic diameter. Furthermore, Zeta potential measurements display a straight forward negative surface charge, indicating that colloids are expected being stable at physiological pH (Table 1).

The stability of Gal-1 AuNPs in solution, was monitored by the Localized Surface Plasmon (LSP) band at 548 nm (Gal-1 ON PEG-AuNPs) and 538 nm (Gal-1 IN PEG-AuNPs). The analysis was carried out at pH 5.5 and electrolytic conditions. The synthesized Gal-1 IN PEG-AuNPs did show an almost negligible change in the LSP band position over a period of three months (Figure S1 in the Supporting Information). Some differences in term of LSP were observed between Gal-1 ON PEG-AuNPs and Gal-1 IN PEG-AuNPs, due to the different chemical behavior of Gal-1as function of size and shape respectively.

The Raman spectra of Gal-1 ON PEG-AuNPs (**black line**) and Gal-1 IN PEG-AuNPs (**red line**) (Fig. 1**-C**) in water exhibit many bands in the region 200-2000 cm^{-1}.One of the Raman fingerprint of the Gal-1 IN PEG-AuNPs is the presence of a band around 263 cm^{-1} and a double peak at 522-430 cm^{-1}. These bands can be assigned to the gold chloride stretches, ν (Au-Cl), and δ (O-Au-O) in aliphatic chains, and is a clear evidence of the formation of a complex between $AuCl_2$-, PEG and Gal-1 in solution. The common peak at 430 cm^{-1} is due to the vibrations δ (OH…O), ν (OH···O) of the PEG. Based on the spectrochemical and previously theoretical results, we assumed that Au^{3+} ions promoted the deprotonation of the PEG [11] in the presence of Gal-1. The spectra of PEG molecules free as control was previously described in literature [13,37]. Only few bands remain as the two bands around 1000 cm^{-1} and the one around 1620 cm^{-1}. The strong band at 1375 cm^{-1} is assigned to CO= carbonyl stretching of PEG-Gal-1and a double peak at 1045-1181 cm^{-1} is due to COC−− stretching in backbone of PEG after stacking onto gold nanoparticles. Furthermore, new bands also appear as an intense triplet at 1211-1243-1289 cm^{-1} due to CO− plane deformation of carboxylic acid and a strong peak at 1471 cm^{-1} and 1616 cm^{-1} assigned to ν COO−− stretching and amide II band with a small peak at 1584 cm^{-1} due to symmetric NH− stretching. In contrast, Gal-1 ON PEG-AuNPs showed Raman bands due to the presence of water and of the PEG molecules onto the gold surface of nanoparticles. Some news bands around 800–900 cm^{-1} appeared, confirming a different Gal-1 orientation onto AuNPs compared to Gal-1 IN-PEG-AuNPs. The main difference consists in the bands located on the range 1400–1500 cm^{-1}. The band at 1464 cm^{-1} confirms the amide band between dicarboxylic PEG molecules onto AuNPs and amino group of Gal-1.All these differences of bands are due to the variation of the steric conformation of the polymers and Gal-1 upon complexation.

3.3. Physicochemical evaluation of Galectin-1/Glucose Interaction

It was proved that Gal-1 binding to carbohydrates cross-links adjacent glycoconjugates to mediate biological activity [32]. Despite individual binding interactions with carbohydrates are weak [18], ligands for galectin-1 typically possess an array of carbohydrates to enhance the binding affinity [32].

In a previous paper [13], we proved the successful of the interaction between a branched polymer lactose-modified chitosan (CTL) with pegylated gold nanoparticles (PEG-AuNPs) and Gal-l.

Gal-1 binds relatively strongly to CTL, and CTL-PEG AuNPs showed a calculated affinity constant (1×10^5 M^{-1}) stronger than that reported in literature by Miller et al. [17]. For these reasons, we developed a novel methodology in which galectin-1 complexed to AuNPs, interacts rectly with carbohydrates (*i.e.* glucose) without chemical intermediate. In latest years, the detection of glucose with nanoparticles has attracted great interest for their optical properties [38].Previously, we described a novel synthesis of nanoparticles, in which Vmh2 protein class I of hydrofobin HFB from *P. ostreatus*, was exploited as original biomolecular probe in glucose with an affinity constant of 7.3 ± 0.3 mg mL^{-1}, corresponding to about 40 mM. Liu et al. have developed a quantitative colorimetric immunoassay based on glucose oxidase (GOx)- of 5 nm AuNPs that can detect prostate-specific antigen (PSA) cancer biomarkers from atto- to pico-molar levels [39].

In this study we present a novel methodology in order to detect the concentration of glucose under nM, in order to generate diagnostic biomarkers based on Galectin-1 protein.

For this purpose, Gal-1 PEG-AuNPs was used as building blocks to detect the biomolecular interaction with glucose. The glucose interaction with Gal-1 PEG-AuNPs was evaluated by UV–vis absorption (Fig. 2) and Raman spectroscopy (Fig. 5).

When Glucose was added to a colloidal solution of Gal-1 IN PEG-AuNps in the range from 10 mM to 100 pM, we observed a dynamic variation of LSP band and a dramatic color change after 15 min depending on the glucose amount (Fig. 2A–B). Lowering the concentration of glucose from 10 mM to 1 mM, a plasmon band red-shifted from 538 nm to 549 nm. This weak red shift of the plasmon band, can be explained by a lower nanoparticle aggregation and a dissociation of agglomerates after the addition of glucose at a concentration of 1 mM (Fig. 2A–C). It means that from 10 mM up to 1 mM, glucose interacts with the Gal-1 IN PEG-AuNPs inducing very small changes on the plasmon band (modification of the dielectric constant around the AuNPs with the addition of Gal-1 proteins and maybe few dissociations). At concentrations lower than 1 mM, a large number of glucose molecules interacts with the Gal-1 IN PEG-AuNPs forming a glucose monolayer at the AuNPs surface. At 100 μM we observed a formation of a broadened band at 748 nm due to the formation of cross-links between Gal-1 IN PEG-AuNPs and glucose. When the concentration of glucose decreases from 100 μM to 100 nM the resulting solution was colorless, with a decrease in the UV–vis spectrum intensity and a red-shift of around 20 nm (from 748 nm to 761 nm). A further decrease of the plasmon at 100 pM of glucose could be attributed to the change of localized refractive index near the NPs surface of a substantial amount

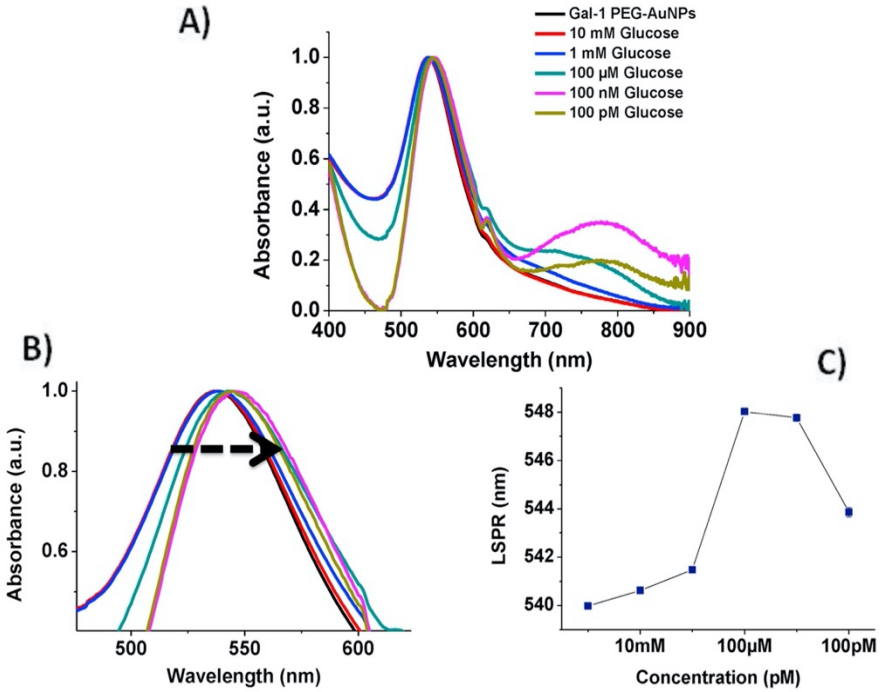

Fig. 2. A) UV–vis absorption spectra in the range 400–900 nm of Gal-1 IN PEG-AuNPs before (black line) and after interaction of glucose (from 10 mM to 100 pM); **B**) Zoom of UV–vis absorption spectra in the range 400–600 nm of Gal-1 IN PEG-AuNPs before and after interaction of glucose. **C**) Dynamic evolution of the Gal-1 IN PEG-AuNPs plasmonic bands *versus* the glucose concentration.

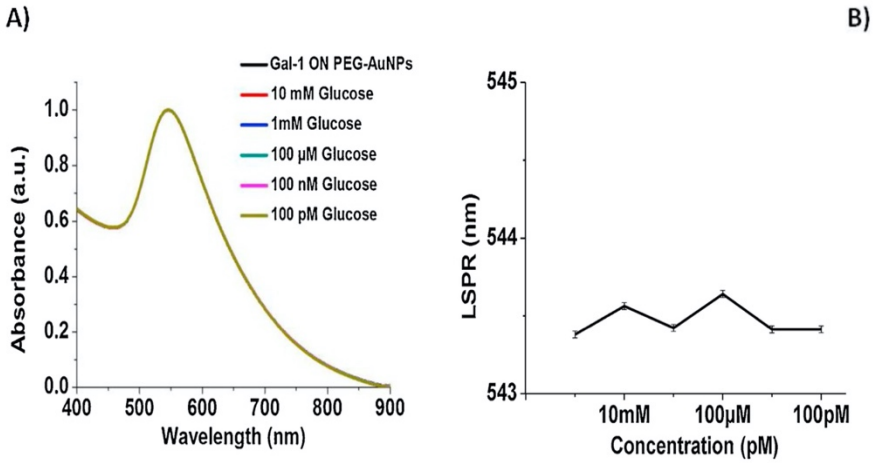

Fig. 3. A) UV–vis absorption spectra in the range 400–900 nm of Gal-1 ON PEG-AuNPs before (black line) and after interaction of glucose (from 10 mM to 100 pM);**B**) Dynamic evolution of the Gal-1 ON PEG-AuNPs plasmonic bands *versus* glucose concentration.

of plasmonic coupling, indicating that the glucose was conjugated to the Gal-1 IN PEG-AuNPs surface. We thus conclude that the selectively interacts with the Gal-1 IN PEG-AuNPs surface. The evolution of the Gal-1 IN PEG-AuNPs plasmonic bands *versus* the Gal-1 concentration is displayed in Fig. 2C.

The experiments carried out with Gal-1 ON PEG-AuNPs in order to evidence the selective binding of Gal-1 with glucose, did not revealed any remarkable spectroscopical modification of plasmonic bands (Figs. 3A–B).

For Gal-1 IN PEG-AuNPs, the formation of cross-links with glucose were further verified both by visual observations and by TEM analysis. We detected a pinkish-red color to the naked eye (Fig. 4panel A) and NPs with a characteristic spherical shape at 0 mM of glucose (Fig. 4panel B inset 1). The addition of 10 mM concentrations of glucose resulted in a slightly more purple color than the initial Gal-1 IN PEG-AuNPs conjugate. We assumed that at 10 mM, the galactoside-binding sites of galectin-1 have been saturated by glucose molecules, the latter forming a thin layer at the surface of nanoparticles. This prevents the link of nanoparticles to form some nanoclusters. When the concentration of glucose decreased at 1 mM, we observed a dramatic color change from red to purple with characteristic linear chains of gold nanoparticles (Fig. 4panel B inset 2). This behaviour is probably due to more galactoside-binding sites available with ensuing formation of nanoclusters between glucose the galectin-1 into nanoparticles [40] (Fig. 4panel B).When the glucose concentration was decreased from 100 µM to 100 pM, the color appeared to turn a purple grey color, and grew progressively transparent at concentrations of 100 pM with a consequent agglomeration of nanoparticles-conjugates until precipitation (Fig. 4panel B inset 3-4). This optical behaviour is opposite to a previous study, in which glucose was monitored in the presence of collagen-gold nanoparticles with a limit of detection of 0.18 mM [41]. In our case, the presence of galectin-1 complexed onto gold nanoparticles, improve the glucose interaction due to their better steric and chemical configuration.

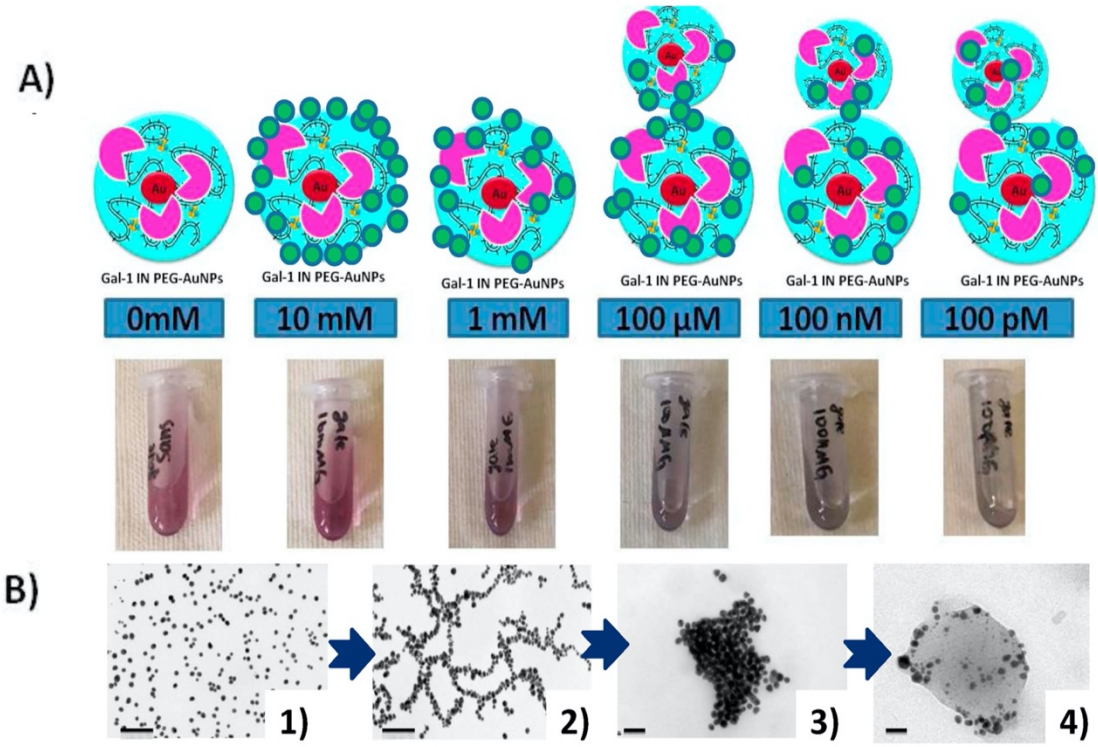

Fig. 4. A) Optical color change at different concentration of glucose and schematic mechanism of glucose interaction onto Gal-1 IN PEG-AuNPs; **B)** TEM images of Gal-1 IN PEG-AuNPs before (1) and after interaction of glucose (2-3–4). Scale bars: 100 nm; 20 nm (Please note that drawings are not in scale and are not intended to be representative of the full samples composition).

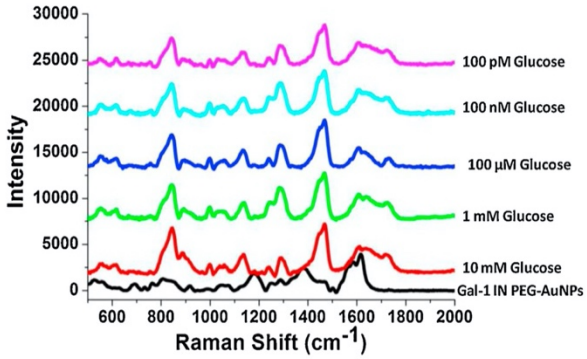

Fig. 5. A) Raman spectra of the Gal-1 IN PEG-AuNPs before (black line) and after interaction of glucose (glucose concentration range 10 mM - 100 pM); directional arrows show the characteristic peaks during glucose interaction. Experimental conditions: λ_{exc} = 785 nm; laser power 20 mW; accumulation time 180 s.

The successful interaction of glucose onto Gal-1 IN PEG-AuNPs surface was established by Raman spectroscopy at different glucose concentrations (10 mM-100 pM) (Fig. 5).The fingerprint detection of glucose onto Gal-1 IN PEG-AuNPs surface was demonstrated through the appearance of the Raman bands and SERS effect at 1250 cm^{-1}, 1472 cm^{-1} and 848 cm^{-1}due to the vibration of C—OH, COC and CO———— chemical groups, respectively (Fig. 5).

After the glucose interaction, 550–610 cm^{-1} the amide II (1587–1620 cm^{-1}) and amide III (1200–1300 cm^{-1} regions), as well as modifications in protein local environments, confirmed the protein interaction [42].

By evaluating the Raman results it is possible to confirm that the chemical and steric conformation of Gal-1 influences the detection of glucose onto Gal-1 IN PEG-AuNPs, when Gal-1 is complexed to gold salt. In fact, the interaction of glucose on the Gal-1 IN PEG-AuNPs will take place due to their great packing density as well as to the forces repulsion between the negatively charged Gal-1.Similar analyses of interaction (UV–vis and Raman) were carried out in the presence of PEG-AuNPs as control, under the same experimental conditions, confirming the selectivity of interaction betweenGal-1 IN PEG-AuNPs and glucose. Infact, after incubating PEG-AuNPs and glucose at maximal concentration (10 mM), we did not observe any signal variation as described previously [27].

3.4. Selectivity of Gal-1 IN PEG-AuNPs towards glucose

To confirm the selectivity of Gal-1 IN PEG-AuNPs *versus* glucose, a preliminary test in the presence of galactose, lactose and maltose were carried out. The interaction between Gal-1 IN PEG-AuNPs galactose, lactose and maltose was monitored by UV–vis and Raman spectroscopy (**Figure S2 in Supporting Information**), and did not show any remarkable spectroscopical modification. This means that there was no capture of the galactose, lactose and maltose at the Gal-1 IN PEG-AuNPs surface even at high concentration of sugar. We thus can conclude that the Gal-1 IN PEG-AuNPs surface selectively interacts with glucose.

3.5. Conclusions

In the present work Galectin-1 (Gal-1) was exploited as both a stabilizer of a nano-biosystem and an active biomolecular probe in glucose monitoring in order to evaluate further human health diseases. All experimental results highlighted that Gal-1IN PEG AuNPs manifested, for the first time, the ability to bind glucose even if intrinsically engaged with a gold complex by chelation methodology. In essence, a new hybrid bio/non-bio nanosystem was developed for both interface stabilization and biomolecular interaction monitoring applications. Indeed, in the second time, news galectin-1 nanoformulations will be internalized

in pancreatic cancer cells to detect the glucose produced under specific conditions. This study not only provides a new colorimetric assay for the simple detection of glucose for specific applications, *e.g.* predicted cancer and treatment, but also potentially offers a new analytical platform for understanding the molecular basis of physiological and pathological events.

Author contributions

The manuscript was written through contributions of all authors. All authors have given approval to the final version of the manuscript.

Acknowledgments

This work has been partly performed on the CNanoMat platform of the University Paris 13.

Appendix A. Supplementary data

Supplementary material related to this article can be found, in the online version, at doi:https://doi.org/10.1016/j.colsurfb.2019.110588.

References

[1] P. Suchomel, L. Kvitek, R. Prucek, A. Panacek, A. Halder, S. Vajda, et al., Simple size-controlled synthesis of Au nanoparticles and their size-dependent catalytic activity, Sci. Rep. 8 (2018) 4589.
[2] S. Ashraf, B. Pelaz, P. del Pino, M. Carril, A. Escudero, W.J. Parak, et al., Gold-based nanomaterials for applications in Nanomedicine, Top. Curr. Chem. 370 (2016) 169–202.
[3] P.-C. Chen, P. Roy, L.-Y. Chen, R. Ravindranath, H.-T. Chang, Gold and silver nanomaterial-based optical sensing systems, Part. Part. Syst. Charact. 31 (2014) 917–942.
[4] N.G. Bastús, J. Comenge, V. Puntes, Kinetically controlled seeded growth synthesis of citrate-stabilized gold nanoparticles of up to 200 nm: size focusing versus ostwald ripening, Langmuir 27 (2011) 11098–11105.
[5] M. Lawrence, A. Testen, T. Koklic, O. Smithies, A simple method for the size controlled synthesis of stable oligomeric clusters of gold nanoparticles under ambient conditions, J. Vis. Exp. (2016) e53388-e.
[6] E.H. Ismail, A.M.A. Saqer, E. Assirey, A. Naqvi, R.M. Okasha, Successful green synthesis of gold nanoparticles using a Corchorus olitorius extract and their antiproliferative effect in Cancer cells, Int. J. Mol. Sci. 19 (2018) 2612.
[7] Z. Molnár, V. Bódai, G. Szakacs, B. Erdélyi, Z. Fogarassy, G. Sáfrán, et al., Green synthesis of gold nanoparticles by thermophilic filamentous fungi, Sci. Rep. 8 (2018) 3943.
[8] A.-L. Morel, S. Giraud, A. Bialecki, H. Moustaoui, M.L. de La Chapelle, J. Spadavecchia, Green extraction of endemic plants to synthesize gold nanoparticles for theranostic applications, Front. Lab. Med. 1 (2017) 158–171.
[9] I. Chakraborty, N. Feliu, S. Roy, K. Dawson, W.J. Parak, Protein-mediated shape control of silver nanoparticles, Bioconjug. Chem. 29 (2018) 1261–1265.
[10] S.M. Celia Arib, A. Gerbino, J. Spadavecchia, Aptamer grafting onto (on) and into (in) pegylated gold nanoparticles: physicochemical characterization and in vitro cytotoxicity investigation in renal cells, J. Nanomed. Nanotechnol. 9 (2018) 520.
[11] H. Moustaoui, D. Movia, N. Dupont, N. Bouchemal, S. Casale, N. Djaker, et al., Tunable design of gold(III)-doxorubicin complex-PEGylated nanocarrier. the golden doxorubicin for oncological applications, ACS Appl. Mater. Interfaces 8 (2016) 19946–19957.
[12] G. Marguerit, H. Moustaoui, M.B. Haddada, N. Djaker, M.L. de la Chapelle, J. Spadavecchia, Taxanes hybrid nanovectors: from design to physico-chemical evaluation of Docetaxel and paclitaxel gold (III)-PEGylated complex nanocarriers, Part. Part. Syst. Charact. 35 (2018) 1700299.
[13] Q. Liu, P. Sacco, E. Marsich, F. Furlani, C. Arib, N. Djaker, et al., Lactose-modified chitosan gold(III)-PEGylated complex-bioconjugates: from synthesis to interaction with targeted Galectin-1 protein, Bioconjug. Chem. 29 (2018) 3352–3361.
[14] H. Blanchard, K. Bum-Erdene, M.H. Bohari, X. Yu, Galectin-1 inhibitors and their potential therapeutic applications: a patent review, Expert Opin. Ther. Pat. 26 (2016) 537–554.
[15] V.L. Thijssen, R. Heusschen, J. Caers, A.W. Griffioen, Galectin expression in cancer diagnosis and prognosis: a systematic review, Biochim. Biophys. Acta 2 (2015) 235–247.
[16] V. Balan, P. Nangia-Makker, A. Raz, Galectins as cancer biomarkers, Cancers. 2 (2010) 592–610.
[17] M.C. Miller, J.P. Ribeiro, V. Roldós, S. Martín-Santamaría, F.J. Cañada, I.A. Nesmelova, et al., Structural aspects of binding of α-linked digalactosides to human galectin-1, Glycobiology. 21 (2011) 1627–1641.
[18] J.M.C.M.J. Cloninger, Glycodendrimers: tools to explore multivalent galectin-1 interactions, Beilstein J. Org. Chem. 11 (2015) 739–747.
[19] E. Croteau, J.M. Renaud, M.A. Richard, T.D. Ruddy, F. Bénard, R.A. deKemp, PET metabolic biomarkers for Cancer, Biomark. Cancer 8 (2016) 61–69.
[20] A. Dyer, B. Schoeps, S. Frost, P. Jakeman, E.M. Scott, J. Freedman, et al., Antagonism of Glycolysis and reductive carboxylation of glutamine potentiates activity of oncolytic adenoviruses in Cancer cells, Cancer Res. 79 (2019) 331–345.
[21] M.B. Haddada, F. Aouidat, M. Monteil, M. Lecouvey, M.L. de la Chapelle, J. Spadavecchia, A simple assay for direct colorimetric detection of prostatic acid phosphatase (PAP) at fg levels using biphosphonated loaded PEGylated gold nanoparticles, Front. Lab. Med. 1 (2017) 186–191.
[22] T. Li, K. Zhu, S. He, X. Xia, S. Liu, Z. Wang, et al., Sensitive detection of glucose based on gold nanoparticles assisted silver mirror reaction, Analyst 136 (2011) 2893–2896.
[23] R.B. Dominguez, M.A. Orozco, G. Chávez, A. Márquez-Lucero, The evaluation of a low-cost colorimeter for glucose detection in salivary samples, Sens. Basel (Basel) 17 (2017) 2495.
[24] C. Li, J. Hu, T. Liu, S. Liu, Stimuli-triggered Off/On switchable complexation between a novel type of charge-generation polymer (CGP) and gold nanoparticles for the sensitive colorimetric detection of hydrogen peroxide and glucose, Macromolecules 44 (2011) 429–431.
[25] Y. Jiang, H. Zhao, Y. Lin, N. Zhu, Y. Ma, L. Mao, Colorimetric detection of glucose in rat brain using gold nanoparticles, Angew. Chemie Int. Ed. 49 (2010) 4800–4804.
[26] M. Chen, G. Zeng, P. Xu, C. Lai, L. Tang, How do enzymes' Meet' nanoparticles and nanomaterials? Trends Biochem. Sci. 42 (2017) 914–930.
[27] J. Politi, L. De Stefano, I. Rea, A.M. Gravagnuolo, P. Giardina, C. Methivier, et al., One-pot synthesis of a gold nanoparticle-Vmh2 hydrophobin nanobiocomplex for glucose monitoring, Nanotechnology 27 (2016) 0957–4484.
[28] J. Spadavecchia, D. Movia, C. Moore, C.M. Maguire, H. Moustaoui, S. Casale, et al., Targeted polyethylene glycol gold nanoparticles for the treatment of pancreatic cancer: from synthesis to proof-of-concept in vitro studies, Int. J. Nanomed. 11 (2016) 791–822.
[29] M. Monteil, H. Moustaoui, G. Picardi, F. Aouidat, N. Djaker, M.L. de La Chapelle, et al., Polyphosphonate ligands: from synthesis to design of hybrid PEGylated nanoparticles toward phototherapy studies, J. Colloid Interface Sci. 513 (2018) 205–213.
[30] J. Spadavecchia, E. Apchain, M. Alberic, E. Fontan, I. Reiche, One-step synthesis of collagen hybrid gold nanoparticles and formation on Egyptian-like gold-plated archaeological ivory, Angew. Chem. Int. Ed. Engl. 53 (2014) 8363–8366.
[31] A.-L.S. Yen-Jang Huang, S.-Y. Chen, Y.-L. Chen, C.-R. Wang, C.-Y. Tsai, M.-Y. Chang, Y.-T. Li, C.-H. Leu, W. Chao-Liang, Multivalent structure of GALECTIN-1-NANOGOLD complex serves as potential therapeutics for rheumatoid arthritisby enhancing receptor clustering, Eur. Cell. Mater. 23 (2012) 170–181.
[32] K. Yamaguchi, Y. Niwa, T. Nakabayashi, H. Hiramatsu, Generation of self-clusters of galectin-1 in the farnesyl-bound form, Sci. Rep. (2016) 6.
[34] J.S. Suk, Q. Xu, N. Kim, J. Hanes, L.M. Ensign, PEGylation as a strategy for improving nanoparticle-based drug and gene delivery, Adv. Drug Deliv. Rev. 99 (2016) 28–51.
[35] D.R. Baer, M.H. Engelhard, G.E. Johnson, J. Laskin, J. Lai, K. Mueller, et al., Surface characterization of nanomaterials and nanoparticles: important needs and challenging opportunities, J. Vac. Sci. Technol. A 31 (2013) 50820-.
[36] H. Halimi, A. Rigato, D. Byrne, G. Ferracci, C. Sebban-Kreuzer, L. ElAntak, et al., Glycan dependence of Galectin-3 self-association properties, PLoS One 9 (2014) e111836-e.
[37] J. Spadavecchia, R. Perumal, S. Casale, J.-M. Krafft, C. Methivier, C.-M. Pradier, Polyethylene glycol Gold-Nanoparticles: facile Nanostructuration of Doxorubicin and its complex with DNA molecules for SERS detection, Chem. Phys. Lett. 648 (2016) 182–188.
[38] P.C. Chen, S.C. Mwakwari, A.K. Oyelere, Gold nanoparticles: from nanomedicine to nanosensing, Nanotechnol. Sci. Appl. 1 (2008) 45–65.
[39] D. Liu, J. Yang, H.-F. Wang, Z. Wang, X. Huang, Z. Wang, et al., Glucose oxidase-catalyzed growth of gold nanoparticles enables quantitative detection of attomolar Cancer biomarkers, Anal. Chem. 86 (2014) 5800–5806.
[40] J. Spadavecchia, S. Casale, S. Boujday, C.M. Pradier, Bioconjugated gold nanorods to enhance the sensitivity of FT-SPR-based biosensors, Colloids Surf. B Biointerfaces 100 (2012) 1–8.
[41] S. Unser, S. Holcomb, R. Cary, L. Sagle, Collagen-gold nanoparticle conjugates for versatile biosensing, Sens. Basel (Basel) 17 (2017) 378.
[42] S. Söderholm, Y.H. Roos, N. Meinander, M. Hotokka, Raman spectra of fructose and glucose in the amorphous and crystalline states, J. Raman Spectrosc. 30 (1999) 1009–1018.

Supporting Information

Galectin-1 protein modified gold (III)-PEGylated complex-nanoparticles: Proof of concept of alternative probe in colorimetric glucose detection.

Qiqian Liu[1-2‡], Fatima Aouidat[1], Pasqule Sacco[3], Eleonora Marsich[3] Nadia Djaker[1], Jolanda Spadavecchia[1-2*]

[1] CNRS, UMR 7244, NBD-CSPBAT, Laboratoire de Chimie, Structures et Propriétés de Bio-matériaux et d'Agents Thérapeutiques Université Paris 13, Sorbonne Paris Cité, Bobigny, France

[2]Department of Clinical Laboratory Medicine, Southwest Hospital, Third Military Medical University, Chongqing, China

[3]Department of Life Sciences, University of Trieste, Via L. Giorgieri 5, I-34127 Trieste, Italy

Corresponding Author*: jolanda.spadavecchia@univ-paris13.fr

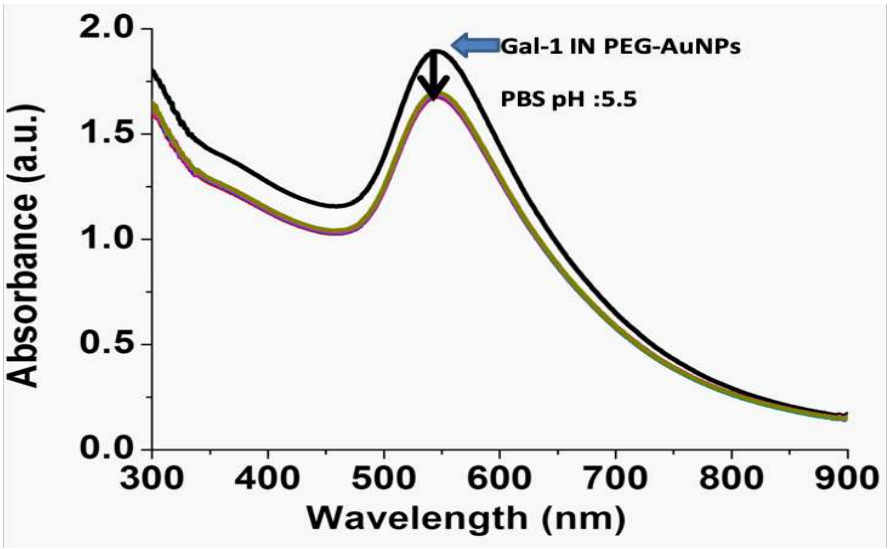

Figure S1: Changes in the UV-Vis absorption spectra of Gal-1 IN PEG-AuNPs (black line) when incubated in PBS solution at pH 5.5 up to one month (green line) and three months (red line).

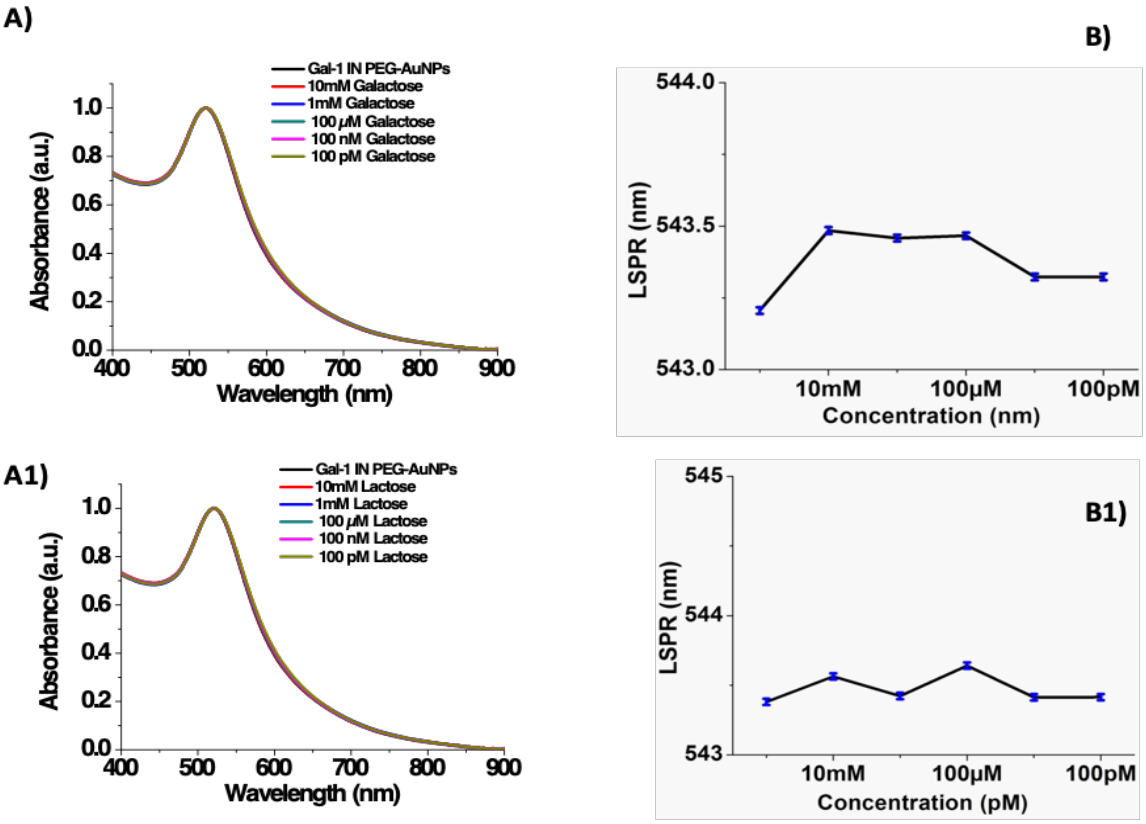

Figure S2: A) UV-Vis absorption spectra in the range 400-900 nm of Gal-1 IN PEG-AuNPs before (black line) and after interaction of galactose (from 10 mM to 100 pM) and A1) lactose (from 10 mM to 100 pM); B) Evolution of the Gal-1 IN PEG-AuNPs plasmonic bands *versus* galactose and B1) lactose concentration.

.

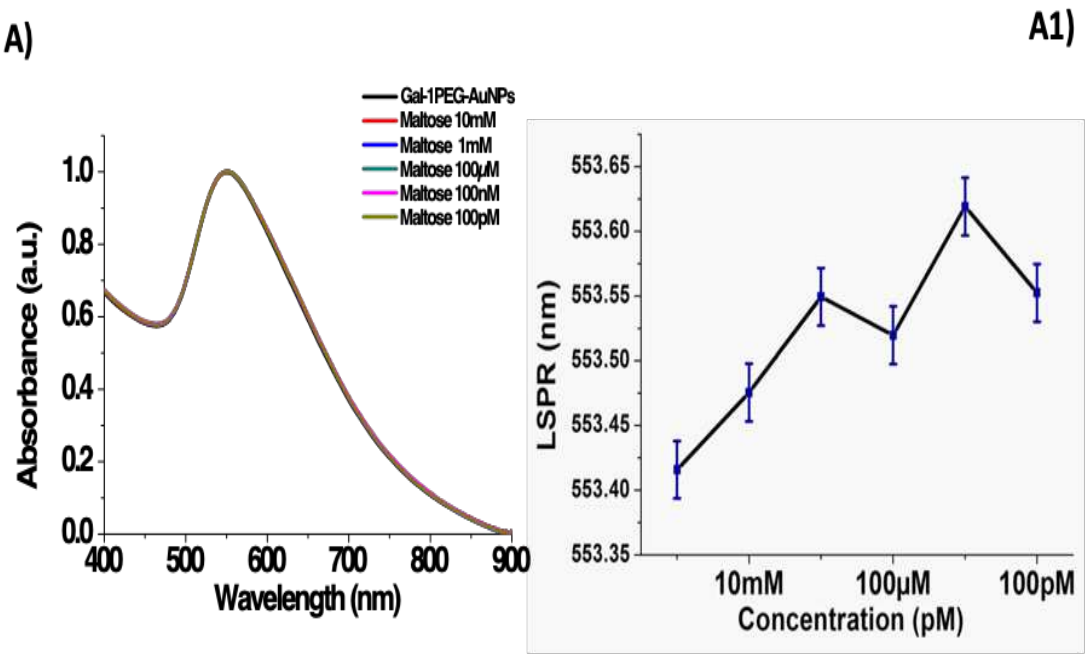

Figure S3: A) UV-Vis absorption spectra in the range 400-900 nm of Gal-1 IN PEG-AuNPs before (black line) and after interaction of maltose (from 10 mM to 100 pM) and A1) Evolution of the Gal-1 IN PEG-AuNPs plasmonic bands versus maltose

2.6 Conclusion

In the present work, Galectin-1 (Gal-1) was exploited as both a stabilizer of a nano-biosystem and as an active biomolecular probe in glucose monitoring in order to evaluate further human health diseases. All experimental results highlighted that Gal-1IN PEG AuNPs exhibited, for the first time, the ability to bind glucose even if if the Gal-1 is intrinsically engaged with a gold complex by chelation methodology. In essence, a new hybrid nanosystem was developed for both interface stabilization and biomolecular interaction monitoring applications. In a second step, new galectin-1 nanoformulations could be internalized in pancreatic cancer cells to detect the glucose produced under specific conditions. This study not only provides a new colorimetric assay for the simple detection of glucose for specific applications, e.g. predicted cancer and treatment, but also potentially offers a new analytical platform for understanding the molecular basis of physiological and pathological events. From the two publications we could conclude that our gold nanosystem could provide a bimodal interest in biomedical diagnosis and therapy. This is the advantage to compare with other detection methods. In the future, the biomodal nanosystem will give patients a faster and better treatment.

2.7 Bibliographic references

1. M. Yalpani, L.D. Hall, M.A. Tung, D.E. Brooks, Unusual rheology of a branched, water-soluble chitosan derivative, Nature 302 (1983) 812-814.

2. C. Storm, J.J. Pastore, F.C. MacKintosh, T.C. Lubensky, P.A. Janmey, Nonlinear elasticity in biological gels, Nature 435 (2005) 191-194.

3. I. Donati, S. Stredanska, G. Silvestrini, A. Vetere, P. Marcon, E. Marsich, P. Mozetic, A. Gamini, S. Paoletti, F. Vittur, The aggregation of pig articular chondrocyte and synthesis of extracellular matrix by a lactose-modified chitosan, Biomaterials 26 (2005) 987-998.

4. E. Marsich, M. Borgogna, I. Donati, P. Mozetic, B.L. Strand, S. Gomez Salvador, F. Vittur, S. Paoletti, Alginate/lactose-modified chitosan hydrogels: a bioactive biomaterial for chondrocyte encapsulation, J. Biomed. Mater. Res A 84 (2008) 364-376.

5. A. Travan, E. Marsich, I. Donati, M.-P. Foulc, N. Moritz, H.T. Aro, S. Paoletti, Polysaccharidecoated thermosets for orthopedic applications: from material characterization to in vivo tests, Biomacromolecules 13 (2012) 1564-1572.

6. P. Marcon, E. Marsich, A. Vetere, P. Mozetic, C. Campa, I. Donati, F. Vittur, A. Gamini, S. Paoletti, The role of Galectin-1 in the interaction between chondrocytes and a lactosemodified chitosan, Biomaterials 26 (2005) 4975-4984

7 Moghadas, Babak; Dashtimoghadam, Erfan; Mirzadeh, Hamid; Seidi, Farzad; Hasani-Sadrabadi, Mohammad Mahdi (19 January 2016). RSC Advances. 6 (10): 7701–7711

8. Moghadas, Babak; Solouk, Atefeh; Sadeghi, Davoud (24 August 2020). "Development of chitosan membrane using non-toxic crosslinkers for potential wound dressing applications". Polymer Bulletin.

9. Agnihotri, Sunil A.; Mallikarjuna, Nadagouda N.; Aminabhavi, Tejraj M. (2004). "Recent advances on chitosan-based micro- and nanoparticles in drug delivery". Journal of Controlled Release. 100 (1): 5–28

10. Aiedeh, K.M.; Taha, M.O.; Al-Khatib, H. (2005). "Evaluation of chitosan succinate and chitosan phthalate as enteric coating polymers for diclofenac sodium tablets". Journal of Drug Delivery Science and Technology. 15 (3): 207–211.

11. Shukla, S. K; Mishra, A. K; Arotiba, O. A; Mamba, B. B (2013). "Chitosan-based nanomaterials: A state-of-the-art review". International Journal of Biological Macromolecules. 59: 46–58.

12. Ryu, J. H; Hong, S; Lee, H (2015). "Bio-inspired adhesive catechol-conjugated chitosan for biomedical applications: A mini review". Acta Biomaterialia. 27: 101–15.

13. Elsabee, M. Z; Abdou, E. S (2013). "Chitosan based edible films and coatings: A review". Materials Science and Engineering: C. 33 (4): 1819–41.

14. Norowski, Peter A.; Fujiwara, Tomoko; Clem, William C.; Adatrow, Pradeep C.; Eckstein, Eugene C.; Haggard, Warren O.; Bumgardner, Joel D. (May 2015).
15. O. WarburgThe metabolism of tumors Constable and Company, London (1930)

16. M.K. SchwartzEnzymes as prognostic markers and therapeutic indicators in patients with cancer Clin Chim Acta, 206 (1992), pp. 77-82

17. A. Herling, M. Konig, S. Bulik, H.G. HolzhutterEnzymatic features of the glucose metabolism in tumor cells FEBS J, 278 (2011), pp. 2436-2459

18. S. Dhup, R.K. Dadhich, P.E. Porporato, P. SonveauxMultiple biological activities of lactic acid in cancer: influences on tumor growth, angiogenesis and metastasis Curr Pharm Des, 18 (2012), pp. 1319-1330

19. E. Madan, R. Gogna, M. Bhatt, U. Pati, P. Kuppusamy, A.A. MahdiRegulation of glucose metabolism by p53: emerging new roles for the tumor suppressorOncotarget, 2 (2011), pp. 948-957

20. R.J. Klement, U. Kammerer Is there a role for carbohydrate restriction in the treatment and prevention of cancer? Nutr Metab (Lond), 8 (2011), p. 75

21.V.C. Fogg, N.J. Lanning, J.P. Mackeigan Mitochondria in cancer: at the crossroads of life and death Chin J Cancer, 30 (2011), pp. 526-539

22. R.B. Hamanaka, N.S. Chandel Targeting glucose metabolism for cancer therapy J Exp Med, 209 (2012), pp. 211-215

Chapter 3

Development of a nanovector for the treatment of liver cancer

In this chapter I developed a specific nanovector for the liver cancer therapy. The originality of this nanovector is the inclusion of chitosan as bioreceptor to target the cancer cells and of doxorubicin as drug to eradicate the tumor. This efficiency of this nanovector was tested in in vivo experiments with nude mice.

3.1 Chitosan Nanoparticles

Many studies have shown that glycated chitosan regulates immune responses and could be a novel adjuvant for cancer vaccin [1]. Chitosan also improves the nanovector's biodistribution, increases their specificity and sensitivity, and reduces their pharmacological toxicity. Thus, nanoparticles combined with chitosan become perfect polymeric platforms for the development of new pharmacological and therapeutic drug release systems [2]. Chitosan nanoparticles (CNPs) can be administrated through noninvasive routes such as oral, nasal, pulmonary, and ocular routes [3]. CNPs have been proposed as nonviral vectors in gene therapy [4] or for the chemotherapy drug delivery by combining them with monoclonal antibody to reduction the drug side effects [5].

CNP may be a safe and efficient adjuvant candidate suitable for therapeutic vaccines. Experimental results have proved that CNP had a strong potential to increase both cellular and humoral immune responses. Wen et al. investigated the promoted immune response to ovalbumin (OVA) in mice by CNP and its toxicity, OVA was used because this protein is considered to be an inert antigen with low capacity to modulate the immune response it's a classic model antigen [6]. The mice were immunized subcutaneously with OVA alone, with OVA dissolved in saline solution containing chitosan or with CNP. The CNP did not cause any cell mortality or side effects. They observed that the serum OVA-specific antibodies were significantly enhanced by CNP as compared with OVA and chitosan groups. CNP remarkably increased the killing activities of NK cells [7]. CNP also significantly promoted the production of Th1 (IL-2 and IFN-γ) and Th2 (IL-10) cytokines and upregulated the mRNA expression of IL-2, IFN-γ, and IL-10 cytokines in splenocytes [7].Wu et al. showed that humoral and cellular immunities were significantly enhanced in immunized mice, which resisted the infection of *E. coli* and survived, while the control mice exhibited clear symptoms and lesions of infection [8]. Their results showed that the inoculation with CNP significantly raised the content of IgG, IgM, and IgA in the sera of immunized mice. Increased number of white blood cells and lymphocytes and elevated levels of IL-2, IL-4, and IL-6 were also observed in the mice of CNP group. It indicates that CNP can be utilized as an effective adjuvant to improve the immune protection and against infectious disease [8].

Modified chitosans can then be used for the wide range of biomedical applications including the interaction and intracellular delivery of genetic materials [9]. Its unique properties help to form a complex with siRNA [10] and Chitosan-based nanoparticles can act as a potential carrier for various gene delivery applications, which indicate its promising perspectives in cancer therapy.

3.1.1 Doxorubicin- and CTL-Doxorubicin-Gold complex Nanoparticles

Doxorubicin (DOX) is a chemotherapy drug used in various cancers (ovarian, bladder, lung, liver, thyroid and stomach). But it induces harmful side effects. The drug can cause a dose-dependent heart toxicity that can lead to a congestive heart failure. Researchers have found an important contributor to that heart pathology: the disruption of the metabolism that controls immune responses in the spleen and heart. This dysregulated immunometabolism impairs the treatment of inflammation and as a consequence, chronic inflammation leads to advanced heart failure. To overcome the side effect of DOX. We considered that the hydrochloride-lactose-modified chitosan, named CTL, is a relevant candidate to act as an immune regulator and a targeting agent for the cancer therapy. This work is a continuation of previous in vitro studies performed in the research group. In 2016 J. Spadavecchia et al published "Tunable Design of Gold (III)−Doxorubicin Complex−PEGylated Nanocarrier. The Golden Doxorubicin for Oncological Applications". In this study the translation of Au (III) complexes into chemotherapeutic agents has permitted to improve their stability under physiological conditions, a crucial parameter in drug development. They reported an innovative four step synthesis of a stable Au (III)−doxorubicin (DOX) complex (Figure 3.1) acting as a key constitutive component of doxorubicin-loaded PEG-coated nanoparticles. This innovative synthesis was called method IN and the associated nanoparticles DOX IN−PEG−AuNPs. For therapeutic purposes, such AuNPs were then functionalized with the anti-Kv11.1 polyclonal antibody (pAb), which specifically recognizes the hERG1 channel that is over expressed on the membrane of human pancreatic cancer cells. In vitro experiments demonstrated that DOX IN-PEG -AuNPs strongly influence the therapeutic potential of AuNPs in pancreatic cancer treatment, with a significant increase of the DOX therapeutic index when complexed to Au (III) ions. This study demonstrated that Au (III)−DOX complexes as building blocks of PEGylated AuNPs constitutes a promising approach to transform Au (III) complexes into real chemotherapeutic drugs for the treatment of pancreatic cancer. Even if the efficiency of in vitro experiments gave us a way to continue our experiments in vivo, it was necessary to go one step beyond and to demonstrate also the in vivo efficiency of such nanovectors. Our in vivo nanovectors use the same innovative synthesis method but to improve the cancer cell targeting, the new nanovectors, DOX-AuGCs) were functionalized with CTL as this one can recognize the Gal-1 protein over expressed on the cancer cells surface (this has already been explained in the chapter 2, publication 1). The nature of interactions between DOX-CTL and Au (III) ions was probed by various analytical techniques (Raman spectroscopy, UV−vis, and TEM) at the different steps of the DOX-AuGCs formation. For in vivo experiments, HepG2 liver cancer cell line was injected in nude mice to induce the formation of liver cancer. To observe the effect of our nanovectors on the cancer evolution but also to identify potential side effects, a wide number of analyzes have been carried out: Ultrason imaging, Blood cells analyze, biodistribution analyze by ICP-MS. We were then able to provide a clear evaluation of the nanovector efficiency, of its toxicity and its biodistribution in the mouse body.

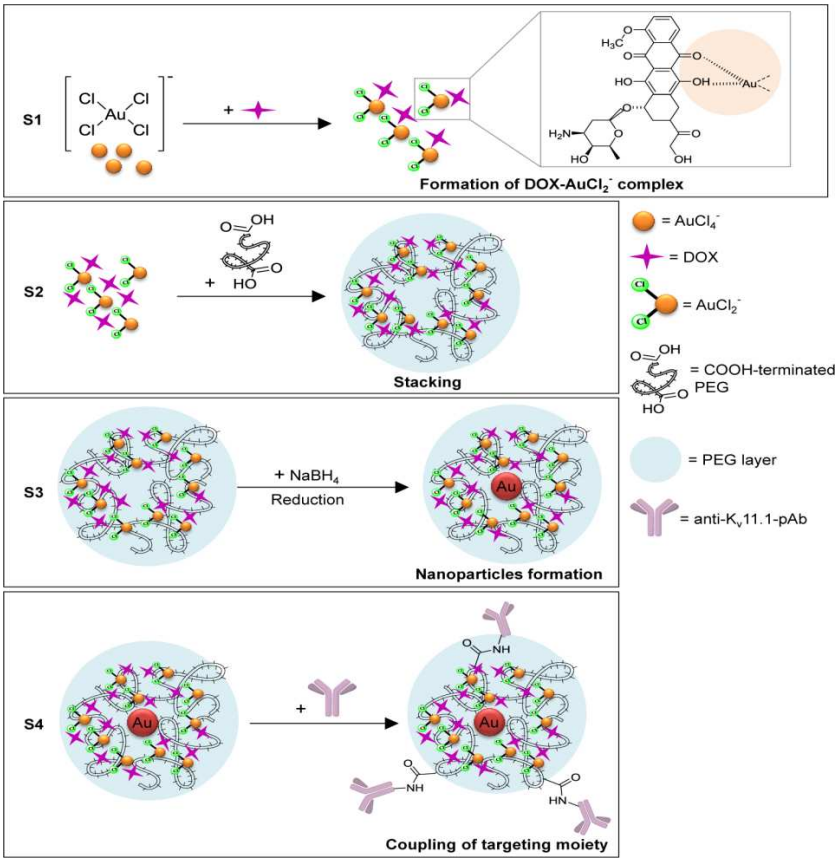

Figure 3.1 –Schematic mechanism of DOX IN PEG AuNPs (Tunable Design of Gold (III)−Doxorubicin Complex−PEGylated Nanocarrie**)**

3.1.2 Method and material for in vivo experiments

a) Group of mice

To evaluate the therapeutic effects of our nanovector, HepG2 cancer cells were injected into 5 groups of mice including:

1. the model group: the mice are treated with only 0.9% sodium chloride solution.

2. the DOX-AuGSs solution group: the mice are treated with gold nanoparticles covered with DOX drug by method-in

3. the DOX IN nanoparticles solution group: the mice are treated with gold nanoparticles including DOX drug and produced using the method IN.

4. the CTL solution group: the mice are treated with DOX-AuGCs produced using the method IN.

5. a positive control group: the mice are treated using the classical chemotherapy drugs 5-fluorouracil (5-FU).

More details can be found in the publication inserted in the following of this chapter.

b) HepG2 Cell cultures

For the preparation of in vivo experiments, we have selected HepG2 as cell line from the Korean Cell Line Bank (Seoul, Korea). HepG2 is an immortalized cell line consisting of human liver carcinoma cells, derived from the liver tissue of a 15-year-old Caucasian male who had a well-differentiated hepatocellular carcinoma, which is the fifth most-common cancer worldwide. The HepG2 cell line is commonly used in drug metabolism and hepatoxicity studies. HepG2 cells exhibit an epithelial-like morphology with a modal chromosome number of 55. They are also non-tumorigenic and have high proliferation rates. Briefly, HepG2 cell lines (2×10 cells/mL) were seeded in a six-well culture plate with RPMI 1640 media containing 10 % FBS and 1 % ABS at 37 °C in an atmosphere humidified at 5 %. Then green fluorescence protein (GFP) was transfected into cell line by using lentiviruses. When the cells reached confluence (70~80 %), the culture media was replaced by RPMI 1640 without FBS. After 24 h of incubation, 3 mL of fresh media containing hexadimethrine bromide (8µg/mL) was added to each well, then gently swirling the plate with DAPI for 10 min. 10 µL of lentiviral particles were added to each well. The cells were incubated at 37°C for 24 h and further cultured in 3 mL of fresh media containing puromycin (3 µL).

c) Cancer cells injection for nide mice

BALB\c nude mouse males (5 weeks aged) have been chosen for drug tests, a total of 25 mices was divided into 5 groups. HepG2 liver cancer cells were resuspended in 0.9% PBS solution, adjusted to a density of 2×10^7 cells/mL, mixed with matrigel 1:1, and inoculated on the left side of the second pair of breast pads (inoculation number 1 $\times10^6$ cells, inoculation volume 100 µL). On the third day after inoculation, the tumor volume was measured and calculated, and the tumor volume was calculated by the following formula: (length × width^2/2). Figure 3.2 shows the third day of one group of nude mice after inoculation of cancer cell line. The tumors reached its optimal volume (between 150 and 200 mm^3) for drug administration after one week of incubation (Figure 3.3).

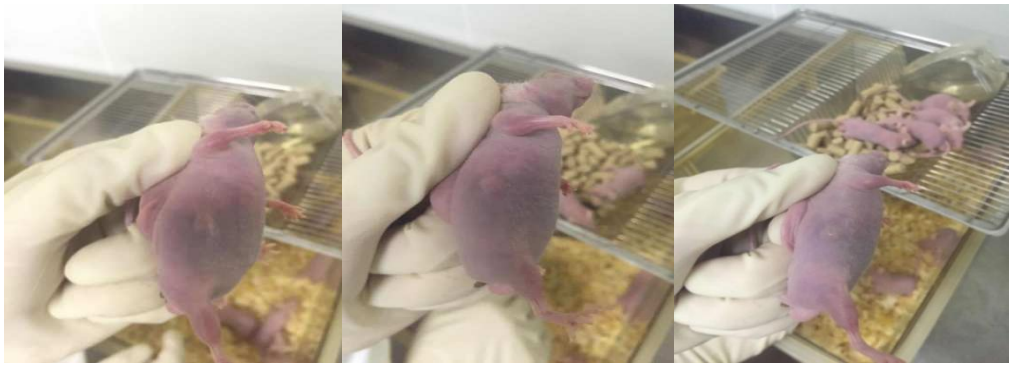

Figur3.2 nude mice 3 days after cancer cell line inoculation

Figure 3.3 nude mice one week after cancer cell line inoculation. The tumors have then reached their optimal volume for drug administration.

d) Administration of the nanovectors and drugs

The nanovectors or drugs were injected intravenously through the tail of the mices: once every 3 days (injection at 10:00 am every day), 2 days a week with continuous administration during 3 weeks. The body weight and tumor volume of nude mice were measured and recorded every 3 days (Figure 3.4). The survival time of the tumor-bearing mice was recorded.

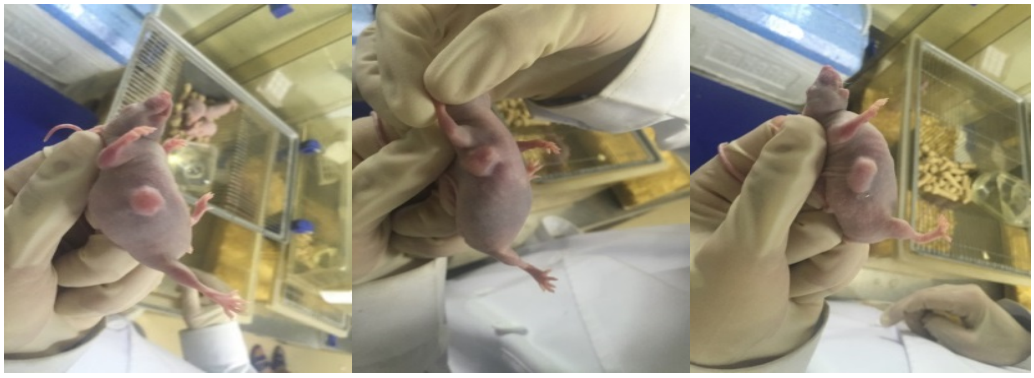

Figure 3.4 after injection of the nanovectors and drugs in one group of nude mices

e) Ultrason imaging preparation

The tumor end point was detected by high-resolution ultrasound imaging. First the nude mice were immobilized and anesthetized with isoflurane. After the hindlimb reflex disappeared, they were placed in the lateral position on the 37 ^{o}C constant temperature physiological monitoring platform. The tumor site was exposed, and a small amount of coupling agents was applied to the limbs and then fixed to the metal. Ultrasound detection of the ventral subcutaneous tumor

was performed with the probe.

f) Blood cells and biodistribution analysis

After the animals were anesthetized with ketamine/xylazine, the tumor, the heart, liver, spleen, lung and kidney tissues of the nude mice were photographed and weighed. The cytokines were used to detect the serum inflammatory factors and the blood cell analyzer was used to determine the blood cell content. Finally, the biodistribution of nanovectors in various tissues was detected by ICP-MS.

This work was carried out in collaboration with the Department of Life Sciences, University of Trieste with doctor Pasquale Sacco who has kindly provided CTL powder. Prof Xiaowu Li, the director of the department of hepato-biliary surgery (Shenzhen University, General Hospital & Guangdong Provincial Key Laboratory of Regional Immunity and Diseases & Carson International Cancer, China), has kindly collaborated with Université Sorbonne Paris Nord for in vivo experiments.

3.2 Publication

CTL–doxorubicin (DOX)–gold complex nanoparticles (DOX–AuGCs): from synthesis to enhancement of therapeutic effect on liver cancer model

Nanoscale Advances

ROYAL SOCIETY OF CHEMISTRY

PAPER

View Article Online
View Journal

Check for updates

Cite this: DOI: 10.1039/d0na00758g

CTL–doxorubicin (DOX)–gold complex nanoparticles (DOX–AuGCs): from synthesis to enhancement of therapeutic effect on liver cancer model†

Qiqian Liu,‡[ae] Hui Liu,‡[be] Pasquale Sacco,[ce] Nadia Djaker,[ae] Marc Lamy de la Chapelle,[de] Eleonora Marsich,[ce] Xiaowu Li*[be] and Jolanda Spadavecchia*[ae]

In this work, we bring back a rapid way to conceive doxorubicin (DOX) hybrid gold nanoparticles, in which DOX and Au(III) ions were complexed with a hydrochloride-lactose-modified chitosan, named CTL and dicarboxylic acid-terminated polyethylene-glycol (PEG), leading to hybrid polymer-sugar-metal nanoparticles (DOX–AuGSs). All formulations were assessed by spectroscopic techniques (Raman and UV-Vis) and transmission electron microscopy (TEM). To estimate the therapeutic effect of DOX–AuGSs in liver cancer, murine HepG2 cells were used to induce a hepatic carcinoma model in nude mice. The survival time of the tumor-bearing mice, body weight and tumor volume were measured and recorded. The cytokines were used to detect the serum inflammatory factors, and the blood cell analyzer was used to determine the blood cell content of different groups of nude mice. The outcomes demonstrate that DOX–AuGCs significantly suppressed the tumor growth derived from human HepG2 injection and reduce the tumor index without affecting the body weight of mice. Moreover, DOX–AuGCs significantly reduced the serum levels of cytokines IL-6, TNF-α and IL-12 P70. Finally, a histological analysis of the heart tissue sections indicated that DOX–AuGCs significantly reduce the chronic myocardial toxicity of DOX during the period of treatment.

Received 9th September 2020
Accepted 29th September 2020

DOI: 10.1039/d0na00758g

rsc.li/nanoscale-advances

1. Introduction

Recently, nanomedicine has led to engineered tunable devices capable to solve unsatisfied issues in the healthcare worldwide. One of the most investigated applications of nanomedicine is the treatment of cancer through the targeted destruction of cancer cells and tumors.[1,2] Among tumors, hepatic cancer is one of the most commonly occurring tumors. There are approximately 800 000 new cases every year worldwide. With respect to common drug therapies, target cancer approaches have recently paved the way for improved patient outcomes. This strategy is based on the principle that specific interactions occur between the tumor and anti-cancer agents.[3,4]

In this context, nanotechnology-based platforms (as nanocarriers) have emerged as adequate candidates for guiding the drug therapeutic massively and selectively to the tumor, thus limiting the common side effects and pharmacokinetic problems related to standard therapies.[5,6] At the tumor site, specific receptors play a key role in determining such host/guest recognition. Exploiting new potential target sites is therefore of primary importance given the heterogeneity of tumors. As an example, galactose-bearing vector systems are extensively studied in hepatic targeted therapy as characteristic targeting ligands for the asialoglycoprotein receptors (ASGP-R) expressed on the surface of liver parenchymal cells.[7,8]

The utilization of biomolecules and biopolymers to tune surface properties and assembly of AuNPs performs greatly attractive overtures that have received remarkable attention.[9,10] Biomolecules and/or biopolymer-conjugated AuNPs are largely used as detection biomarkers, and theranostics in medicine/pharmaceutical fields, as well as components of cosmetic products. The safety profile of AuNPs can be finely realized by modifying the size and/or composition of the gold nanocarrier. Lastly, gold nanomaterials have great potential as multimodal

[a]CNRS, UMR 7244, NBD-CSPBAT, Laboratoire de Chimie, Structures et Propriétés de Biomatériaux et d'Agents Thérapeutiques Université Paris 13, Sorbonne Paris Nord, Bobigny, France. E-mail: jolanda.spadavecchia@univ-paris13.fr

[b]Department of Hepato-biliary Surgery, Shenzhen University General Hospital, Guangdong Provincial Key Laboratory of Regional Immunity and Diseases, Carson International Cancer, Shenzhen, 518055, China

[c]Department of Life Sciences, University of Trieste, Via L. Giorgieri 5, I-34127 Trieste, Italy

[d]Department of Medicine, Surgery and Health Sciences, University of Trieste, Piazzale Europa 1, I-34127 Trieste, Italy

[e]IMMM – UMR 6283 CNRS, Université du Mans, Avenue Olivier Messiaen, 72085 Le Mans, Cedex 9, France

† Electronic supplementary information (ESI) available. See DOI: 10.1039/d0na00758g

‡ These authors contributed equally to this work.

agents. AuNPs are in fact good labels for real-time *in vivo* imaging and/or probes for photothermal therapy through their thermoplasmonic properties.[11,12] Biopolymers are actively employed for the synthesis of anisotropic AuNPs showing relevant results for the specific treatment of cancer cells by hyperthermia using Near-Infra-Red (NIR) irradiation.

The present contribution proposes a novel drug nano-based platform designed to specifically target and attack hepatic cancer. A novel type of composite nano-system consisting of chitosan derivative/gold–PEGylated bioconjugates capped by the anticancer drug doxorubicin (DOX–AuGCs) is synthetized and characterized. CTL (in other papers termed chitlac) is a branched polysaccharide composed of a chitosan backbone to which lactitol moieties have been chemically inserted *via* a reductive *N*-alkylation reaction by lactose.[13] The role played by CTL is investigated here since it was already shown to stabilize gold clusters in CTL–PEGylated gold nanoparticles, and to target the Galectin-1 (Gal-1) protein.[14,15] Gal-1 is in fact considered a novel therapeutic target for cancer due to its widespread presence in the extracellular medium of different tumors.[16]

The therapeutic effects *in vivo* of DOX–AuGCs were evaluated in the HepG2-induced liver cancer of nude mice in comparison with a negative control group (mice treated with a saline solution), and mice treated with the polymer CTL *per se* and with DOX in PEG–AuNPs (DOX–Au nanoparticles without CTL).

2. Experimental section

Materials and methods

Tetrachloroauric acid ($HAuCl_4$), sodium borohydride ($NaBH_4$), dicarboxylic polyethylene glycol (PEG)-600 (PEG), sodium chloride NaCl (0.9%), phosphate-buffered saline (PBS), EDTA, doxorubicin hydrochloride (DOX), 5-fluoro uracile (5-FU), isoflurane, and paraformaldehyde were purchased from Sigma Aldrich at maximum purity grade. Hydrochloride CTL was kindly provided by BiopoLife S.r.l. (Trieste, Italy). The chemical composition of CTL was determined by ^{1}H-NMR spectroscopy, and results showed a fraction of deacetylated units (F_D) 0.36, fraction of lactose-modified units (F_L) 0.56, and fraction of acetylated units (F_A) 0.08. The physical properties were determined by viscometry: the intrinsic viscosity, [ν], of CTL was checked at 25 °C by means of a CT1150 Schott Geräte automatic measuring apparatus and a Schott capillary viscometer. A buffer solution composed of 20 mM AcOH/AcNa, pH 4.5, and 100 mM NaCl was used as the solvent.[17] The resulting mass was 511 mL g^{-1}. The estimated viscosity average molecular weight of CTL was around 870 000.

HEMAVET950FS animal blood analyzer special reagents (Drew Scientific, Inc., USA); Cytokine detection kit (Brand: Biolegend, USA). Cultrex®Basement membrane matrix high concentration, 10× (Manufacturer: Corning, USA). Coupling agent (300 mL), Manufacturer: Shandong Huikang Medical. 68.8–69.8% electronic grade nitric acid; electronic grade hydrochloric acid, Manufacturer: South Korea's DUKSAM company; tuning solution for ICP-MS: ^{7}Li, ^{59}CO, ^{115}In, ^{238}U, Manufacturer: Thermo, 1.0 μg L^{-1}; internal standard solution: ^{6}Li, ^{45}Sc, ^{72}Ge, ^{89}Y, ^{103}Rh, ^{115}In, ^{159}Tb, ^{175}Lu, ^{209}Bi, Manufacturer: National Nonferrous Metals and Electronic Materials Analysis and Testing Center, 1000 μg mL^{-1}; gold single element standard solution, Manufacturer: National Nonferrous Metals and Electronic Materials Analysis and Testing Center, 1000 μg mL^{-1}.

Instruments

Animal Weight Balance (Mettler – Toledo instruments (Shanghai) Co., LTD, Serial number: PL3001-s), HEMAVET 950 Animal Blood Analyzer (Drew Scientific, Inc., USA-Model: HEMAVET 950FS), Automatic biochemical analyzer (Hitachi-Model: 7100), BD Accuri C6 Flow cytometer (BD company), High Resolution Small Animal Ultrasound Imaging System (Visual Sonics-Model: Vevo2100, probe MS400, frequency 30 MHz), Inductively Coupled Plasma Mass Spectrometer (ICAP-Q) (American Thermo Company). DB-3EFS type hot plate (Tianjin Gongxing Laboratory Instrument Co., Ltd), Milli-Q ultrapure water treatment system (American Millipore Company).

Synthesis of doxorubicin–PEG–AuNPs (DOX in PEG–AuNPs)

DOX in PEG–AuNPs was synthetized and used as a control under the previously described methodology.[18]

Synthesis of doxorubicin in CTL–PEG–AuNPs (DOX–AuGCs)

Colloids of doxorubicin in CTL–PEG–AuNPs (DOX–AuGCs) were synthesized by a chelation process, as previously described.[14]

Determination of DOX–AuGCs concentration

The AuNPs concentration was determined by exploiting the standard mathematical calculations in the colloidal solution, as described previously.[14]

Physical–chemical characterization

All characterizations were carried out in triplicate determinations, as described previously.[19,20]

UV/Vis measurements

Absorption spectra were recorded using a double-beam Varian Cary 500 UV-Vis spectrophotometer (Agilent, France). UV-Vis spectra of the NPs were recorded in water at a concentration of 1 mM in the 200–900 nm spectral range.

Transmission electron microscopy (TEM)

Transmission electron microscopy (TEM) images were recorded with a JEOL JEM 1011 microscope operating (JEOL, USA) at an accelerating voltage of 100 kV. TEM specimens were prepared after separating the surfactant from the metal particles by centrifugation under a protocol described elsewhere.[20]

Raman spectroscopy

The Raman experiments have been performed on an Xplora spectrometer (Horiba Scientifics-France). The Raman spectra were recorded using an excitation wavelength of 785 nm (diode laser) at room temperature. For measurements in solution,

a macro-objective with a focal length of 40 mm (NA = 0.18) was used in the backscattering configuration. The achieved spectral resolution was 2 cm^{-1}.

Dynamic light scattering (DLS) and zeta potential measurements

The size and zeta potential measurements were performed using a Zetasizer Nano ZS (Malvern Instruments, Malvern, UK) equipped with a He–Ne laser (633 nm, fixed scattering angle of 173°) at room temperature, as described previously.[19]

DOX loading efficiency

The amount of the drug incorporated into DOX–AuGCs was measured by UV-Vis absorption spectroscopy, as previously described.[18]

DOX release from DOX in PEG–AuNPs

DOX release was evaluated by UV-Vis absorption spectroscopy at 485 nm under experimental conditions at physiological temperature (37 °C) and pH 7.0 and 5.0. The experimental conditions are described in a previous work of some of the authors.[18]

Stability of DOX–AuGCs in DMEM

The stability of DOX–AuGCs was detected by UV-Vis. All nanoparticles were dissolved in Dulbecco Modified Eagle's Medium (DMEM) and stored for 144 h (Fig. S1 in ESI†).

Animal tests

In vivo tests were performed using male nude mice (strain: BALB/cA-Grade: SPF; age 5 weeks; Animal production license number SCXK (Yue) 2018-0002, Guangdong Medical Laboratory Animal Center; Animal certificate number no. 44007200064015; no. 44007200070200; Animal Use License number SYXK (Yue) 2018-0001, Laboratory Animal Center, Guangzhou University of Chinese Medicine).

The animals were fed in an animal room of SPF grade of Guangzhou University of Chinese Medicine. The nude mice had free access to food and water throughout the experiment, and were housed under 12:12 h light/dark conditions in a temperature controlled environment (23 ± 3 °C). The humidity was controlled at 40–70%. Experimental procedures were conducted in accordance with the NIH, and were approved by the Experimental Animal Ethics Committee of Guangzhou University of Chinese Medicine.

After entering the SPF-level experimental center, the nude mice were quarantined in strict accordance with the relevant technical requirements of the SPF-level experimental animal center of Guangzhou University of Chinese Medicine. The quarantine time was 5–7 days. The general appearance and exercise conditions (including state of consciousness, gait, response to stimulation, walking balance and limb coordination) in rats were observed and recorded. Animals were randomly divided into five groups: saline model groups (5 mice), CTL group (2 mice), DOX in PEG–AuNPs (4 mice), DOX–AuGCs (5 mice), and the positive control (5-FU).

Grouping and administration

After the formation of the tumor model of the nude mice (tumor volume reached 150–200 mm^3, about 7 days), 80 μL of each group (Table 1) was intravenously administered once every 3 days (injection at 10:00 a.m.) for 3 weeks.

Detection indicators

Observation of the general health conditions, body weight and organ indexes of nude mice. The general health conditions of mice were evaluated, observing the mental state, skin color, diet, water intake and urine output. The body weight (BW) was weighed every 3 days to evaluate the effects of the tumors, and the effects of the drug-nanoparticles and drug alone.

At the end of the experiments, the hearts, livers, spleen, lungs, kidneys and tumor tissues were separated and accurately weighted. Then, the mice were sacrificed and the heart, liver, spleen, lung, kidney and tumor index were calculated according to the formula tissue weight (mg)/body weight (g).

Tumor volume detection. During the experiment, the length and width of the tumor were measured using a Vernier caliper at intervals of 3 days.

Tumor size detection using high-resolution small animal ultrasound imaging. Nude mice were anesthetized by isoflurane and placed in the lateral position at 37 °C under physiological conditions. The tumor site was exposed, and a small amount of coupling agent was applied to the limbs and then fixed to the metal. Ultrasound detection of the ventral subcutaneous tumor was performed on the probe.

The tumor was coated with an ultrasonic coupling agent, and then covered with the tumor. The ultrasound probe was placed on the ventral tumor. At the maximum cut surface, a B-Mode ultrasound image was recorded. The Vevo imaging software package was used to analyze the area, long diameter and short diameter of the tumor section.

Whole blood cell count detection. Samples of whole blood were sampled on EDTA tubes and analysed by means of an automated HEMAVET950FS animal blood analyzer to determine the concentrations of white blood cells (WBC), red blood cells (RBC), haemoglobin (HGB), hematocrit (HCT), mean corpuscular volume (MCV), mean corpuscular haemoglobin (MCH), mean corpuscular haemoglobin concentration (MCHC), platelets (PLT), lymphocytes (LY), monocytes (MO), neutrophil granulocytes (NE), platelet volume distribution width (PDW), mean platelet volume (MPV), and platelet larger cell ratio (P-LCR).

Multiplex bead-based assay for pro-inflammatory cytokine

After collection, the blood was allowed to clot by leaving it undisturbed at room temperature for 1 h, and the supernatant was collected by centrifugation at 3500 rpm for 10 min. Serum levels of pro-inflammatory cytokine was measured using the Bio Legend LEGEND plex™ multiplex bead-based assay (#740007) from Bio Legend (San Diego, CA, USA).

Table 1 Experimental conditions of drug-nanoparticles administration

Group	Dosage	Number	Method of administration	Frequency
Model, 0.9% NaCl	80 μL	5	i.v.	Once every 3 days
CTL	80 μL	2	i.v.	Once every 3 days
DOX in PEG–AuNPs	80 μL	4	i.v.	Once every 3 days
DOX–AuGCs	80 μL	5	i.v.	Once every 3 days
5-FU	2.5 mg kg^{-1}	5	i.v.	Once every 3 days

Sample preparation and ICP-MS analysis

All tissues were digested using aqua regia in a DB-3EFS type hot plate (Tianjin Gongxing Laboratory Instrument Co., Ltd., china) for 30 min at 200 °C. The digested samples were diluted with a solution containing 2% HCl, 2% HNO_3, and 5 g L^{-1} rhodium (internal standard). Analyses were carried out on an Inductively Coupled Plasma Mass Spectrometer (ICAP-Q) (Thermo-Fisher). Instrumental control and data analysis were performed using an Agilent Chem Station software. Between each analysis, the instrument was rinsed with 2% HNO_3 for 2 min. Furthermore, after every 8 analyses, the blank sample was run to test if there were remaining Au in the system.

Calculations

To calculate the Au content, the ICP-MS results in μg L^{-1} were transformed to pg Au for each organ, taking into account the sample dilution factor and the volume. In addition, the blank Au value obtained for the control samples was subtracted from the result. The Au content, ω_{Au}, was calculated based on the following equation:

$$\omega_{Au}(\mu g\ kg^{-1}) = \frac{(m_1 - m_0)}{m}$$

where m_1 stands for the amount of Au (Ug L^{-1}) after injection of the nano drug, m_0 stands for the amount of Au (Ug L^{-1}) before injection of the nano drug, and m denotes the amount of Au (in μg L^{-1}) taken up by the tissue. Recovery was calculated by dividing the sum of the Au mass in all three fractions by the Au mass obtained for the control sample, containing only a solution with the same concentration of control samples.

Statistical analysis

Statistical analysis of the experimental data was performed by Graph Pad Prism 5.0 software. The data were expressed by mean ± SEM. One-way ANOVA and Tukey test methods were used for comparison between groups. Results were considered statistically significant when $p < 0.05$.

3. Results and discussion

Synthesis and spectroscopic analysis of DOX–AuGCs

DOX–AuGCs were synthesized using a novel methodology previously developed to design nano-therapeutic agents and hybrid gold nanomaterials based on a gold–biomolecule complex, and called Method IN.[18] The choice of CTL as the polymeric component of the NPs is mainly due to its binding affinity to Galectin-1,[14,21] a protein that is overexpressed in many tumors, and with the possibility of being recognized by the asialoglycoprotein receptors (ASGPR) exposed by the hepatocytes.[22]

The originality with the previously reported methodologies of the hybrid nanovector is that DOX, CTL and the polymer molecules are involved in the stabilization of AuNPs *via* electrostatic interactions between their carboxylic and amino groups. The synthesis of DOX–AuGCs foresees three main steps (Scheme 1). The first step included the complexation between gold salt and DOX to form DOX–$AuCl_2$.[18]

Successively, CTL and the COOH-terminated PEG molecules adsorb onto DOX–Au complexes *via* electrostatic interactions. The final reduction by $NaBH_4$ occurs in the third step to generate the gold hybrid nanovector. The synthesized nanoparticles were widely characterized by UV-Vis absorption spectroscopy, TEM and Raman spectroscopy. As described in the literature, the individual DOX molecules (Fig. 1B, cyan line) exhibit three pronounced absorption peaks at 239 nm, 300 nm and 490 nm with a shoulder at 530 nm. After the nucleation and growth process, the absorption spectrum of DOX–AuGCs appeared by a strong peak at 250 nm with a shoulder at 310 nm and a plasmon band at 550 nm (Fig. 1B, black line). PEG–COOH and CTL react as stabilizing polymers for AuNPs, thanks to the formation of coordination bands between the Au ions and the chetone or the hydroxyl groups of DOX, respectively. This chemical comportment is due to the π–π* electronic transitions

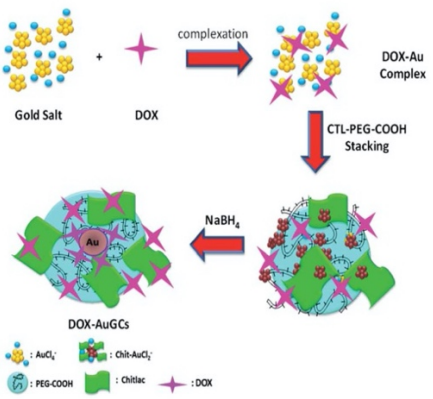

Scheme 1 Chemical representation of DOX–AuGCs synthesis (all drawings are not to scale).

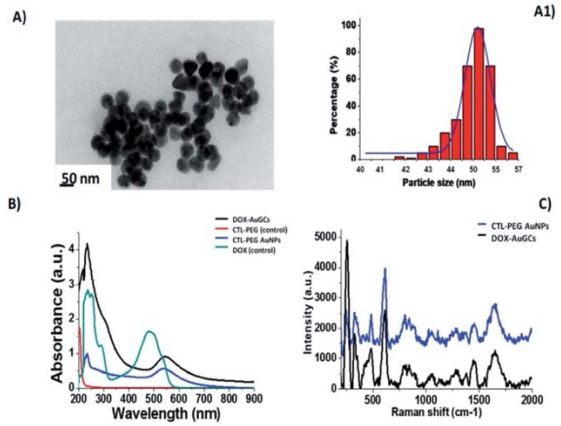

Fig. 1 (A) TEM images of DOX–AuGCs and (A1) histogram size nanoparticles (scale bars: 50 nm); (B) UV-Vis of DOX–AuGCs and (C) Raman spectra of-AuGCs (DOX and CTL–PEG diacide are also reported for comparison). The spectra were normalized on the intensity of the band at 990 cm^{-1}. Experimental conditions: $\lambda_{exc} = 785$ nm; laser power 20 mW; 1200 Tof 180 s.

from the interactions between the anthracycline ring and $AuCl_4^-$ ions, giving strong evidence of the complex formation.[18]

TEM images of DOX–AuGCs display a spherical shape and a narrow dispersion of the nanoparticle size with an average diameter of 50 ± 3 nm (Fig. 1A and A1). Based on the previously reported findings, we presume that when the DOX and the CTL/dicarboxylic PEG mixture were mixed with the $AuCl_4$-solution, PEG–CTL was bound initially to Au(III) in a mushroom conformation followed by a conformational change to the brush mode.[19] In order to confirm the success of the reaction, the UV-Vis spectrum of DOX–AuGCs was compared to that of CTL PEG–AuNPs as the control. The spectrum showed a small band at 233 nm and prominent peak at 540 nm assigned to the AuNP plasmon band (Fig. 1A, blue line). The CTL/dicarboxylic PEG mixture only showed an absorption peak at 204 nm relative to the polymers (Fig. 1A, red line). Consequently, the bright pink-violet color of the DOX–AuGCs solution, as well as the UV-Vis spectrum stayed unaltered after storage for 144 h in DMEM at room temperature, suggesting the formation of a stable particle suspension. The zeta potential and DLS measurements show that DOX–AuGCs was a colloidal solution that was stable under physiological conditions (Table S1 in ESI†). This stability was improved with the presence of the CTL/PEG coating.[14] The chemical conformation of DOX during the synthetic process of DOX–AuGCs was confirmed by Raman spectroscopic analysis, and compared to the Raman spectra of CTL–PEG AuNPs (Fig. 1C, blue line). In detail, the Raman spectra of DOX–AuGCs (Fig. 1C, black line) in water exhibit many bands in the region of 500–2000 cm^{-1}. The wide band observed at around 1600 cm^{-1} on both Raman spectra can be assigned to the bending mode of the water molecule. Previous studies demonstrated remarkable differences between the Raman spectra of DOX before and after complexation with the biomolecules or metal.[23] Considering the spectra of DOX–AuGCs, the Raman bands at 1205, 1445 and 1595 cm^{-1}, corresponding to the (ν_{C-O}) and ($\nu_{C=C}$) vibration of ring A, from DOX are relevant to the variation of the steric conformation of DOX. The bands at 1445 and 430 cm^{-1} become more prominent upon complexation.[18,23] Consequently, we believe that DOX, after chelation with $AuCl_2^-$, was electrostatically adsorbed to the CTL–PEG chains. The DOX molecule is located in the CTL–PEG layer with a characteristic steric arrangement within the AuNPs. Indeed, the steric orientation of DOX onto the AuNPs surface was influenced by the electrostatic interactions between the amino group and phenol group in the presence of polymeric molecules (CTL, PEG) under the definite conditions of pH and ionic strength. Besides, this chemical behavior influences the electronic distribution within DOX, Au^{3+}, and the polymeric chains during the synthesis process with the realization of a new drug-gold nanoparticle system.

Stability of DOX–AuGCs and drug release

The stability of DOX–AuGCs in the colloidal solution is essential to estimating their therapeutic application. The DOX–AuGCs stability was assessed by evaluating the position and intensity of the Localized Surface Plasmon (LSP) band at 550 nm of the AuNPs. Analysis was performed in the cell culture medium (Dulbecco's Modified Eagle's Medium-DMEM) over a period of 144 hours. The DOX–AuGCs exhibited no change in the LSP band position after 72 h (Fig. S1 in ESI†), indicating that the AuNPs are highly stable and that their size remains unchanged during the time. While the LSP band intensity slightly decreased overtime, we believe that no major aggregation occurred over 144 h, indicating that the DOX–AuGCs could be applied as clinical drug-delivery systems.[17] The zeta potential measurements confirmed the spectroscopic results, showing that the DOX–AuGCs colloidal solution is stable at physiological pH (z-potential = −31 ± 1 mV with a PdI equal to 0.259 ± 0.002). We assume that the DOX–AuGCs stability is due to the presence of the CTL–PEG polymer chains. The DOX loading efficiency was 88%, as previously described.[18] The DOX release was pH- and time-dependent (Fig. S2 in ESI†). In particular, after 96 h, the DOX release at acidic pH (pH: 5) (~98%) was higher than at neutral pH (~10%). We assumed that the release of DOX was checked by a dynamic equilibrium between the free Au(III)–DOX complexes in the colloidal solution and trapped into AuNPs by the hydrophobic interactions between CTL–PEG and DOX. The mechanism by which the acidic pH triggers drug release is due to the presence of carboxylate groups of PEG molecules.[18] We can see that the low release at physiological pH within the first hours allows DOX in-PEG–AuNPs to achieve the therapeutic target following intravenous administration without causing toxicity in healthy tissues, thus limiting the side effects.[24]

In vivo antitumor efficacy and drug distribution

The therapeutic effect of DOX–AuGCs on liver cancer was evaluated using nude mice, in which human HepG2 cells were hypodermically injected to generate a subcutaneous liver cancer. All figures show the results from the mice groups with five different treatments: control group (saline solution) to estimate tumor progression without any treatment, CTL group to evaluate the effects of the polysaccharide alone, DOX in PEG–

AuNPs group to evaluate the efficacy of the nano drug system without CTL, DOX–AuGCs group to evaluate the efficiency of the nano drug system with CTL (DOX–AuGCs), and 5-FU group as the reference for a classic cancer therapy.[25,26]

The safety of DOX–AuGCs was determined by observing the animal body weight changes. The measurements of the body weight were taken every 3 days (Fig. 2A). If the control group (saline solution) is compared to the DOX–AuGCs group, it can be observed that the latter did not have a significant reduction of the body weight in the following 30 days. The tumor growth was evaluated by estimating the tumor volume (length × width) every 3 days (Fig. 2B). After the HepG2 cell line injection, the cancer volume quickly increased in all the animals. However, CTL showed a slight inhibition of tumor growth. Conversely, the injection of DOX–AuGCs dramatically decreased the tumor growth compared to DOX in PEG–AuNPs and 5-FU as the control ($p < 0.05$) (Fig. 2B and C). Fig. 2D shows the ultrasound images of the tumor for each group. A very important regression of the tumor marked by the blue line in the images can be observed in the groups treated with the DOX–AuGCs, DOX-in PEG–AuNPs and 5-FU groups. Conversely, the control and CTL groups showed non-significant regression of the tumor. At the end of the experiment, the tumor and spleen tissues of the mice were separated and photographed. The experimental result images are shown in Fig. S3 in the ESI.†

Effect of DOX–AuGCs on the heart, liver, spleen, lung, kidney and tumor indices

To evaluate the effect of DOX–AuGCs on the heart, liver, spleen lung, kidney and tumor indices, the organs and the tumors were collected at the end point of the experiments, weighed, and the weight ratio was calculated.

Fig. 3 shows that all treatments had no significant effect on the indices of the heart, liver, lung and kidney compared to the control group. However, CTL, DOX IN PEG–AuNPs, DOX–AuGCs and 5-FU had significant effects on the spleen index ($p < 0.05$), which can be ascribed to their organ filtration and tissue penetration ability. Otherwise, CTL and DOX IN PEG–AuNPs reduced the tumor index without significance compared with the DOX–AuGCs and 5-FU treatments, which had a significant reduction of the tumor index ($p < 0.05$). This behavior is probably due to the specific chemical affinity of the DOX conjugate to CTL in the gold core nanoparticle, which induced a better steric arrangement and consequent therapeutic effect.

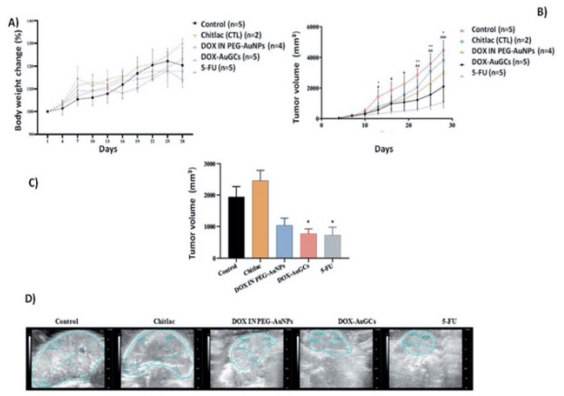

Fig. 2 (A) Body weight changes of DOX–AuGCs compared with each control group in the HepG2 cell line injected in nude mice models. (B) Tumor volume at different time points. Values were shown as mean ± S.E.M. *$p < 0.05$ *vs.* model. (C) Tumor volume of each group at the study end point calculated by ultrasound images. (D) Ultrasound images of the tumor of each group at the study end point. Data are shown as the mean ± S.E.M. *$P < 0.05$, **$P < 0.01$, ***$P < 0.001$ compared to the controls group, as indicated.

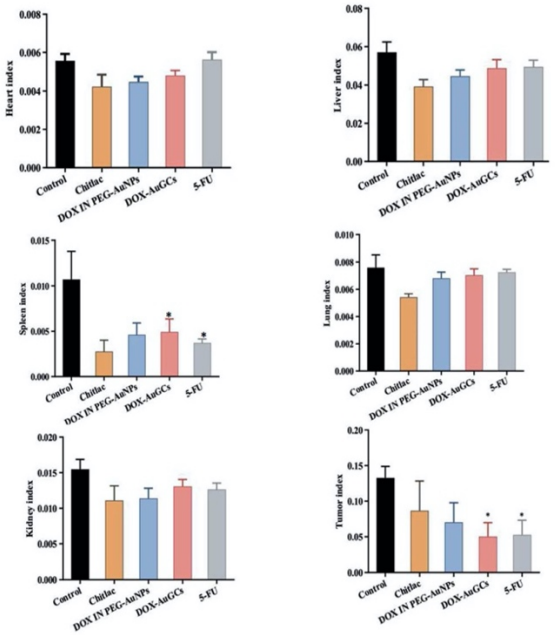

Fig. 3 Effect of each group treatment on the index (heart, liver, spleen, lung, kidney and tumor) in nude mice with HepG2 cells injection.*$p < 0.05$ *vs.* model. Bars represent the mean ± standard deviation. Data were analyzed using the analysis of variance with SPSS13.0. *Represents the significant differences from the control.

Effects of DOX–AuGCs on blood cells

Previously, some authors showed that various parameters related to red blood cell function are negatively influenced by anthracycline drugs and your metabolites,[27,28] stimulating the pentose phosphate pathway (PPP). Indeed, changes in the membrane permeability,[29] variation of sodium transporters,[29] inhibition of inositol lipid metabolism,[30] enhancement of lipid peroxidation,[30] and alterations of the membrane structure have been reported.[28]

As exhibit in Fig. S4 in ESI,† DOX–AuGCs significantly reduced the number of WBC, PLT, LY, MO, NE cells in the blood, which is in line with the features of common chemotherapy drugs and with the data from 5-FU and DOX in PEG–AuNPs. However, the effect of DOX–AuGCs on NE is not as great as that of the traditional chemotherapy drug 5-FU, although there is no statistical difference. The effect of 5-FU on the reduction of MO is significantly different. Interestingly, CTL significantly increased EO and BA compared to the control

group, but this effect cannot be observed in animals treated with DOX–AuGCs, where CTL is a component of the nanostructure. On the contrary, 5-FU and DOX–AuGCs similarly reduced EO BA cells at an extent higher than that observed for DOX in PEG–AuNPs.

Effects of DOX–AuGCs on cytokine expression

Recently, it was established that several chemotherapeutics provoke a form of apoptosis known as immunogenic cell death (ICD), alerting the immune system to the presence of dying cancer cells.[31] ICD is characterized by the release of molecules with danger-associated molecular patterns (DAMPs). Multiple studies indicate that the dosage of ICD agents is a key component associated with the release of DAMPs, as well as the activation of the immune system.[32,33] Previously, it was established that DOX treatment causes apoptosis in the cancer cell studied,[34] and the dose at which this drug triggered ICD was mostly higher than the dose needed to achieve cytotoxicity.[35]

It was proved that AuNPs are efficient nanocarriers as they are inert, chemically robust and able to protect molecules like antigens and cytokines from degradation.[31] As discussed above, AuNPs alone have been shown to stimulate the immune system, and thus provide attractive candidates for adjuvant delivery. For example, Bastús *et al.* showed that 10 nm AuNPs functionalized with two peptides stimulated macrophage activation, as evidenced by the induction of TNF, IL-1β, IL-6, while the macrophages did not recognize the peptides or AuNP alone.[36] Other groups have found that AuNPs can inhibit IL-1β-mediated inflammatory responses and toll-like receptor 9 (TLR9) responses, also in a size-dependent manner.[31] These studies looked at particles in the 2 to 50 nm size, range and found that the smallest particles (<5 nm) had the highest impact on the immune response. The absorption of the cytokine to the nanoparticle surface also induced a conformational change that reduced the biological activity of TGF-β1.[37] In our case, the level of IL-6 in the serum was remarkably reduced by DOX–AuGCs and CTL. However, other treatments have no effects on the expression of IL-6 (Fig. 4). The DOX–AuGC particles have the potential of anti-inflammatory agents, as they significantly reduced the serum levels of IL-6, TNF-α and IL-12 P70 probably due to the anti-inflammatory properties of CTL.[38] Besides, DOX–AuGCs dramatically decreased the level of GMF-CSF (Granulocyte Macrophage Colony Stimulating Factor), a white blood growth factor. The decreases of GMF-CSF results in less infection compared with other groups. This is mainly due to CTL, which protects the immune system that can be collapsed by the drug and tumors (Fig. S5 in ESI†).

On the basis of these results, we can intimate that DOX–AuGCs improve the immune inhibitory effects (Scheme 2), due to a probable different activation of calreticulin and consequent decrease of the serum level of IL-6, IL-12, TNF-α and CM-CSF[32] that could be valorized in the treatment of metastatic disease.[39]

Biodistribution of DOX–AuGCs

In vivo tissue distribution of the two groups of nanoparticles, namely DOX IN PEG–AuNPs (group 4) and DOX–AuGCs (group

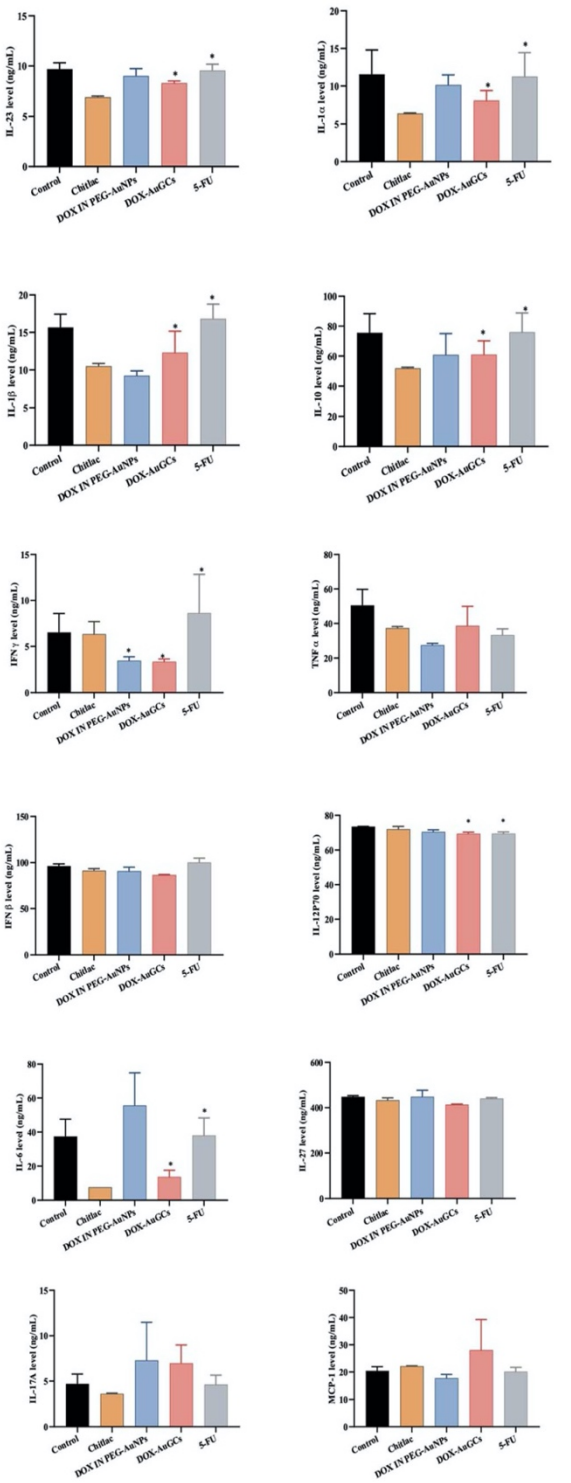

Fig. 4 Effect of DOX–AuGC nanoparticle on cytokine expression. Values were shown as the mean ± S.E.M. *$p < 0.05$, **$p < 0.01$ *vs.* saline group.

5), were investigated by ICP-MS analysis. DOX–AuGCs and DOX IN PEG–AuNPs concentrations in the normal (including, liver, spleen, lung and kidney) and tumor tissues of treated mice are shown in Fig. 5. Both groups of nanoparticles were mostly distributed in the liver, followed by the spleen, and then the

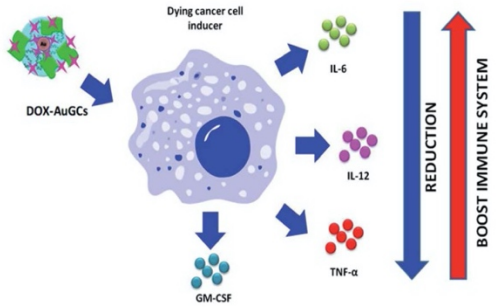

Scheme 2 Schematic representation of the effect of DOX–AuGCs on cytokine level after cancer cell induction (all drawings are not in scale).

lung, kidney and tumor tissues. The data shown in the biodistribution results are the normalized DOX concentrations calculated from the DOX–AuGCs. It is notable that the cardiotoxicity is the main side effect of DOX,[40] and the concentration and retention of DOX in the heart is closely related with the toxicity of DOX-containing formulations. As shown in Fig. 5, DOX–AuGCs concentrations in the spleen are higher than those of group 4 at all time points after administration. This result intimates that DOX–AuGCs exhibited higher retention in the spleen, stimulating the production of the blood cells due to the synergic effect of CTL. This result can be demonstrated by the rapid drug distribution of free DOX in the whole body, and the subsequent quick elimination from the circulation. This phenomenon was due to the protection effect of PEG and CTL on the outer layer of the particle, which caused sustained circulation and effective passive tumor targeting *via* enhanced permeability and retention effect *in vivo*.[41,42] In other normal tissues, including the liver, spleen, lung, and kidney, DOX–AuGCs appeared to show a higher early accumulation. Moreover, the rapid elimination rate of the drug and its formation caused minor injury in normal tissues. Otherwise, the retention of nanoparticles DOX–AuGCs (group 5) in the tumor tissues is higher than that in DOX IN PEG–AuNPs (group 4). This result suggests that CTL allows for the recognition and targeting of the tumor tissue. In a previous study, we demonstrated that CTL in PEG–AuNPs specifically recognizes a cancer biomarker (Galectin-1) involved in the regulation of cancer progression, immune responses and tumor aggressiveness.[16] Furthermore, it cannot be excluded that the molecular recognition between the hepatic asialoglyprotein receptors and galactose-pending groups on CTL may also contribute to the targeting and internalization process into the hepatic tumor.

DOX–AuGCs cardiotoxicity: hypothesis

Since the discovery of DOX, oxidative stress is the best frequently suggested mechanism to clarify the pathophysiology of DOX-induced cardiotoxicity (DIC).[43,44] It was exhaustively discussed that the chemical structure of DOX showed quinone groups that can be reduced to a semiquinone, an unstable metabolite that can react with molecular oxygen (an electron acceptor) and promptly revert to the parent compound. This redox cycle takes the formation of superoxide anion radicals within mitochondria, producing cardiotoxicity due to their affinity to complex Fe^{3+}/Fe^{2+}.[45,46]

Indeed, DOX is able to alter iron metabolism due to its great affinity for this metal, thus forming iron–DOX complexes which, in turn, react with oxygen and trigger ROS production.[46] Thus, the scientists supposed that only oxidative stress was liable for the cardiotoxicity induced by iron–DOX complexes. However, under physiological conditions, there would not be enough free iron to interact with DOX to the extent necessary to generate cardiomyopathy. Moreover, another theory suggests that the effect of DOX on iron metabolism is due to the interference of this drug in the activity of proteins that transport and bind intracellular iron. To evaluate the chronic myocardial toxicity of DOX, a group of mice were also treated with free DOX. The observation time was extended to 8 weeks after the last administration. As shown in Fig. 6, the heart tissue sections from free DOX and 5FU-treated mice exhibited serious myocardial pathological changes. The myocardial fibers became thin and loose, and even presented varying degrees of rupture.[47] However, the heart tissue sections from the DOX–AuGCs nanoparticle-treated mice only showed normal muscle fibers without serious myocardial pathological changes. In comparison with free DOX, this indicated that DOX–AuGCs under DOX–gold complex significantly eliminated the chronic myocardial toxicity of DOX during the period of treatment. In

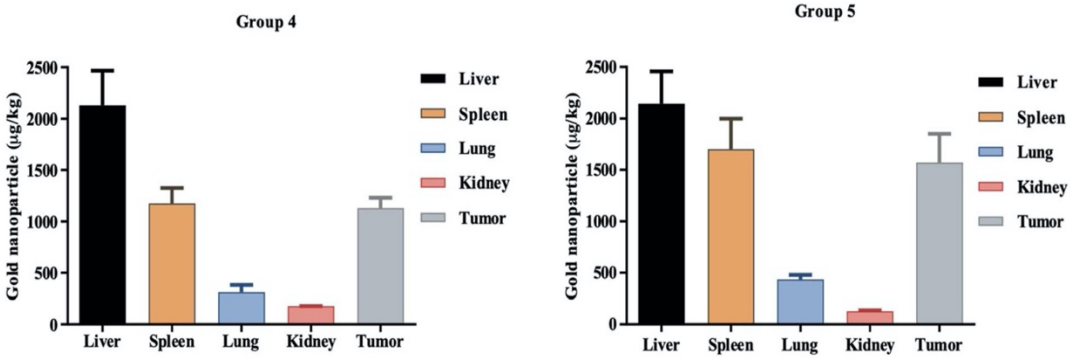

Fig. 5 Biodistribution profiles of DOX IN PEG–AuNPs (group 4) and Dox–AuGCs (group 5) cs in normal tissues including the liver, spleen, lung, kidney and tumor tissue.

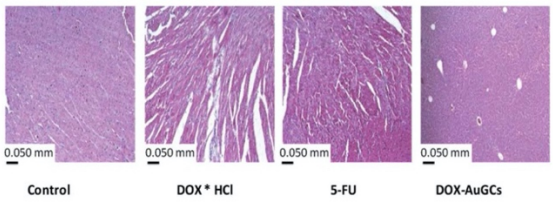

Fig. 6 Histological observation of heart tissue sections from the control and test groups 3 days post-injection. The scale bar is 0.050 mm.

our methodology, DOX was complexed to gold salt by chelation of hydroquinone/quinine by deprotonation of C24 before staking to polymer chains. Anyway, the chitlac and chitosane polymers showed a strong antioxidant power, as described previously.[48,49] In this configuration, DOX as a component of the gold complex does not bind Fe^{3+}/Fe^{2+}, and so it does not promote the ROS production that is responsible for cardiotoxicity (Scheme S1 in ESI†). We also hypothesize that the diffusion mechanism of DOX into the membrane cell can bypass the P-glycoprotein 1-mediated mechanism with the consequent elimination of multi-drug resistance (MDR).[50]

4. Conclusions

This work reports the capability of DOX–AuGCs to target liver cancer and to amplify (in certain respects) the antitumor efficacy of 5-FU. More specifically, a novel synthetic protocol was adopted to acquire a hybrid nanovector. The steric conformation of the drugs onto gold nanoparticles was modulated in the presence of a diacide polymer (PEG) and a polysaccharide (CTL), in which the drug position can resolve the principal issues of drug-conjugated AuNPs. The advanced antitumor efficacy of DOX–AuGCs compared to 5-FU is exhibited not only in the repression of tumor growth, but also in the higher stimulation of immune system. Therefore, the results in this work confirmed that the molecular design plays a key role in modulating the *in vivo* properties and functionalities of the nanocarriers, and enhances their performance and safety in tumor therapeutics. Overall, these results pave the wave for the development of an innovative theranostic platform, allowing for the detection of protein-associated tumors and for the simultaneous cancer treatment with a multimodal agent that combines chemotherapy (drug delivery associated with an increased payload release or enhanced spreading into the cancer cells) with photothermal therapy.

Conflicts of interest

There are no conflicts of interest.

Acknowledgements

This work was supported by the National Natural Science Foundation of China [81430063], and Guangdong Provincial Science and Technology Program [2019B030301009].

References

1 S. Tran, P.-J. DeGiovanni, B. Piel and P. Rai, Cancer nanomedicine: a review of recent success in drug delivery, *Clinical and Translational Medicine*, 2017, **6**, 44.
2 K. Chen, S. Liao, S. Guo, X. Zheng, B. Wang, Z. Duan, H. Zhang, Q. Gong and K. Luo, Multistimuli-responsive PEGylated polymeric bioconjugate-based nano-aggregate for cancer therapy, *Chem. Eng. J.*, 2020, **391**, 123543.
3 R. Bayat Mokhtari, T. S. Homayouni, N. Baluch, E. Morgatskaya, S. Kumar, B. Das and H. Yeger, Combination therapy in combating cancer, *Oncotarget*, 2017, **8**, 38022–38043.
4 D. Pan, X. Zheng, Q. Zhang, Z. Li, Z. Duan, W. Zheng, M. Gong, H. Zhu, H. Zhang, Q. Gong, Z. Gu and K. Luo, Dendronized-Polymer Disturbing Cells' Stress Protection by Targeting Metabolism Leads to Tumor Vulnerability, *Adv. Mater.*, 2020, **32**, 1907490.
5 R. Zeineldin and J. Syoufjy, Cancer Nanotechnology: Opportunities for Prevention, Diagnosis, and Therapy, *Methods Mol. Biol.*, 2017, 3–12.
6 H. Cai, X. Dai, X. Wang, P. Tan, L. Gu, Q. Luo, X. Zheng, Z. Li, H. Zhu, H. Zhang, Z. Gu, Q. Gong and K. Luo, A Nanostrategy for Efficient Imaging-Guided Antitumor Therapy through a Stimuli-Responsive Branched Polymeric Prodrug, *Adv. Sci.*, 2020, **7**, 1903243.
7 H. Chen, M. Li, T. Wan, Q. Zheng, M. Cheng, S. Huang and Y. Wang, Design and synthesis of dual-ligand modified chitosan as a liver targeting vector, *J. Mater. Sci.: Mater. Med.*, 2012, **23**, 431–441.
8 S. Alonso, Exploiting the bioengineering versatility of lactobionic acid in targeted nanosystems and biomaterials, *J. Controlled Release*, 2018, **287**, 216–234.
9 J. Politi, L. De Stefano, S. Longobardi, P. Giardina, I. Rea, C. Methivier, C. M. Pradier, S. Casale and J. Spadavecchia, The amphiphilic hydrophobin Vmh2 plays a key role in one step synthesis of hybrid protein-gold nanoparticles, *Colloids Surf., B*, 2015, **136**, 214–221.
10 J. Spadavecchia, E. Apchain, M. Albéric, E. Fontan and I. Reiche, One-step synthesis of collagen hybrid gold nanoparticles and formation on Egyptian-like gold-plated archaeological ivory, *Angew. Chem., Int. Ed. Engl.*, 2014, **53**, 8363–8366.
11 R. S. Riley and E. S. Day, Gold nanoparticle-mediated photothermal therapy: applications and opportunities for multimodal cancer treatment, *Wiley Interdiscip. Rev.: Nanomed. Nanobiotechnol.*, 2017, **9**(4), 2–16.
12 P. A. Jarzyna, A. Gianella, T. Skajaa, G. Knudsen, L. H. Deddens, D. P. Cormode, Z. A. Fayad and W. J. M. Mulder, Multifunctional imaging nanoprobes, *Wiley Interdiscip. Rev.: Nanomed. Nanobiotechnol.*, 2010, **2**, 138–150.
13 I. Donati, S. Stredanska, G. Silvestrini, A. Vetere, P. Marcon, E. Marsich, P. Mozetic, A. Gamini, S. Paoletti and F. Vittur, The aggregation of pig articular chondrocyte and synthesis

of extracellular matrix by a lactose-modified chitosan, *Biomaterials*, 2005, **26**, 987–998.

14 Q. Liu, P. Sacco, E. Marsich, F. Furlani, C. Arib, N. Djaker, M. Lamy de la Chapelle, I. Donati and J. Spadavecchia, Lactose-Modified Chitosan Gold(III)-PEGylated Complex-Bioconjugates: From Synthesis to Interaction with Targeted Galectin-1 Protein, *Bioconjugate Chem.*, 2018, **29**, 3352–3361.

15 P. Marcon, E. Marsich, A. Vetere, P. Mozetic, C. Campa, I. Donati, F. Vittur, A. Gamini and S. Paoletti, The role of Galectin-1 in the interaction between chondrocytes and a lactose-modified chitosan, *Biomaterials*, 2005, **26**, 4975–4984.

16 V. L. Thijssen, R. Heusschen, J. Caers and A. W. Griffioen, Galectin expression in cancer diagnosis and prognosis: a systematic review, *Biochim. Biophys. Acta*, 2015, **2**, 235–247.

17 P. Sacco, F. Furlani, S. Paoletti and I. Donati, pH-Assisted Gelation of Lactose-Modified Chitosan, *Biomacromolecules*, 2019, **20**, 3070–3075.

18 H. Moustaoui, D. Movia, N. Dupont, N. Bouchemal, S. Casale, N. Djaker, P. Savarin, A. Prina-Mello, M. L. de la Chapelle and J. Spadavecchia, Tunable Design of Gold(III)-Doxorubicin Complex-PEGylated Nanocarrier. The Golden Doxorubicin for Oncological Applications, *ACS Appl. Mater. Interfaces*, 2016, **8**, 19946–19957.

19 J. Spadavecchia, D. Movia, C. Moore, C. M. Maguire, H. Moustaoui, S. Casale, Y. Volkov and A. Prina-Mello, Targeted polyethylene glycol gold nanoparticles for the treatment of pancreatic cancer: from synthesis to proof-of-concept in vitro studies, *Int. J. Nanomed.*, 2016, **11**, 791–822.

20 M. Monteil, H. Moustaoui, G. Picardi, F. Aouidat, N. Djaker, M. L. de La Chapelle, M. Lecouvey and J. Spadavecchia, Polyphosphonate ligands: from synthesis to design of hybrid PEGylated nanoparticles toward phototherapy studies, *J. Colloid Interface Sci.*, 2018, **513**, 205–213.

21 S. Q. Liu, Y. W. Tong and Y. Y. Yang, Incorporation and in vitro release of doxorubicin in thermally sensitive micelles made from poly(N-isopropylacrylamide-co-N,N-dimethylacrylamide)-b-poly(D,L-lactide-co-glycolide) with varying compositions, *Biomaterials*, 2005, **26**, 5064–5074.

22 A. A. D'Souza and P. V. Devarajan, Asialoglycoprotein receptor mediated hepatocyte targeting - strategies and applications, *J. Controlled Release*, 2015, **203**, 126–139.

23 J. Gautier, E. Allard-Vannier, E. Munnier, M. Soucé and I. Chourpa, Recent advances in theranostic nanocarriers of doxorubicin based on iron oxide and gold nanoparticles, *J. Controlled Release*, 2013, **169**, 48–61.

24 J. Yang, B. Benyamin, B. P. McEvoy, S. Gordon, A. K. Henders, D. R. Nyholt, P. A. Madden, A. C. Heath, N. G. Martin, G. W. Montgomery, M. E. Goddard and P. M. Visscher, Common SNPs explain a large proportion of the heritability for human height, *Nat. Genet.*, 2010, **42**, 565–569.

25 N. Zhang, Y. Yin, S. J. Xu and W. S. Chen, 5-Fluorouracil: mechanisms of resistance and reversal strategies, *Molecules*, 2008, **13**, 1551–1569.

26 H. Nagano, A. Miyamoto, H. Wada, H. Ota, S. Marubashi, Y. Takeda, K. Dono, K. Umeshita, M. Sakon and M. Monden, Interferon-alpha and 5-fluorouracil combination therapy after palliative hepatic resection in patients with advanced hepatocellular carcinoma, portal venous tumor thrombus in the major trunk, and multiple nodules, *Cancer*, 2007, **110**, 2493–2501.

27 D. Dhamecha, S. Jalalpure, K. Jadhav, S. Jagwani and R. Chavan, Doxorubicin loaded gold nanoparticles: implication of passive targeting on anticancer efficacy, *Pharmacol. Res.*, 2016, **113**, 547–556.

28 F. Misiti, B. Giardina, A. Mordente and M. E. Clementi, The secondary alcohol and aglycone metabolites of doxorubicin alter metabolism of human erythrocytes, *Braz. J. Med. Biol. Res.*, 2003, **36**, 1643–1651.

29 J. R. Harper Jr, E. P. Orringer and J. C. Parker, Adriamycin inhibits Ca permeability and Ca-dependent K movements in red blood cells, *Res. Commun. Chem. Pathol. Pharmacol.*, 1979, **26**, 277–284.

30 T. Miura, S. Muraoka and T. Ogiso, Adriamycin-induced lipid peroxidation of erythrocyte membranes in the presence of ferritin and the inhibitory effect of ceruloplasmin, *Biol. Pharm. Bull.*, 1993, **16**, 664–667.

31 J. P. Almeida, E. R. Figueroa and R. A. Drezek, Gold nanoparticle mediated cancer immunotherapy, *Nanomedicine*, 2014, **10**, 503–514.

32 A. Showalter, A. Limaye, J. L. Oyer, R. Igarashi, C. Kittipatarin, A. J. Copik and A. R. Khaled, Cytokines in immunogenic cell death: applications for cancer immunotherapy, *Cytokine*, 2017, **97**, 123–132.

33 J. Zhou, G. Wang, Y. Chen, H. Wang, Y. Hua and Z. Cai, Immunogenic cell death in cancer therapy: present and emerging inducers, *J. Cell. Mol. Med.*, 2019, **23**, 4854–4865.

34 S. Siddharth, A. Nayak, D. Nayak, B. K. Bindhani and C. N. Kundu, Chitosan-dextran sulfate coated doxorubicin loaded PLGA-PVA-nanoparticles caused apoptosis in doxorubicin resistance breast cancer cells through induction of DNA damage, *Sci. Rep.*, 2017, **7**, 2143.

35 J. Wu and D. J. Waxman, Immunogenic chemotherapy: dose and schedule dependence and combination with immunotherapy, *Cancer Lett.*, 2018, **419**, 210–221.

36 N. G. Bastús, E. Sánchez-Tilló, S. Pujals, C. Farrera, M. J. Kogan, E. Giralt, A. Celada, J. Lloberas and V. Puntes, Peptides conjugated to gold nanoparticles induce macrophage activation, *Mol. Immunol.*, 2009, **46**, 743–748.

37 Y. S. Tsai, Y. H. Chen, P. C. Cheng, H. T. Tsai, A. L. Shiau, T. S. Tzai and C. L. Wu, TGF-β1 conjugated to gold nanoparticles results in protein conformational changes and attenuates the biological function, *Small*, 2013, **9**, 2119–2128.

38 E. Tarricone, R. Elia, E. Mattiuzzo, A. Faggian, A. Pozzuoli, P. Ruggieri and P. Brun, The Viability and Anti-Inflammatory Effects of Hyaluronic Acid-Chitlac-Tracimolone Acetonide-β-Cyclodextrin Complex on Human Chondrocytes, *Cartilage*, 2020, **28**, 1947603520908658.

39 O. S. Blomberg, L. Spagnuolo and K. E. de Visser, Immune regulation of metastasis: mechanistic insights and therapeutic opportunities, *Dis. Models Mech.*, 2018, **11**, 036236.

40 B. Kalyanaraman, Teaching the basics of the mechanism of doxorubicin-induced cardiotoxicity: have we been barking up the wrong tree?, *Redox Biol.*, 2020, **29**, 101394.
41 S. K. Golombek, J.-N. May, B. Theek, L. Appold, N. Drude, F. Kiessling and T. Lammers, Tumor targeting via EPR: strategies to enhance patient responses, *Adv. Drug Delivery Rev.*, 2018, **130**, 17–38.
42 R. Bazak, M. Houri, S. E. Achy, W. Hussein and T. Refaat, Passive targeting of nanoparticles to cancer: a comprehensive review of the literature, *Mol. Clin. Oncol.*, 2014, **2**, 904–908.
43 M. Gou, X. Zheng, K. Men, J. Zhang, L. Zheng, X. Wang, F. Luo, Y. Zhao, X. Zhao, Y. Wei and Z. Qian, Poly(ε-caprolactone)/Poly(ethylene glycol)/Poly(ε-caprolactone) Nanoparticles: Preparation, Characterization, and Application in Doxorubicin Delivery, *J. Phys. Chem. B*, 2009, **113**, 12928–12933.
44 D. Cappetta, A. De Angelis, L. Sapio, L. Prezioso, M. Illiano, F. Quaini, F. Rossi, L. Berrino, S. Naviglio and K. Urbanek, Oxidative Stress and Cellular Response to Doxorubicin: A Common Factor in the Complex Milieu of Anthracycline Cardiotoxicity, *Oxid. Med. Cell. Longevity*, 2017, 1521020.
45 M. F. Xu, P. L. Tang, Z. M. Qian and M. Ashraf, Effects by doxorubicin on the myocardium are mediated by oxygen free radicals, *Life Sci.*, 2001, **68**, 889–901.
46 G. Minotti, S. Recalcati, P. Menna, E. Salvatorelli, G. Corna and G. Cairo, Doxorubicin cardiotoxicity and the control of iron metabolism: quinone-dependent and independent mechanisms, *Methods Enzymol.*, 2004, **378**, 340–361.
47 S. H. Kim, K. J. Kim, J. H. Kim, J. H. Kwak, H. Song, J. Y. Cho, D. Y. Hwang, K. S. Kim and Y. S. Jung, Comparision of doxorubicin-induced cardiotoxicity in the ICR mice of different sources, *Lab. Anim. Res.*, 2017, **33**, 165–170.
48 W. Xie, P. Xu and Q. Liu, Antioxidant activity of water-soluble chitosan derivatives, *Bioorg. Med. Chem. Lett.*, 2001, **11**, 1699–1701.
49 X. Sun, J. Zhang, Y. Chen, Y. Mi, W. Tan, Q. Li, F. Dong and Z. Guo, Synthesis, Characterization, and the Antioxidant Activity of Carboxymethyl Chitosan Derivatives Containing Thiourea Salts, *Polymers*, 2019, **11**, 1810.
50 G. D. Kruh and L. J. Goldstein, Doxorubicin and multidrug resistance, *Curr. Opin. Oncol.*, 1993, **5**, 1029–1034.

Electronic Supplementary Material (ESI) for Nanoscale Advances.

Supporting Information

CTL-Doxorubicin (DOX)-Gold complex Nanoparticles (DOX-AuGCs): From Synthesis to Enhancement of Therapeutic Effect on Liver Cancer Model

Quiqian Liu[1‡], Hui Liu[2‡], Pasquale Sacco[3-4], Nadia Djaker[1], Marc Lamy de la Chapelle[5], Eleonora Marsich[3-4], Xiaowu Li[2*], Jolanda Spadavecchia[1-2*]

[1] *CNRS, UMR 7244, NBD-CSPBAT, Laboratoire de Chimie, Structures et Propriétés de Biomatériaux et d'Agents Thérapeutiques Université Paris 13, Sorbonne Paris Nord, Bobigny, France*

[2] *Department of hepato-biliary surgery, Shenzhen University General Hospital &Guangdong Provincial Key Laboratory of Regional Immunity and Diseases &Carson International Cancer Shenzhen 518055, China*

[3] *Department of Life Sciences, University of Trieste, Via L. Giorgieri 5, I-34127 Trieste, Italy*

[4] *Department of Medicine, Surgery and Health Sciences, University of Trieste, Piazzale Europa 1, I-34127 Trieste, Italy*

[5] *IMMM – UMR 6283 CNRS, Université du Mans, Avenue Olivier Messiaen, 72085 Le Mans, Cedex 9, France*

Corresponding Author*: lixw1966@163.com; jolanda.spadavecchia@univ-paris13.fr

Table S1: z-potential and hydrodynamic diameter of **DOX AuGCs**.

Synthetic product	Zeta potential (mV)	Hydrodynamic diameter (nm)	PdI
DOX AuGCs	-31,4±1,06	50 ± 3	0,259±0,002

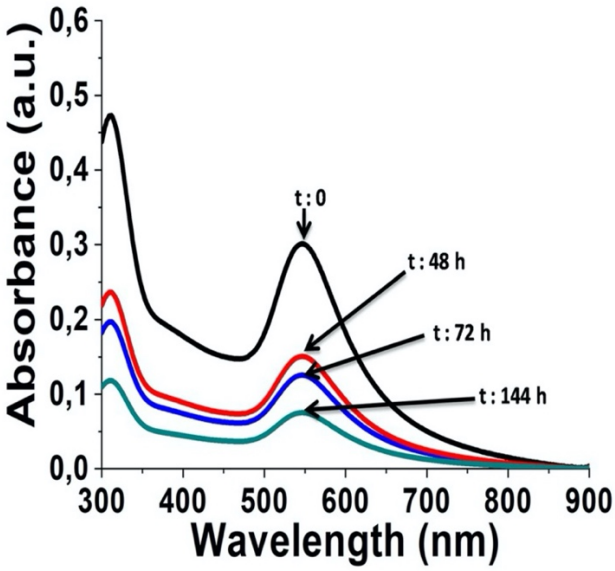

Figure S1. UV-Vis spectra of DOX-AuGCs in DMEM as function of time (black spectrum: 0 h, red spectrum: 48 h, blue spectrum: 72 h, green spectrum: 144 h)

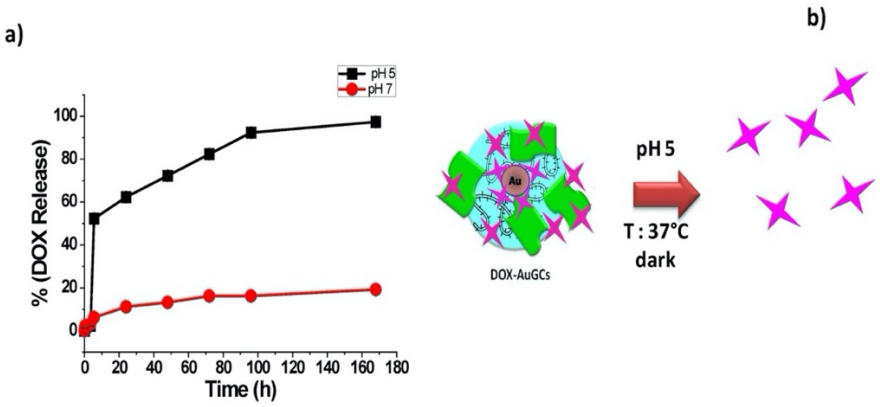

Figure S2. (a) Percentage (%) of DOX released from DOX-AuGCs overtime in PBS (37 °C) at pH 7 (red curve) and 5 (black curve). Data are reported as average ± standard deviation.
(**b**) Schematic diagram of DOX release under acidic conditions.

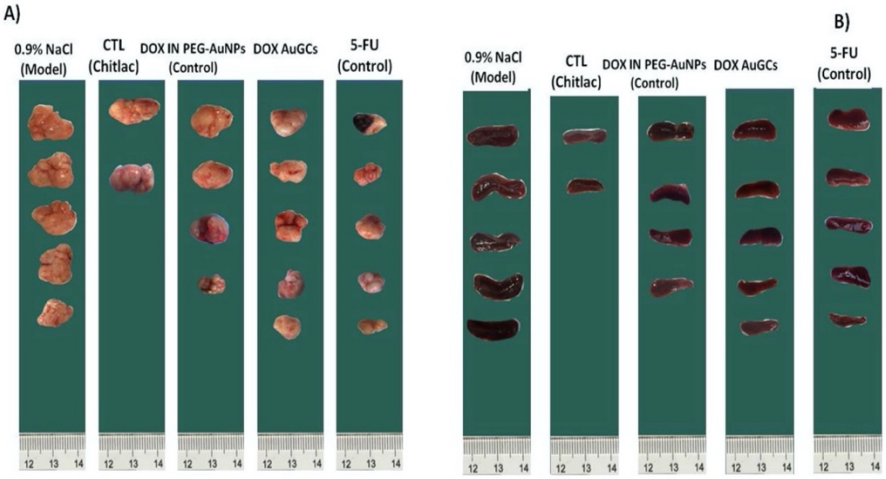

Figure S 3. Morphology of the tumor (A) and spleen tissues (B) of each group taken out from the sacrificed mice at the study end point.

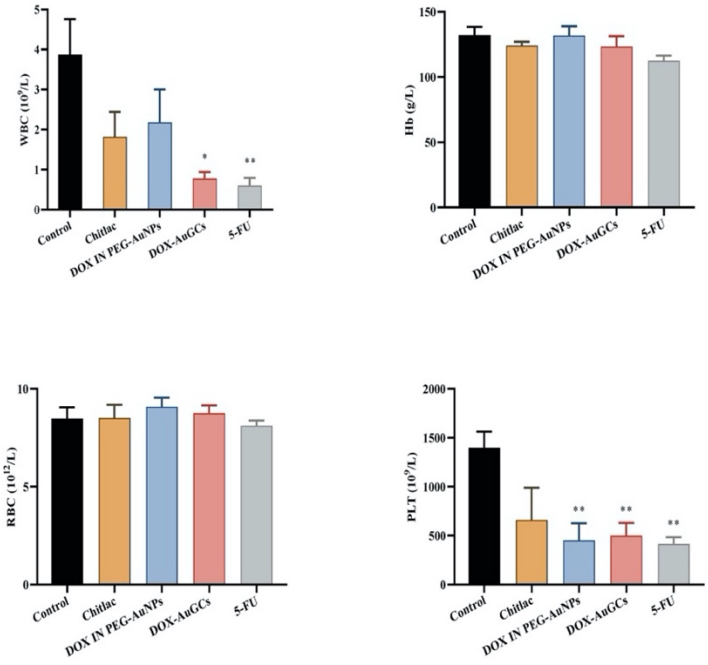

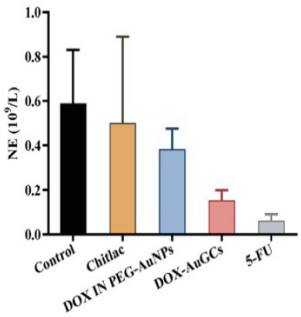
NE (10^9/L)
1.0
0.8
0.6
0.4
0.2
0.0
Control
Chitlac
DOX IN PEG-AuNPs
DOX-AuGCs
5-FU

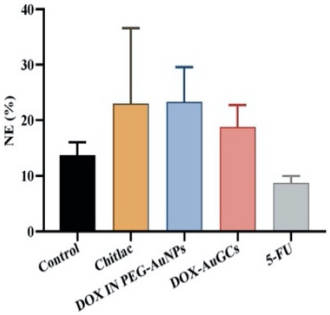
NE (%)
40
30
20
10
0
Control
Chitlac
DOX IN PEG-AuNPs
DOX-AuGCs
5-FU

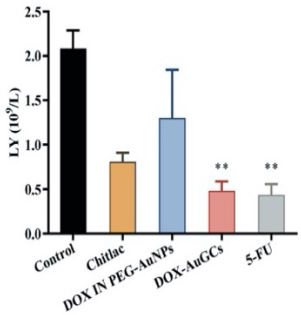
LY (10^9/L)
2.5
2.0
1.5
1.0
0.5
0.0
**
**
Control
Chitlac
DOX IN PEG-AuNPs
DOX-AuGCs
5-FU

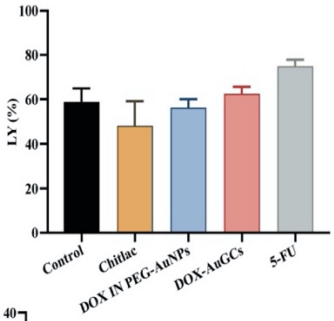
LY (%)
100
80
60
40
20
0
Control
Chitlac
DOX IN PEG-AuNPs
DOX-AuGCs
5-FU

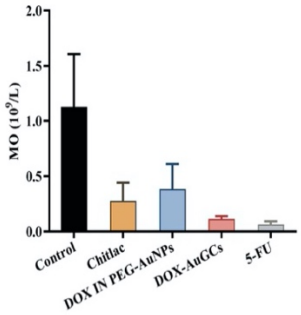
MO (10^9/L)
2.0
1.5
1.0
0.5
0.0
Control
Chitlac
DOX IN PEG-AuNPs
DOX-AuGCs
5-FU

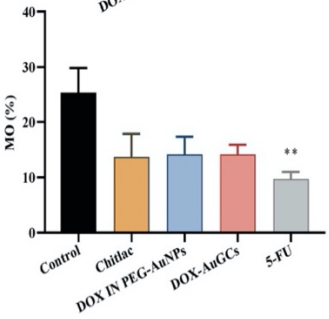
MO (%)
40
30
20
10
0
**
Control
Chitlac
DOX IN PEG-AuNPs
DOX-AuGCs
5-FU

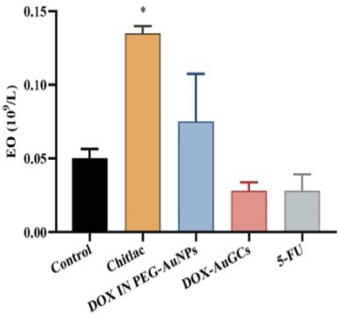
EO (10^9/L)
0.15
0.10
0.05
0.00
*
Control
Chitlac
DOX IN PEG-AuNPs
DOX-AuGCs
5-FU

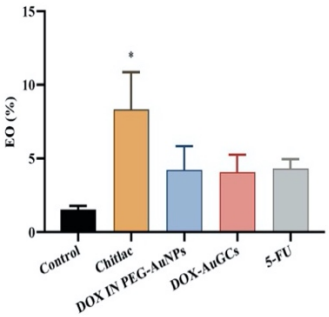
EO (%)
15
10
5
0
*
Control
Chitlac
DOX IN PEG-AuNPs
DOX-AuGCs
5-FU

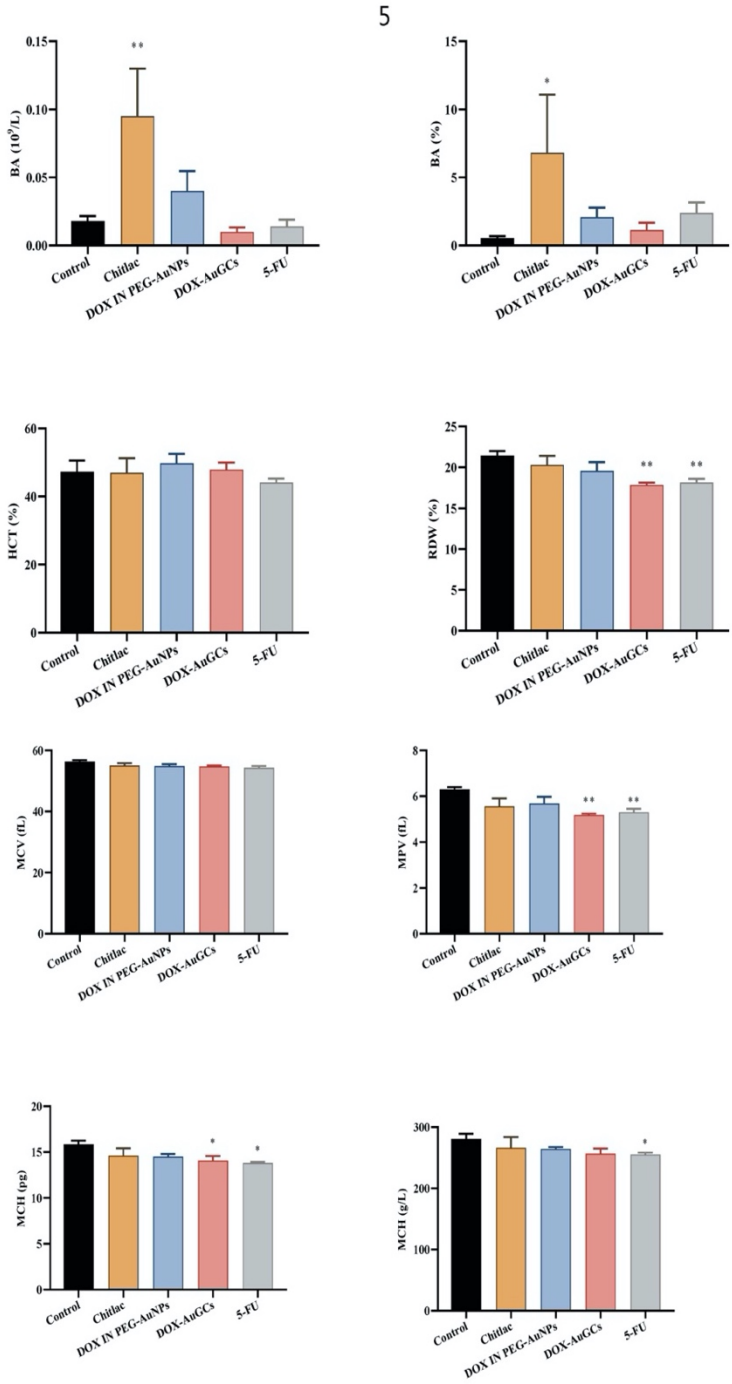

Figure S4. Effects of DOX-AuGCs on blood cells. The statistical significance was determined by the paired Student *t*-test (*P < 0.05).

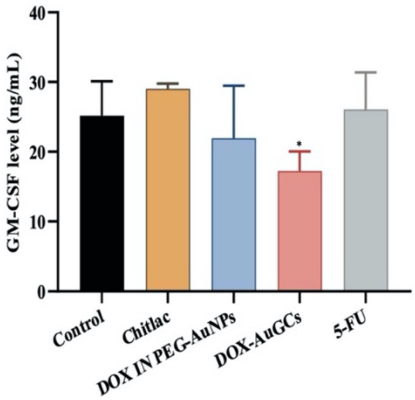

Figure S5. Effect of DOX-AuGCs on serum level of GM-CSF. The statistical significance was determined by the paired Student *t*-test (*P < 0.05).

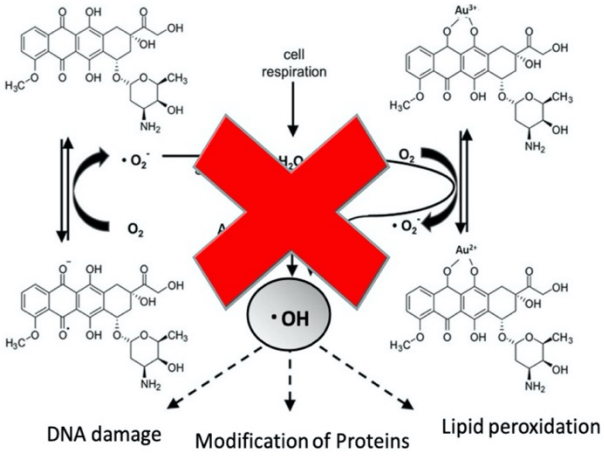

Scheme S1. Schematic **hypothesis** of cardiotoxicity inhibition from DOX AuGCs complex

3.3 Conclusion

This work reports the capability of DOX-AuGCs to target liver cancer in nude mice. As we demonstrated in the publication 1 of chapter 2, CTL can recognize the Gal-1. CTL targeted nanovector with doxorubicin could thus specifically target liver cancer and amplify in certain respects the antitumor efficiency of Doxorubicin. A novel synthetic protocol was adopted to acquire a hybrid nanovector in the presence of diacide polymer (PEG) and a polysaccharide (CTL). ICP-MS biodistribution experiments give us an insight on an important accumulation of nanovectors in tumor tissues. The anti-tumor efficiency of DOX-AuGCs compared to 5-FU was demonstrated not only in the regression of tumor size by ultrason imaging, but also in higher stimulation of immune system and in the reduction of the side effects of DOX. In the future the development of an innovative diagnostic and theragnostic platform should be established for patients, allowing the detection of protein-associated tumors and the simultaneous cancer treatment with a multimodal agent that combine chemotherapy (drug-delivery associated to an increase payload release or enhanced spreading into the cancer cells). In addition, gold nanoparticles can easily generate heat by near-infrared light absorption close to their plasmon resonance. Thus, they have special advantages in the photothermal treatment of late-stage metastatic cancers. Further investigations are needed to understand the interaction mechanisms between the DOX-AuGCs and cancer cells to explore optimal treatment protocols for future clinical applications.

3.4 Bibliographic references

1.Chitin, Chitosan, and Glycated Chitosan Regulate Immune Responses: The Novel Adjuvants for Cancer VaccineXiaosong Li, Min Min, Nan Du, Ying Gu, Tomas Hode, Mark Naylor, Dianjun Chen, Robert E. Nordquist, Wei R. Chen Clin Dev Immunol. 2013; 2013: 387023.

2. Peniche H, Peniche C. Chitosan nanoparticles: a contribution to nanomedicine. Polymer International. 2011;60(6):883–889.

3. Sharma S, Mukkur TK, Benson HA, et al. Enhanced immune response against pertussis toxoid by IgA-loaded chitosan-dextran sulfate nanoparticles. Journal of Pharmaceutical Sciences. 2012;101(1):233–244.

4. Wang JJ, Zeng ZW, Xiao RZ, et al. Recent advances of chitosan nanoparticles as drug carriers. International Journal of Nanomedicine. 2011;6: 765–774.

5. Yousefpour P, Atyabi E F, Vasheghani-Farahani E, et al. Targeted delivery of doxorubicin-utilizing chitosan nanoparticles surface-functionalized with anti-Her2 trastuzumab. International Journal of Nanomedicine. 2011;6: 1977–1990.

6. Wen ZS, Xu YL, Zou XT, Xu ZR. Chitosan nanoparticles act as an adjuvant to promote both Th1 and Th2 immune responses induced by ovalbumin in mice. Marine Drugs. 20 ;9(6) :1038–1055.

7. Wu KY, Wu M, Fu ML, et al. A novel chitosan CpG nanoparticle regulates cellular and humoral immunity of mice. Biomedical and Environmental Sciences. 2006 ;19(2) :87–95.

8. Danesh-Bahreini MA, Shokri J, Samiei A, et al. Nanovaccine for leishmaniasis: preparation of chitosan nanoparticles containing Leishmania superoxide dismutase and evaluation of its immunogenicity in BALB/c mice. International Journal of Nanomedicine. 2011; 6 :835–842.

9. Saranya N, Moorthi A, Saravanan S, Devi MP, Selvamurugan N. Chitosan and its derivatives for gene delivery. International Journal of Biological Macromolecules. 2011;48(2):234–238.

10. Park S, Jeong EJ, Lee J, et al. Preparation and characterization of nonaarginine-modified chitosan nanoparticles for siRNA delivery. Carbohydrate Polymers. 2013; 92:57–62.

Chapiter 4

Study of the interaction of one protein (MnSOD) with its aptamer by scattering correlation spectroscopy

In this chapter, we will focus on the interaction of one aptamer with its target protein. This interaction was studied by scattering correlation spectroscopy (SCS), under specific conditions on the aptamer length and on the MnSOD concentrations. For this purpose, we exploit a specific chemical strategy to graft the aptamers onto pegylated gold nanoparticles: the carbodiimide chemistry (EDC/NHS method). We also study the influence of the presence of a spacer of 15 thymine bases at the aptamer's extremity on the aptamer/MnSOD affinity. The interaction of the aptamer with MnSOD were characterized by SCS on a large range of MnSOD concentrations (from 10^{-12} up to 10^{-5}M). This study is in the continuity of previous works published in 2018 (Influence of aptamer grafting on its conformation and its interaction with targeted protein) [1].In this latter publication, the interaction was studied by using UV-Visible spectroscopy. Interestingly the results with SCS studies are highly correlated with the results presented in this publication.

We observed that the interaction is strongly dependent on the aptamer structure when grafted at the surface of the gold nanoparticles. We demonstrate that the highest affinity is obtained for the aptamer with the spacer of 15 thymine bases. We assume that SCS is a powerful technique to deeply study the aptamer/analyte interaction.

4.1 MnSOD

Manganese superoxide dismutase (MnSOD or SOD2, figure 4.1) is one of the primary antioxidant enzymes, capable of maintaining intracellular reactive oxygen species (ROS) and redox balance for the cell equilibrium. The SOD2 enzyme is an important constituent in apoptotic signaling and oxidative stress, most notably as part of the mitochondrial death pathway and cardiac myocyte apoptosis signaling. Programmed cell death is a distinct genetic and biochemical pathway essential to metazoans while protecting normal tissue against oxidative stress [2-4]. An over-expression of MnSOD in cancerous cell lines increases the activity of MnSOD and of its levels in serum have also been correlated to severe chronic liver diseases and can lead to enhanced malignant transformation inducing the development of various cancers [5-11]

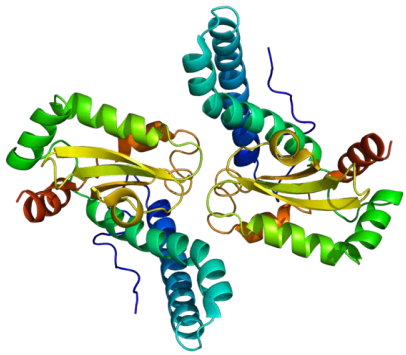

Figure 4.1 The chemical structure of MnSOD protein

4.2 Aptamers

Aptamers are single DNA strands that exhibit a higher affinity to proteins than antibodies. They have become increasingly important molecular tools for diagnostics and therapeutics since they can be synthesized with high reproducibility and purity from commercial sources, showing a high chemical stability [12]. In our studies we have specially designed two aptamers which can interact with MnSOD.

Apt-wT : 5′HS-(C_6)-TTTTTTTTTTTTTTT-TCT TCT CTA GCT GAA TAA CCG GAA GTA ACT CAT CGT TTC GAT GAG TTA CTT CCG GTT ATT CAG CTA GAG AAG 3′.

Apt-w/oT : 5′HS-(C_6)- TCT TCT CTA GCT GAA TAA CCG GAA GTA ACT CAT CGT TTC GAT GAG TTA CTT CCG GTT ATT CAG CTA GAG AAG-3′.

Both sequences are identical except the inclusion of a spacer of 15 thymines in the Apt-w/T. We assume that both aptamers should have the same conformation and the same affinity with the MnSOD. The 15 thymines spacer is only used to increase the distance of the active part of the aptamer from the gold surface and provide higher flexibility to the active part of the aptamer.

4.2.1 The grafting aptamer method onto gold spherical nanoparticles

In previous studies, [1]. we have studied two different methods for the aptamer grafting as described in the following.

a) Aptamer Graftings onto PEG-AuNPs by Carbodiimide Cross-Linker Chemistry

Aptamers were immobilized on the surface of the activated nanoparticles through the formation of amide links between the COOH groups decorating the surface of the PEG-AuNPs and the NH_2 groups of the aptamers (EDC/NHS method, Figure 4.2). The aptamers were immobilized directly at the gold surface through the formation of a covalent bond between the NH_2 group located in 5′ of the aptamer and the COOH group located at the AuNPs surface. The key role of carbodiimide chemistry procedure is that it involves no lengthy linker species, allowing the hydrodynamic radius of the NP to be minimized This strategy has already been demonstrated to couple enzymes to the NPs surface, with retention of up to 80% of enzymatic activity, depending on the enzyme. The aim is to show that carbodiimide chemistry plays a key role in the optimal chemical and steric arrangement of aptamer allowing a better interaction with MnSOD protein.

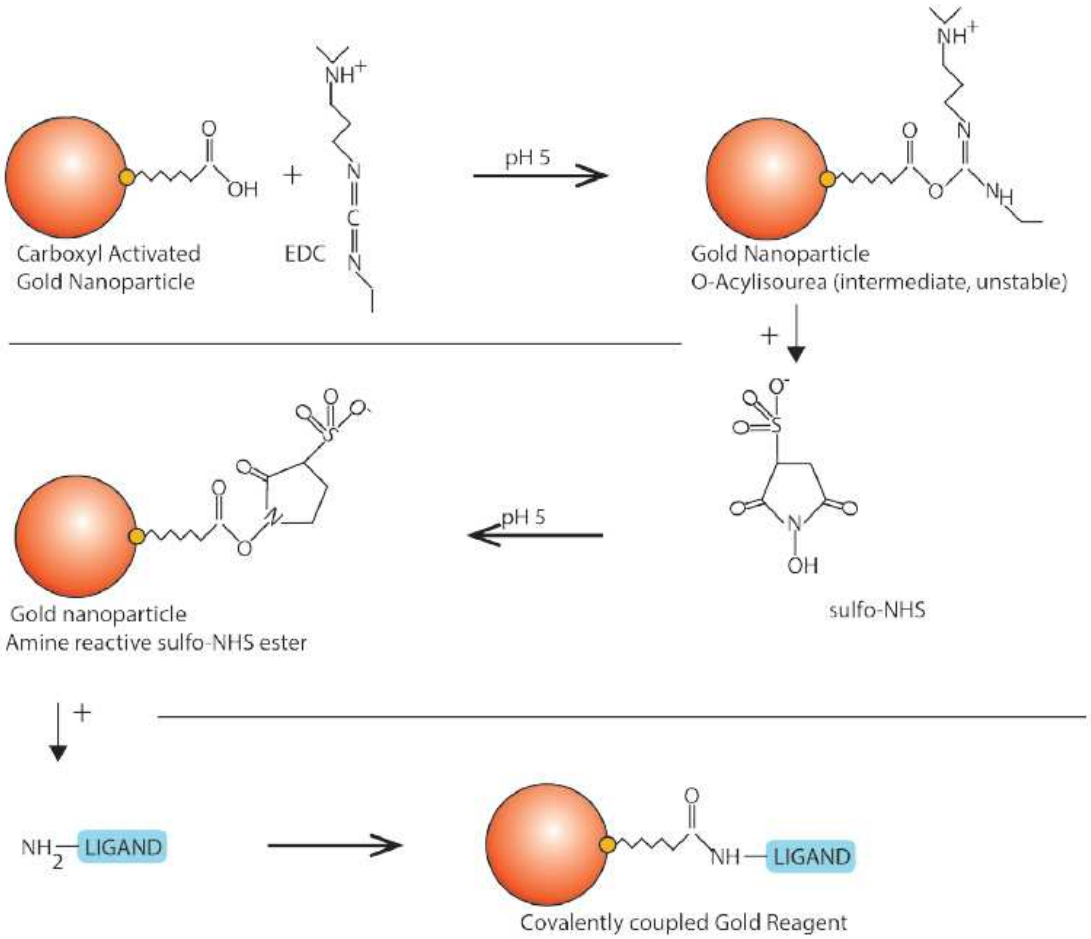

Figure 4.2 Covalent conjugation of Carboxyl-functionalized GNS: reaction scheme EDC/sulfo-NHS activation at pH 5 results in an amine reactive sulfo-NHS ester, immediately followed by binding of the sulfo-NHS ester to free amine on the target molecule (ligand).

b) Aptamer Grafting onto PEG-AuNPs by S covalent bond

Thiol-covalent binding (Figure 4.3) is a conventional grafting strategy, it consists in the immobilization of the aptamers onto PEG-AuNPs by S covalent binding.

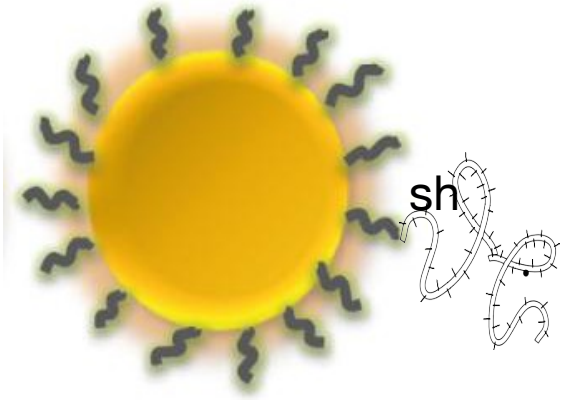

Figure 4.3 Thiol-covalent binding onto PEG- AuNPs

4.2.2 Monitoring of the aptamer graftings by UV-visible absorption

To verify the grafting of the aptamers at the surface of the AuNPs, we used the UV-visible absorption technique to observe the surface plasmon of the nanoparticle and monitor its potential shift through the capture of the aptamer at the surface. Indeed, as the aptamers have a dielectric constant higher than the solution where the nanoparticles are diluted, the formation of an aptamer layer on the nanoparticles should induce a redshift of the plasmon resonance. The UV-visible spectra of PEG-AuNPs exhibit a surface plasmon band at 518 nm (Fig. 4.4, black line). After the Apt-w/T and Apt wo/T binding onto the PEG-AuNPs, the plasmon band is red shifted whatever the grafting methods used [13]. However, one can notice that the plasmon band modification depends on the grafting method and on the different types of APT (Apt-w/T or Apt wo/T). For the carbodiimide method, the plasmon band is red shifted to 535 nm for Apt-w/T with a broadening and to 525 nm for Apt wo/T with also a broadening but more limited than for Apt-w/T. For the thiol method, the redshift is similar (to 524 nm for Apt-w/T and Apt wo/T) without any broadening. The red shift can be explained by the modification of the dielectric environment of the nanoparticles and thus confirms the successful functionalization of the AuNPs surface in all the cases. The broadening is due to aggregation between the gold nanoparticles associated to the formation of classical Van der Waals inter-aptamer or aptamer/PEG interactions [13]. The observation of different plasmon band modification suggests that each condition induces a specific chemical behavior of the APT from the Apt-w/T to Apt wo/T and from the carbodiimide method to the thiol grafting. First, the chemical method will influence the grafting position of the APT (Figure 4.5). With the thiol grafting, the aptamer is located directly at the gold surface and for the carbodiimide method, the aptamer will be located at the surface of the PEG layer. In the former case (thiol method), one can assume that the aptamer is embedded in the PEG layer and they are less accessible than the ones grafted by carbodiimide directly at the PEG layer surface. It will induce lower surface modification of the AuNPs and thus no AuNPs aggregation on the contrary of the carbodiimide method. Such observation is of first importance since the nature of capping layer onto AuNPs play a key role on the success of bioconjugation and comparative kinetic. The similar redshift for the thiol method means that the efficiency of the grafting is similar than for the carbodiimide method.

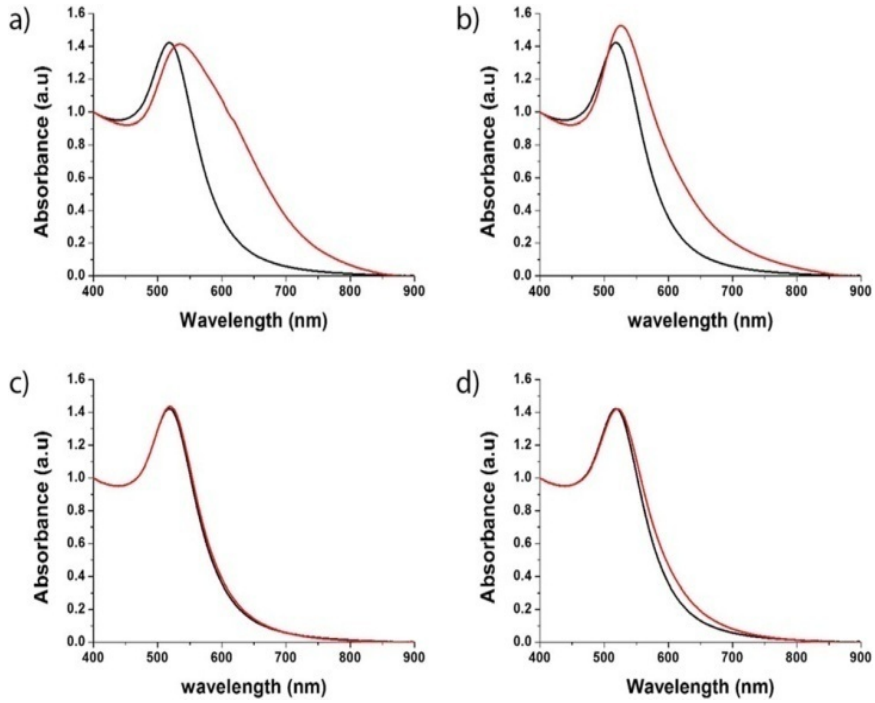

Fig. 4.4 UV-Vis absorption spectra of PEG- AuNPs **before (black line) and after (red line) grafting of aptamer at the PEG- surface by (a, b) carbodiimide chemistry (EDC/NHS) (a Apt-w/oT ; b Apt-w/oT) and (c and d) thiol binding (c Apt-wT ; d Apt-w/oT)**

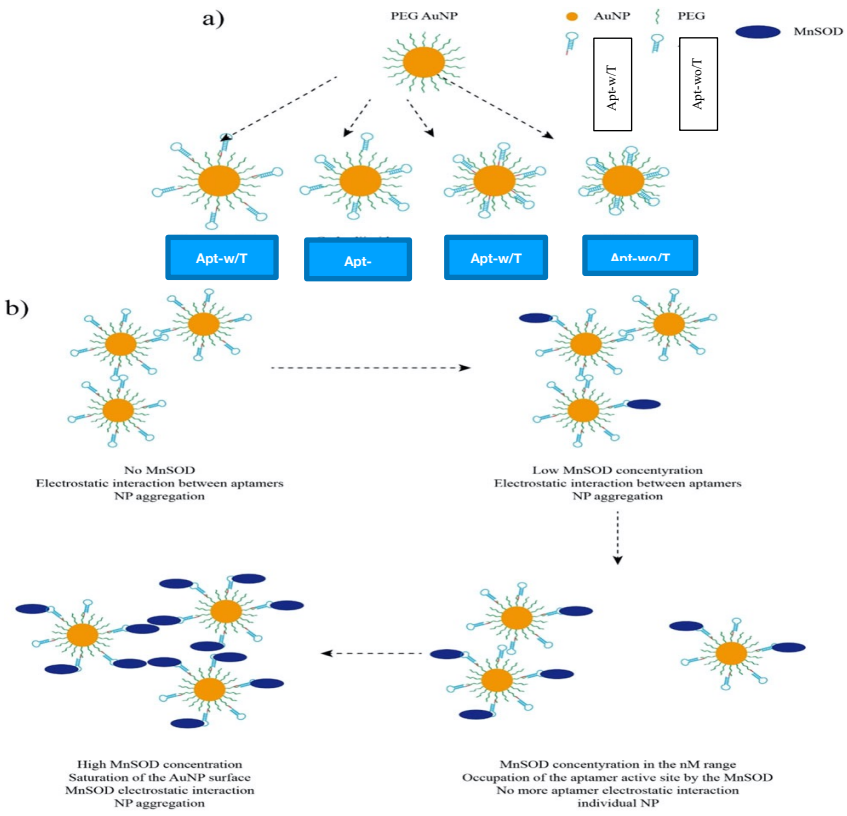

Figure 4.5 Schematic representation of the aptamer grafting on theAuNPs(a) and of the interaction between AuNP under specific concentrations of proteins (b) (please note that drawings are not in scale and are not intended to be representative of the full samples composition)

These results demonstrated that Carbodiimide Cross-Linker Chemistry method has a better grafting ability than by the S covalent bond methods. This is the reason why we have chosen carbodiimide cross-linker chemistry method as our grafting methods for SCS measurements.

4.3 The scattering correlation spectroscopy

The scattering correlation spectroscopy (SCS) is a technique widely used to analyze the temporal fluctuations of different types of optical or spectroscopic signals such as fluorescence [14] (Fluorescence Correlation Spectroscopy FCS), luminescence or even scattering [15] (in the case of the Dynamic Light Scattering DLS or of the scattering Correlation Spectroscopy SCS). DLS is a well-known and widely used method to determine the hydrodynamic diameter of nanoparticles. However, this technique does not make it possible to characterize nanoparticles at very low concentration. SCS is a method that has been recently used to characterize nanoparticles. Its principle is similar to that of the FCS technique [16]. The main idea of this technique is to analyze the temporal fluctuations of an optical signal emitted by molecules or individual particles diffusing light in a very low detection volume (in the order of femtoliter, fL) called the confocal volume. This effective volume is essentially given by the strong focusing of a laser generated by an immersion lens.

If the particle concentration is low enough (nM-pM), the particles do not interact with each other, and the time between particle entry and exit respect the Poisson distribution, meaning that each particle passing through the confocal volume contributes significantly to the signal measured. This makes it possible to perform a statistical correlation analysis (see the paragraph below) in order to obtain the number and the diffusion time of the particles in the confocal volume.

4.3.1 Theoretical aspect of scattering correlation spectroscopy

SCS is an excellent technique based on the use of a confocal optical microscope to extract information within the limits of conventional optical resolution. This technique uses a statistical method which analyzes the scattering signal fluctuations. These fluctuations typically arise from Brownian motions of particles crossing the confocal volume. The size of these particles determines the average time they spend in the confocal volume. A very sensitive detector (usually avalanche photodiode, APD) records the photons scattered by the nanoparticles in the confocal volume ($2r_0$ represents the diameter and $2Z_0$ represents the height of confocal volume on the figure 4.4). Relevant information on the nanoparticle dynamics such as diffusion time, particle size, particle number and concentration can be extracted using the correlation function. The latter converts the intensity fluctuation signal into a correlation curve, the general principle of which is shown in Figure 4.6

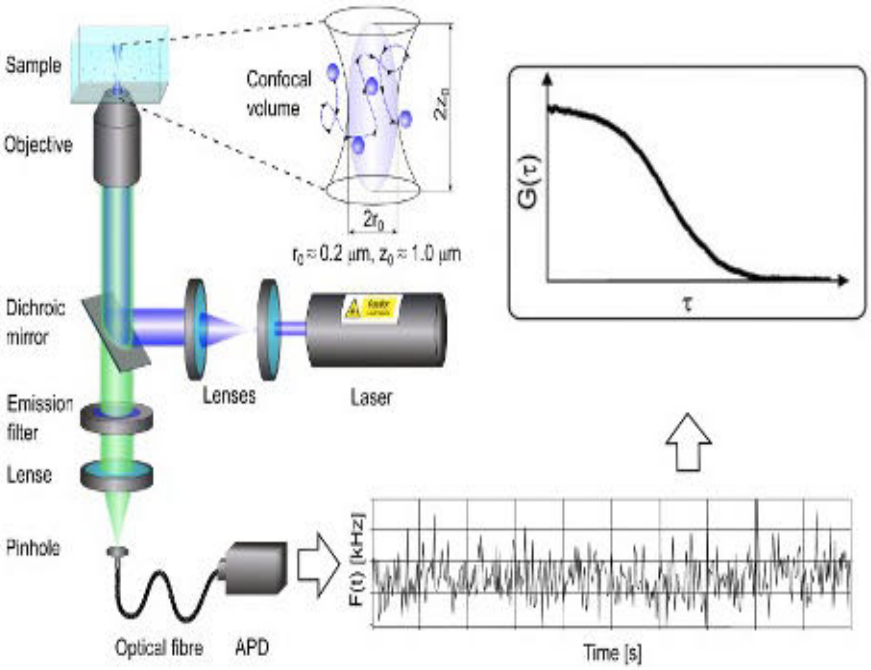

Figure 4.6 - General principle of correlation spectroscopy

The intensity is recorded as a function of time (figure 4.5) and can be written as follows:

$$F(t) = < F(t) > + \delta F(t) \qquad \text{(Equation 3.1)}$$

where <F (t)> is the mean intensity over time and δF (t) is the fluctuation of the intensity with respect to the mean intensity at time t. The correlation function is a measure of the similarity of a signal F (t) with the signal F (t + τ) which is emitted by the particles after a very short time τ. In other words, the intensity recorded at time t is correlated with that recorded at time t + τ. If the signal strength has not changed significantly during this period (meaning there is no time lag), the correlation is high. Conversely, if the signal is completely different (meaning a large time lag), the correlation is weak. We can therefore assume that the correlation function is a "memory" function which measures the length of time during which a signal remains the same over a specific time interval.

The correlation function G (τ) is defined as [12]

$$\boldsymbol{G(\tau) = \frac{< F(t).F(t+\tau) >}{< F(t) >^2} = 1 + \frac{< \delta F(t).\delta F(t+\tau) >}{< F(t) >^2}}$$

(Equation 3.2)

Knowing that the signal strength, F (t), is proportional to physical parameters such as:

- Quantum efficiency: q,

- The effective excitation cross-section of the particles: σ,

- The effective excitation section of the particles: σ_{ABS},

- The collection efficiency function: CEF ($\vec{r}$), for example the fraction of light emitted by a particle at point $\vec{r}$ and collected by the detector,

- The excitation intensity at the position r : I ($\vec{r}$),

- The concentration of particles at position $\vec{r}$ and at time t: C ($\vec{r}$,t)

It is possible to inject these parameters into equation 3.2 [18, 19] and rewrite the correlation function (G (τ)) as follows:

$$G(\tau) = 1+\frac{1}{N} \cdot \frac{1}{1+\frac{\tau}{\tau D}} \cdot \frac{1}{\sqrt{1+s^2\frac{\tau}{\tau D}}} \qquad \text{Equation (3.3)}$$

Basically three important pieces of information can be extracted from the correlation function:

The average number of particles in the detection volume, N, from the amplitude of the correlation curve at time τ = 0s. knowing that G(0)=1+1/N (figure 4.7)

The structure parameter, *s*, which describes the shape of the confocal volume. The size of the confocal volume (ω_{xy} (radial distance) and ω_z (axial distance)) was previously determined for our experimental set-up by performing reference measurements with a fluorescent molecule having a known diffusion constant (Rhodamine, Alexa).

The average time required for a particle to cross the confocal volume (τ_D). τ_D allows to calculate the particle diffusion coefficient (D) (figure 4.7)

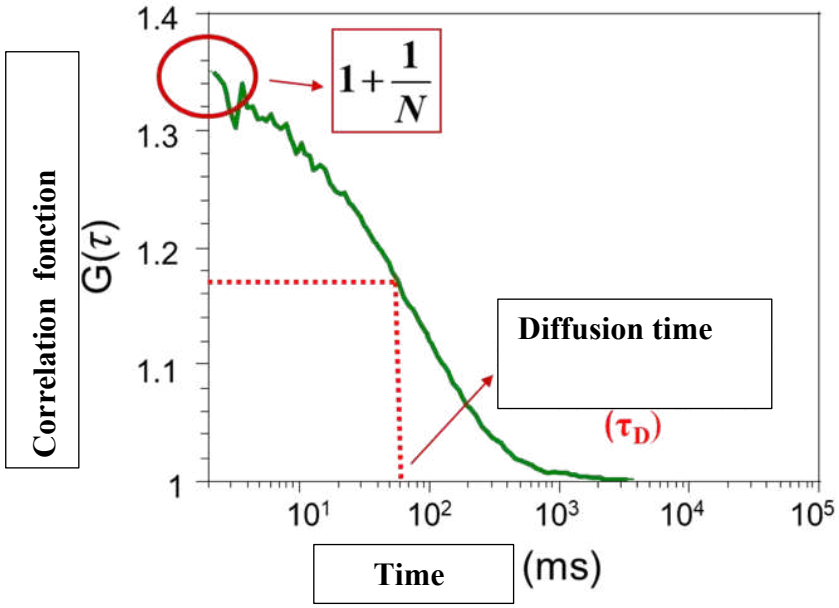

Figure 4.7 Correlation curve whose amplitude at G (0) is inversely proportional to the average number of particles present in the effective volume and the width at mid-height corresponds to the diffusion time, τ_D.

Figure 4.8 shows that a higher concentration and then a greater number of particles present within the confocal volume induce very low signal fluctuations and thus a reduction of the intensity of the correlation curve. The SCS is then quite sensitive at low concentrations. It should be noted that this technique allows detection up to picomolar in the case of gold nanoparticles [1].

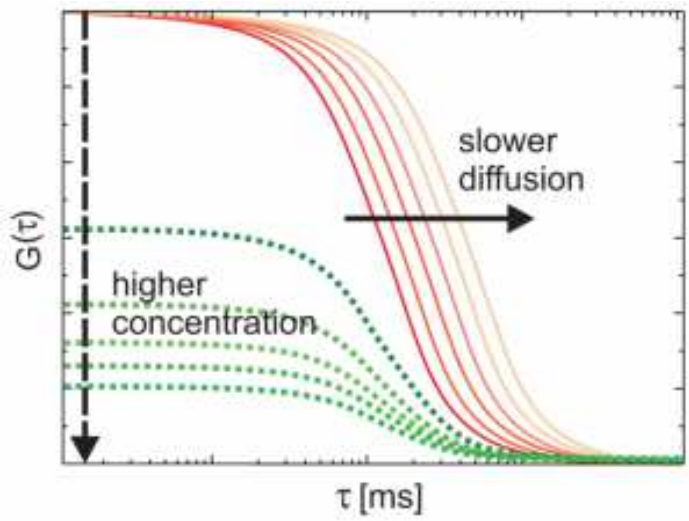

Figure 4.8 Effect of concentration on fluctuations in signal strength and correlation curve [17].

The diffusion time is related to the diffusion coefficient (D) of a particle by the following equation:

$$\tau_D = \frac{W_{xy}^2}{4D}$$

(Equation 3.4)

The value of the hydrodynamic radius (Rh) can then be deduced from D using the Stokes-Einstein equation:

$$D = \frac{kT}{6\pi\eta Rh}$$ (Equation 3.5)

Where η is the viscosity of the surrounding medium, T is the temperature and k is the Boltzmann constant. The diffusion time τ_D is inversely proportional to the diffusion coefficient D. The diffusion coefficient being inversely proportional to the size of the particle, the more the radius Rh increases, the more the diffusion time τ_D of the particle increases (Figure 4.7)

4.3.2 SCS setup

The correlation spectroscopy experimental setup used is illustrated in **Figure 4.8**. The excitation source comes from different continuous lasers of different wavelengths ranging from visible to near IR: a 488nm laser (Cobolt MLDTM lasers), a 532nm laser (Optoelectronics, United Kingdom), a 633nm laser (Thorlabs, France) and a tunable sapphire-titanium laser from 750 to 950 nm (Coherent, USA). The system is based on an inverted microscope (Nikon, Japan) combined with a water immersion objective (x60) with a numerical aperture of 1.2. The laser beam is widened (from 2 to 8 mm) via a telescope to completely cover the entrance pupil of the lens to reach the limit of optical resolution. A dichroic mirror (in the case of FCS) or a 50/50 splitter cube (in the case of SCS) is used in order to reflect the excitation beam directly into the microscope objective which allows it to be focused in the analysed solution. The light emitted (or scattered) by the molecules (or particles) present in the solution is collected by the same objective, transmitted through the dichroic mirror or the splitter cube and focused on a confocal hole of size ranging from 30 to 50 µm (depending on the laser used) and placed in the image plane of the objective to reject light emitted outside the focal plane. Subsequently, the signal is recorded by two avalanche photodiodes. The detectors are connected to a multichannel correlator (ALV-Laser GmbH, Langen, Germany) which is connected to a computer for data analysis via LabView software (National Instruments, USA).

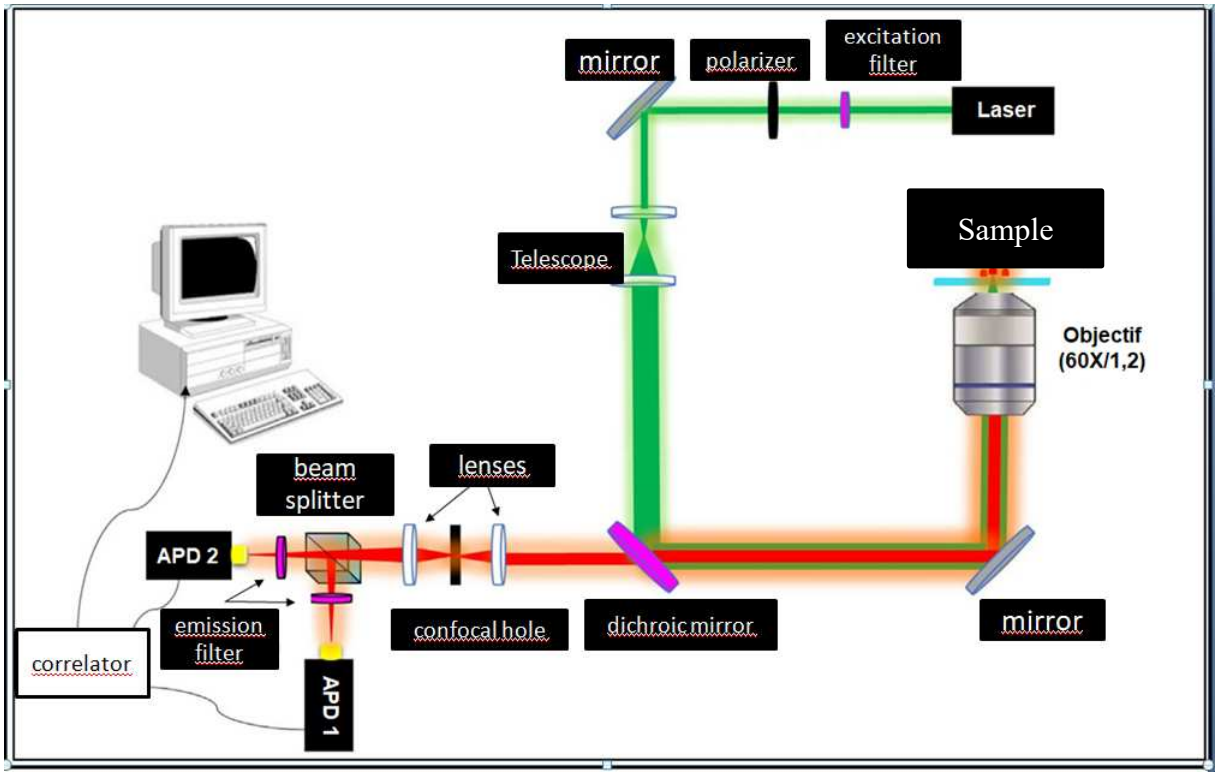

Figure 4.9 Setup of the correlation spectroscopy used in the experiences

4.4 Study of the interaction of MnSOD with its aptamer by SCS

The objective of this study is to understand the mechanism of interaction between a protein of interest and its aptamers designed to specifically capture the protein. The aptamers were grafted at the surface of gold nanoparticles using the carbodiimide method described previoulsy (section 4.2.1.a) and the study was performed for different concentrations of proteins. MnSOD was chosen as a model molecule as we already have a large experience on this protein in terms of detection and identification.

4.4.1 Materials and methods

Gold spherical nanoparticles PEG 50nm (GNS-PEG 50), dicarboxylic, N-hydroxysuccinimide (NHS),1-(3-dimethylaminopropyl)-N′-ethylcarbodiimidehydrochloride (EDC) and phosphate-buffered solution (PBS) were all provided by Sigma Aldrich at maximum purity grade. Human manganese superoxide dismutase (MnSOD) was provided by Euromedex and MnSOD aptamers were purchased from Eurogentec.

a) MnSOD Aptamers

Two types of aptamers for MnSOD were used both purchased from Eurogentec. The aptamers were dispersed in PBS buffer (pH = 9).

The sequence of the first aptamer (APT-w/T) is:
5′HS-(C_6)-TTTTTTTTTTTTTTT-TCT TCT CTA GCT GAATAA CCG GAA GTA ACT CAT CGT TTC GAT GAG TTA CTT CCG GTT ATT CAG CTA GAG AAG 3′.

The sequence of the second aptamer (APT-wo/T) is:
5′HS-(C_6)- TCT TCT CTA GCT GAA TAA CCG GAA GTA ACT CAT CGT TTC GAT GAG TTA CTT CCG GTT ATT CAG CTA GAG AAG-3′.
Both sequences are identical except the inclusion of a spacer of 15 thymines in the APT-w/T. We assume that both aptamers should have the same conformation and the same affinity with the MnSOD. The 15 thymines spacer is only used to increase the distance of the active part of the aptamer from the gold surface and provide higher flexibility to the active part of the aptamer.

b) MnSOD Protein

The MnSOD protein solution was prepared from a MnSOD (LF-P0013, Superoxide Dismutase 2, Human, Euromedex) lyophilized powder in a buf-iron (50 mM Tris-Acetate, 100 mM $NaCl_2$, 5 mM $MgCl_2$, (Sigma-Aldrich) in Mili-Q water at pH = 8.2). Once the MnSOD solution is ready, we prepare several solutions of different concentrations which are ranging from 1 pM to 1µM. A solution of 450 µL of functionalized gold nanoparticles with the aptamers was added in 1.5-ml eppendorf tubes, to which 50 µL of MnSOD of different concentrations are added in it.

c) Bioconjugation of 50nm PEG-GNS with Aptamers

The aptamer grafting onto 50nm PEG-GNS was performed by Carbodiimide Cross-Linker Chemistry. The grafting strategy consists in the immobilization of the APTw/T or APTwo/T at the PEG-AuNPs surface by carbodiimide bonds. Briefly, 50 µl of EDC/NHS (40/10

w/w ratio) aqueous solution was added into 5 ml PEG-GNS dispersion (42 nM). After 2 h, 50 µl of aptamer solution (10 µM in PBS pH 9) were added in 2 ml of the reaction mixture and stirred for 2 h at room temperature. Such concentrations correspond to an average of 2.6 aptamers per AuNPs. The APT-PEG-GNS thus obtained were centrifuged two times at 9000 rpm for 30 min to remove excess of non-conjugated APT and dried under nitrogen.

4.4.2 Characterization of raw 50nm PEG-GNS by SCS

SCS was used to characterize the hydrodynamic radius of the primary gold nanoparticles. Figure 4.9 shows the correlation curve measured for the commercial 50nm PEG-GNS (the acquisition time was set at 300 seconds). This measurement gave us a radius Rh=25.36 nm (diameter of 50.72nm) and a diffusion time t_D=6.25ms. This measurement is in good agreement with the expected one of 50 nm for the commercial PEG-GNS.

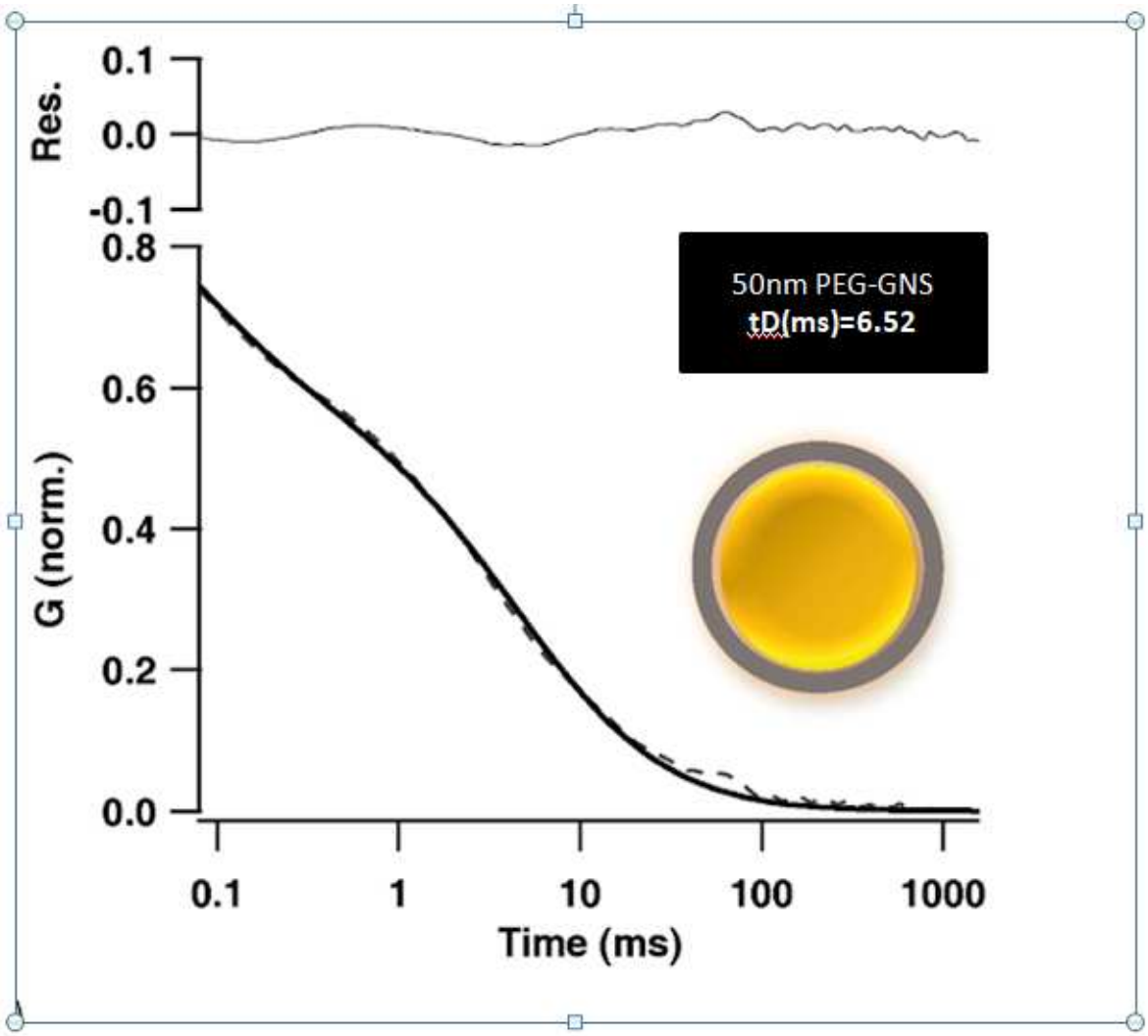

Figure 5.0 Correlation curve measured for the commercial 50nm PEG-GNS

4.4.3 Characterization of Apt-w/T-PEG-GNS and Apt-w/oT-PEG-GNS by SCS

We analyzed the variation in the hydrodynamic radius of gold nanoparticles after the grafting of both aptamers. The cross-correlation curves were recorded for GNS solution and were normalized to 1 (Figure 5.1) to facilitate comparison of the diffusion time under the two conditions.

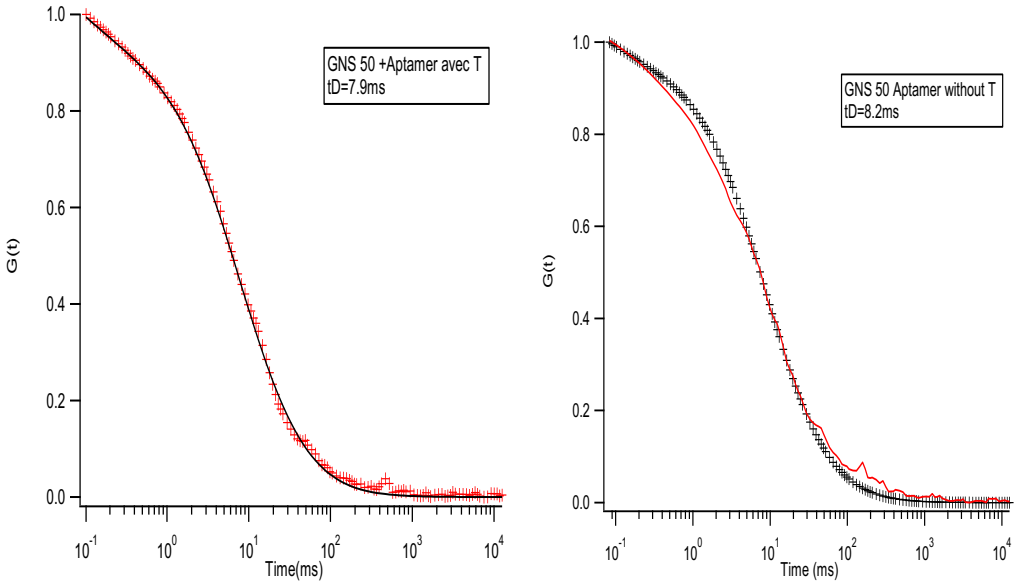

Figure 5.1 Correlation curves measured for the Apt-w/T-PEG-GNS and Apt-w/oT-PEG-GNS

The diffusion time (τ_D) was determined for each nanoparticle by fitting the curve with the equation (3.3), and then the Rh of the nanoparticles was calculated for each case using the equations (3.4) and (3.5). The results obtained are summarized in Table 4.1 below.

	Aptamer	**τ_D(ms)**	**Rh by SCS ($\pm$0.2nm)**
GNS	**without**	**6.52**	**25.36**
GNS	**APTw/T**	**7.91**	**30.77**
GNS	**APTwo/T**	**8.23**	**32.01**

Table 4.1 mesurements of APT-GNS by SCS

Without aptamer, the raw GNS show a Rh of 25.36 ± 0.2 nm. After the grafting of the aptamers with EDC/NHS method, the Rh increases at 30.77± 0.2 nm for APTw/T and at 32.01± 0.2 nm for APTwo/T, which confirms the grafting of the aptamers on the surface of the GNS. This matches perfectly with the UV-visible measurements from the previous publication[1]. From the Rh measured at each stage of the aptamer grafting onto the nanoparticles, the difference in Rh (ΔRh) was determined for each aptamer. In the case of GNS incubated with aptamer with 15T (APTw/T), ΔRh is approximately 5.4 ± 0.2 nm, which corresponds to the thickness of the aptamer monolayer. In the case of GNS incubated at the same concentration of aptamer without 15T (APTwo/T), a ΔRh of 6.6 ± 0.2 nm. We can see that aptamer without 15T induces a greater ΔRh than aptamer with 15T. This can be explained by the fact that the 15T spacer provides a better flexibility to the aptamer on the surface of the GNS. In this case, the aptamer can be closer to the gold surface and as a consequence forms a layer with lower thickness. Figure 5.1 shows the flexibility of the 15T.

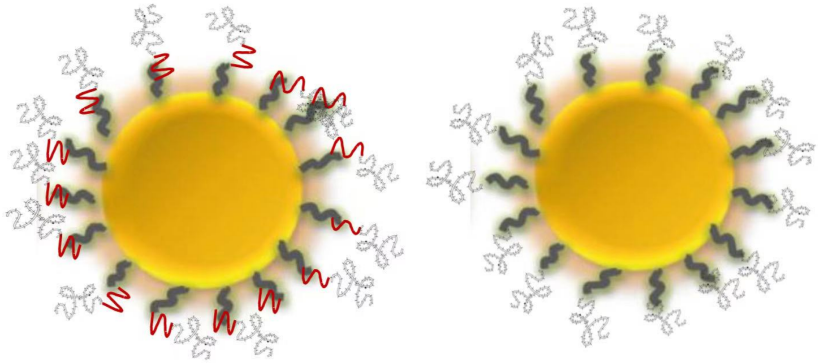

Aptamer with 15T spacer	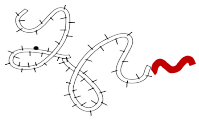
aptamers	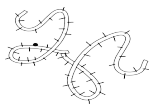
GNS 50nm PEG	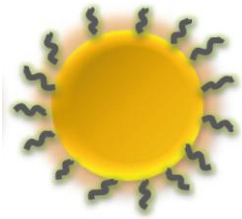

Figure 5.2 scheme of monolayer of Apt and GNS

From the figure 5.2 we can clearly see that the 15 T of aptamer gives a larger flexibility to aptamer and the Rh of GNS 15 T is less important than the Rh of GNS with APTwo/T.

4.4.4 Interaction with the MnSOD

By using SCS, we analyzed the variation in the hydrodynamic radius of gold nanoparticles by adding the different concentrations of MnSOD from 1pM to 1μM. Each concentration has been probed by SCS for one hour. In figure 5.2, it shows before and after the adding of 1μM MnSOD. The results obtained are summarized in Table 4.2 below.

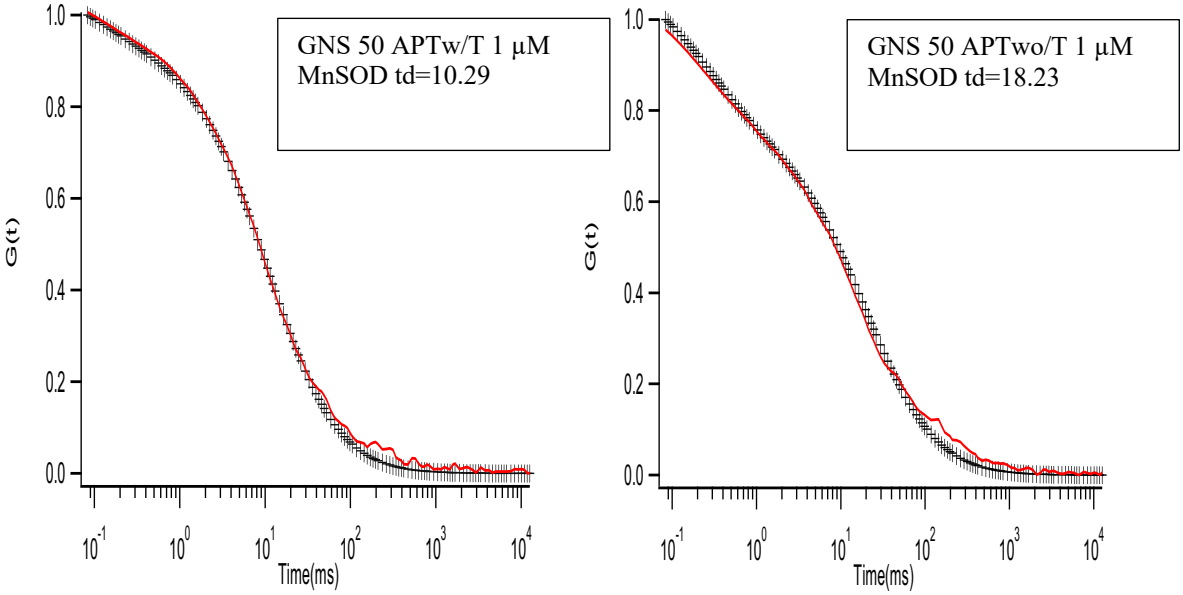

Figure 5.3 Correlation curve measured for the Apt-w/T-PEG-GNS PEG-and Apt-w/oT-PEG-GNS in interaction with 1µM of MnSOD

	Aptamer	MnSOD(μM)	t_D(ms)	Rh by SCS (±0.2nm)
GNS	APTw/T	0	7.91	30.77
GNS	APTwo/T	0	8.23	32.01
GNS	APTw/T	1	10.29	50.95
GNS	APTwo/T	1	18.23	70.95

Table 2 the mesurements of APT-GNS with MnSOD(1μM) **by SCS**

After adding 3μM of MnSOD in the GNS Aptamer solution, we could see a significant increase of Rh. It shows that MnSOD interacts with the aptamers, but GNS with APTw/T has smaller Rh compared with GNS with APTwo/T. This may be due to the conformation of the APTw/T which induces a better interaction between aptamer and MnSOD. This latter one will then saturate the aptamer layer and avoid any interaction between the nanoparticles and as a consequence avoid their aggregation. On the contrary the lower flexibility of APTwo/T would induce a lower interaction between aptamer and MnSOD resulting in an aggregation of the GNS and as a consequence an artificially higher Rh.

The following tables give the variation of Rh depending on the concentration of MnSOD from 10pM up to 3μM for both aptamers.

Table 3 the mesurments of APT-w/T-GNS with MnSOD(3μM to 10pM) **by SCS**

	MnSOD	**tD(ms)**	**Rh by SCS ($\pm$0.2nm)**
GNS	10pM	7.89	30.71
GNS	100pM	11.69	45.5
GNS	1nM	11.73	45.62
GNS	10nM	11.64	45.27
GNS	20nM	11.59	45.07
GNS	30nM	11.56	44.96
GNS	40nM	10.37	41.27
GNS	50nM	10.03	39.02
GNS	100nM	8.69	33.80
GNS	200nM	8.38	32.59
GNS	300nM	8.97	34.89
GNS	400nM	9.09	35.36
GNS	500nM	9.32	36.25
GNS	600nM	10.26	39.9
GNS	700nM	10.29	40.03
GNS	800nM	10.88	42.32

GNS	900nM	11.02	42.90
GNS	1μM	13.06	50.95
GNS	2 μM	13.54	52.67
GNS	3 μM	11.80	45.89

Table 4 the mesurments of APT-wo/T-GNS with MnSOD(3μM to 10pM) **by SCS**

	MnSOD	**tD(ms)**	**Rh by SCS (±0.2nm)**
GNS	10pM	7.71	30.01
GNS	100pM	11.11	43.23
GNS	1nM	10.54	41.26
GNS	10nM	11.29	43.91
GNS	20nM	9.31	36.25
GNS	30nM	9.29	36.14
GNS	40nM	10.51	40.89
GNS	50nM	9.25	35.98
GNS	100nM	9.29	36.14
GNS	200nM	8.78	34.15
GNS	300nM	8.01	31.16
GNS	400nM	7.71	30.01
GNS	500nM	8.77	34.15
GNS	600nM	10.38	40.37
GNS	700nM	9.73	37.86
GNS	800nM	10.57	41.13
GNS	900nM	16.71	65

GNS	1μM	18.23	70.95
GNS	2μM	19.88	77.32
GNS	3μM	13.01	50.62

From the tables 3 and 4, we could figure out the Δ_{Rh} of GNS for the different concentrations of MnSOD. For both aptamers, we could see a clear increase of Rh on the 10nM range to 100nM range, (figure 5.4). This is due to the occupancy of the aptamer layer by the MnSOD that induces a lower interaction between the NP through the DNA strands. For higher concentrations, one can observe a continuous decrease of the Rh that corresponds to 200nM to 500nM. This is due to the optmal occupancy of the aptamer layer by the MnSOD that induces a lower interaction between the NP through the DNA strands and reduce the aggregation. For concentrations higher than 500nM, a increase of the Rh is observed indicating a new interaction between the nanoparticles. With the saturation of the surface of the AuNP, we can suppose that it could induce a reorientation of the MnSOD or a change of its conformation due to chemical hindrance and also due to aptamer conformation changes. These results are in agreement with the previous work made with UV-visible experiments (Figure 5.5). In these experiments, the MnSOD interaction was monitored through the evolution of the plasmon resonance of the nanoparticles depending on the MnSOD concentration.

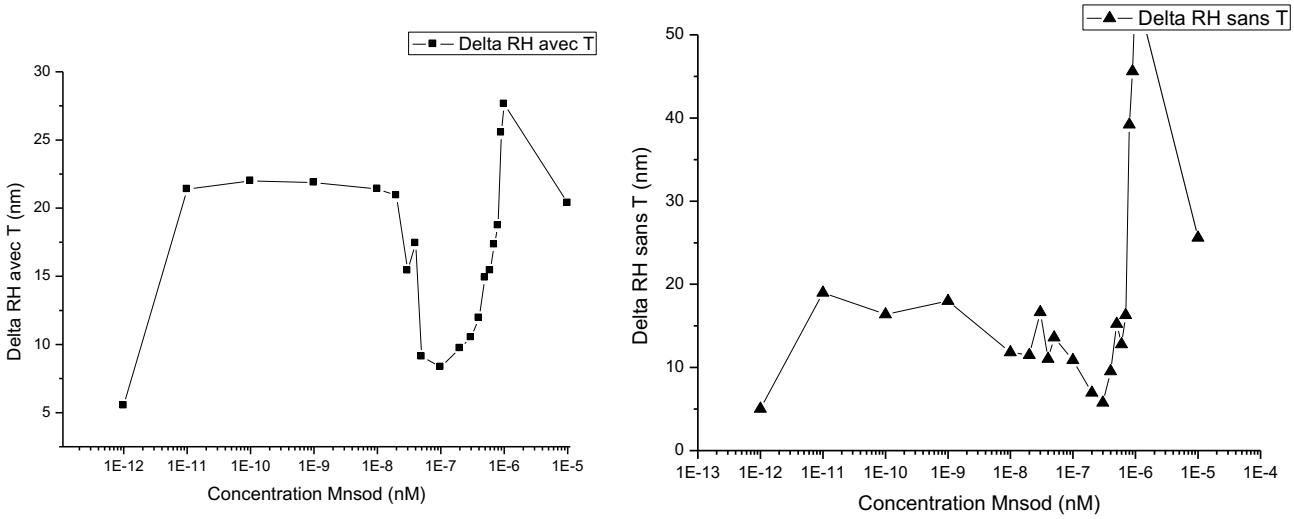

Firgue 5.4 evolution of the ΔRH of Apt-w/T-PEG-GNS and Apt-w/oT-PEG-GNS for different concentrations of MnSOD

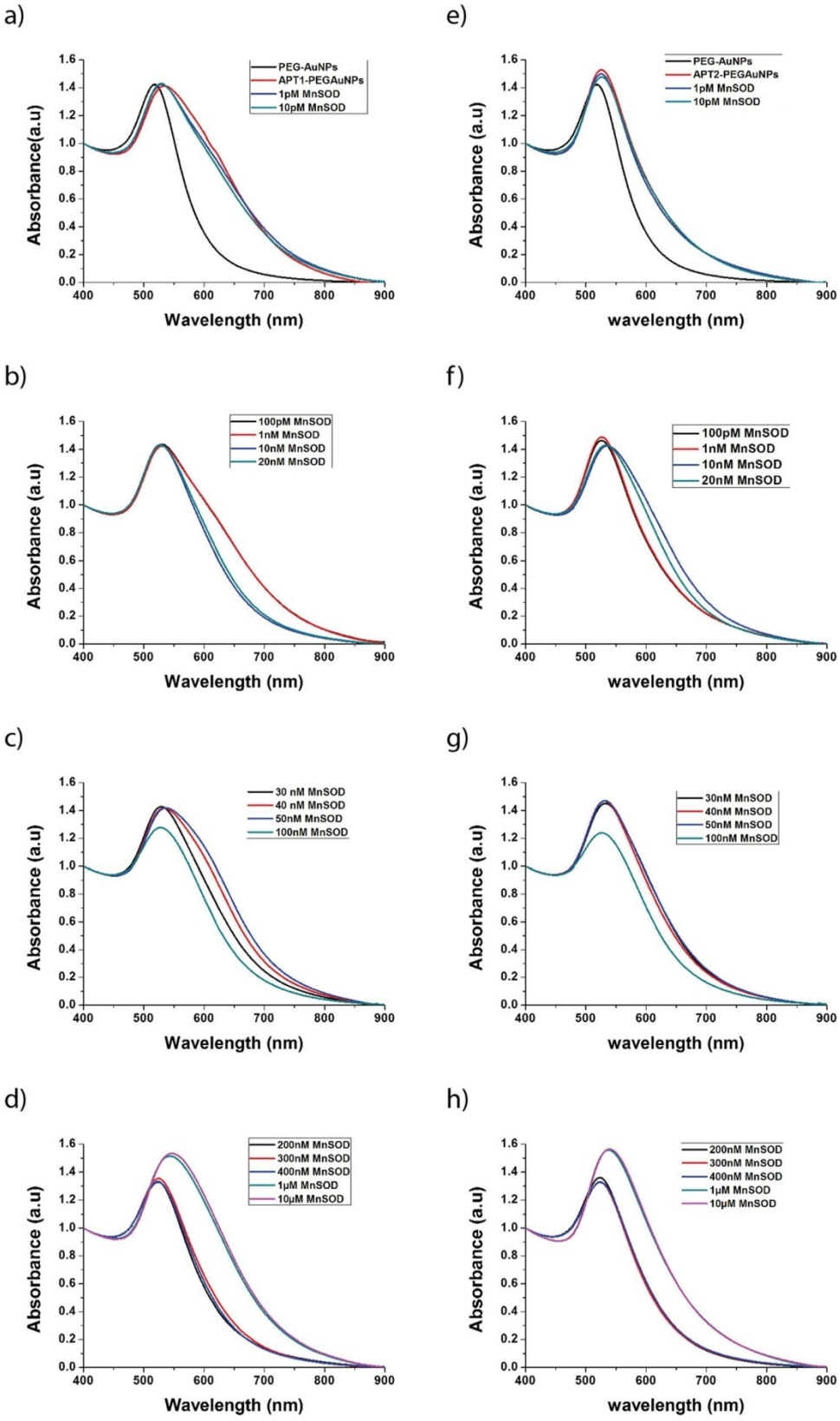

Figure. 5.5 a–d Extinction spectra of Apt-w/T-PEG-GNS and e–h Apt-wo/T-PEG-GNS by carbodiimide chemistry before and after conjugation to MnSOD at different concentrations

To compare the SCS results with UV-Visible results, in last publication [1]. we have fitted all the plasmon bands of UV-visible by two lorentzian peaks to describe the evolution of the plasmon resonance during the interaction process, corresponding to two kinds of nano-objects: individual AuNP (peak called P1 in red and green lines on figure 5.6) and aggregated AuNP (peak called P2 in black and blue lines on figure 5.6). Thus, the observation of each one will give some information on the evolution of these two kinds of objects with the concentration and more especially on the dissociation and aggregation of the AuNP depending on the MnSOD concentrations. Indeed, the intensity of P2 tells us about the amount of aggregated AuNP whereas its width gives information on the number of AuNP in the agglomerates. (Fig.5.6). The P1 and P2 curves can be essentially splitted in three intervals: from 0 to 10^{-9} M, from 10^{-8} to 4×10^{-7} M and from 10^{-6} to 10^{-5} M. In the first and third concentration ranges, the curves are nearly constant with few variations whereas in the second range, strong variations can be observed. These results are correlated with SCS measurements show that SCS is a perfect technique to study the interaction of aptamer and MnSOD in a much more precise way.

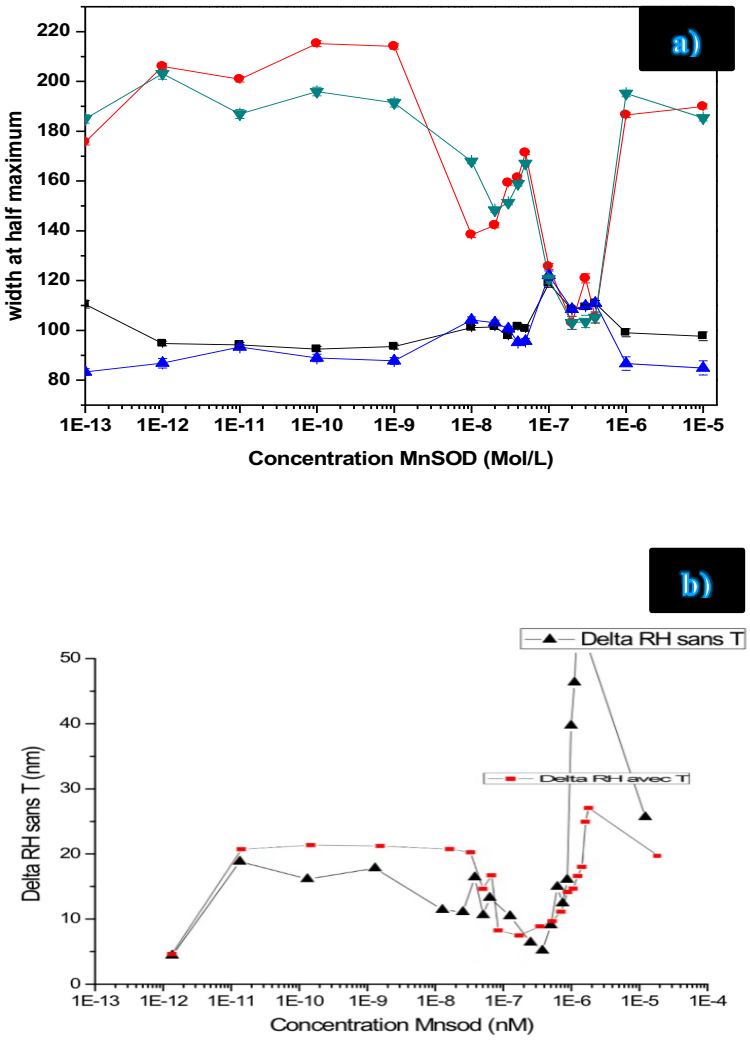

Figure 5.6 a) Evolution of the intensity and width of plasmon bands b) evolution of the ΔRH of APT-GNS for different concentrations of MnSOD

4.5 Monitoring of the aptamer/protein interaction by Real time surface enhanced Raman scattering

Aptamer is a macromolecule made of a long chain of nucleosides; it is flexible [18]. and could present different structural configurations when it is alone or when it is in interaction. To probe this complexity, one should screen the different configurations experienced by the aptamer under specific conditions and determine their effects on the aptamer structure.

To provide a clear and relevant insight, we propose the real time approaches of a SERS surface covered by aptamers

The methodology was applied to one aptamer specific to the Manganese Superoxide Dismutase (MnSOD). We were able to observe different structures and orientations of the aptamer in relation to the SERS surface depending on its interaction with the MnSOD.

This work has been done in collaboration with Dr Aymeric Leray and Pr Eric Finot from the Laboratoire Interdisciplinaire Carnot de Bourgogne (UMR 6303 CNRS, Université de Bourgogne Dijon, France)

4.5.1 Methods

a) Chemicals

The aptamer for MnSOD was purchased from Eurogentec and dispersed in a PBS buffer (pH = 7.4). Manganese Superoxyde Dismutase (MnSOD), was purchased by Ab FRONTIER (LF-P0013, Super oxyde Dismutase 2, Humain, Euromedex).

b) Aptamers

One sequence of aptamer has been used. This is the one including the spacer of 15 thymines (Apt/wT).

c) Gold spherical nanoparticles synthesis

Colloids of COOH-terminated PEG-coated AuNPs (PEG-AuNPs) were prepared by a well assessed chemical reduction process by reducing tetrachlororoauric acid ($HAuCl_4$) in the presence of PEG-diacid using sodium borohydride ($NaBH_4$) as a reducing agent. The color of the dispersion indeed instantly changed from yellow to red when sodium borohydride was added to a solution of gold precursor in the presence of PEG-diacid, confirming the formation of PEG-AuNPs in the solution

d) Deposition of AuNPs covered by aptamer and MnSOD

We have deposited few drops of AuNPs- Apt on a surface of a Glass slide well cleaned. After one hour we have added different concentrations of MnSOD (10nM and 500nM) on the dry area of AuNPs -Apt. faire une phrase

e) Real time SERS measurements

Dynamic SERS measurements are conducted using a home-made confocal Raman setup. The substrate is illuminated by the laser (784 nm) through a water immersion objective (60x, NA=1.20). The Raman scattering is recorded simultaneously on an avalanche photodiode and a spectrometer associated with a cooled CCD camera cadenced at 1 second acquisition time.

4.5.2 Results

SERS gave us some interesting results. From figure 5.7 a) we could observe large fluctuations of the SERS signal from the aptamer alone, with strong modifications of the band positions and intensities during time. Such fluctuations could be due to the fact that the aptamer is highly flexible and that its conformation is continuously modified.
After the deposition of 10nM of MnSOD (figure 5.7 b), less fluctuations of the SERS signal can be observed. At the end point with 500nM of MnSOD (figure 5.7 c), we could observe nearly no fluctuations. This indicates that the structure of the aptamer stay constant with time and no modification of the conformation occurs when the aptamer is interacting with the MnSOD.
Thus, during the interaction between the aptamer and the MnSOD, the aptamer flexibility is highly reduced and the MnSOD interaction freezes the aptamer conformation. The aptamer is then a highly flexible molecule that can experience various conformations to recognise the MnSOD but the aptamer conformation is blocked in a specific one to capture the MnSOD.

a)

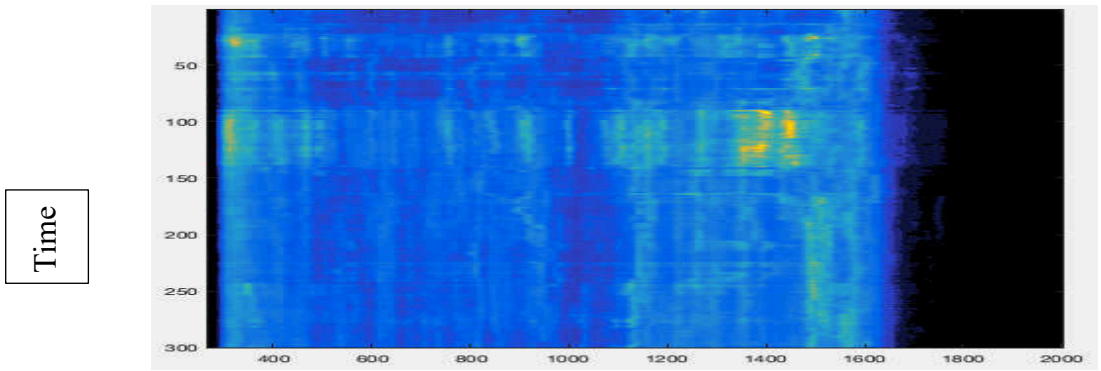

b)

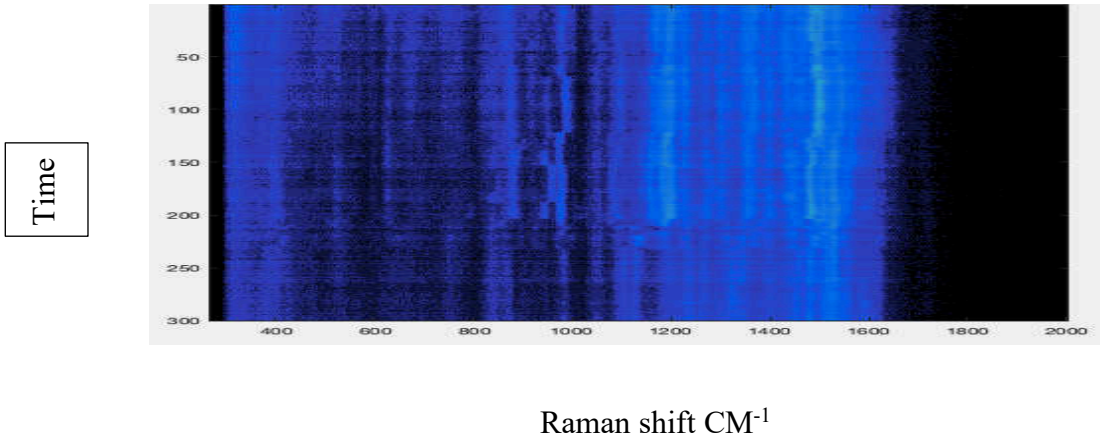

c)

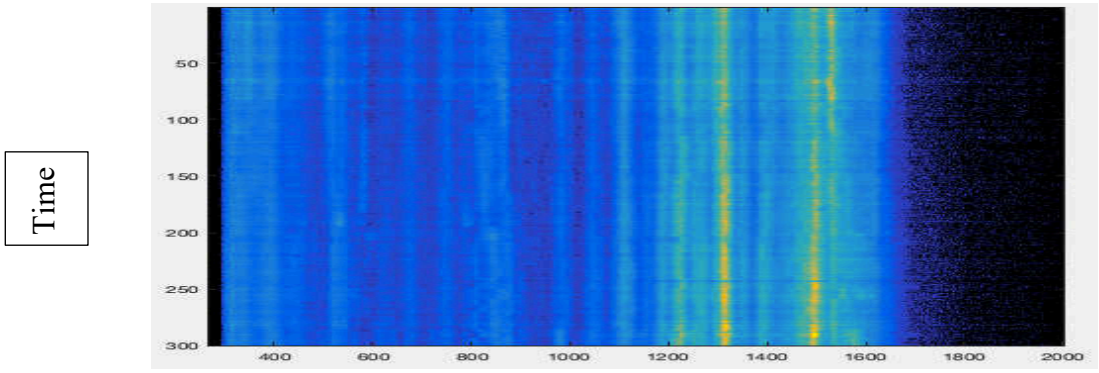

Figure 5.7 SERS signal evolution with time. The colors indicate the SERS intensity from the black (lowest intensity) to the yellow (highest intensity) colors. a) Apt w/T alone; b) Apt w/T with 10nM of MnSOD; C) Apt w/T with 1000 nM of MnSOD.

4.6 Conclusion

In this work, we have used UV-visible, SCS and SERS to provide a new way to understand the interaction of aptamer with the MnSOD. It's the first time we have associated the 3 methods for a deep study between aptamer and proteins. First the SCS allows us to investigate the protein binding in situ by determining the hydrodynamic radius in the case of nanospheres 50nm PEG by EDC/NHS grafting with aptamers. Different values of GNS aptamer and MnSOD thickness were measured, reflecting a specific interaction of the MnSOD on the GNS surface. Moreover, our results were highly correlated with the results of UV-visible experiments.

In the SCS analysis, the GNS Rh is dependent not only on the GNS size but also on the aptamer sequence which affects its flexibility. We found that Apt-w/T has more flexibility than Apt-wo/T. We have shown that by UV-visible the binding affinity for Apt-w/T was stronger than for Apt-wo/T, indicating that the MnSOD interacts much more strongly with Apt-w/T than Apt-w/T. This can be explained by a higher surface of interaction. As Apt-GNS could be injected into the blood for therapeutic applications (often as nanovector for targeted delivery), it is of major importance to study their interaction with proteins. This study is a primordial step to study the actual interaction between aptamer and MnSOD by SCS. To better understand the detection mechanism in biologic environments and in the future, we shall investigate more the interaction of other relevant proteins with aptamer nanovectors.

Furthermore, the SERS experiences give evidence of the dynamic of the aptamer/protein interaction. By monitoring temporally, the interaction, we think that it will be possible to observe its influence on the aptamer conformation.

4.7 Bibliographic references

1 Celia Arib & Qiqian Liu & Nadia Djaker & Weiling Fu& Marc Lamy de la Chapelle & Jolanda Spadavecchi Influence of the Aptamer Grafting on its Conformation and its Interaction with Targeted Protein lasmonics https://doi.org/10.1007/s11468-018-0890-4

2 Borrelli, A.; Schiattarella, A.; Bonelli, P.; Tuccillo, F. M.; Buonaguro, F. M.; Mancini, A., The Functional Role of MnSOD as a Biomarker of Human Diseases and Therapeutic Potential of a New Isoform of a Human Recombinant MnSOD. BioMed. Res. Int. 2014, 2014.

3 Epperly, M. W.; Defilippi, S.; Sikora, C.; Gretton, J.; Greenberger, J. S. Radioprotection of Lung and Esophagus by Overexpression of the Human Manganese Superoxide Dismutase Transgene. Mil. Med. 2002, 167, 71−73.

4 Mukhopadhyay, S.; Das, S. K.; Mukherjee, S. Expression of Mn- Superoxide Dismutase Gene in Nontumorigenic and Tumorigenic Human Mammary Epithelial Cells. J. Biomed. Biotechnol. 2004, 4, 195− 202.

5 McGlynn, K. A.; Tarone, R. E.; El-Serag, H. B. A Comparison of Trends in the Incidence of Hepatocellular Carcinoma and Intrahepatic Cholangiocarcinoma in the United States. Cancer Epidemiol. Biomarkers Prev. 2006, 15, 1198−203.

6 Tamai, T.; et al. Serum Manganese Superoxide Dismutase and Thioredoxin Are Potential Prognostic Markers for Hepatitis C Virus- Related Hepatocellular Carcinoma. World J. Gastroenterol. 2011, 17, 4890−8.

7 Kawaguchi, T.; et al. Serum-Manganese-Superoxide Dismutase: Normal Values and Increased Levels in Patients with Acute Myocardial Infarction and Several Malignant Diseases Determined by an Enzyme- LinkedImmunosorbentAssayUsingaMonoclonalAntibody.J. Immunol. Methods 1990, 127, 249−254.

8 Ishikawa, M.; Yaginuma, Y.; Hayashi, H.; Shimizu, T.; Endo, Y.; Taniguchi, N. Reactivity of a Monoclonal Antibody to Manganese Superoxide Dismutase with Human Ovarian Carcinoma. Cancer Res. 1990, 50, 2538−42.

9 Li, J. J.; Oberley, L. W.; Stclair, D. K.; Ridnour, L. A.; Oberley, T. D. Phenotypic Changes Induced in Human Breast-Cancer Cells by Overexpression of Manganese-Containing Superoxide-Dismutase. Oncogene 1995, 10, 1989−2000.

10 Church, S. L.; Grant, J. W.; Ridnour, L. A.; Oberley, L. W.; Swanson, P. E.; Meltzer, P. S.; Trent, J. M. Increased Manganese Superoxide-Dismutase Expression Suppresses the Malignant Pheno- type of Human-Melanoma Cells. Proc. Natl. Acad. Sci. U.S.A. 1993, 90, 3113−3117.

11 Zhong, W. X.; Oberley, L. W.; Oberley, T. D.; StClair, D. K. Suppression of the Malignant Phenotype of Human Glioma Cells by Overexpression of Manganese Superoxide Dismutase. Oncogene 1997, 14, 481−490.

12 O'sullivan, C. K.; Guilbault, G. G. Commercial Quartz Crystal Microbalances−Theory and Applications. Biosens. Bioelectron. 1999, 14, 663−670.

13 Spadavecchia J, Perumal R, Casale S, Krafft J-M, Methivier C, Pradier C-M (2016) Poly-ethylene glycol gold-nanoparticles: facile nanostructuration of doxorubicin and its complex with DNA mol- ecules for SERS detection. Chem Phys Lett 648:182–188

14 Haustein, E. and P. Schwille, Fluorescence Correlation Spectroscopy: Novel Variations of an Established Technique. Annual Review of Biophysics and Biomolecular Structure, 2007. 36(1) : p. 151-169.

15Tcherniak, A., et al., One-Photon Plasmon Luminescence and Its Application to Correlation Spectroscopy as a Probe for Rotational and Translational Dynamics of Gold Nanorods. The Journal of Physical Chemistry C, 2011. 115(32) : p. 15938-15949.

16 Wang, K., et al., Single-Molecule Technology for Rapid Detection of DNA Hybridization Based on Resonance Light Scattering of Gold Nanoparticles. ChemBioChem, 2007. 8(10) : p. 1126-1129.

17 Sabanayagam, C.R. and J.R. Lakowicz, Fluctuation correlation spectroscopy and photon histogram analysis of light scattered by gold nanospheres. Nanotechnology, 2007. 18(35) : p. 355402.

18 Borrelli, A., Schiattarella, A., Bonelli, P., Tuccillo, F.M., Buonaguro, F.M., Mancini, A., The functional role of MnSOD as a biomarker of human diseases and therapeutic potential of a new isoform of a human recombinant MnSOD, *Biomed Res Int.* **2014**, 476789 (2014)

Conclusions and perspectives

This work consisted first in the synthesis of a hybrid gold nanoparticle for biomolecule detection using a one-step approach. This approach allows for the use of few reagents and steps, and therefore allows a simple and inexpensive synthesis. Thus, an important part of this thesis was devoted to the development of this synthetic strategy, which consists of the complexation between the auric ions and the Chitlac for fast detection of Galectin-1. This latter one is considered as a cancer biomaker in human body. In a second step, as Galectin-1 has a special glycan site, we have done a complexation of the auric ions with this protein and demonstrated its efficiency for the Glucose detection. This could be a new method for fast diabet detection in the future.

In the framework of the development of the third generation of nanovectors, we need to design a complex system which will not only provide an analyte detection, but will also allow the cancer therapy. To reach such objectives, we combine in a single nanovector CTL and Doxorubicin for both targeting and treatment functions, respectively. This new strategy has been exploited as part of a systematic study with other molecules such as docetaxel, paclitaxel and bisphosphonates. This new method of synthesis (DOX IN-CTL) was compared to another classic drug 5-Fu. The results show on the one hand a better immunity system protection, but also a better therapeutic efficiency on cancer cells. In addition, the first in vivo tests were carried out on nude mice, in order to study the biodistribution of this nanovector. The results showed that the mice accepted the nanovector well and no excess mortality was observed. These mice were then sacrificed in order to get the organs (liver, spleen, kidneys, lungs, heart). A part of these organs was treated for histological study and another part was used to quantify the level of gold present in mice by ICP MS.

The last work concerns the characterization by SCS of the interaction between the protein MnSOD and its specific aptamer grafted on the surface of gold nanoparticles. We first quantitatively analyzed the adsorption of aptamer on the nanoparticles. This study showed an increase in the size of nanoparticles with the formation of an aptamer layer. In addition, we demonstrated that the aptamer sequence (inclusion of a spacer) influences its interaction with the MnSOD. We gave evidence that the spacer has a strong influence on the affinity between the MnSOD and the aptamer. We demonstrated that the highest affinity is obtained for the aptamer with the a spacerof 15 Thymines. This study opens the way to a better understanding of the interaction mechanism (chemical structure modifications, kinetic interaction…) and to the sensing optimization since the detection sensitivity is directly related to the affinity of the bioreceptor to the analyte. It also gives evidence on the dynamic of the aptamer/protein interaction that go largely beyond the simple key/lock model and how the aptamer should be flexible to capture efficiently the protein.

During this thesis, numerous synthesis was developed and gave numerous results thanks to a multitude of characterization techniques. Especially in vivo study reports the ability of DOX-AuGCs to target liver cancer and to amplify in certain respects the antitumor efficiency of 5-FU. More specifically an original synthetic protocol was adopted to obtain a hybrid nanovector in which the steric conformation of the drugs onto gold nanoparticles was modulated in the presence of diacide polymer (PEG) and a polysaccharide (CTL) in which the drug position can solve the main issues of drug-conjugated AuNPs. The higher antitumor efficiency of DOX-AuGCs compared to 5-FU is shown not only in the suppression of tumor growth but also in higher stimulation of immune system. Therefore, the results in this work confirmed that the molecular design plays a key role to modulate *in vivo* properties and functionalities of nanocarriers and improves their performances and safety in tumor therapeutics. Overall, these results

pave the way for the development of an innovative theranostic platform, allowing for the detection of protein-associated tumors and for the simultaneous cancer treatment with a multimodal agent that combines chemotherapy (drug-delivery associated to an increase payload release or enhanced spreading into the cancer cells). In addition, it would be interesting to study the phototherapy treatment in vivo for the next step.

Appendices

UV-visible spectroscopy

UV-visible spectroscopy is an instrument largely used in the most laboratories. It is not only carrying out quantitative and qualitative analyzes, but also follows the kinetics reaction. It is an instrument that is based on the phenomenon of absorption of electromagnetic radiations by a material. Indeed, when a molecule interacts with light, there will be an electronic transition between the different energy levels of the material. In this case, the electromagnetic radiations take place in the range from the near ultraviolet to the near infrared, between 180 and 1100 nm. When this absorption corresponds to the visible range, the substance is colored. This instrument therefore consists of sending monochromatic radiations through a solution (solid, liquid, gas) and of measuring the luminous flux transmitted as a function of the incident flux. It measures the intensity of light after passing through a sample (I), and compares it to the intensity of light before it passes through a reference sample (I_0The ratio is called the transmittance, and is usually expressed as a percentage (%T). The absorbance A is based on the transmittance.

Transmission electron microscopy (TEM)

Transmission electron microscopy (TEM) is a microscopy technique in which a beam of electrons is transmitted through a specimen to form an image. The specimen is most often an ultrathin section less than 100 nm thick or a suspension on a grid. An image is formed from the interaction of the electrons with the sample as the beam is transmitted through the specimen. The image is then magnified and focused onto an imaging device, such as a fluorescent screen, a layer of photographic film, or a sensor such as a scintillator attached to a charge-coupled device. Transmission electron microscopes are capable of imaging at a significantly higher resolution than light microscopes, owing to the smaller de Broglie wavelength of electrons. This enables the instrument to capture fine detail—even as small as a single column of atoms, which is thousands of times smaller than a resolvable object seen in a light microscope. Transmission electron microscopy is a major analytical method in the physical, chemical and biological sciences. TEMs find application in cancer research, virology, and materials science as well as pollution, nanotechnology and semiconductor research, but also in other fields such as paleontology and palynology. TEM instruments boast an enormous array of operating modes including conventional imaging, scanning TEM imaging (STEM), diffraction, spectroscopy, and combinations of these.

Dynamic light scattering (DLS)

DLS is a spectroscopic for measuring the hydrodynamic diameter of particles of submicron size. This technique is based on the fact that the particles in suspension are subjected to Brownian motions. Thus, large particles will tend to move slowly while smaller particles will move faster. When the particles are excited by a laser, they will start scattering light in a random fashion, the scattered light is recorded and detected at a certain angle. The presence of Brownian motion causes a fluctuation in the intensity of the scattered light which will be recorded, then with the help of a correlator, these fluctuations will be processed in order to obtain an autocorrelation function. This autocorrelation function will make it possible to obtain the coefficient of diffusion which itself is linked to the hydrodynamic radius thanks to the Stokes-Einstein relationship (See chapter 3). The hydrodynamic radius obtained for the case of spherical

particles, for example, corresponds to the radius of the sphere surrounded by its double solvation layer, which is different from the “geometric” radius measured by microscopy.

Inductively coupled plasma mass spectrometry (ICP-MS)

Inductively coupled plasma mass spectrometry is a type of mass spectrometry that uses an inductively coupled plasma to ionize the sample. It atomizes the sample and creates atomic and small polyatomic ions, which are then detected. It is known and used for its ability to detect metals and several non-metals in liquid samples at very low concentrations. It can detect different isotopes of the same element, which makes it a versatile tool in isotopic labeling. Compared to atomic absorption spectroscopy, ICP-MS has greater speed, precision, and sensitivity. However, compared with other types of mass spectrometry, such as thermal ionization mass spectrometry (TIMS) and glow discharge mass spectrometry (GD-MS), ICP-MS introduces many interfering species: argon from the plasma, component gases of air that leak through the cone orifices, and contamination from glassware and the cones. In vivo studies, the ICP-MS could very efficiently detection the biodistribution of nanovectors in different organs. This could led us have a clear understand of the toxicity and accumulation of nanoparticles in the animals model.

High-resolution small animal ultrasound imaging

Ultrasound are sound waves with frequencies which are higher than those audible to humans (>20,000 Hz). Ultrasonic images, also known as sonograms, are made by sending pulses of ultrasound into tissue using a probe. The ultrasound pulses echo off tissues with different reflection properties and are recorded and displayed as an image.

Many different types of images can be formed. The most common is a B-mode image (Brightness), which displays the acoustic impedance of a two-dimensional cross-section of tissue. Other types can display blood flow, motion of tissue over time, the location of blood, the presence of specific molecules, the stiffness of tissue, or the anatomy of a three-dimensional region.

Compared to other dominant methods of medical imaging, ultrasound has several advantages. It provides images in real-time and is portable and can be brought to the bedside. It is substantially lower in cost than other imaging modalities and does not use harmful ionizing radiation. Drawbacks include various limits on its field of view, such as the need for patient cooperation, dependence on physique, difficulty imaging structures behind and air or gases, and the necessity of a skilled operator, usually a trained professional.

Plex TM multiplex bead-based assay

The Cytokine Human Plex TM multiplex bead-based assay platform is specifically designed for quantifying human cytokines, chemokines and growth factors in serum, plasma, and tissue culture supernatant. By measuring 35 analytes simultaneously, the assay panel helps provide more data from each sample, saving both money and time compared to more traditional systems (such as ELISA) used in research. The panel employs magnetic beads, facilitating automation, decreasing hands-on time, and increasing throughput and precision.

1) Superior performance—accurate, reproducible, and sensitive quantitation of multiple proteins

2) High quality—fully qualified antibodies permit excellent specificity and sensitivity

3) Fast and easy protocols—perform your multiplex assay and analyze your data typically in less than one day